AN ABSTRACT OF THE DISSERTATION OF

Rong Fang for the degree of Doctor of Philosophy in Sustainable Forest Management presented on May 6, 2020.

Title: Measuring and Modeling the Structure of Coniferous Trees with Point Clouds Data

Abstract approved: _____

Bogdan Strimbu

Coniferous trees are a major North American crop that has been intensively managed for its commercial value, while also serving as critical habitat for abundant wildlife and as carbon sinks. Having diverse functions, North American temperate coniferous forests have become a research hotspot for numerous scientific studies aiming to integrate ecological and economic objectives, such as examining the contribution of the conifer crown architecture to long-term forest management schemes. Point clouds have become an important source of forest inventory data and forest ecological studies, as provide accurate and comprehensive estimates of many structural variables.

The present thesis aims to improve the understanding of conifer crown structure by estimating crown variables and developing stem and crown models using point clouds derived from images or laser scanning. The utilizations of point clouds were tested on loblolly pine plantations and mature Douglas-fir trees in a natural stand. Various types of 3D models were constructed for tree stems and branch attributes using point clouds. The 3D models provide direct volume estimates, as well as estimates of tree structural variables including tree height, stem diameter, branch basal diameter, length, insertion angle, and azimuth. The variable extractions were executed with semi-automatic methods, which combine human interpretation with an automatic estimation algorithm. The accuracy and reliability of point-clouds-based estimates were assessed with ground measurements and estimates from existing equations through simulations. Stem taper equations were developed using point-clouds-based stem diameter estimates.

Nonlinear models of branch variables, as well as systematic crown models, were developed using lidar-based estimates by considering neighboring competition effects.

The results demonstrate the reliability and efficiency of using point clouds data as alternatives or complements to traditional fieldwork. Stem and branch variables estimated nondestructively from lidar and photogrammetry point clouds agreed with ground measurements and fit in the range of observations from existing equations. Workflows developed and presented in this thesis can be employed by forestry practitioners and researchers to acquire fast and accurate tree structural variables, while models of stem and branch attributes can guide forest inventory and silvicultural practices as well as advance ecological research.

Measuring and Modeling the Structure of Coniferous Trees with Point Clouds Data

by
Rong Fang

A DISSERTATION

submitted to

Oregon State University

in partial fulfillment of
the requirements for the
degree of

Doctor of Philosophy

Presented May 6, 2020
Commencement June 2020

Doctor of Philosophy dissertation of Rong Fang presented on May 6, 2020

APPROVED:

Major Professor, representing Sustainable Forest Management

Head of the Department of Forest Engineering, Resources and Management

Dean of the Graduate School

I understand that my dissertation will become part of the permanent collection of Oregon State University libraries. My signature below authorizes release of my dissertation to any reader upon request.

Rong Fang, Author

ACKNOWLEDGMENTS

First and foremost, I deeply thank my advisor Dr. Bogdan Strimbu, who has been dedicated to supporting me to conduct the research for the past four and a half years. Dr. Bogdan Strimbu has always given me inspiring insights to develop scientific research and encouraged me to persist. I thank my committee members Dr. Temesgen Hailemariam, Yuan Jiang, Darrell Ross, and Dave Shaw for their guidance and support. I would like to express my gratitude to my parents Yang Liu and Jie Fang for their endless love and support. I thank my boyfriend Max Boath for his support and encouragements, which guide me through the tough journey of PhD study. I express my appreciation to my dear friend Fangli Zhang, who had made lifelong impact on me.

TABLE OF CONTENTS

Page

Chapter 1 Introduction 1
1.1. Importance of conifer architecture 1
1.2. Application of point clouds in tree structural studies 3
1.3. Objectives of this study 7
Reference 9
Chapter 2 Stem measurements and taper modeling using photogrammetric point clouds 13
2.1. Introduction 14
2.1. Methods 16
2.1.1. Field data collection 16
2.1.2. Photogrammetric point cloud generation and diameter measurements. 19
2.1.3. Assessment of measurements and bias correction 23
2.1.4. Taper modeling 25
2.2. Results 27
2.2.1. Tree construction and diameter measurement 27
2.2.2. Taper equations 35
2.3. Discussions 43
2.4. Conclusion 46
References 48
Chapter 3 Comparison of total stem volume estimates from point clouds of terrestrial lidar and empirical equations for mature Douglas-fir (Pseudotsuga menziessi (Mirb.) Franco) 53
3.1. Introduction 54
3.2. Methods 58
3.2.1. Study area and point cloud acquisition and processing 58
3.2.2. Stem measurements 60
3.2.3. Taper equations 62
3.2.4. Volume estimation 64
3.2.5. Simulation 66
3.3. Results 69

TABLE OF CONTENTS (Continued)

Page

3.3.1. Taper equations 69
3.3.2. Volume estimation 72
3.3.3. Simulated trees 74
3.4. Discussion 78
3.4.1. Sensitivity of point-cloud-based volume estimates to segment length of cylinder models 79
3.4.2. Difference of total stem volume estimates from various methods 80
3.5. Conclusion 82
References 84
Chapter 4 Comparison of mature Douglas-firs' crown structures developed with two quantitative structural models using TLS point clouds for neighboring trees in a natural regime stand 88
4.1. Introduction 90
4.2. Data and methods 94
4.2.1. Study sites and data collection 94
4.2.2. Cyclone-based estimation of stems and branch dimensions 96
4.2.3. Automatic estimates of stem and branches dimensions using TreeQSM 99
4.2.4. Cleaning TreeQSM estimates 101
4.2.5. Comparison of the Cyclone and TreeQSM estimates 102
4.2.6. Simulation of crown architecture 105
4.3. Results 111
4.3.1. Tree level estimates 111
4.3.2. Estimation of branch attributes 112
4.3.3. Simulated crowns 121
4.3.3.1. Branch Diameter 121
4.3.3.2. Branch length 123
4.4. Discussion 124
4.4.1. Comparison of TreeQSM and Cyclone crown attribute estimates 124
4.4.2. Crown architecture and development stage derived with TLS-based estimates 129

TABLE OF CONTENTS (Continued)

Page

4.5. Conclusion 132
References 133
Chapter 5 Modeling mature Douglas-fir crown attributes using point clouds-based measurements 138
5.1. Introduction 139
5.2. Data and method 142
5.2.1. Study site and field data collection 142
5.2.2. TSL-based branch estimates in Cyclone 143
5.2.3. Competition indices 146
5.2.4. anch attribute modeling 149
5.2.5. Model evaluation 158
5.3. Results 158
5.3.1. Branch attribute models 158
5.3.2. Systematic crown profile modeling 169
5.4. Discussion 175
5.4.1. Branch attributes models 175
5.4.2. Crown form modeling 180
5.4.3. Application and limitation 182
5.5. Conclusion 183
References 184
Chapter 6 General Discussion and Conclusion 189
6.1. Summary of contributions 194
6.2. Limitation and future work 196
Reference 198

LIST OF FIGURES

Figure Page

2.1 Study area showing the location of the trees. a. general position within Louisiana; b. locations of all the trees photographed and cut; c. the four most southern trees; d. lidar point cloud of the rectangle contain the southern four trees. 18

2.2 Workflow of the photogrammetric-based stem reconstruction and diameter measurement. a. field photographs for an individual tree; b. SfM process of reconstruction (tie points, densified points, surface); c. scaling the ppc with reference bar and d1.3; d. diameter measurements in AutoCAD. 20

2.3 An example of a reconstructed stem, with the lower part continuous, (i.e, measurable surface), and the upper part fragmented (i.e., unsuitable for accurate measurements) 29

2.4 Diameter measurements on cross sections of the stem. a. successfully identified by the convex hull algorithm at height 4 m; b. unsuccessfully identified by convex hull algorithm at height 11 m. The red line is the circumference of the tree as computed by the convex hull algorithm. 30

2.5 Variation with height of diameters measured in the field and from the ppc.....31

2.6 The ppc-based error vs. the stem height; a. uncorrected b. after bias correction with Eq. 2-7. The dots represent outliers, which are estimated using the interquartile range approach. 32

2.7 Comparisons of the models developed with the ppc-based measurement and the ground-based measurement. a. Max and Burkhart b. Baldwin and Feduccia c. Lenhart et al d. Kozak.....41

3.1 A rendering of sample tree point clouds. The grey scale of the point clouds are represented by their intensity values.....59

LIST OF FIGURES (Continued)

Figure Page

3.2 Fitting cylinder models; a. cylinder fitting in Cyclone with region grow; b. Region Grow fits stem sections with missing points on one side; c. Imputation of the tree top: A is the highest fitted cylinder, B is the imputed cone shape, and C is the estimated tree top from point clouds. d_A is the diameter of highest fitted cylinder; h_{BC} is the length between A and C. 60

3.3 Illustration of cylinder models with three segment length. a. The length of the cylinder segment is 0.5 m; b. the length of cylinder segment is 1 m; c. the length of the cylinder segment is 2 m. 61

3.4 Simulation process of volume estimation with different methods. dbhi is the simulated dbh of *ith* tree and is generated from the uniform distribution of U(a, b), where a and b are the boundary of dbh class. H is simulated total tree height based on Eq. 3-10. $\mathrm{VolumeFIA-PNW}$ is the estimated stem total volume with the FIA-PNW eequation. VolumeM05, VolumeM1, and VolumeM2 are stem volume estimated with point-cloud-based taper equations, in which dibs are estimates of equation M05, M1 and M2 as it describes in Table 3.1. VolumePoudel18 is the estimated stem volume with the taper equation of Poudel et al. (2018). VolumeC05, VolumeC1, and VolumeC2 are volumes of direct cylinder estimates. 69

3.5 Residuals of fitted Kozak 04 equations with the point-cloud-based dib estimates against predicted dib. a. equation M05, b. equation M1, and c. equation M2.....71

3.6 Comparisons of taper equations for different tree size. Upper row (a – d): predicted dib curves with the point-cloud-based taper equations; lower row (e – h): cumulative stem volume estimates with the point-cloud-based taper equations. Predictions of Poudel et al. (2018) serve as references. 71

LIST OF FIGURES (Continued)

Figure Page

3.7 Comparison between stem volume estimates of the FIA-PNW equation and other methods. a. Volume estimates of cylinder models. b. Volume estimates of taper-based equations. 73

3.8 Simulation results of the 10,000 generated trees by dbh classes: 1 (40 – 60 cm); 2 (60 – 80 cm); 3 (80 – 100 cm); 4 (100 – 120 cm). a. Estimated mean stem volume; b. Mean relative difference between estimates of other methods and the FIA-PNW equation; c. Standard deviation of volume estimates; d. Standard deviation of relative difference. 76

4.1 Lidar point clouds. a. Rendering of the segmented sample tree point clouds; b. Point clouds of the entire plot and the locations of the 10 sample trees within the plot; c. Nadir view of the sample tree crowns 96

4.2 Crown measurements in Cyclone. a. The point clouds of a sample tree. b. Incomplete point clouds of the top section of crown. c. Cylinder models of a branch. Branch insertion angle is measured as the angle between the stem axis and branch cylinder axis. d. Branch length measurements: sum of the length of line segments. The maximum horizontal distance from the stem is the branch projected distance. e. Cylinder model of the stem. f. Dead branch without leaves attaches on it. 98

4.3 An example of QSM created tree model. Different colors represent segments...100

4.4 The algorithm used to simulate individual trees crown using existing models ...109

4.5 TLS identified individual branches by insertion height and azimuth. 113

LIST OF FIGURES (Continued)

Figure Page

4.6 Cumulative probability of branch insertion height. The p-values are for the Kolmogorov–Smirnov test used to compare the branch insertion height distribution of TreeQSM and Cyclone. The null hypothesis of the test is that two sets of values have the same distribution. Red dots mark the height at which the largest difference in the cumulative probability of Cyclone and TreeQSM measured height is found. 114

4.7 Cumulative probability of branch azimuth. The p-values are for the Kolmogorov–Smirnov test used to compare the branch azimuth distributions estimated by TreeQSM and Cyclone. The null hypothesis of the test is that two sets of values have the same distribution. Red dots mark the azimuth at which the largest difference in cumulative probability of Cyclone and TreeQSM estimates are found. 115

4.8 Branch diameter estimates at insertion point by height section. a. Comparison of branch diameter estimates of Cyclone and TreeQSM by height section; reference lines connect the mean of the aggregated estimates. b. The difference of the branch diameter estimates between Cyclone and TreeQSM by height section..117

4.9 Branch length estimates by height section. a. Estimates for Cyclone and TreeQSM; reference lines connect the mean of the aggregated estimates. b. Difference between the branch length estimates of Cyclone and TreeQSM. The dots represents outliers identified with the quantile approach.....118

4.10 Branch angle estimates by height section. a. Estimates for Cyclone and TreeQSM; reference lines connect the mean of the aggregated estimates. b. Difference between branch insertion angle estimates of Cyclone and TreeQSM by height section. 120

LIST OF FIGURES (Continued)

Figure Page

4.11 Mean (a - c) and maximum (d - f) branch diameter of the 10 trees by DBH class as a function of depth into the crown. The reference lines are second-order polynomial regression lines fit to the simulations and observations. Green and red lines are the simulated trees with second- and old-growth models, namely Ishii and Wilson (2001) and Maguire (1999) models. The shades represent the 95% confidence intervals of the simulated results of 10000 trees.....122

4.12 Mean (a - c) and maximum (d - f) branch length of the 10 trees by DBH class as a function of depth into the crown. The reference lines are second order polynomial regression lines fit to the individual simulations and observations. Green and red lines are the simulated trees with second- and old-growth models, namely Ishii and Wilson (2001) and Maguire (1999) models. The shades represent the 95% confidence intervals of the simulated results of 10000 trees. 124

4.13 Comparisons of quantitative structural models constructed with TreeQSM and Cyclone. Identification of some typical errors of structural models developed with TreeQSM. a. Accurate stem model (silver cylinder) developed in Cyclone. b. Inaccurate stem models developed with TreeQSM (blue cylinders). c. A first-order branch was categorized as second-order in TreeQSM (red cylinder). d. Cyclone rendering of the point clouds of the same branch shown in c. e. Stem models at breast height of Tree #3 in Cyclone. f. Incorrect stem models at breast height of Tree #3 in TreeQSM. Cylindrical models (blue cylinder) deviate from the stem point clouds resulting overestimation of DBH. g. Accurate stem model (silver cylinder) constructed in Cyclone. h. TreeQSM misidentified stem points as branch points and constructed models for a nonexistent branch (green cylinders shown in the right). 126

LIST OF FIGURES (Continued)

Figure Page

4.14 Conceptual Douglas-fir tree architectures developed based on TreeQSM crown attribute estimates by DBH classes.....131

4.15 Conceptual Douglas-fir tree architectures developed based on Cyclone crown attribute estimates by DBH classes.....131

5.1 An example of tree estimation in Cyclone. a. Tree-level attribute measurements: total height (THT), crown length (CL) and diameter at breast height (DBH). b. a considerable number of points were missing inside the crown, but branch skeletons were still traced with line segments. c. Branch diameter (BD) and insertion angle estimates with the cylinder models. d. Branch length (BL) and crown radius (CR) estimates.....146

5.2 Illustration of angular measures in competition indices. a. The horizontal angular measure between the focal and the neighboring trees. The tree in the center is the focal tree; b. vertical angular measures between the focal and the neighboring trees . The tree in the middle is the focal tree. $\alpha i = \arctan DBHi Dist0i$. $\beta i = \arctan THTi Dist0i$. $\gamma i = \arctan THTi Dist0i - \arctan THTi - CLi Dist0i$, where DBHi is the DBH of the ith neighbor of the center tree, Dist0i is the distance between the center tree and the neighbor tree i, THTi and THT0 are the total tree height of the neighbor tree i and the center tree respectively, CLi is the crown length of the neighbor tree i.....148

5.3 a. Residual plot of model L: all branch length observations; b. Residual plot of model ML: the maximum branch length. 160

5.4 TLS-based branch length and maximum branch length estimates and their model fits for nine sample trees.....162

5.5 Residual plot of model MD: the maximum branch diameter. 164

LIST OF FIGURES (Continued)

Figure Page

5.6 TLS-based branch diameter and maximum branch diameter estimates and maximum branch diameter models fit for nine sample trees. 165

5.7 a. Residual plot of model AMD: the insertion angle of branches with maximum diameter; b. Residual plot of model AML: the insertion angle of branches with maximum length. 167

5.8 TLS-based branch insertion angle estimates and model fits for nine sample trees. 168

5.9 Crown radius estimates from four models. C1 and C2 are branch model systems fitted with NSUR. 173

5.10 Crown width estimation error distributions of systemic models. Upper: model estimation error of model C1; Lower: model estimation error of model C2. 174

LIST OF TABLES

Table Page

2.1 Parameter for generation of the ppc with SfM implemented in Agisoft.....21

2.2 Taper equations used for modeling diameter outside bark.....26

2.3 Variation along the stem of diameter measurement error from ppc. Diameter is the diameter measured in the field.....33

2.4 Performance of existing taper models on field and ppc-based measurements. Max –Burkhart Model 4 was used for assessment.....36

2.5 Taper models developed from ground-based measurements.....38

2.6 Taper models developed from the bias corrected ppc-based measurements.....39

2.7 Validation of the ppc – based models with ground measured data.....42

3.1 Summary of methods that are used for stem volume estimates.....66

3.2 Fitted coefficients of the Kozak 04 equation with AR(1) structure for point clouds measured inside bark diameter. The standard errors is abbreviated SE. Coefficients b4 and b6 are associated with random effects. The given estimates of b4 and b6 are the mean estimates of individual trees.....70

3.3 Evaluation of the three point-cloud-based equations using the leave-one-out validation. 71

3.4 Summary of volume estimation (i.e., mean and standard deviation) and relative difference to the FIA-PNW volume estimates.....73

3.5 GLM of volumes estimates as response variable of computation methods and dbh class.....75

3.6 Simulation results of volume estimates. 77

LIST OF TABLES (Continued)

Table Page

4.1 Summary of involved crown attributes. 95

4.2 Summary of number of branches by height section. 103

4.3 Semi-automatic (Cyclone) and automatic (TreeQSM) tree attribute estimates. 112

4.4 Summary of mean branch diameter estimates by height section. 117

4.5 Difference in branch diameter estimates between Cyclone and TreeQSM as a function of height section, within a repeated measurements framework. 117

4.6 Summary of branch length estimates by height section. 119

4.7 Summary of branch angle estimates by height section. 120

5.1 Summary of involved variables branch profile modeling. 145

5.2 Definitions of competition indices. 149

5.3 Selected model forms for developing branch models 153

5.4 System modeling model forms 157

5.5 Fitted coefficients of individual branch attributes models. 161

5.6 Evaluation of individual branch models. 161

5.7 Fitted coefficients of crown shape models. C1 and C2 systematic crown model sets developed with nonlinear seemly unrelated regression (NSUR). C1 is model set developed based on maximum branch length. C2 is model set developed based on maximum branch diameter. 171

5.8 Evaluation of individual models within each systematic model set. 172

LIST OF TABLES (Continued)

Table Page

5.9 Correlation between residuals of individual models in each systematic model set. 172

LIST OF APPENDICES

Appendix Page

A. Photogrammetric trees 201

B. Proof of the linear bias reduction for PPC-based tree stem diameter estimates . 208

C. Doulgas-fir double bark thickness equation 211

Chapter 1 Introduction

1.1. Importance of conifer architecture

In North America, conifer trees are a major crop that has been intensively managed for their high commercial value. At the same time, as home to enormous amounts of wildlife and serving as large carbon sinks, North American temperate coniferous forests have become a critical research hotspot for numerous scientific studies. To help integrate and balance ecological and economic objectives, one important research topic is to investigate the crown architecture of the conifer species, which is crucial in designing long-term forest management strategies (Franklin et al., 2002).

Quantitative information on trees and numeric models describing individual tree structure such as stem and crown profiles are essential components of comprehensive forest growth and yield prediction systems (Harold E Burkhart and Tomé, 2012). In the context of the present research, structure is defined as the attributes describing the tree dimensional variables and the relationship among them, which is an application of the general systems theory developed by von Bertalanffy to forest. Acquisition of accurate estimates of forest volume and biomass is the primary goal of forest inventory (Kangas and Maltamo, 2006). Due to the difficulty of direct volume and biomass estimation in the field, tree structural variables, including diameter at breast height (DBH), total height (THT), stem taper, and crown radius are used as indirect inputs in empirical allometric models for stem volume and biomass estimation. Furthermore, numerical descriptions of tree structure guide silvicultural practices seeking to achieve desired tree forms. Tree branch geometry and size are important indicators of timber quality (Maguire et al., 1999; Osborne and Maguire, 2015). Small limbs are preferred on crop

trees, as large limbs form large internal knots that discontinue the wood fiber and reduce the strength and value of the lumber products. Tree spacing aims at optimal stem biomass allocation while reducing the crown volume. A system of equations or databases documenting branch size, growth, and geometry assists in designing silvicultural treatments to maximize timber yield.

Knowledge of forest canopy architecture is also needed to better understand forest productivity (Bohn and Huth, 2017), forest fire resilience (Stephens et al., 2015), variability of forest microclimate (Aussenac, 2000; Chen and Franklin, 1997), and forest biodiversity and habitat connectivity (Franklin et al., 2002; Michel and Winter, 2009; Van Pelt and Nadkarni, 2004). Clement and Shaw (1999) found the abundance of large limbs on old-growth Douglas-fir trees promotes the mass of epiphytes, which determines the microclimate condition forest substrates expose to. Michel and Winter (2009) observed a positive relationship between tree size and the numbers of microhabitat groups within individual Douglas-fir trees. They found that only a few large trees (DBH > 80 cm) provide the majority of bark-related microhabitats, which suggests a possible increase in tree structural complexity through management that enhances the trees' ability to host diverse organisms.

Acquiring accurate structural information is fundamental for successful structural studies. Among all the structural variables, DBH is the most commonly used variable in describing tree volume, biomass, height, and branch variables. Although DBH alone could adequately explain basic mass metrics, such as total biomass and volume, other dimensional metrics are also important for describing tree structure. Updated tree

structure for plantation and natural regime trees improve the understanding of tree structural allocation and can be easily linked to other biological processes.

Traditional field measurement methods are limited in their ability to acquire fast and accurate structural estimates in locations that are difficult to access, such as dense forests and very high canopy. Traditionally, the upper stem diameters are destructively measured from fallen trees. Tree falling requires tremendous efforts, time, and resources, and the representativeness of sampled stem diameters are limited by the randomness and the size of the measured samples (Harold E Burkhart and Tomé, 2012). Even more, tree falling causes a considerable loss of branch information. Branch measurements on standing trees are usually performed by formally trained tree climbers, which is inexistent operationally only in research.

1.2. Application of point clouds in tree structural studies

The light detection and ranging (lidar) allows for measurement of forest structure even in dense forests, as laser beams can penetrate dense canopy and allows estimation of canopy metrics in substantially less time than conventional fieldwork methods. In the last decades, the application of lidar data acquisition has been gradually incorporated into forest inventory techniques (Johnson et al., 2014). Information provided by lidar scans is represented as points with coordinate and intensity attributes. Airborne lidar has been widely used to estimate stand- or plot-level forest structural variables, which are eventually used to predict tree aboveground biomass (Chen et al., 2012; Lim and Treitz, 2004, 2004; Sheridan et al., 2015), species diversity (Clawges et al., 2008; Hernández-Stefanoni et al., 2014; Simonson et al., 2012), and photosynthetic activities

(Chen et al., 2008; Hilker et al., 2010a; Thomas et al., 2006). However, as airborne lidar is operated from aircraft flying above the canopy, it tends to perform poorly in acquiring detailed structural information inside the crown and in the lower canopy.

By contrast, terrestrial lidar can supply precise structural information inside the canopy, as the estimates have at most several centimeters error. Point clouds from terrestrial sensors depict detailed dimensional attributes of stems, branches, and leaves. Having a simpler structure relative to tree branches, conifer stems can be relatively easily modeled using lidar point clouds. To estimate tree stem diameter, the cross-section of the stem is commonly approximated with two geometries: circle and a convex hull developed from point clouds. The former is a fitted circular shape by minimizing a predefined loss function, whereas the latter is the smallest convex envelope that encompasses all the selected points. The reported error of DBH estimates from terrestrial lidar ranges from 1 cm to 3 cm (Henning and Radtke, 2006; Hopkinson et al., 2004; Huang et al., 2011; Liang et al., 2014b; Watt and Donoghue, 2005). Despite the advantages of lidar, the expensive cost of the sensors, as well as demanding operational and data processing skill level needed from forest practitioners, are factors limiting terrestrial lidar to forest research. Point clouds developed from images have recently become increasingly popular, as an affordable alternative to lidar point clouds. Structure from motion (SfM) is a technique that ties together a series of 2D photographs to convert them to 3D point clouds (Ullman, 1979). SfM extracts key feature points that define edges of objects in individual images, then aligns these feature points across multiple images, thereby mimicking the visual depth of the human eye. After images

are aligned, tie points outlining the 3D structures are retrieved and represented as relative 3D coordinates. Dense point

clouds are created starting from the surface of the modeled 3D structures. Due to the underlining mechanisms of SfM, it is most effective in scenes with well-defined details, where distinct edges distinguish objects from their surroundings. Therefore, SfM usually is successful in developing 3D models for individual tree stems located in sparse forest understory. In fact, many studies have shown similar stem diameter and volume estimates derived from photogrammetry-based point clouds (PPC) to ground measurements or lidar point clouds (Mikita et al., 2016; Miller et al., 2015; Wallace et al., 2016). However, exceeding complexity of branches and dense canopy usually decreases the success of 3D model construction with SfM.

Compared with stem models, branch models are more difficult to reconstruct from point clouds due to their relatively small size, interlocking effects among branches, and noise from evergreen foliage. Aggregating branch point clouds with convex hulls or voxels provides rough estimates of entire crown volumes and surface areas (Kato et al., 2009; Li and Liu, 2019; Stovall et al., 2017). In the process of creating a convex hull, only the points at the crown surface are actually used to define the crown shape. Voxel, in comparison, more precisely approximate crown shape by dividing the point clouds into small cubic units. Different sizes of voxels result in different levels of precision of the structural estimates (Grau et al., 2017; Hauglin et al., 2013). However, both convex hull and voxel methods neglect the topological relationship between points inside the unit. Côté et al (2009) developed an algorithm to extract tree skeleton from

terrestrial lidar point clouds by tracing the central line of defined node sets of points. Unfortunately, their study did not yield readily measurable branch models, and the final algorithm is not available as an open-source product.

Quantitative structural modeling (QSM) is a solution to utilize the topological relations between points to develop tree structural models. Starting from the bottom of the stem, QSM segments point clouds into subsections of varying lengths until the bifurcation of branches happens. Then, it repeats the same procedure recursively for all suborder branches. The segments of branch and stem point clouds are locally approximated with cylindrical models of varying sizes. Eventually, branch and stem structural and locational attributes can be estimated from these cylindrical models. Various QSM methods and corresponding algorithm products were provided in the last quinquennial (Delagrange et al., 2014; Hackenberg et al., 2015a; Raumonen et al., 2013b; Zhang et al., 2014). Among the QSM products, TreeQSM, developed by Raumonen et al. (2013b) is the most successful, as it was applied to many tree structural studies, some aiming at the structure of broadleaf species (Lau et al., 2019, 2018; Malhi et al., 2018), some at the tree volume (Calders et al., 2015; Tanago et al., 2018).

Attributed to the dissimilar crown structures between broadleaf and coniferous species, as well as the seasonality of their foliage growth, the challenges of TreeQSM's application on coniferous species are twofold. First, when using TreeQSM it is assumed that point clouds were collected during the leaf-off season. Filtering leaf points is an extra step required by TreeQSM to enable accurate 3D model reconstruction for conifer species (Brede et al., 2019a). Second, although TreeQSM is not designed to be

dependent on species, the relatively smaller branch diameters of coniferous species can impact the accuracy of reconstructed models. Lau et al. (2018) found that TreeQSM accurately estimated approximately 45% of the branches with a diameter at insertion point between 10 – 20 cm. For young to mature conifer trees, most of the branches are less than 10 cm. Thus, the reliability of accurately using TreeQSM on conifer trees is still in question.

Despite the uncertainties associated with automatic branch model reconstruction, the branch attributes estimated with QSM techniques are still encountered in crown studies. For one, it supplies fast crown attribute estimates as a complement to field measurements. It also helps drive crown studies from model-driven to data-driven, the latter of which provides a more inclusive view of crown structure and free the crown studies from rigid and cumbersome model systems.

1.3. Objectives of this study

With the goal of improving scientific understanding of conifer crown structure while also advancing point cloud research in contemporary tree structural studies, the present thesis aims to: 1) test the utilization of point clouds derived from both photogrammetry and lidar in estimating tree structural variables; and 2) develop conifer tree stem and crown models using estimates acquired from point clouds. The substance of the thesis is contained in four chapters whose major goals are:

Chapter 2: assess the accuracy of diameter measurements executed from the photogrammetric point clouds (PPC) obtained with SfM technique for loblolly pine

trees located at a plantation in central Louisiana, and developing stem taper equations using corresponding estimates from PPC;

Chapter 3: compare stem volume estimates using terrestrial lidar point clouds with volume estimates from existing equations and assess the effects of sample segment lengths on lidar-based volume estimates;

Chapter 4: test the performance of TreeQSM in estimating branch structural variables for mature Douglas-fir trees and develop conceptual tree crown models using estimates from terrestrial lidar for Douglas-fir trees;

Chapter 5: develop nonlinear models for mature Douglas-fir branch attributes using estimates from lidar point clouds by incorporating competition effects from neighboring trees in the branch models and develop systematic crown model sets.

Reference

Aussenac, G., 2000. Interactions between forest stands and microclimate: Ecophysiological aspects and consequences for silviculture. Ann. For. Sci. 57, 287–301. https://doi.org/10.1051/forest:2000119

Bohn, F.J., Huth, A., n.d. The importance of forest structure to biodiversity–productivity relationships. Royal Society Open Science 4, 160521. https://doi.org/10.1098/rsos.160521

Brede, B., Calders, K., Lau, A., Raumonen, P., Bartholomeus, H.M., Herold, M., Kooistra, L., 2019. Non-destructive tree volume estimation through quantitative structure modelling: Comparing UAV laser scanning with terrestrial LIDAR. Remote Sensing of Environment 233, 111355. https://doi.org/10.1016/j.rse.2019.111355

Burkhart, H.E., Tomé, M., 2012. Modeling forest trees and stands. Springer Science & Business Media.

Calders, K., Newnham, G., Burt, A., Murphy, S., Raumonen, P., Herold, M., Culvenor, D., Avitabile, V., Disney, M., Armston, J., Kaasalainen, M., 2015. Nondestructive estimates of above-ground biomass using terrestrial laser scanning. Methods in Ecology and Evolution 6, 198–208. https://doi.org/10.1111/2041-210X.12301

Chen, J., Franklin, J., 1997. Growing-season microclimate variability within an old-growth Douglas-fir forest. Climate Research 8, 21–34. https://doi.org/10.3354/cr008021

Chen, Q., Baldocchi, D., Gong, P., Dawson, T., 2008. Modeling radiation and photosynthesis of a heterogeneous savanna woodland landscape with a hierarchy of model complexities. Agricultural and Forest Meteorology 148, 1005–1020. https://doi.org/10.1016/j.agrformet.2008.01.020

Chen, Q., Laurin, G.V., Battles, J.J., Saah, D., 2012. Integration of airborne lidar and vegetation types derived from aerial photography for mapping aboveground live biomass. Remote Sensing of Environment 121, 108–117.

Clawges, R., Vierling, K., Vierling, L., Rowell, E., 2008. The use of airborne lidar to assess avian species diversity, density, and occurrence in a pine/aspen forest. Remote Sensing of Environment, Earth Observations for Terrestrial Biodiversity and Ecosystems Special Issue 112, 2064–2073. https://doi.org/10.1016/j.rse.2007.08.023

Clement, J.P., Shaw, D.C., 1999. Crown structure and the distribution of epiphyte functional group biomass in old-growth Pseudotsuga menziesii trees. Ecoscience 6, 243–254.

Côté, J.-F., Widlowski, J.-L., Fournier, R.A., Verstraete, M.M., 2009. The structural and radiative consistency of three-dimensional tree reconstructions from

terrestrial lidar. Remote Sensing of Environment 113, 1067–1081. https://doi.org/10.1016/j.rse.2009.01.017
Delagrange, S., Jauvin, C., Rochon, P., 2014. PypeTree: a tool for reconstructing tree perennial tissues from point clouds. Sensors 14, 4271–4289.
Franklin, J.F., Spies, T.A., Van Pelt, R., Carey, A.B., Thornburgh, D.A., Berg, D.R., Lindenmayer, D.B., Harmon, M.E., Keeton, W.S., Shaw, D.C., 2002. Disturbances and structural development of natural forest ecosystems with silvicultural implications, using Douglas-fir forests as an example. Forest Ecology and Management 155, 399–423.
Grau, E., Durrieu, S., Fournier, R., Gastellu-Etchegorry, J.-P., Yin, T., 2017. Estimation of 3D vegetation density with Terrestrial Laser Scanning data using voxels. A sensitivity analysis of influencing parameters. Remote Sensing of Environment 191, 373–388. https://doi.org/10.1016/j.rse.2017.01.032
Hackenberg, J., Spiecker, H., Calders, K., Disney, M., Raumonen, P., 2015. SimpleTree—an efficient open source tool to build tree models from TLS clouds. Forests 6, 4245–4294.
Hauglin, M., Astrup, R., Gobakken, T., Næsset, E., 2013. Estimating single-tree branch biomass of Norway spruce with terrestrial laser scanning using voxel-based and crown dimension features. Scandinavian Journal of Forest Research 28, 456–469. https://doi.org/10.1080/02827581.2013.777772
Henning, J.G., Radtke, P.J., 2006. Detailed stem measurements of standing trees from ground-based scanning lidar. Forest Science 52, 67–80.
Hernández-Stefanoni, J.L., Dupuy, J.M., Johnson, K.D., Birdsey, R., Tun-Dzul, F., Peduzzi, A., Caamal-Sosa, J.P., Sánchez-Santos, G., López-Merlín, D., 2014. Improving Species Diversity and Biomass Estimates of Tropical Dry Forests Using Airborne LiDAR. Remote Sensing 6, 4741–4763. https://doi.org/10.3390/rs6064741
Hilker, T., Hall, F.G., Coops, N.C., Lyapustin, A., Wang, Y., Nesic, Z., Grant, N., Black, T.A., Wulder, M.A., Kljun, N., Hopkinson, C., Chasmer, L., 2010. Remote sensing of photosynthetic light-use efficiency across two forested biomes: Spatial scaling. Remote Sensing of Environment 114, 2863–2874. https://doi.org/10.1016/j.rse.2010.07.004
Hopkinson, C., Chasmer, L., Young-Pow, C., Treitz, P., 2004. Assessing forest metrics with a ground-based scanning lidar. Canadian Journal of Forest Research 34, 573–583.
Huang, H., Li, Z., Gong, P., Cheng, X., Clinton, N., Cao, C., Ni, W., Wang, L., 2011. Automated Methods for Measuring DBH and Tree Heights with a Commercial Scanning Lidar [WWW Document]. https://doi.org/info:doi/10.14358/PERS.77.3.219
Johnson, K.D., Birdsey, R., Finley, A.O., Swantaran, A., Dubayah, R., Wayson, C., Riemann, R., 2014. Integrating forest inventory and analysis data into a LIDAR-based carbon monitoring system. Carbon balance and management 9, 3.

Kangas, A., Maltamo, M., 2006. Forest Inventory: Methodology and Applications. Springer Science & Business Media.
Kato, A., Moskal, L.M., Schiess, P., Swanson, M.E., Calhoun, D., Stuetzle, W., 2009. Capturing tree crown formation through implicit surface reconstruction using airborne lidar data. Remote Sensing of Environment 113, 1148–1162. https://doi.org/10.1016/j.rse.2009.02.010
Lau, A., Bentley, L.P., Martius, C., Shenkin, A., Bartholomeus, H., Raumonen, P., Malhi, Y., Jackson, T., Herold, M., 2018. Quantifying branch architecture of tropical trees using terrestrial LiDAR and 3D modelling. Trees 32, 1219–1231. https://doi.org/10.1007/s00468-018-1704-1
Lau, A., Martius, C., Bartholomeus, H., Shenkin, A., Jackson, T., Malhi, Y., Herold, M., Bentley, L.P., 2019. Estimating architecture-based metabolic scaling exponents of tropical trees using terrestrial LiDAR and 3D modelling. Forest Ecology and Management 439, 132–145. https://doi.org/10.1016/j.foreco.2019.02.019
Li, L., Liu, C., 2019. A new approach for estimating living vegetation volume based on terrestrial point cloud data. PLoS ONE 14, e0221734. https://doi.org/10.1371/journal.pone.0221734
Liang, X., Kankare, V., Yu, X., Hyyppa, J., Holopainen, M., 2014. Automated stem curve measurement using terrestrial laser scanning. IEEE Transactions on Geoscience and Remote Sensing 52, 1739–1748.
Lim, K.S., Treitz, P.M., 2004. Estimation of above ground forest biomass from airborne discrete return laser scanner data using canopy-based quantile estimators. Scandinavian Journal of Forest Research 19, 558–570. https://doi.org/10.1080/02827580410019490
Maguire, D.A., Johnston, S.R., Cahill, J., 1999. Predicting branch diameters on second-growth Douglas-fir from tree-level descriptors. Canadian Journal of Forest Research 29, 1829–1840.
Malhi, Y., Jackson, T., Patrick Bentley, L., Lau, A., Shenkin, A., Herold, M., Calders, K., Bartholomeus, H., Disney, M.I., 2018. New perspectives on the ecology of tree structure and tree communities through terrestrial laser scanning. Interface Focus 8, 20170052.
Michel, A.K., Winter, S., 2009. Tree microhabitat structures as indicators of biodiversity in Douglas-fir forests of different stand ages and management histories in the Pacific Northwest, U.S.A. Forest Ecology and Management 257, 1453–1464. https://doi.org/10.1016/j.foreco.2008.11.027
Mikita, T., Janata, P., Surový, P., 2016. Forest stand inventory based on combined aerial and terrestrial close-range photogrammetry. Forests 7, 165.
Miller, J., Morgenroth, J., Gomez, C., 2015. 3D modelling of individual trees using a handheld camera: Accuracy of height, diameter and volume estimates. Urban Forestry & Urban Greening 14, 932–940. https://doi.org/10.1016/j.ufug.2015.09.001
Osborne, N.L., Maguire, D.A., 2015. Modeling knot geometry from branch angles in Douglas-fir (Pseudotsuga menziesii). Canadian Journal of Forest Research 46, 215–224.

Raumonen, P., Kaasalainen, M., Åkerblom, M., Kaasalainen, S., Kaartinen, H., Vastaranta, M., Holopainen, M., Disney, M., Lewis, P., 2013. Fast Automatic Precision Tree Models from Terrestrial Laser Scanner Data. Remote Sensing 5, 491–520. https://doi.org/10.3390/rs5020491

Sheridan, R.D., Popescu, S.C., Gatziolis, D., Morgan, C.L.S., Ku, N.-W., 2015. Modeling Forest Aboveground Biomass and Volume Using Airborne LiDAR Metrics and Forest Inventory and Analysis Data in the Pacific Northwest. Remote Sensing 7, 229–255. https://doi.org/10.3390/rs70100229

Simonson, W.D., Allen, H.D., Coomes, D.A., 2012. Use of an Airborne Lidar System to Model Plant Species Composition and Diversity of Mediterranean Oak Forests. Conservation Biology 26, 840–850. https://doi.org/10.1111/j.1523-1739.2012.01869.x

Stephens, S.L., Lydersen, J.M., Collins, B.M., Fry, D.L., Meyer, M.D., 2015. Historical and current landscape-scale ponderosa pine and mixed conifer forest structure in the Southern Sierra Nevada. Ecosphere 6, art79. https://doi.org/10.1890/ES14-00379.1

Stovall, A.E.L., Vorster, A.G., Anderson, R.S., Evangelista, P.H., Shugart, H.H., 2017. Non-destructive aboveground biomass estimation of coniferous trees using terrestrial LiDAR. Remote Sensing of Environment 200, 31–42. https://doi.org/10.1016/j.rse.2017.08.013

Tanago, J.G. de, Lau, A., Bartholomeus, H., Herold, M., Avitabile, V., Raumonen, P., Martius, C., Goodman, R.C., Disney, M., Manuri, S., Burt, A., Calders, K., 2018. Estimation of above-ground biomass of large tropical trees with terrestrial LiDAR. Methods in Ecology and Evolution 9, 223–234. https://doi.org/10.1111/2041-210X.12904

Thomas, V., Finch, D.A., McCaughey, J.H., Noland, T., Rich, L., Treitz, P., 2006. Spatial modelling of the fraction of photosynthetically active radiation absorbed by a boreal mixedwood forest using a lidar–hyperspectral approach. Agricultural and Forest Meteorology, The Fluxnet-Canada Research Network: Influence of Climate and Disturbance on Carbon Cycling in Forests and Peatlands 140, 287–307. https://doi.org/10.1016/j.agrformet.2006.04.008

Ullman, S., 1979. The interpretation of structure from motion. Proceedings of the Royal Society of London. Series B. Biological Sciences 203, 405–426.

Van Pelt, R., Nadkarni, N.M., 2004. Development of canopy structure in Pseudotsuga menziesii forests in the southern Washington Cascades. Forest Science 50, 326–341.

Wallace, L., Lucieer, A., Malenovský, Z., Turner, D., Vopěnka, P., 2016. Assessment of forest structure using two UAV techniques: A comparison of airborne laser scanning and structure from motion (SfM) point clouds. Forests 7, 62.

Watt, P., Donoghue, D., 2005. Measuring forest structure with terrestrial laser scanning. International Journal of Remote Sensing 26, 1437–1446.

Zhang, X., Li, H., Dai, M., Ma, W., Quan, L., 2014. Data-Driven Synthetic Modeling of Trees. IEEE Trans. Visual. Comput. Graphics 20, 1214–1226. https://doi.org/10.1109/TVCG.2014.2316001

Chapter 2 Stem measurements and taper modeling using photogrammetric point clouds

Abstract

Estimation of tree biomass and products that can be obtained from stem focused forest research for more than two centuries. Traditionally, measurements of entire tree bole were expensive or inaccurate, even that sophisticated remote sensing techniques were used. I propose a fast and accurate procedure for measuring diameters along the merchantable portion of the stem at any given height. The procedure uses unreferenced photos captured with consumer grade camera. A photogrammetric point cloud (ppc) is produced from the acquired images using structure from motion, which is a computer vision range imaging technique. A set of 18 loblolly pines (Pinus taeda L.) from east Louisiana, USA, were photographed, subsequently cut, and diameter measured every meter. Same diameters were measured on the point cloud with AutoCAD Civil3D. Ground point cloud reconstruction provide useful information for at most 13 m along the stem. The ppc measurements are biased, overestimating real diameters with 17.2 mm, but with reduced standard deviation (8.2%). A linear equation with parameters the error at diameter at breast height (d1.3)bh and the error of photogrammetric rendering reduced bias to 1.4 mm. The usability of the ppc measurements in taper modeling was assessed with four models: Max and Burkhart [1], Baldwin and Feduccia [2], Lenhart et al. [3] and Kozak [4]. The evaluation reveled that data fit well all the models ($R2 \geq 0.97$), with Kozak and Baldwin & Feduccia performing the best. The results support replacement of taper with ppc, as faster, more accurate and precise product estimations are expected.

Keywords: structure from motion; merchantable stem; bias; accuracy; precision

2.1. Introduction

Forest inventory is focused on estimation of existing resources with techniques that are simultaneously fast, accurate, precise, and cost effective [5-7]. Ground estimates are enhanced by remote sensing techniques, particularly lidar, which provide a wealth of data at reduced costs [8,9]. However, looking at the forest from above limits access to valuable information in respect to product identification from individual trees. Regardless the sensor (i.e., active or passive), nadir view fails to capture relevant information about the stem. Therefore, either ground inventory focused on stem product is executed or taper models are used to predict the products that can be obtained from each stem. In practical applications, stem is described from ground measurements with two procedures: one based on measuring diameter at various height with optical devices [10-13] and one based on point clouds, such as terrestrial laser scanning [14-17]. Both approaches are time-consuming and not necessarily unexpansive. Besides significant time needed to acquire the information, accuracy issues are present. Optical devices overestimate actual diameter with more than 1 mm on average, which could seem insignificant. However, the standard deviation is at least 10 times larger than mean [10], which suggests that quality of the measurements depends on the operator as much as on the method or device. Overestimation of diameter also occurs when lidar serves as input, depending on the approach, by as much as 25 mm [17]. Compared with ground measurements, taper models require a significant development effort, but once completed the only information needed to estimate products allocation along stem is diameter at breast height ($d_{1.3}$) and total height [18]. However, mixed results were

obtained when taper is used in products identification and estimation, some arguing for [19] some against [20,21].

An alternative to time - consuming (i.e., ground measurements) or expensive point clouds (i.e., terrestrial lidar) is reconstruction of reality with computer vision techniques. The main product of computer vision procedures is a point cloud built from 2D images [22,23]. The distinction between the computer vision based point clouds and the clouds produced from stereo images is the reduced importance, up to elimination, of the stereometric information in the former. Creation of point clouds with stereopsis is possible, but is slow, difficult to implement in the field, and requires a significant post-processing. Image processing is implemented in many instances with expensive software, such as ENVI [24] or IMAGINE Photogrammetry (former Leica Photogrammetry Suite) [25]. The need for performant software is rooted on the stereopsis (i.e., operates with one pair of images at a time), which supplies only a partial view of the trees. To render the entire tree multiple image acquisition positions are needed, each location producing point clouds that have to be merged subsequently. Therefore, stereometric techniques focused on 3D rendering are not considered operationally feasible for activities occurring under forest canopy. The lack of stereometry labeled the computer vision derived points as photogrammetric [26,27]. Representation of reality with 3D points is not new [28,29], but gained momentum in forestry when commercial applications become available, such as Agisoft [30], Pix4D [31] or VisualSFM [32]. A large number of papers using photogrammetric point clouds (henceforth ppc) describe forest from above, similarly with aerial lidar [33]. However, the presence of a passive sensor limits the ability of ppc to reach the ground; therefore,

they were used either in combination with other data (such as digital terrain models) or confined to upper canopy. Currently, researchers investigate the applicability of structure from motion (SfM) technique, a computer vision procedure, in reconstructing the lower portion of tree stem [34,35]. Success was noticed in estimation of d1.3, in many instances with precision superior to terrestrial lidar [34]. The encouraging SfM results recommended expansion from d1.3to diameter along the stem. Therefore, the objective of this research is assessment of the accuracy of diameter measurements executed from the ppc obtained with SfM technique. A secondary objective is comparison between the diameters measured from ppc and the diameters estimated from taper equations.

2.1. Methods

2.1.1. Field data collection

The accuracy and precision of diameter measurements executed on ppc was assessed using 18 loblolly pines (Pinus taeda Lindl.) from west central Louisiana (Figure 2.1 a,b). The trees were chosen to describe stands that are ready for a silvicultural prescription (Figure 2.1 c) (i.e., thinning or regeneration harvest), and mirror other studies focused on taper modeling [36-38]. The selected trees were positioned in the dominant and codominant crown classes (Figure 2.1 d), according to Nyland [39]. Trees located in the upper crown classes are the focus of active forest management, as they are not only the most valuable trees but also the ones that define the ecosystem dynamics [40]. The trees were scheduled for either the first thin (i.e., mechanical thinning) or for final cut (i.e., clearcut). The average d1.3 was on average 306.1 mm (variance 68.5), ranging from 213.0 mm to 449.6 mm. Total height (H) varied from

15.9 m to 26.8 m, with an average of 22.2 m and a variance of 12.8. The trees grew on productive sites, with site indices ≥ 60 at base age 25. Each tree was photographed with a Nikon D3200 (i.e., CMOS sensor of 23.2 mm × 15.4 mm) equipped with a Nikkor AF-S DX VR 18-55 mm zoom lens (aperture 3.5 – 5.6). To capture as much as possible from the tree the images were acquired at the focal length 18 mm. For calibration, each tree had the d1.3 painted circularly, and on opposite sides of d1.3 two metal rods of 304.8 mm (i.e., 1 foot) were freely hanged. Shortly after the images were captured, the trees were felled and diameter along the stem was measured every meter with a Spencer D-tape starting from d1.3, which was marked at 1.3 m. The accuracy of measurements was 1 mm for diameters and 10 mm for lengths along the stem (i.e., height). To verify total length after the tree was felt, total height was extracted from lidar data. The lidar flight scanning the area was executed in March 2012, at most four months before the trees were photographed and cut. To accommodate for the growth between flight time and field measurements I considered that trees could have increased their height with at most 1 m. The point density was on average 30 points / m2.

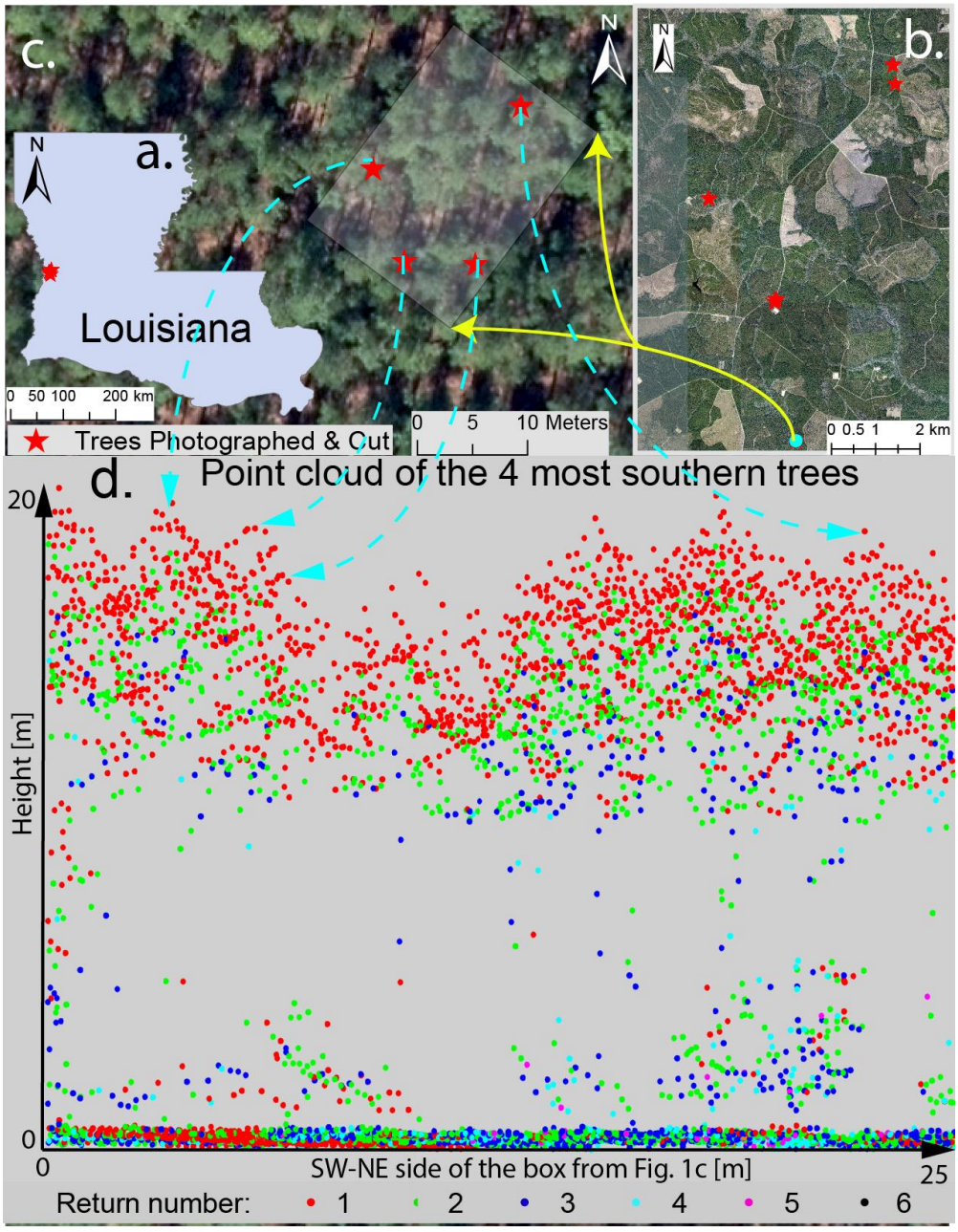

Figure 2.1 Study area showing the location of the trees. a. general position within Louisiana; b. locations of all the trees photographed and cut; c. the four most southern trees; d. lidar point cloud of the rectangle contain the southern four trees.

2.1.2. Photogrammetric point cloud generation and diameter measurements.

The ppc were generated using SfM implemented in Agisoft PhotoScan ver 1.2 [30]. Tree reconstruction and stem diameter measurements from ppc were executed in four steps (Figure 2.2 a, b, c and d): 1) photo alignment, 2) build the point cloud, 3) scale the point cloud, and 4) measure diameter along the stem. Three sample ppc trees were documented in Appendix A in detail. The crucial step of SfM is concerned with alignment of images, which if not completed properly will render an unusable ppc. Depending on computational power (i.e., microprocessor), the amount of detail existing inside the image (i.e., number of pixels), and time available for processing the alignment can be executed in few seconds or few hours. In Agisoft, there are four parameters determining the time and quality of photo alignment: accuracy of camera position, matching detected features across images, the number of key points (i.e., image specific feature points that can represent same entities in multiple images), and tie points (i.e., image specific points used for matching images). Accurate camera locations are obtained when original images are used unaltered, which in Agisoft is coded as “high” [41]. However, this option is time-consuming; therefore, lower accuracy can be used [42], such as medium, which downscale each side of the image by a factor of two. Liang et al. [42] obtained good results by low alignment of photos with resolution 5472 × 3648 pixels, which employed only 16th of the information recorded (i.e., 1368 × 912). In our study, the image resolution was 3872 × 2592 pixels, and I aligned the photos by downscaling the original images by half (i.e., 1936 × 1296). Thru experimentation the maximum number of key points was set to 100,000 and of tie-points at 60,000.

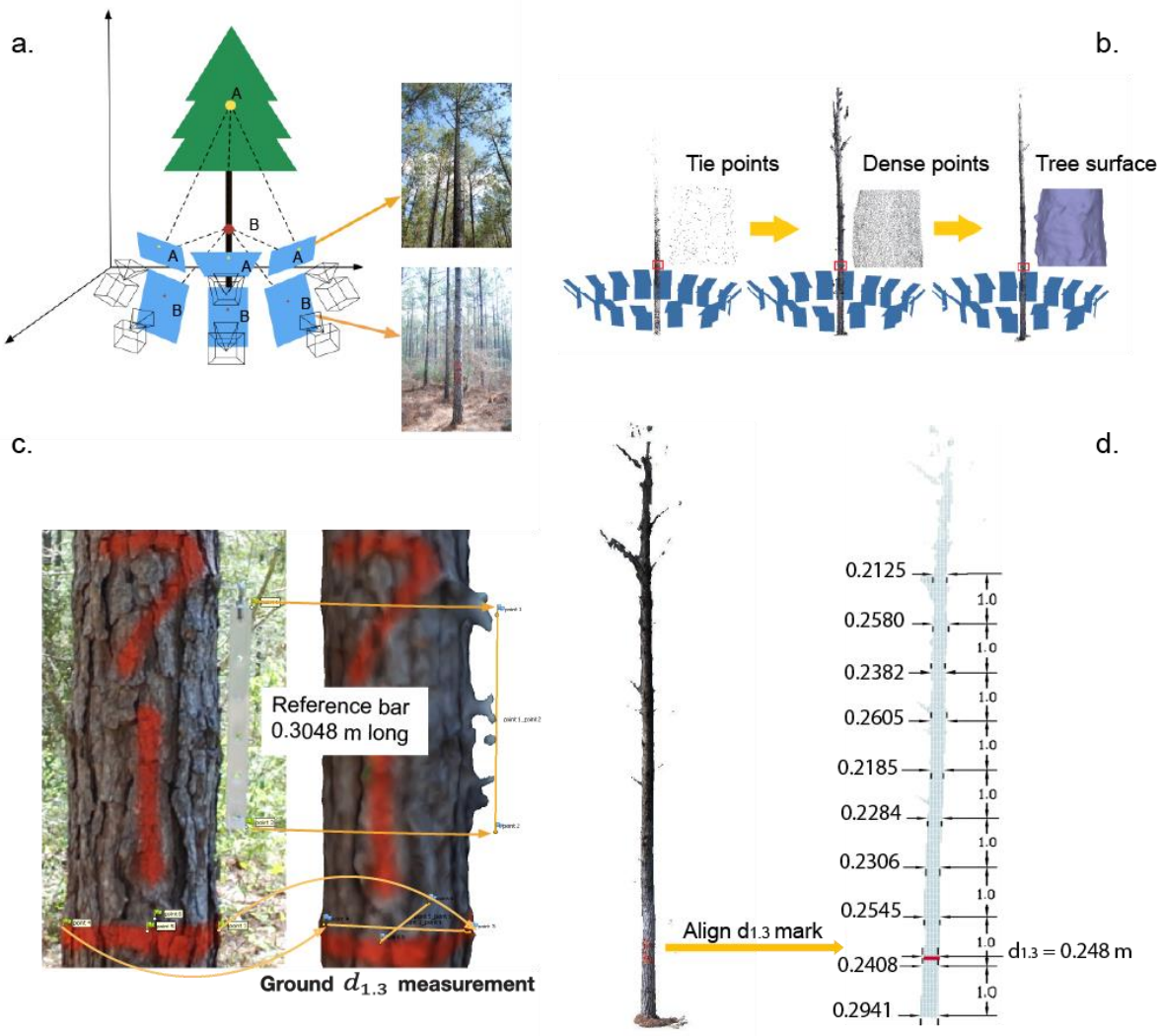

Figure 2.2 Workflow of the photogrammetric-based stem reconstruction and diameter measurement. a. field photographs for an individual tree; b. SfM process of reconstruction (tie points, densified points, surface); c. scaling the ppc with reference bar and d1.3; d. diameter measurements in AutoCAD.

Photos were captured around the trees in pairs to cover the lower and higher portions of the stem (Figure 2.2 a). Each pair overlapped ≥ 50%, to ensure sufficient common features for successful photo alignment. Georeference provides auxiliary information that helps camera positioning. However, by operating below canopy no reliable GPS coordinates were acquired; therefore, the photos were aligned by relying only on presence of same features on multiple images. At least 10,000 tie-points / image were used for photo alignment and camera positioning.

The second step occurs after photos alignment and consists in densification of the tie-points (Figure 2.2 b). For each tree, the final ppc was created by downscaling the images by a factor of 2, which produced enough points for precise measurements without sacrificing processing time. All trees were described with a ppc of at least 600,000 points (the maximum was approximately 2 millions), at least 25,000 points/ m2. To ensure precise measurements I reconstructed the surface of the trunk with at least 500,000 faces (Figure 2.2 b). The faces were built with a ratio of 1:5 to the number of points. Compared with previous studies of image-based forest inventories [34,35,42] the selected parameter for SfM in Agisoft (Table 2.1) were either similar or provided superior solutions.

Table 2.1 Parameter for generation of the ppc with SfM implemented in Agisoft

Photo alignment		Point cloud densification		Mesh building	
Accuracy	Medium & High	Quality	High	Face count	High
Key points	100,000	Depth filtering	Disabled	Interpolation	Disabled
Tie points	60,000				

Because the images were not georeferenced and no ground control points were present, the ppc is in relative not absolute units. Therefore, to measure diameters, the ppc and the associated surface had to be scaled. To minimize the errors, scaling was implemented using measurements executed on two perpendicular planes. On the horizontal plane, the ground measured d1.3 was assigned to the corresponding segment from the ppc. The scale on the vertical plane was carried out by allocating the known length of the metal bar (i.e., 304.8 mm) to the distance between the points delineating the bar inside ppc (Figure 2.2 c). Scaling is one of the three main sources of errors when ppc are used for actual measurements, as usually increases the magnitude of the investigated attributes with at least one order of magnitude (in our case three orders, from 1 to 1000). Current guidelines consider field measurements accurate if difference between actual and measured d1.3 is < 5% [43]. The average d1.3 measured in the field is 306 mm. Because the calibrating metal bar was 304.8 mm (i.e., close to the d1.3 of measured trees), I considered that a vertical error of 5% is also admissible, even that field measurements for heights accepts errors < 10% [43]. Therefore, the accepted total error for accurate field measurements is 21.6 mm (i.e., $0.05\sqrt{306_{average\ dbh}{}^2 + 304_{metal\ bar}{}^2}$). For consistency, a similar value could have been used for ppc accuracy, but I decided to tighten the requirements. Consequently, I considered that scaling will have a limited impact of measurements if total error (i.e., horizontal and vertical) is < 10 mm (less than half from the field accepted accuracy).

The last step consists in measuring the diameters every meter along the stem (Figure 2.2 d), which was executed in AutoCAD Civil 3D [44]. The second source of ppc

measurement errors is matching the ground diameters with ppc-estimated diameters. The matching can be implemented in two ways: 1) identify d1.3 as the middle of the colored band marking the d1.3 in the ppc, then measure all diameters starting from the identified d1.3 (i.e., 1.3 m), or 2) identify the ground in the ppc, then measure diameters in respect with the ground. Both ways offer a check, as either ground should be at height (length) 0 (i.e., former), or d1.3 should fall inside the colored band (i.e., later). Even that the difference between the d1.3 identified using the two ways should by minor, its propagation could have significant impact, particularly for the upper section of the stem. Therefore, diameters were measured in both ways. In AutoCAD the diameters were measured on a plane perpendicular to the axis of the tree. The surface generated from ppc, on which the measurements are executed, describes the tree by its outer shape. Therefore, values larger then ground measured values are expected. Measurements on the surface is the third source of errors, and probably the largest one. Because, the ppc – based diameters likely overestimate the actual diameters, biased estimates are likely.

2.1.3. Assessment of measurements and bias correction

The main statistics used to assess the accuracy of the ppc-based diameter measurements was the difference between the ground diameter measured at height h (i.e., diameter@h field) and its correspondent from AutoCAD (i.e., diameter@h ppc):

$$error_h = diameter@h_{field} - diameter@h_{ppc} \quad (2\text{-}1)$$

Error analysis is necessary not only because overestimates are expected from ppc-based measurements but also because estimates from SfM could be biased [45]. Bias is assessed with three statistics, similar to other studies [46-49]

$$Bias = \sum_{i=1}^{n}\left(\sum_{h=1}^{H_i} error_{i,h}/(H_i+1)\right)/n \quad 2\text{-}2$$

$$Mean\ Absolute\ Bias = MAB = \sum_{i=1}^{n}\left(\sum_{h=1}^{H_i} |error_{i,h}|/(H_i+1)\,|\right)/n \quad 2\text{-}3$$

$$RootMeanSquareError = RMSE = \sqrt{\sum_{i=1}^{n}\sum_{h=1}^{H_i} error^2{}_{i,h}/(H_i+1)\,|\,/n} \quad 2\text{-}4$$

where errori,h is the ppc-based error at height h for tree i that has total height Hi, and n is the number of trees.

If possible, bias would be corrected using a linear function, as it is more robust and parsimonious than nonlinear approaches [50,51]. For practicality, the proposed linear model should include variables easy to estimate accurately, either in the field (e.g., d1.3 or total height) or during processing (e.g., software scaling errors). Furthermore, considering that the images were recorded from the ground the upper sections of a tree will be described by fewer points than the lower sections, which will render the measurement process less accurate close to terminal bud. Therefore, I expect that bias will change with height. Consequently, I will be using the following linear model for bias correction (Eq. 2-5):

$$BC_h = b_0 + b_1 d_{1.3 basedvariable} + b_2 h_{basedvariable} + b_3 RH \times d_{1.3 basedvariable} + b_4 RH \times Scaling_{basedvariable} \quad 2\text{-}5$$

where BCh is bias correction at height h, RH is the relative height, RH=h/H, d1.3 based variable and scalingbased variable are linear variables derived from d1.3 and ppc scaling, and bi, i=0, .. 4, are coefficients to be estimated.

Preference will be given to a model that has coefficient bi 0 or 1, which are easy to implement. However, this simplistic approach will likely not remove the bias. Nevertheless, if bias is reduced to ≤ 1% while RMSE is larger, the simplification becomes operationally justified.

The common approach of testing bias significance is through the null hypothesis stating that the statistics measuring bias are not different than 0 [49]. Assuming normality and no outliers, paired t-test will be used for accepting or rejecting the null hypothesis. However, the t-test is relatively sensitive to outliers [50]; therefore, the existence of large errors will be investigated with Grubbs test [52]. Grubbs' test assumes normality, which will be assessed with the Kolmogorov-Smirnov test [53]. When one of the previous two assumptions is violated, the Wilcoxon signed-rank test will be used, which is robust to outliers and lack of normality [54]. All tests were executed in SAS 9.4 [55].

2.1.4. Taper modeling

Diameters provide a cross-sectional perspective of a tree, which is also supplied by taper equations. Therefore, it is natural to compare the values obtained from taper models with the ppc-based diameters. The comparison employed four taper models (Table 2.2), out of each three are widely used for loblolly pine: Max and Burkhart [1], Baldwin and Feduccia [2], Lenhart et al. [3], and Kozak [4]. Max-Burkhart (1976) model has been extensively used to develop compatible taper equations of loblolly pine in central Louisiana and East Texas [18,56-58]. Instead of describing the tree bole with a single equation, Max-Burkhart partitions the tree bole in two sections. The partitions approximate better the neiloid and paraboloid forms associated with the respective

sections of the stem. Comparatively, Kozak's model 2 (2004) integrates neiloid, paraboloid, and conic forms of the stem as a continuous function by using "changing exponents"[4]. Baldwin and Feduccia [2] and Lenhart et al. [3] models have a relatively simple model form, as only contain two coefficients. The four models were fit to the field and ppc based data with the package nls2 [59] from R version 3.2.4 [60].

Table 2.2 Taper equations used for modeling diameter outside bark

Model	Equation
Max-Burkhart Eq.4 in original paper	$d_h = d_{1.3} \times \left[b_1 (\frac{h_d}{H} - 1) + b_2 \left(\frac{{h_d}^2}{H^2} - 1 \right) + b_3 \left(u_1 - \frac{h_d}{H} \right)^2 I_1 + b_4 \left(u_2 - \frac{h_d}{H} \right)^2 I_2 \right]^{0.5}$ $where\ I_1 = \begin{cases} 1 if h_d/H \le a_1 \\ 0 if h_d/H > a_1 \end{cases}$ $I_2 = \begin{cases} 1 if h_d/H \le a_2 \\ 0 if h_d/H > a_2 \end{cases}$ $a_1 < a_2$
Baldwin- Feduccia Eq. 2 in original paper	$d_h = d_{1.3} \times \{ b_1 + b_2\, ln[1 - (1 - e^{-b_1/b_2}) \times (h_d/H)^{1/3}] \}$
Lenhart et al. Eq.26 in original paper	$d_{ht} = d_{1.3} \times \left(\frac{H - h_d}{H - 1.3} \right)^b$
Kozak Eq. 3 in original paper	$d = a_0 \times {d_{1.3}}^{a_1} X_i^q,$ $where\ X_i = [1 - (h_d/H)^{1/4} / (1 - 0.01^{1/4})]$ $q = b_0 + b_1 \times (1/e^{h_d/H}) + b_2 \times {d_{1.3}}^{X_i} + b_3 \times X_i^{d1.3/H}$

Similar fit statistics used for bias assessment were employed to evaluate the taper models: bias, mean absolute bias (MAB), and root mean square error (RMSE). For the taper models, the error present in the fit statistics is computed as the difference between the measured diameter, di,h, and the estimated dimeter, $\hat{d}_{i,h}$, at height h for tree i. Besides the previous three fit statistics I have included the coefficient of determination R2, to mirror other taper studies [61,62]. Because errors have different signs, bias is usually smaller than MAB and RMSE, which are always non-negative. MAB and RMSE are similar in the evaluation power [63], with the observation that RMSE is slightly higher than MAB, a direct result of the Cauchy-Bunyakovsky-Schwarz inequality [64].

$$R^2 = 1 - \frac{\sum_{i=1}^{n}\left(\sum_{h=1}^{H_i}(d_{i,h}-\hat{d}_{i,h})^2\right)}{\sum_{i=1}^{n}\left(\sum_{h=1}^{H_i}(d_{i,h}-\bar{d}_i)^2\right)} \qquad 2\text{-}6$$

where di,h is the ppc –based diameter of tree i at height ht, Hi is the total height of tree i, $\hat{d}_{i,h}$ is the diameter predicted from taper equations for tree i at height h, and $\bar{d}_i$is the average diameter of tree i. A 1 was added to the denominator of each statistics to account for the d1.3 measurement.

Same tests used for assessing the accuracy of ppc – measurements (i.e., paired t-test or signed Wilcoxon) were employed to evaluate performances of the taper models.

2.2. Results

2.2.1. Tree construction and diameter measurement

Ground based methods of measuring taper of standing trees with optical devices [10,13] or by climbing the tree with a Swedish ladder is accurate but requires at least 15

min/tree (this includes preparatory time and measurement time). For a timber inventory plot, commonly 500 m2 [65], on which 5-7 trees are measured, the total time to acquire the data is approximately two hours. The acquisition of images for SfM reconstruction is less than 2 min/tree, with a total time of at most 15 min/plot. The ppc processing time for one tree with the parameters from Table 2.1 on a Dell Precision workstation 7910 CPU E5-2630 v3 @ 2.40 GHz and 32 Gb RAM was on average 15 min (i.e., ranging from 11 min to 18 min). Therefore, the total processing time for one plot would have been approximately 2 hours, same with ground measurements. However, the advantages of using ppc over ground data is tremendous, as a snapshot of the trees is obtained that can be used for subsequent investigations, including audit. Furthermore, while the field measurement time remained almost unchanged for the last 50 years, the technological advances will most likely reduce the computation time. Therefore, the desired results will likely be obtained faster than ground measurements.

SfM successfully constructed the lower portion of the stem for all 18 trees (Figure 2.3). SfM was able to produce a usable reconstruction for only three trees above 13 m and seven for 12 m. Therefore, diameters were measured only on the part of the stem where the tree surface was continuous and has a shaped according to visual expectations.

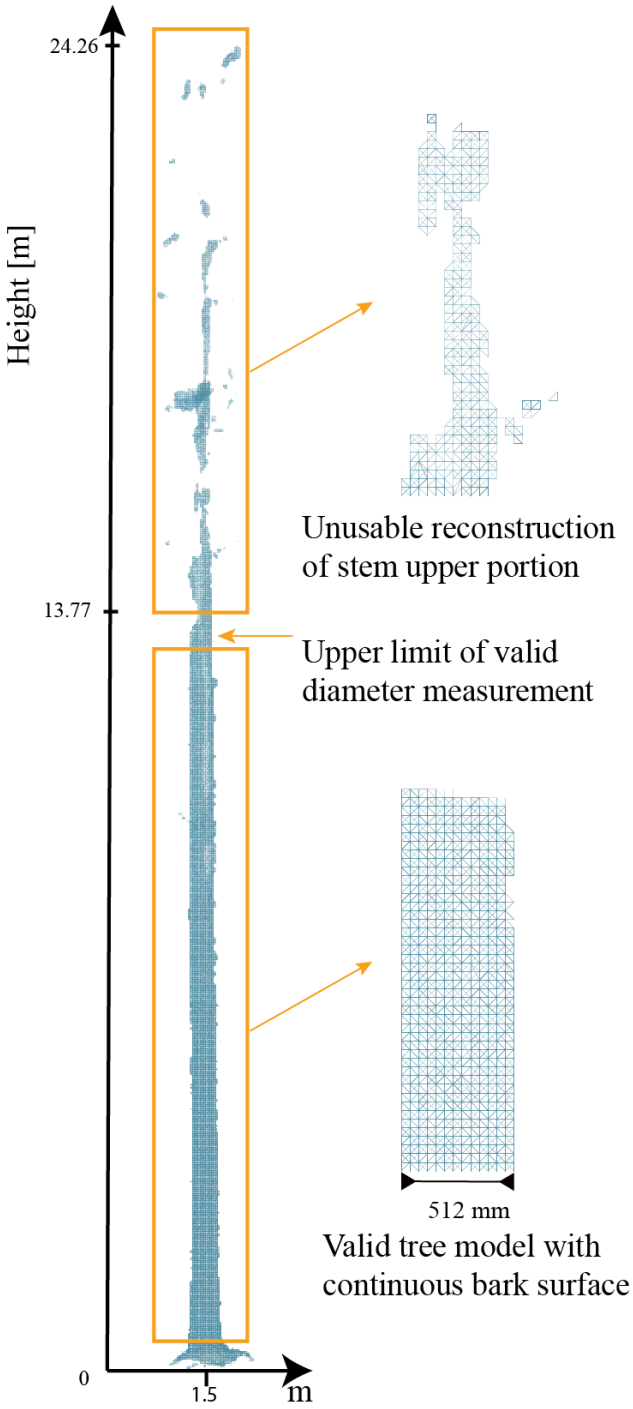

Figure 2.3 An example of a reconstructed stem, with the lower part continuous, (i.e, measurable surface), and the upper part fragmented (i.e., unsuitable for accurate measurements)

The side-view measured diameters were constantly larger than the circumference-based diameters (Figure 2.4 a), with a significant difference of 5.2 mm ($p = 0.007$ for the pair t-test). However, there were many heights for which the convex hull algorithm did not produce the expected polygon, as the PPC cross-section did not have the points evenly distributed along the circumference (Figure 2.4 b). To obtain valid results, an algorithm that compensates for a lack of points in some area of the cross-section of the stem should be executed before the implementation of the convex hull algorithm. However, such algorithms are not readily available, and the augmentation of PPC introduces errors, as a model is used. Therefore, to carry the subsequent analyses with all of the ground measured diameters, the side-view measured diameters were used. The decision to use the side-view diameter instead of the circumferential diameter was enforced by an overestimation of diameter with more than 10 mm by both approaches, which requires a subsequent bias correction anyway.

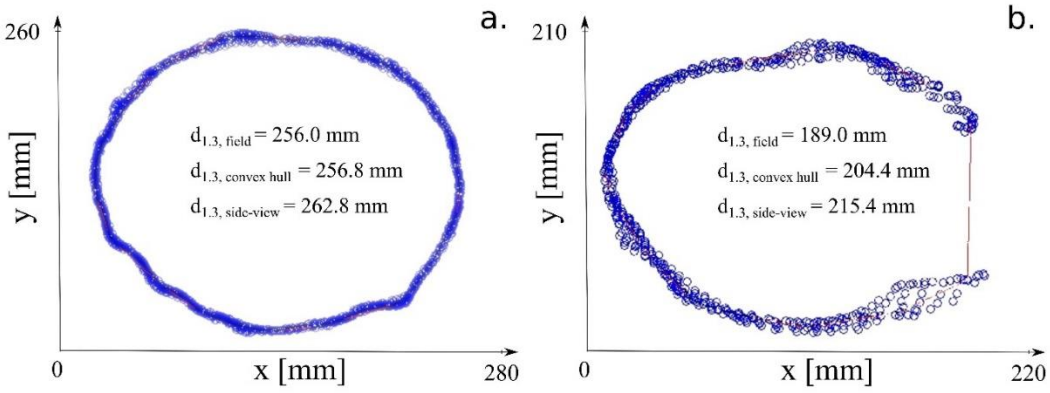

Figure 2.2 Diameter measurements on cross sections of the stem. a. successfully identified by the convex hull algorithm at height 4 m; b. unsuccessfully identified by convex hull algorithm at height 11 m. The red line is the circumference of the tree as

Irrespective height on the stem, the ppc measured mean diameter is constantly larger than the mean ground diameter (Figure 2.5), supporting the existence of bias. The variability of field and ppc measurements is similar along the stem, with standard deviation between 61.9 - 82.7 mm, and 40.0 ~ 88.4 mm, respectively (Figure 2.5). For heights < 9 m, the variance decreased along the stem for both ground and the ppc-based measurements, the largest occurring at 1.0 m for ppc (i.e., 782.9) and 1.3 m for field (i.e., 685.3). While diameter tapered with height, at 13 m I noticed the largest mean diameter (Figure 2.5) and the smallest variances for both ground and ppc-based measurements. This unnatural situation occurred because only three measurements were recorded at 13 m, and those were for largest trees (i.e., $d_{1.3}$ > 35 cm). Therefore, in further analyses only results for heights ≤ 12 m were considered.

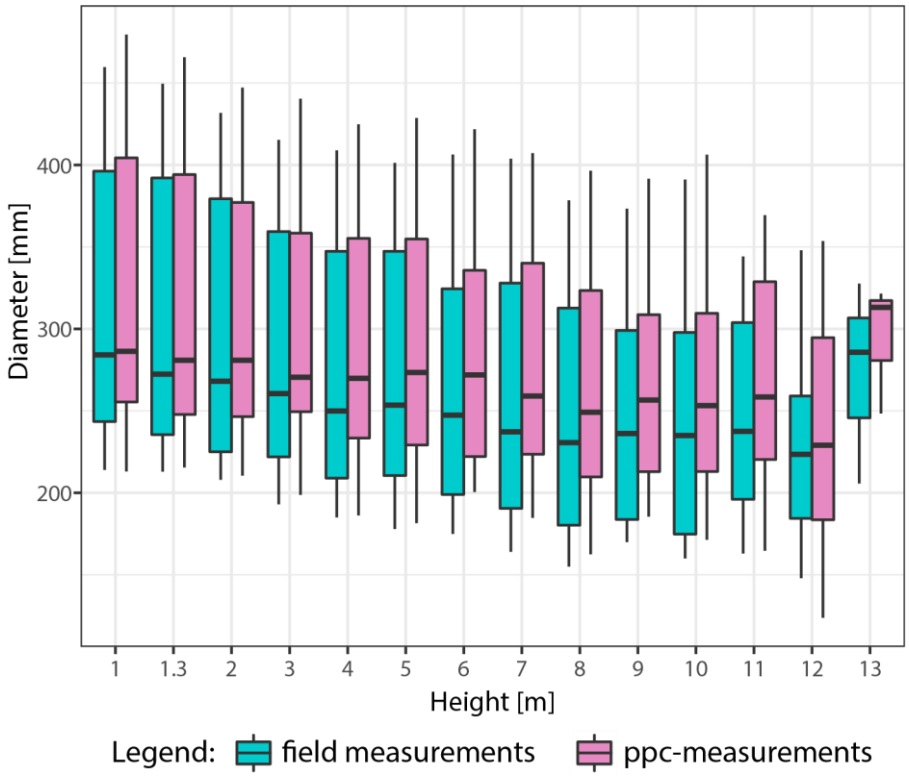

Figure 2.5 Variation with height of diameters measured in the field and from the ppc.

The overall mean error is -17.2 mm, which is 6.3% larger than the mean diameter (Table 2.3). The estimates from ppc are biased and not acceptable by the current field guides, which requires at least 5% accuracy. As expected MAB was larger than bias but not significantly (i.e., 7.2 % or 18.9 mm MAB). RMSE was the largest fit statistics employed for assessment, and was almost 30% greater than bias (i.e., 22.5 mm or 7.9%). The range of ppc – based measurements errors is fairly constant along the stem height (Figure 2.6). The smallest deviations of the ppc-based measurement occur close to the ground (i.e., ≤14 mm for heights ≤ 2.0 m). The largest deviation happens at 9 m, with the mean error = -23.7mm, almost 10% of the corresponding diameter.

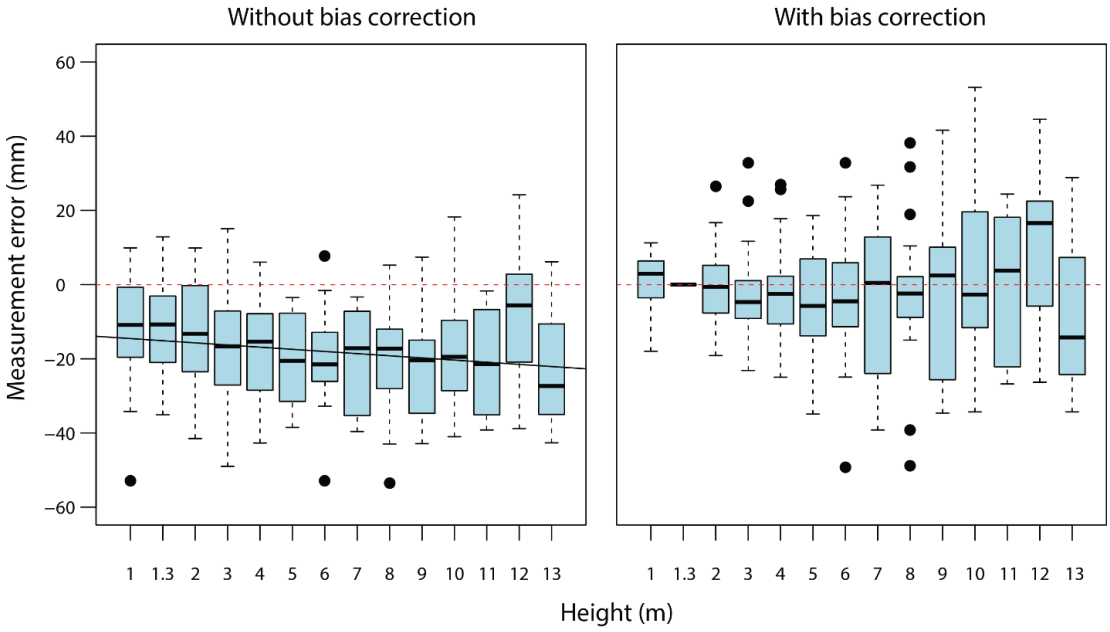

Figure 2.6 The ppc-based error vs. the stem height; a. uncorrected b. after bias correction with Eq. 2-7. The dots represent outliers, which are estimated using the interquartile range approach.

Table 2.3 Variation along the stem of diameter measurement error from ppc. Diameter is the diameter measured in the field.

Height	Diameter	Bias		Mean absolute error		RMSE	
[m]	[mm]	[mm]	[%]	[mm]	[%]	[mm]	[%]
1	312	-12.1	-3.9	14.8	4.8	19.4	6.2
1.3	306	-12.0	-3.9	13.5	4.4	17.1	5.6
2	296	-13.5	-4.6	16.1	5.4	20.4	6.9
3	287	-16.4	-5.7	19.2	6.7	22.5	7.8
4	278	-17.2	-6.2	18.2	6.6	22.4	8.0
5	270	-20.3	-7.5	20.3	6.5	23.3	8.6
6	263	-19.5	-7.4	20.3	7.7	23.3	8.9
7	256	-20.0	-7.8	20.0	7.8	23.8	9.3
8	247	-20.0	-8.1	20.5	8.3	24.2	9.8
9	244	-22.4	-9.2	23.8	9.8	26.7	11.0
10	242	-18.2	-7.5	20.9	8.6	22.9	9.4
11	249	-19.9	-8.0	19.9	8.0	24.1	9.7
12	229	-8.1	-3.5	18.1	7.9	22.1	9.6
Total	-	-17.2	-6.3	18.8	6.9	22.5	8.2

Kolmogorov – Smirnov test supports the normal distribution of the difference between ground and ppc-based diameters ($p>0.1$), except for 5 m and 6 m height ($p=0.02$ and 0.04, respectively). Grubbs' test revealed no outliers in the data ($p>0.05$), which justifies *t*-test for assessing bias significance at all heights, except 5 m and 6 m. The *t*-test provided strong evidence ($p<0.01$) that both bias and MAB are significantly different from 0, when applicable. For 5 m and 6 m, at which the *t* – test was not appropriate, Wilcoxon test confirms the presence of a significant bias.

To correct the bias the preferred form of the Eq. 2-5 has bi either 0 or 1. Coefficients different than 0 or 1 require field measurements, which in most instances not only that are not available but preclude the remote sensing approach advocated by the paper. Multiple trials revealed that bias can be reduced with a linear function derived from Eq. 2-4 (i.e., b1 and b4 are 1, rest are 0):

$$BC_h = error_{d1.3} + (scaling\ error) \times RH \qquad 2\text{-}7$$

where BC is the bias correction, $error_{d1.3}$ is the ppc-based measurement error at d1.3 (i.e., d1.3 field – d1.3 ppc), and scaling error is the horizontal calibration error estimated by Agisoft.

Being unfitted to data or distribution of errors, Eq. 2-7 will likely not eliminate the bias but will reduce it. However, since the only field measurements needed is d1.3, commonly recorded anyway, Eq. 2-7 delivered the intended results: measurements bias is operational and statistical insignificant. Nevertheless, a formal assessment of the residual error, errorht, residual, is required:

$$error_{h,\ residual} = error@h - BC_h \quad \text{2-8}$$

The remaining bias was less than 1.8 mm (~0.5%), which was shown by the t-test to be unsignificantly different from 0 (p=0.2). However, t-test provides only empirical evidence that bias was reduced to insignificant values. Nevertheless, assuming that bias is linearly related with height, the residual bias is approximately 10% d1.3 errors, at most 1% of the diameter (proof in the Appendix B). For the 18 trees, the bias reduction was almost 10 times (i.e., 17.2/ 1.8 = 9.5 times), which proved that biased corrected ppc-measurements are accurate and precise.

2.2.2. Taper equations

Since the highest valid stem measurement is at the stem height = 13 m, the four taper models evaluated the shape of the lower and middle portions of the stem. Only three of the four selected models (Table 2.2) could be used directly on the data, as they were developed specifically for loblolly pine. Irrespective the source of data (i.e., field or ppc), all three models performed as intended by the authors in respect with MAB, even that Lenhart et al. [3] had MAB three times larger than Max-Burhart or Baldwin and Feduccia (Table 2.4). For the 18 trees, bias was larger than the original model (e.g., 5.7 mm vs 3.6 mm for Max- Burkhart), and significantly greater than other taper studies [66]. However, even that RMSE was comparable with other taper studies [4,67], I refitted the models to the data, such that a formal assessment of capacity to supply input data for taper modeling by ppc is executed.

Table 2.4 Performance of existing taper models on field and ppc-based measurements. Max –Burkhart Model 4 was used for assessment.

Equation	Coeff	Original	Bias [mm]		MAB [mm]		RMSE [mm]	
			Field	ppc	Field	ppc	Field	ppc
Max-Burkhart	b_1	-3.0257	5.7	12.4	14.1	19.4	18.1	24.4
	b_2	1.4586						
	b_3	-1.4464						
	b_4	39.1081						
	a_1	0.7431						
	a_2	0.1125						
Baldwin-Feduccia	b_1	1.22467	-6.2	0.1	14.7	17.9	18.6	21.9
	b_2	0.3563						
Lenhart et al.	b	0.841837	16.0	23.2	19.5	25.4	27.3	34.9

When developed from field measurements the models performed similarly, all measures of fit being within the expected range: R2>0.97, bias <1 mm, MAB and RMSE around 10 mm (Table 2.5). The models refitted from ppc-based measurements supplied comparable fit statistics with ground based data (Table 2.6), except for bias, who was twice as large (i.e., 1.4 mm for Baldwin and Feduccia and 2.2 mm for Max-Burkhart vs 0.6 mm and 0.9 mm, respectively). It should be noted that because the upper portion of the stem could not be rendered from ppc, the upper inflection point of the Max-Burkhart equation was not identified. Therefore, a simplified version of the best Max-Burkhart equation (in Table 2.2) was used for ppc based values (equation 2 in the original article) Irrespective the equation, the fit statistics are slightly higher for ppc-derived models than the ground-based models. Overall, Kozak model performed the best, with the smallest bias, MAB, RMSE, and largest R2.

Table 2.5 Taper models developed from ground-based measurements

Equation	Coeff.	Data	p-value	R^2	Bias [mm]	MAB [mm]	RMSE [mm]	RMSE [%]
Max-Burkhart	b_1	-0.48	<0.001	0.98	-0.9	8.7	12.2	4
	b_2	-0.41	0.01					
	b_3	2.72	0.02					
	a	0.29	<0.001					
Baldwin-Feduccia	b_1	1.11	<0.001	0.98	-0.6	8.6	11.7	5
	b_2	0.24	<0.001					
Lenhart et al.	b	0.5288	0.01	0.97	-2.0	9.8	12.9	5
Kozak	a_0	1.35	<0.001	0.98	-0.01	8.4	11.9	5
	a_1	0.94	<0.001					
	b_0	0.19	<0.001					
	b_1	0.3	0.02					
	b_2	0.01	0.25					
	b_3	-0.05	0.19					

Table 2.6 Taper models developed from the bias corrected ppc-based measurements

Equation	Coeff.	Estimates	p-value	R^2	Bias [mm]	MAB [mm]	RMSE [mm]	RMSE [%]
Max-Burkhart	b_1	-0.64	<0.001	0.95	-2.2	13.5	18.4	6
	b_2	-0.33	<0.001					
	b_3	3.53	0.37					
	a	0.2	<0.001					
Baldwin-Feduccia	b_1	1.12	<0.001	0.95	-1.4	13.3	18.3	6
	b_2	0.24	<0.001					
Lenhart et.al	b	0.519	<0.001	0.94	-0.7	13.6	18.6	7
Kozak	a_0	1.81	<0.001	0.95	-0.1	12.5	16.7	5
	a_1	0.84	<0.001					
	b_0	0.15	<0.001					
	b_1	0.42	0.02					
	b_2	-0.01	0.54					
	b_3	-0.04	0.77					

The Max-Burkhart model have the inflection point at relative height 0.29 for ground measurements and 0.20 from ppc- measurements. However, the ppc-based model does not generate a significant estimate of α (p=0.37), indicating that a single polynomial curve can approximate the tree bole. Apparent divergence between the field and ppc curves can be observed for the relative height between 0.18 – 0.40 (Figure 2.6 a). The coefficients of the nonlinear term in the Baldwin and Feduccia model are the same (i.e., 0.24), while the one for the linear term are practically indistinguishable between the two datasets (Figure 2.6 b). The model fit from ground - measurements is superior to the ppc-based model (i.e., MAB is 9.2 mm vs. 13.3 mm, and RMSE is 13.2 mm vs. 18.3 mm, respectively). Similarly to Baldwin and Feduccia model, regardless of measurements source, the Lenhart at al model has the same estimates of the power term (Figure 2.6 c). Mirroring Max-Burkhart model, Kozak's model has insignificant estimates for two coefficient (i.e., $p > 0.10$ for b_2 and b_3). The lack of significance is noticed for relative heights >0.5 (Figure 2.6 d).

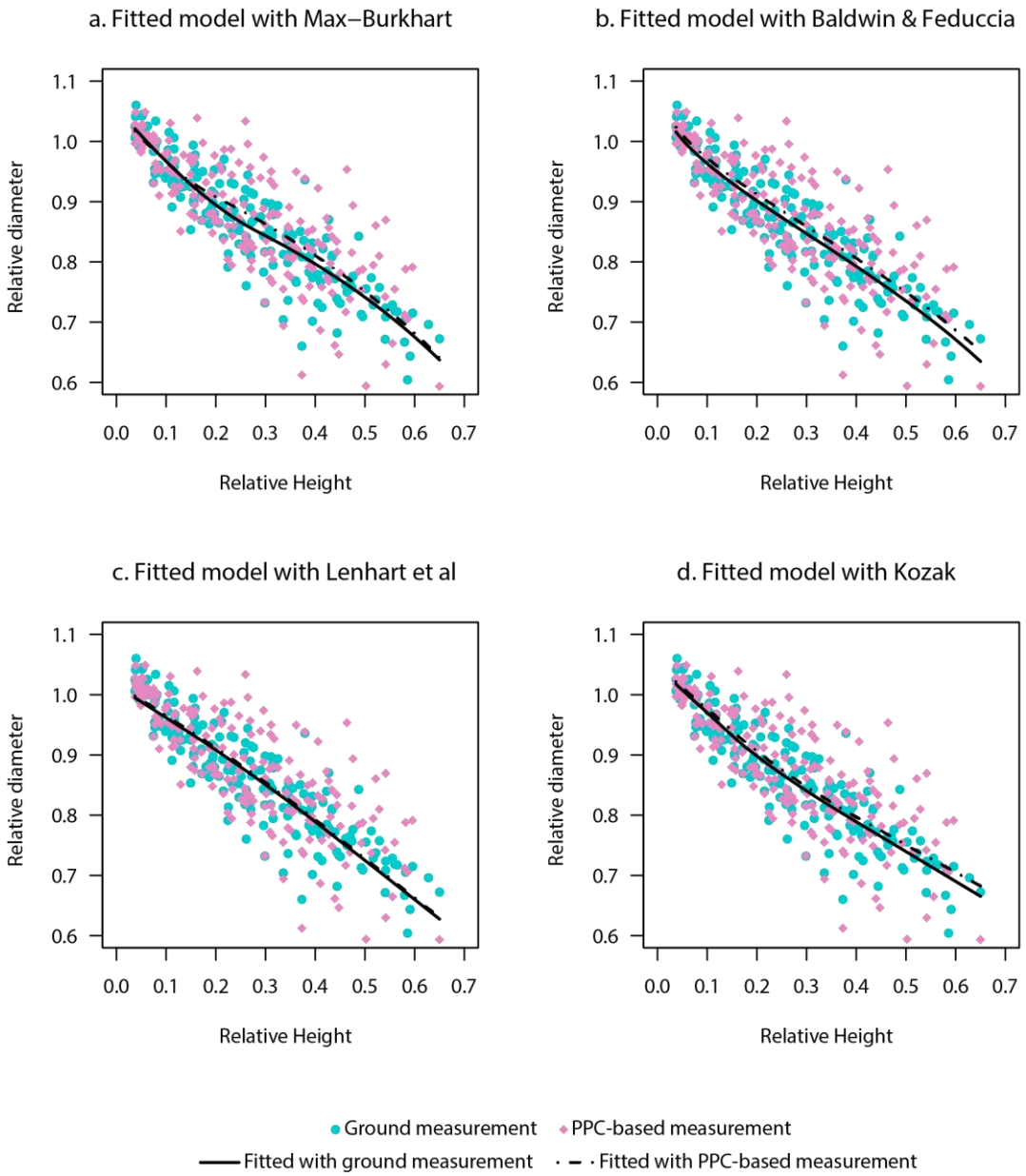

Figure 2.7 Comparisons of the models developed with the ppc-based measurement and the ground-based measurement. a. Max and Burkhart b. Baldwin and Feduccia c. Lenhart et al d. Kozak

The cross-validation of the ppc based models with the field data reveals agreement for all fit statistics (Table 2.7), with R2≥0.97 irrespective the model type, bias <4 mm, MAB <10 mm, and RMSE<15 mm. Even that Kozak's proved to be most suited to represent diameter variation along the stem, the Baldwin and Feduccia model, which is simpler, supplied similar fit statistics with a significant increase in parsimony.

Table 2.7 Validation of the ppc – based models with ground measured data

Equation	R^2	Bias [mm]	MAB [mm]	RMSE [mm]
Max- Burkhart	0.98	-3.6	9.7	14.0
Baldwin -Feduccia	0.97	-2.9	9.4	13.7
Lenhart et al.	0.97	-2.5	10	14.2
Kozak	0.98	-2.0	9.4	13.2

2.3. Discussions

Current applications of SfM in forest inventory are limited by irregular stems geometry and complex background, which challenge camera location, key point extraction, and lack of geo-reference under dense canopy. Oblique perspective limits the ability of 3D reconstruction of the entire tree, particularly the higher portion of the trunk. Therefore, diameter measurements were below 12 m (i.e., the first two logs), which is approximately half of the total tree height. Nevertheless, higher diameters can be measured if the photographic information is captured with unnamed aerial vehicles flying along and around the tree.

Lightning and background of the objected to be rendered with SfM plays a significant role in accuracy of the reproduction process [68,69], particularly the lack of features and low light (called “bad lighting” by Koutsoudis et al. [68]). Considering that all images were acquired under canopy where limited light is present I have chosen only spring and summer bright days, with almost no cloud coverage and no rain for three days. The lack of details and a homogeneous background were not a concern, as forest provides plenty of variation to allow for identification of a multitude of key-points.

The diameter measurements directly from ppc are constantly higher than ground measurements, which is the result of two assumptions: first, the stem is circular, and second, the length along stem is measured without error. This combination impact AutoCAD measurements, as rotation of the stem could, and likely would, lead to small variations in diameter at the same location along the stem. Therefore, besides calibration errors measurements errors are also present. The bias correction equation that I proposed (Eq. 2-7) is practical and intuitive rather than mathematically based.

The measurement bias seems to be positively related to the stem height. I assumed that projective direction of the camera is almost horizontal, at the eye of the operator; therefore, the best-estimated diameter is $d_{1.3}$. The measurement error expands along the stem as the distance is increasingly away from the projection center. Consequently, I select the relative height as correcting term. A higher order polynomial of relative height or even a rotation correction term could lead to better results than the proposed affine transformation (Eq. 2-7), as images are restructured with a nonlinear process. It is possible that accuracy is influenced by errors occurring from multiple directions [70]. Even so, the largest error, relative to diameter, was 4% (i.e., at 12 m), the rest being ≤ 2%. The accuracy and precision of diameter measurements from ppc are not the only advantages of using 3D reconstruction from images. The ppc allows for diameter measurements at any height, not only at preset ones (e.g., every meter). Furthermore, high-density ppc supply information for detection and estimation of trunk defects, such as catface or sweep.

The results show that the equations developed from the ppc-based measurements are comparable with the equations developed from the ground-based measurements, when the same model forms were applied. The four models developed by ppc-based measurement could be used to estimate ground diameter with accuracy < 4 mm. The bias of ppc-based diameter models does not vary remarkably among four model forms. The most evident difference between ground and ppc-based occurs for the Max-Burkhart model (Figure 2.7a). The Kozak model 02 was not originally developed for diameter estimation of loblolly pine. However, the goodness-of-fit of Kozak models is slightly better than other models, consistent with the finding of Li and Weiskittel [71].

According to their study, Kozak model 02 will fit the diameters of other species across a wide range of biogeographic zones [71]. Diameter estimated with Baldwin and Feduccia [2] equation are the closest to the ground measurement at relative height > 0.22, compared with Max-Burkhart and Lenhart et al. equations. A possible explanation of relatively weak performance of Lenhart et al (1987) equation could rest with its development, which was confined to small trees ($d_{1.3}$< 33 cm). Nevertheless, our study results show that the selection of model forms would not significantly influence the model fit. Among the four models selected for taper assessment, I consider Baldwin and Feduccia [2] approach to be the most trustworthy, as it is intuitive and relatively simple. Kozak [4] model 02 outperformed all other models, but its lack of realism and low parsimony (e.g., 6 parameters compared to 2 for Baldwin and Feduccia) is not appealing. In fact, the difference between Kozak's model 02 and Baldwin and Feduccia is minute, as bias, MAB, and RMSE are almost the same (Table 2.7). Therefore, the ppc measurements can be used not only for direct estimation of diameter (bias was < 2 mm), but also on taper modeling (bias <4 mm and $R^2 \geq 0.97$).

Diameter estimation and taper modeling was possible for loblolly pine because the crown is concentrated on a small portion along the trunk (usually <30%) and lack of dead branches on the lower portion of the stem. However, for species that keep for long time the lower branches, such as Douglas fir (Pseudotsuga menziesii Mirb.) or Norway spruce (Picea abies L.), the usage of SfM is difficult not only because of difficulty to navigate but also because pf the poor light conditions. In these situations a combination of active-passive sensors could deliver the desired point clouds.

The ppc proved that can be used for modeling taper, and consequently the amount and type of products that can be obtained from individual stems. I expect that subsequent studies on taper, particularly for genetic studies where branching is also important, will be almost entirely based on ppc. New equipment that allows diameter measurements along the stem, such as Criterion RD by Laser Technology, did not reduced significantly the time to acquire accurate data significantly. Furthermore, while measurements based optical devices exhibits increase in variability with distance from the tree, the ppc is not affected by these issues. Large sample size balances the estimates of various taper modeling methods, but all approaches, except the ones based on ppc, are either expensive (i.e., terrestrial lidar) are have larger variability. The costs of producing ppc will decrease, which would make it even more attractive. I expect that real time ppc creation will occur in the next decade, which will allow estimation of products during forest operations, which will increase the value of each stand.

2.4. Conclusion

In this paper, I proposed an accurate procedure for measuring diameter along the stem from consumer grade cameras. Limited training and fieldwork is required for capturing oblique images of the trees and execution of scaling operation. The images are rendered to a 3D point cloud using a structure form motion algorithm, hence the name photogrammetric point cloud (ppc). Diameter measurements executed on the ppc along the stem are biased, overestimating the real diameter. However, a simple, intuitive, and easy to implement correction will reduce the bias to millimeters, majority $\leq$ 2%. Diameter measurements from ppc can successfully replace ground measurements not only by being accurate while reducing the costs and time, but also by allowing a

continuous examination of the stem. Therefore, taper models can be developed from ppc-based measurements that would trace closely the stem, (e.g., every 10 cm). I assessed the diameter measurements with four popular taper models, and I found no operational and statistical difference between the models developed from ground data and from ppc-corrected data. In fact, two models [Kozak [4] model 02 and Baldwin and Feduccia [2]] had the bias less than 1 mm. Although the application of SfM is still limited in the context of vegetation with high complexity, our results suggest that ppc based models are as accurate as conventional inventory. Reconstruction of the entire stem can be achieved by combining images acquired by unmanned aerial systems with ground-based photographs. Examination of the entire trunk can expand beyond dendrometric attributes, such as diameter or length, and can include stem defects, such as catface, knots, or sweep. For accurate product estimation in the lower portion of the bole (e.g., the first two logs), our results recommend replacement of taper with ppc, as being fast, more accurate and precise.

References

1. Max, T.A.; Burkhart, H.E. Segmented polynomial regression applied to taper equations. *Forest Science* **1976**, *22*, 283-289.
2. Baldwin, V.C.; Feduccia, D.P. Compatible tree-volume and upper-stem diameter equations for plantation loblolly pines in the west gulf region. *Southern Journal of Applied Forestry* **1991**, *15*, 92-97.
3. Lenhart, J.D.; Hackett, T.L.; Laman, C.J.; Wiswell, T.J.; Blackard, J.A. Tree content and taper functions for loblolly and slash pine trees planted on non-old-fields in east texas. *Southern Journal of Applied Forestry* **1987**, *11*, 147-151.
4. Kozak, A. My last words on taper equations. *The Forestry Chronicle* **2004**, *80*, 507-515.
5. Avery, T.E.; Burkhart, H. *Forest measurements*. Mcgraw-Hill Ryerson: New York, 2001; p 1-480.
6. Husch, B.; Beers, T.W.; Kershaw, J.A. *Forest mensuration*. 4th ed.; Wiley: 2002; p 456.
7. Burkhart, H.E.; Tome, M. *Modeling forest trees and stands*. Springer: New York NY, 2012; p 460.
8. Lee, J.-H.; Ko, Y.; McPherson, E.G. The feasibility of remotely sensed data to estimate urban tree dimensions and biomass. *Urban Forestry & Urban Greening* **2016**, *16*, 208-220.
9. Lu, D.; Chen, Q.; Wang, G.; Liu, L.; Li, G.; Moran, E. A survey of remote sensing-based aboveground biomass estimation methods in forest ecosystems. *International Journal of Digital Earth* **2016**, *9*, 63-105.
10. Williams, M.S.; Cormier, K.L.; Briggs, R.G.; Martinez, D.L. Evaluation of the barr & stroud fp15 and criterion 400 laser dendrometers for measuring upper stem diameters and heights. *Forest Science* **1999**, *45*, 53-61.
11. Shimizu, A.; Yamada, S.; Arita, Y. Diameter measurements of the upper parts of trees using an ultra-telephoto digital photography system. *Open Journal of Forestry* **2014**, *4*, 316-326.
12. Nunes, M.H.; Görgens, E.B. Artificial intelligence procedures for tree taper estimation within a complex vegetation mosaic in brazil. *PLOS ONE* **2016**, *11*, e0154738.
13. Cushman, K.C.; Muller-Landau, H.C.; Condit, R.S.; Hubbell, S.P. Improving estimates of biomass change in buttressed trees using tree taper models. *Methods in Ecology and Evolution* **2014**, *5*, 573-582.
14. Saarinen, N.; Kankare, V.; Vastaranta, M.; Luoma, V.; Pyörälä, J.; Tanhuanpää, T.; Liang, X.; Kaartinen, H.; Kukko, A.; Jaakkola, A., *et al.* Feasibility of terrestrial laser scanning for collecting stem volume information from single trees. *ISPRS Journal of Photogrammetry and Remote Sensing* **2017**, *123*, 140-158.
15. Olofsson, K.; Holmgren, J. Single tree stem profile detection using terrestrial laser scanner data, flatness saliency features and curvature properties. *Forests* **2016**, *7*, 207.

16. You, L.; Tang, S.; Song, X.; Lei, Y.; Zang, H.; Lou, M.; Zhuang, C. Precise measurement of stem diameter by simulating the path of diameter tape from terrestrial laser scanning data. *Remote Sensing* **2016**, *8*, 717.
17. Henning, J.G.; Radtke, P.J. Detailed stem measurements of standing trees from ground-based scanning lidar. *Forest Science* **2006**, *52*, 67-80.
18. Coble, D.W.; Hilpp, K. Compatible cubic-foot stem volume and upper-stem diameter equations for semi-intensive plantation grown loblolly pipe trees in east texas. *Southern Journal of Applied Forestry* **2006**, *30*, 132-141.
19. Farrar, R.M. Stem-profile functions for predicting multiple-product volumes in natural longleaf pines. *Southern Journal of Applied Forestry* **1987**, *11*, 161-167.
20. Westfall, J.A. *Modifying taper-derived merchantable height estimates to account for tree characteristics*; USDA Forest Service: Washington DC, 2006; p 126.
21. Newnham, R.M. Variable-form taper functions for four alberta tree species. *Canadian Journal of Forest Research* **1992**, *22*, 210-223.
22. Lowe, D.G. Distinctive image features from scale-invariant keypoints. *International Journal of Computer Vision* **2004**, *60*, 91-110.
23. Smith, R.C.; Cheeseman, P. On the representation and estimation of spatial uncertainty. *The International Journal of Robotics Research* **1986**, *5*, 56-68.
24. Harris Geospatial Solutions *Envi*, Exelis Visual Information Solutions: Boulder CO, 2016.
25. Hexagon Geospatial *Erdas imagine*, Hexagon AB: Stockholm, SE, 2016.
26. Schindler, K.; Bischof, H. On robust regression in photogrammetric point clouds. In *Pattern recognition: 25th dagm symposium, magdeburg, germany, september 10-12, 2003. Proceedings*, Michaelis, B.; Krell, G., Eds. Springer Berlin Heidelberg: Berlin, Heidelberg, 2003; pp 172-178.
27. Soule, S.; Maurice, K.; Walcher, W.; Szabo, J. In *Advanced point cloud generation for photogrammetric modeling of complex 3d objects*, Proceedings. International Conference on Image Processing, 24-28 June 2002, 2002; pp 529-532 vol.523.
28. Lucas, B.D.; Kanade, T. In *An iterative image registration technique with an application to stereo vision*, IJCAI, 1981; pp 674-679.
29. Haralick, R.M. Digital step edges from zero crossing of second directional derivatives. *IEEE Transactions on Pattern Analysis and Machine Intelligence* **1984**, *PAMI-6*, 58-68.
30. Agisoft LLC *Agisoft photoscan*, Agisoft: St. Petersburg, Russia, 2014.
31. Pix4D *Pix4d*, Pix4D: Lausanne Switzerland, 2014.
32. Wu, C. *Visualsfm v0.5.26*, 2017.
33. Fritz, A.; Kattenborn, T.; Koch, B. Uav-based photogrammetric point clouds—tree stem mapping in open stands in comparison to terrestrial laser scanner point clouds. *Int. Arch. Photogramm. Remote Sens. Spat. Inf. Sci* **2013**, *40*, 141-146.
34. Forsman, M.; Börlin, N.; Holmgren, J. Estimation of tree stem attributes using terrestrial photogrammetry with a camera rig. *Forests* **2016**, *7*, 61.

35. Mikita, T.; Janata, P.; Surový, P. Forest stand inventory based on combined aerial and terrestrial close-range photogrammetry. *Forests* **2016**, *7*, 165.
36. Mensah, S.; Glèlè Kakaï, R.; Seifert, T. *Patterns of biomass allocation between foliage and woody structure: The effects of tree size and specific functional traits*. 2016.
37. Garber, S.M.; Maguire, D.A. Modeling stem taper of three central oregon species using nonlinear mixed effects models and autoregressive error structures. *Forest Ecology and Management* **2003**, *179*, 507-522.
38. Valentine, H.T.; Gregoire, T.G. A switching model of bole taper. *Canadian Journal of Forest Research* **2001**, *31*, 1400-1409.
39. Nyland, R.D. *Silviculture. Concepts and applications*. McGraw-Hill: New York, 1996; p 1-633.
40. Smith, D.M. *The practice of silviculture : Applied forest ecology*. 9th ed.; Wiley: New York, 1997; p xvii, 537 p.
41. Turner, D.; Lucieer, A.; Wallace, L. Direct georeferencing of ultrahigh-resolution uav imagery. *IEEE Transactions on Geoscience and Remote Sensing* **2014**, *52*, 2738-2745.
42. Liang, X.L.; Jaakkola, A.; Wang, Y.S.; Hyyppa, J.; Honkavaara, E.; Liu, J.B.; Kaartinen, H. The use of a hand-held camera for individual tree 3d mapping in forest sample plots. *Remote Sensing* **2014**, *6*, 6587-6603.
43. Robertson, F.D. *Timber cruising handbook*; USDA Forest Service: Washington DC, 2000; p 268.
44. Autodesk *Autocad civil 3d*, Autodesk: SanRafael CA, 2016.
45. Daniilidis, K.; Spetsakis, M.E. Understanding noise sensitivity in structure from motion. In *Visual navigation*, Aloimonos, Y., Ed. Lawrence Erlbaum Associates: Hillsdale NJ USA, 1996; pp 61-88.
46. Stängle, S.M.; Sauter, U.H.; Dormann, C.F. Comparison of models for estimating bark thickness of picea abies in southwest germany: The role of tree, stand, and environmental factors. *Annals of Forest Science* **2017**, *74*, 16.
47. Montealegre, A.; Lamelas, M.; Riva, J. Interpolation routines assessment in als-derived digital elevation models for forestry applications. *Remote Sensing* **2015**, *7*, 8631.
48. Powell, S.L.; Cohen, W.B.; Healey, S.P.; Kennedy, R.E.; Moisen, G.G.; Pierce, K.B.; Ohmann, J.L. Quantification of live aboveground forest biomass dynamics with landsat time-series and field inventory data: A comparison of empirical modeling approaches. *Remote Sensing of Environment* **2010**, *114*, 1053-1068.
49. Bilskie, M.V.; Hagen, S.C. Topographic accuracy assessment of bare earth lidar-derived unstructured meshes. *Advances in Water Resources* **2013**, *52*, 165-177.
50. Schabenberger, O.; Pierce, F.J. *Contemporary statistical models for the plant and soil sciences*. CRC Press: Boca Raton FL, 2002; p 730.
51. Neter, J.; Kutner, M.H.; Nachtsheim, C.J.; Wasserman, W. *Applied linear statistical models*. WCB McGraw-Hill: Boston, 1996; p 1-1408.

52. Grubbs, F.E. Sample criteria for testing outlying observations. *Annals of Mathematical Statistics* **1950**, *21*, 27-58.
53. Thode, H.C. *Testing for normality*. Marcel Dekker: New York, 2002; p 1-368.
54. Hollander, M.; Wolfe, D.A. *Nonparametric statistical methods*. John Wiley and Sons: New York, 1973; p 1-503.
55. SAS Institute *Sas*, 9.1; SAS Institute: Cary NC, 2010.
56. Cao, Q.V. Calibrating a segmented taper equation with two diameter measurements. *Southern Journal of Applied Forestry* **2009**, *33*, 58--61.
57. Trincado, G.; Burkhart, H.E. A generalized approach for modeling and localizing stem profile curves. *Forest Science* **2006**, *52*, 670-682.
58. Williams, M.S.; Reich, R.M. Exploring the error structure of taper equations. *Forest Science* **1997**, *43*, 378-386.
59. Grothendieck, G. *Nls2: Non-linear regression with brute force*, R package version 0.2: CRAN, 2013.
60. R Core Team *R: A language and environment for statistical computing*, R Foundation for Statistical Computing: Vienna, Austria, 2016.
61. Jiang, L.-c.; Liu, R.-l. Segmented taper equations with crown ratio and stand density for dahurian larch (larix gmelinii) in northeastern china. *Journal of Forestry Research* **2011**, *22*, 347-352.
62. Sharma, M.; Zhang, S.Y. Variable-exponent taper equations for jack pine, black spruce, and balsam fir in eastern canada. *Forest Ecology and Management* **2004**, *198*, 39-53.
63. Grimmett, G.D.; Stirzaker, D.R. *Probability and random processes*. Oxford University Press: New York, 2002; p 1-600.
64. Poole, D. *Linear algebra*. Thomson Brooks/Cole: Toronto, 2005; p 1-712.
65. Vidal, C.; Alberdi, I.A.; Mateo, L.H.; Redmond, J.J. *National forest inventories: Assessment of wood availability and use*. Springer: Cham CH, 2016; p 845.
66. Lejeune, G.; Ung, C.-H.; Fortin, M.; Guo, X.; Lambert, M.-C.; Ruel, J.-C. A simple stem taper model with mixed effects for boreal black spruce. *European Journal of Forest Research* **2009**, *128*, 505-513.
67. Newberry, J.D.; Burkhart, H.E. Variable-form stem profile models for loblolly pine. *Canadian Journal of Forest Research* **1986**, *16*, 109-114.
68. Koutsoudis, A.; Vidmar, B.; Ioannakis, G.; Arnaoutoglou, F.; Pavlidis, G.; Chamzas, C. Multi-image 3d reconstruction data evaluation. *Journal of Cultural Heritage* **2014**, *15*, 73-79.
69. Nikolov, I.; Madsen, C. Benchmarking close-range structure from motion 3d reconstruction software under varying capturing conditions. In *Digital heritage. Progress in cultural heritage: Documentation, preservation, and protection: 6th international conference, euromed 2016, nicosia, cyprus, october 31 – november 5, 2016, proceedings, part i*, Ioannides, M.; Fink, E.; Moropoulou, A.; Hagedorn-Saupe, M.; Fresa, A.; Liestøl, G.; Rajcic, V.; Grussenmeyer, P., Eds. Springer International Publishing: Cham, 2016; pp 15-26.

70. Weng, J.; Huang, T.S.; Ahuja, N. Motion and structure from two perspective views: Algorithms, error analysis, and error estimation. *IEEE Transactions on Pattern Analysis and Machine Intelligence* **1989**, *11*, 451-476.
71. Li, R.; Weiskittel, A.R. Comparison of model forms for estimating stem taper and volume in the primary conifer species of the north american acadian region. *Annals of Forest Science* **2010**, *67*, 302-302.

Chapter 3 Comparison of total stem volume estimates from point clouds of terrestrial lidar and empirical equations for mature Douglas-fir (Pseudotsuga menziessi (Mirb.) Franco)

Abstract

Total stem volume is desirable information for estimating timber yields and tree aboveground biomass. Terrestrial light detection and ranging (lidar) can provide nondestructive stem estimates through a sequence of cylindrical segments that locally approximate the point clouds of the stem. This study estimated the total stem volume of mature Douglas-fir trees using two point-cloud-based methods: one is to integrate taper equations developed with stem diameter estimated on the cylinder segments, and another is to sum up the volume of cylinder segments. Point-cloud-based volume estimates were compared with estimates yielded by a total volume equation of the Forest Inventory Analysis in the Pacific Northwest (FIA-PNW) and a taper equation developed by Poudel et al. (2018). The primary objective is to assess the discrepancy of volume estimates yielded by various methods. The secondary objective is to test the sensitivity of the point-cloud-based volume estimates to the segment length (0.5 m, 1 m, and 2 m) of the cylindrical models constructed from point clouds. The ANOVA suggests a significant difference in mean volume estimates yielded by various methods and the difference increases with increasing tree DBH class. I found the volume estimates yielded by point-cloud-based taper equations are only slightly sensitive to the segment length of cylindrical models. However, the mean volume estimates using summations of cylindrical models differ in segment lengths, in which cylindrical models with the smallest segment length (0.5 m) produced up to 8% greater volume

estimates than models with the largest segment length (2 m). We concluded that not only the data sources but also the method of using these data can cause inconsistency in volume estimates. Calibration is needed to bring consistency to stem volume estimates produced by different methods.

Keywords: Point clouds; cylinder models; taper equations; stem volume estimates; Forest Inventory and Analysis

3.1. Introduction

Accurate tree stem volume estimation is ecologically and economically essential for accessing forest carbon stocks and timberland assets (Avery and Burkhart, 2015; Harold E Burkhart and Tomé, 2012; West and West, 2009). Douglas-fir, a major tree species of the Pacific Northwest (PNW), provides considerable value through timber and biomass; therefore, total stem volume can be desirable information. Total stem volume of Douglas-fir is usually estimated from the equations of Forest Inventory Analysis in the Pacific Northwest (FIA-PNW), which are multiple-entry equations that include diameter at breast height (DBH) and total tree height (Harold E Burkhart and Tomé, 2012; Fang et al., 2000; Kershaw et al., 2017). However, total stem volume equations fail to take into consideration the stem shape variation along the trunk and yield the same volume estimates for trees with identical DBH and height. Taper equations enhance volume estimation by modeling the evolvement of the upper stem diameter (West and West, 2009) and flexibly yield total or sectional stem volume estimates for given stem sections. A series of taper equations have been incorporated into the volume estimation system of Douglas-fir in PNW to enhance the estimation accuracy (Biging, 1984; Rustagi and Loveless Jr, 1991; Walters and Hann, 1986). The

acquisition of accurate stem diameter measurements is essential for the development of taper equations. In comparison with field measurements, which require tremendous effort, point clouds, developed from light detection and ranging (lidar) or thru photogrammetric techniques, have been increasingly used to provide stem diameters and volumes (Mikita et al., 2016; Pitkänen et al., 2019; Raumonen et al., 2013b). To estimate the upper stem diameter, convex hull or circular models are usually used to approximate thin slices of points surrounding the cross-sectional area of the stem at a specific height. The difference between values obtained from point and field measurements are within 2 cm, which render as unnecessary the acquisition of the DBH on the ground (Fang and Strimbu, 2017; Henning and Radtke, 2006; Hopkinson et al., 2004; Mikita et al., 2016). For stem volume estimation, quantitative structural models (QSM) are commonly used to construct segments of the stem or branches with cylinders developed from sectional point clouds (Hackenberg et al., 2015a; Raumonen et al., 2013b). Many studies have demonstrated the accuracy of tree stem diameter and volume estimates from QSM-developed models for broadleaf species (Burt et al., 2013; Lau et al., 2018; Tanago et al., 2018). However, its application to tall conifer species is challenging due to scarce point cloud density at higher sections of the canopy. An alternative to the QSM approach is to use a point cloud processing software, like Cyclone (Leica Geosystems, 2019), which fits cylinder models by visually selecting the seed points. To date, human interaction with computer aid software supplies more accurately reconstructed models of complex structures, like tree stems. Regardless of the approach used (i.e., visual or automatic), stem volume can be computed with cylindrical models. The precision of lidar-based estimation can vary with the length of

the segment used to fit cylinders. When point clouds densely cover the stem, cylinder models with smaller segment length can lead to precise tree volume estimation, as they approximate stem shape in fine detail. However, obstruction can lead to point clouds unevenly distributed around and along the stem, which can lead to early termination of the algorithms fitting cylinders due to point gaps. Short segments could fit curved shapes at the expense of the algorithm's performance, in many instances preferred, whereas longer segment could increase the success of reconstructing the stembut sacrifices the accuracy.

Stem volume estimation can be performed nondestructively using lidar through two methods: integrating the taper equations developed from lidar-based stem diameter estimates, and direct volume estimates with cylinder models. The former combines auxiliary tree structural information obtained from point clouds data and traditional modeling approach to provide numeric models that could be repeatedly used for other inventory purposes. The latter supplies more accurate individual tree volume estimates and drives inventory from model-based to data-based, reducing uncertainties introduced by model specification. Currently, terrestrial point-cloud-based stem volume estimation remains at local scales, and its connection with regional volume estimation, such as the FIA equation system, is unclear. Empirical equations that use only DBH and tree height fail to account for tree structural information which can be crucial for volume estimates and produced biased estimates, especially for volume estimates in commercial use (Dassot et al., 2011).

As lidar has been widely used in contemporary forest inventory but empirical equations are still used as reference volume estimates, there is an increasing need to bring consistency to stem volume estimates from various methods. Especially for studies of forest dynamics, the evolvement of inventory methods and technology allows more accurate and more frequent forest inventory but also bring inconsistency in volume estimates at different time (Kangas and Maltamo, 2006; Smith, 2002; White et al., 2016), which might overestimate or underestimate the change of forest stem volumes overtime. The information on the difference between lidar-based volume estimates and estimates from empirical equations is needed to update the current equation-based estimation systems and to develop stem volume estimation with the frontier technology. The overarching objective of the present study is to compare lidar-based estimates with the values supplied by the FIA-PNW equations and existing taper equations. First, we developed three sets of cylinder models of the stems from lidar point clouds. The three sets of cylinder models are distinguished by their segment lengths: 0.5 m, 1 m, and 2 m. The three lengths represent the level of precision, as we assumed that the shorter the segment length, the more precise the volume is estimated. Next, three taper equations were developed by using stem diameter estimates from the cylinder models. Third, Douglas-fir total stem volume was estimated with taper equations, cylinder models and the FIA-PNW equation. Finally, we used simulation to assess the volume estimation discrepancy between different methods for trees with various DBH classes. The specific objective of our study is twofold: 1) to assess the sensitivity of volume estimates to the parameters defining the cylindrical stem models, and 2) to evaluate the

difference between the stem volume estimates obtained from point clouds and from empirical equations.

3.2. Methods

3.2.1. Study area and point cloud acquisition and processing

The study site is located in the Oregon Cascade, at the HJ Andrews Long Term Ecological Forest. An 80 m × 100 m secondary Douglas-fir-dominated plot was scanned with a RIEGL VZ-400 terrestrial laser scanner from 22 scan locations. Scan 1, located at the plot center, was a 10 min scan for highest density, whereas the rest of the scans were performed at 5 min each. To register the 22 scans, I placed 76 targets inside the plot and their geographic coordinates were surveyed with Leica TS15 P1 total station. I registered the scan with Cyclone (Leica Geosystems, 2019), using the targets with known coordinates and cloud-to-cloud comparison. Mean absolute error of target and cloud-to-cloud alignments were 0.009 m and 0.016 m respectively. Point clouds of 10 dominant and codominant trees were randomly selected within the plot. Figure 3.1 provides a rendering of sample trees' point clouds. The point clouds associated with each tree were visually delineated in Cyclone. The dbh of the 10 trees ranged from 49 cm to 110 cm, with an average of 64 cm. Tree height ranged from 39 m to 53 m, with an average of 44 m.

Figure 3.1 A rendering of sample tree point clouds. The grey scale of the point clouds are represented by their intensity values.

3.2.2. Stem measurements

I fitted the tree stem with cylinder models using the Region Grow function in Cyclone (Figure 3.2 a). Region Grow requires a manual selection of initial seed points, then automatically expands those user-selected points to include all other points likely belonging to the same cylinder segment. Region Grow can fit cylinders to stems that have missing points on one side by estimating the geometric center of the arc (Figure 3.2 b). The cylinder models were obtained by minimizing the sum of distances between the point clouds to the cylinder surface. To account for taper, I developed three sets of cylinder models (Figure 3.3), defined by their sub-cylinder segment length: 0.5 m, 1.0 m, and 2 m.

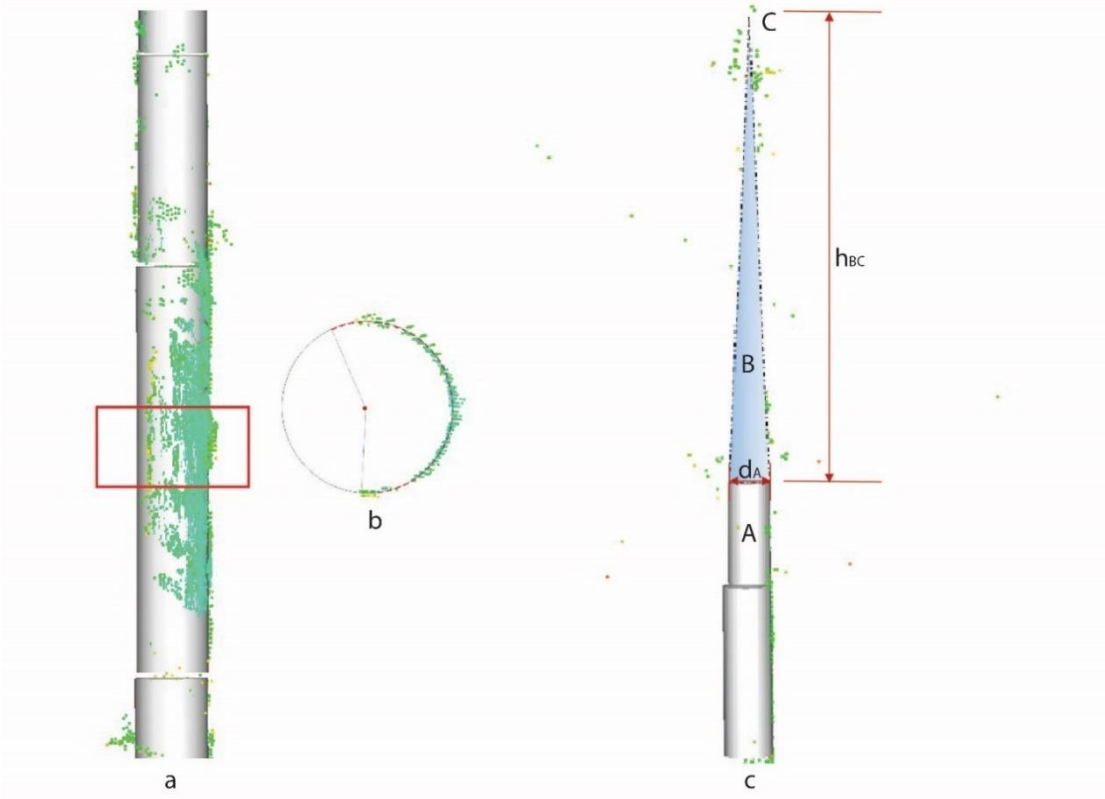

Figure 3.2 Fitting cylinder models; a. cylinder fitting in Cyclone with region grow; b. Region Grow fits stem sections with missing points on one side; c. Imputation of the tree top: A is the highest fitted cylinder, B is the imputed cone shape, and C is the

estimated tree top from point clouds. d_A is the diameter of highest fitted cylinder; h_{BC} is the length between A and C.

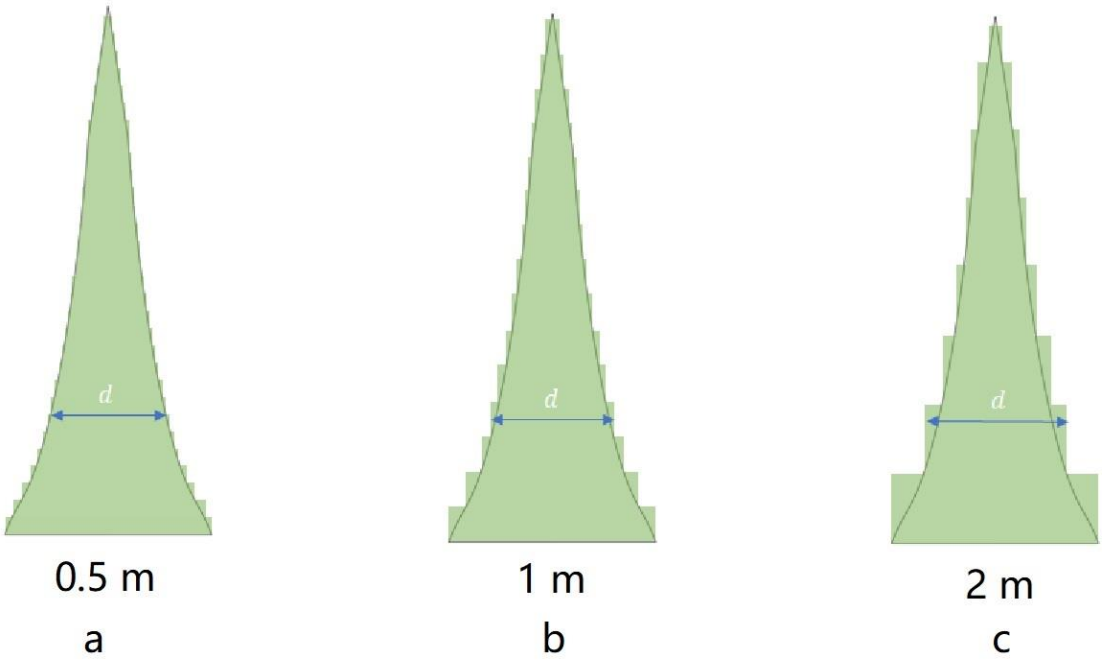

Figure 3.3 Illustration of cylinder models with three segment length. a. The length of the cylinder segment is 0.5 m; b. the length of cylinder segment is 1 m; c. the length of the cylinder segment is 2 m.

For each cylinder length, I measured the diameter outside bark (dob) as the diameter of the cylinder cross section. Stem model at the top, particularly for height above 35 m, was missing due to insufficient points for constructing lidar models. The missing model at stem top was filled with cone shape by assuming linear relationship between stem diameter and specific height (Figure 3.2 c). Conic or parabolic shapes are usually present at the stem top (Avery and Burkhart, 2015). Defining conic shape only requires the bottom diameter and height. Defining parabolic shape, however, requires three parameters of bottom diameter, height, and an additional diameter measurement along the stem to be able to complete the equation. As the point clouds in upper sections of trees was not dense enough to provide a reliable third measurement for diameter along the stem needed for parabolic modeling, and in light of the nature of trees holding

relatively less volume in the upper stem that would be important to capture, we considered the conic model to be sufficient for this study.

3.2.3. Taper equations

Diameter outside bark is converted to diameter inside bark (dib) by subtracting bark thickness:

$$dib_{ij} = dob_{ij} - dbt_{ij} \qquad 3\text{-}1$$

where dib_{ij} is the predicted diameter inside bark of tree i at height j;

dob_{ij} is the the diameter outside bark measurement from point clouds for tree i at height j; dbt_{ij} is the predicted double bark thickness with Maguire and Hann's equation (1990) (see Appendix C).

Despite abundance of taper equation forms, variable exponent developed by Kozak (2004) has been found by some studies (Fang and Strimbu, 2017; Poudel et al., 2018) as having the least bias. In this study, I fit dib equations with the three datasets using variable exponent equation from Kozak (2004):

$$d_{ij} = a_0 DBH_i^{a_1} H_i^{a_2} X_{ij}^{b_1 RH_{ij}^4 + b_2 \left(e^{DBH_i/H_i}\right)^{-1} + b_3 X_{ij}^{0.1} + b_4 \frac{1}{DBH_i} + b_5 H_i^{1-RH_{ij}^{1/3}} + b_6 X_{ij}} + e_{ij} \qquad 3\text{-}2$$

where $X_{ij} = \frac{1-RH_{ij}^{1/3}}{1-p^{1/3}}$, $p = \frac{1.3}{H_i}$, $RH_{ij} = \frac{h_{ij}}{H_i}$,

DBH_i is the diameter breast height of tree i;

H_i is the total tree height of tree i;

h_{ij} is the particular height;

e_{ij} is the error term, modeled as first order autoregressive (AR(1)), with the covariance $\mathrm{cov}(e_{ij}, e_{ik}) = \sigma^2 \Phi^{k-j}\ k \geq j$, σ^2 the mean squared error, and Φ the estimated correlation between two consecutive observations.

All the coefficients are tested as random effect of individual trees. Final models were selected as these having the lowest value of Akaike information criterion (AIC). Coefficients b_4 and b_6 are modeled as random effects with distributions: $b_4 \sim N(0, \sigma_{b_4}^2)$ and $b_6 \sim N(0, \sigma_{b_6}^2)$, where $\sigma_{b_4}^2$ and $\sigma_{b_6}^2$ are the variance of b_4 and b_6 respectively.

Coefficients of Eq.3-2 were computed with weighed least squares to alleviate heteroscedasticity of residuals. Since the precision of the point-cloud-based stem diameter estimates decreases as stem height increases , less weight is given to estimates at the relatively higher section of the stem. After seeking different weight functions, I eventually selected the weight as $v_{ij} = \frac{1}{RH_{ij}^4}$, which lead to the lowest value AIC and a normal distribution of residuals.

The computations were executed in R 3.5.2 (Gentleman and Ihaka, 2014) using the nlme package (Pinheiro and Bates, 2019). Taper equations are evaluated with leave-one-out validation, using three measures, namely pseudo R^2 (Eq. 3-3), bias (Eq. 3-4), and root mean square error (RMSE) (Eq. 3-5).

$$\text{Pseudo } R^2 = 1 - \frac{\sum_{i=1}^{N}(y_{ij} - \hat{y}_{ij})^2}{\sum_{i=1}^{N}(y_{ij} - \bar{y})^2} \qquad 3\text{-}3$$

$$\text{Bias} = \frac{1}{\text{N}}\sum_{\text{i}=1}^{\text{N}}\frac{\sum_{j=1}^{n_i}(y_{ij} - \hat{y}_{ij})}{n_i} \quad 3\text{-}4$$

$$\text{RMSE} = \frac{\sum_{\text{i}=1}^{\text{N}}\sqrt{\frac{\sum_{j=1}^{n_i}(y_{ij} - \hat{y}_{ij})^2}{n_i}}}{\text{N}} \quad 3\text{-}5$$

where y_{ij} is the measured dib of tree i at height j;

$\hat{y}_{ij}$ is the predicted dib of tree i at height j;

N is the total number of trees;

n_i is the number of stem diameter measurement of tree i.

Although other taper equations are available for Douglas-fir in Pacific Northwest (Garber and Maguire, 2003; Rustagi and Loveless Jr, 1991), I decided to compare our results with the Kozak 04 equation fitted by Poudel et al. (2018), as it is the most recent equation and was obtained from a large sample covering the sample trees' DBH range of this study.

3.2.4. Volume estimation

Total stem volume was estimated using point clouds through two methods. One is to use the summation of the cylinder segments' volume as a surrogate of total stem volume, which is expressed as:

$$V_{i(s)} = \sum_{j=1}^{n_{i(s)}} \pi\left(\frac{dib_{ij(s)}}{200}\right)^2 L_{ij(s)} \quad 3\text{-}6$$

where $V_{i(s)}$ (m^3) is the stem volume of tree i based on cylinder length s, s = 0.5, 1, and 2 m;

$n_{i(s)}$ is the number of fitted cylinders with length s;

$dib_{ij(s)}$ (cm) is the diameter inside bark of j^{th} cylinder models of tree i;

$L_{ij(s)}$ (m) is the j^{th} cylinder length of tree i and length s.

Another is to integrate the stem cross-sectional area computed with Eq. 3-2, and the total stem volume estimates can be described as:

$$V_i = 0.00007853981 \int_0^{H_i} dib_i^2 dh \qquad 3\text{-}7$$

where V_i (m^3) is the stem total inside bark volume of tree i;

dib_i (cm) is the diameter inside bark predicted with taper equations (i.e., M05, M1, M2, and Poudel et al. (2018)) for tree i;

H_i (m) is the total tree height for tree i.

Altogether, six types of point-cloud-based volume estimates were computed (Table 3.1), three of which were based on the direct cylinder model estimates and the other three were based on the taper equations developed with stem diameter estimates from the cylinder models.

As references, stem total volume is also estimated with two empirical equations. One is the FIA-PNW total volume equation developed by Brackett (1977) for western Oregon Douglas-fir:

$$V_i = 0.0283168 \times 10^{\begin{matrix}\{-3.21809+0.04948\times\log_{10}(3.2808\times H_i)\times\log_{10}(0.3937\times dbh_i)-0.15664(\log_{10}(0.3937\times dbh_i))^2+ \\ 2.02132*\log_{10}(0.3937\times dbh_i)+1.63408*\log_{10}(3.2808\times H_i)-0.16185*(\log_{10}(3.2808\times H_i))^2\}\end{matrix}} \qquad 3\text{-}8.$$

Another is the Kozak 04 taper model developed by Poudel et al. (2018). The model form of Poudel et al.'s equation is the same as Eq. 3-2 and the fitted coefficients were provided in Poudel et al. (2018).

Since the FIA-PNW equation has been widely used for stem volume estimation, all the volume estimates are compared with FIA-PNW equation as their relative difference:

$$\text{Relative Difference} = \frac{\text{Volume}_{\text{FIA}} - \text{Volume}_{\text{x}}}{\text{Volume}_{\text{FIA}}} \times 100\% \qquad 3\text{-}9$$

where $\text{Volume}_{\text{FIA}}$ is the stem volume estimates with the FIA-PNW equation;

Volume_{x} is the volume estimates with taper equations (i.e., M05, M1, M2 and Poudel et al. (2018)), and cylinder models (i.e., C05, C1 and C2).

Table 3.1 Summary of methods that are used for stem volume estimates.

Volume estimation	Dataset	Cylinder length	Name
Cylinders	I	0.5 m	C05
	II	1 m	C1
	III	2 m	C2
Taper equations	I	0.5 m	M05
	II	1 m	M1
	III	2 m	M2

3.2.5. Simulation

To access the discrepancy of stem volume estimates produced by various methods, I have simulated trees. I generated simulated trees of DBH classes ranging from 40 – 120 cm and computed their stem volume with the compared methods. The simulated DBH classes were divided into four intervals: 40 – 60 cm, 60 – 80 cm, 80 – 100 cm, and 100 – 120 cm. For each of the four DBH classes, generated 10,000 trees realizations and estimated their volume with all four methods: 1) the point-cloud-based taper equations, 2) cylinder models, 3) taper equation of Poudel et al. (2018), and 4) the FIA-PNW regional equation (Figure 3.4). An iteration contained the following four steps:

Step 1. Identify the DBH of a simulated tree by with a randomly selecting ed a value from a uniform distribution with the range defined by each DBH class;

Step 2. Compute the total height of simulated tree with the DBH-height equation for Douglas-fir Temesgen et al. (2007):

$$H_{sim_i} = 1.3 + \exp(a + b * dbh_{sim_i}^{c}) + \varepsilon_i \quad 3\text{-}10$$

where a = 5.7567, b = -6.7792, and c = - 0.2795;

$\varepsilon_i \sim N(0, \delta_i^2)$;

H_{sim_i} is the simulated tree height in m;

DBH_{sim} is the randomly drawn value from Step 1 in cm;

Step 3. Starting from the bottom of the stem, compute tree dib at specific heights along given sampling intervals (0.5 m, 1 m, and 2 m) with Poudel et al. (2018):

$$dib_{sim_{ij}} = b_{20} dbh_{sim}^{b_{21}} H_{sim}^{b_{22}} X_{ij}^{b_{23} RH_{ij}^4 + \frac{b_{24}}{e^{dbh_{sim}/H_{sim}}} + b_{25} X_{ij}^{0.1} + \frac{b_{26}}{dbh_{sim}} + b_{27} H_{sim}^{1-(\frac{h}{H_{sim}})^{1/3}} + b_{28} X_{ij}} + e_{sim_{ij}} \quad 3\text{-}11$$

$$e_{sim_{ij}} = e_{sim_{i1}} * \varphi_{sim_i} + \epsilon_{ij} \quad 3\text{-}12$$

where $b_{20}, b_{21}, \ldots, b_{28}$ are estimated coefficients of Poudel et al. (2018);

$dib_{sim_{ij}}$ is the predicted dib of simulated tree i at specific height j;

dbh_{sim} and H_{sim} are simulated DBH and tree height from Step 1 and 2;

$X_{ij} = \left(1 - RH_{ij}^{1/3}\right) / \left(1 - k^{1/3}\right)$;

$k = 1.3 / H_{sim}$;

$e_{sim_{ij}}$ is the random error of the predicted dib;

$e_{sim_{i1}}$ is the random error of the first dib prediction of tree i;

φ_{sim_i} is simulated autogressive correlation of tree i;

$\varphi_{sim_i} \sim U(0.6, 1)$, the range of autocorrelation is tested by the pre-modeling of our data set;

ϵ_{ij} is the random effect of error term, $\epsilon_{ij} \sim N(0, \sigma^2_{sim_i})$;

$\sigma^2_{sim_i}$ is the variance of random effect ϵ_{ij}.

Step 4. Compute the volume of the simulated tree with equations defined in section 3.2.4.

Generalized linear model (GLM), allowing the non-normal distribution of error terms, was executed to assess the effects of the computation method and dbh class on stem volume estimates. The GLM is expressed as:

$$volume = Computation\ Method + dbh\ class + Computation\ Method \times dbh\ class \quad \text{3-13}$$

where computation method has 8 levels;

DBH class has four levels.

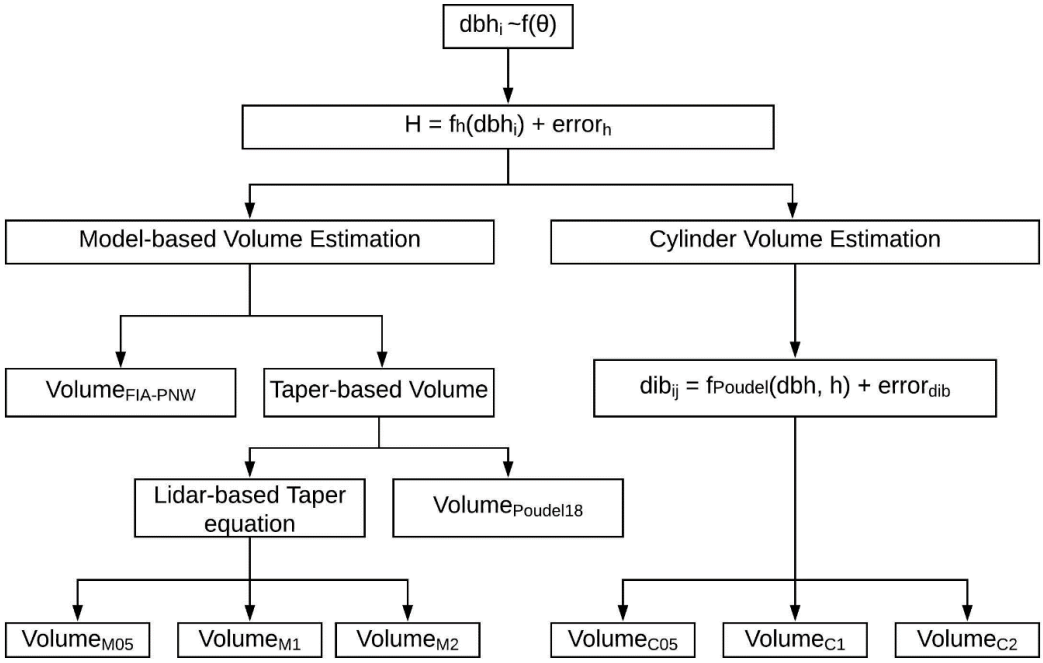

Figure 3.4 Simulation process of volume estimation with different methods. dbh_i is the simulated dbh of *ith* tree and is generated from the uniform distribution of U(a, b), where a and b are the boundary of dbh class. H is simulated total tree height based on Eq. 3-10. $Volume_{FIA-PNW}$ is the estimated stem total volume with the FIA-PNW eequation. $Volume_{M05}$, $Volume_{M1}$, and $Volume_{M2}$ are stem volume estimated with point-cloud-based taper equations, in which dibs are estimates of equation M05, M1 and M2 as it describes in Table 3.1. $Volume_{Poudel18}$ is the estimated stem volume with the taper equation of Poudel et al. (2018). $Volume_{C05}$, $Volume_{C1}$, and $Volume_{C2}$ are volumes of direct cylinder estimates.

3.3. Results

3.3.1. Taper equations

I found that not all the coefficients from Kozak 04 equation are significant (Table 3.2), which supported their elimination from the final model (the case of a2). The autoregressive correlation, Φ, is inversely related to the length of sub-cylinder, indicating error correlation between adjacent pairs of estimates declines with the increasing distance between them. (Table 3.2). The residual plots (Figure 3.5) shows

normality, and homoscedasticity. Leave-one-out validation exhibited little difference in pseudo-R^2, RMSE and bias for all stem diameter equations (Table 3.3). The predicted dib curves of all equations (i.e., M05, M1 and M2) were very similar (Figure 3.6 a - d), with equation M05 yielding slightly higher dib estimates for the lower portion of the stem for large trees (Figure 3.6 c and d). The point-cloud-based taper equations exhibited different patterns from the equation of Poudel et al. (2018) (Figure 3.6), as they yielded smaller dib estimates at the lower third of the stem but larger dib estimates at the middle and upper thirds of the stem, which consequently leads smaller volume estimates from point-cloud-based taper equations for lower two thirds of the stem but greater estimates for total stem volume than estimates from Poudel et al.'s (2018) (Figure 3.6 e – h).

Table 3.2 Fitted coefficients of the Kozak 04 equation with AR(1) structure for point clouds measured inside bark diameter. The standard errors is abbreviated SE. Coefficients b_4 and b_6 are associated with random effects. The given estimates of b_4 and b_6 are the mean estimates of individual trees.

	M05		M1		M2	
Coefficients	Estimates	SE	Estimates	SE	Estimates	SE
a_0	1.0858	0.2274	1.1347	0.2501	1.2026	0.2431
a_1	0.9504	0.0491	0.9416	0.0531	0.9318	0.0563
b_1	0.5529	0.0427	0.5486	0.0441	0.5470	0.0468
b_2	-0.4759	0.2112	-0.4424	0.2256	-0.4682	0.2372
b_3	0.2882	0.0577	0.2700	0.0609	0.2643	0.0650
b_4	-1.3222	0.0844	-1.3266	0.0863	-0.9745	0.0863
b_5	0.0237	0.0104	0.0326	0.0106	0.0472	0.0098
b_6	0.1182	0.0210	0.1093	0.0213	0.0748	0.0213
Φ	0.7246		0.5605		0.3878	

Table 3.3 Evaluation of the three point-cloud-based equations using the leave-one-out validation.

Equation	Measurements (m)	pseudo-R^2	Bias (cm)	RMSE (cm)
M05	0.5	0.94	-0.0650	4.6231
M1	1.0	0.94	-0.1328	4.5354
M2	2.0	0.95	-0.0756	4.5642

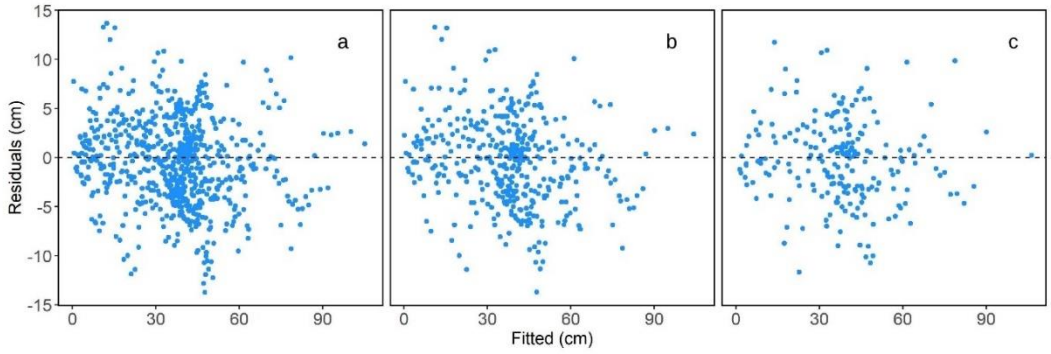

Figure 3.5 Residuals of fitted Kozak 04 equations with the point-cloud-based dib estimates against predicted dib. a. equation M05, b. equation M1, and c. equation M2.

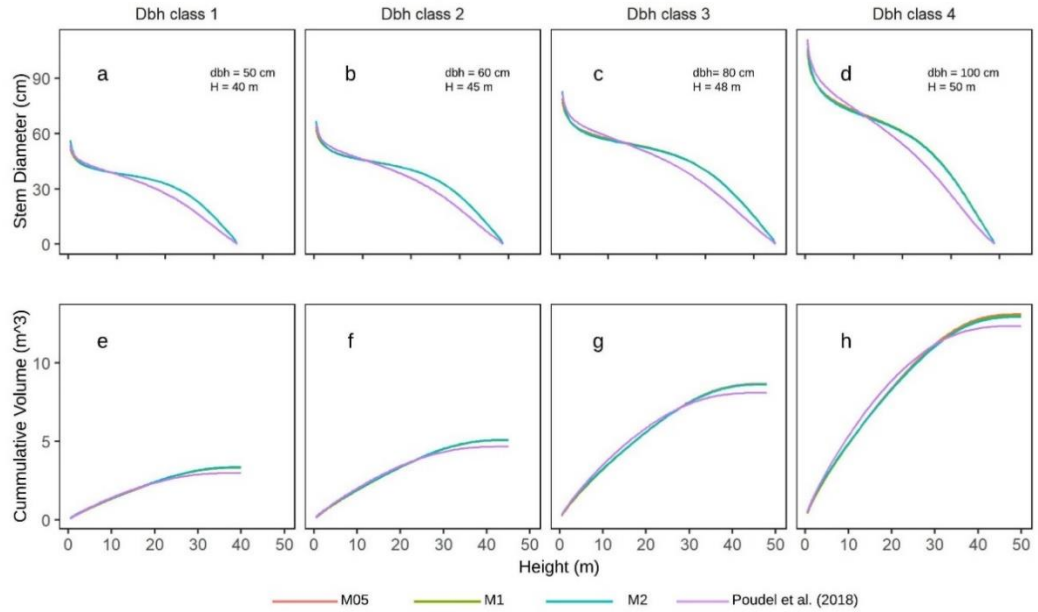

Figure 3.6 Comparisons of taper equations for different tree size. Upper row (a – d): predicted dib curves with the point-cloud-based taper equations; lower row (e – h): cumulative stem volume estimates with the point-cloud-based taper equations. Predictions of Poudel et al. (2018) serve as references.

3.3.2. Volume estimation

Strong correlations (R > 0.98) are present among the point-cloud-based and the FIA-PNW volume estimates (Figure 3.7). Among all the methods, the FIA-PNW equation produced the lowest mean volume estimates, as well as lowest standard deviation of the estimates (Table 3.4). Poudel et al. (2018) produced the most similar total volume estimates to the FIA-PNW equation, with a relative difference of -6% (Table 3.4). Overall, mean volume estimates from point-cloud-based methods are 12% - 17% higher than the mean FIA-PNW estimate. Point-cloud-based taper equations produced the greatest mean volume estimates, as well as the highest standard deviation of the estimates (Table 3.4). The segment length (i.e., 0.5, 1, and 2 m) did not strongly impact the volume estimates of the point-cloud-based taper equations (i.e., M05, M1, and M2). The mean volume estimates and standard deviations are similar across all point-cloud-based taper equations (Table 3.4). The cylinder model estimates were slightly smaller than the taper-based estimates developed with the same segment length, but were 12 - 15% and 7 - 8% higher than the FIA-PNW and Poudel et al. (2018) mean estimates respectively (Table 3.4). Increasing segment length leads to declines in mean volume estimates and the estimate standard deviation of cylinder models (C05 > C1 > C2) (Table 3.4). The point-cloud-based taper equations (i.e., M05, M1, and M2) produced higher mean relative difference to FIA estimates than cylinder models (i.e., C05, C1 and C2), but the standard deviations of the relative difference are much lower in taper-based methods (Table 3.4).

Table 3.4 Summary of volume estimation (i.e., mean and standard deviation) and relative difference to the FIA-PNW volume estimates.

Methods	Model Type	Volume Estimation		Relative difference	
		Mean	St. Dev.	Mean	St. Dev.
Cylinder	C05	5.7200	3.1490	-0.1613	0.13900.1380
	C1	5.6316	3.0880	-0.1449	0.1398
	C2	5.4471	2.9555	-0.1115	0.1400
Taper	M05	5.8191	3.3278	-0.1645	0.0174
	M1	5.8033	3.3035	-0.1627	0.0157
	M2	5.8138	3.2568	-0.1691	0.0199
	Poudel et al. (2018)	5.3783	3.1979	-0.0664	0.0211
FIA-PNW	Total volume	5.0100	2.9000		

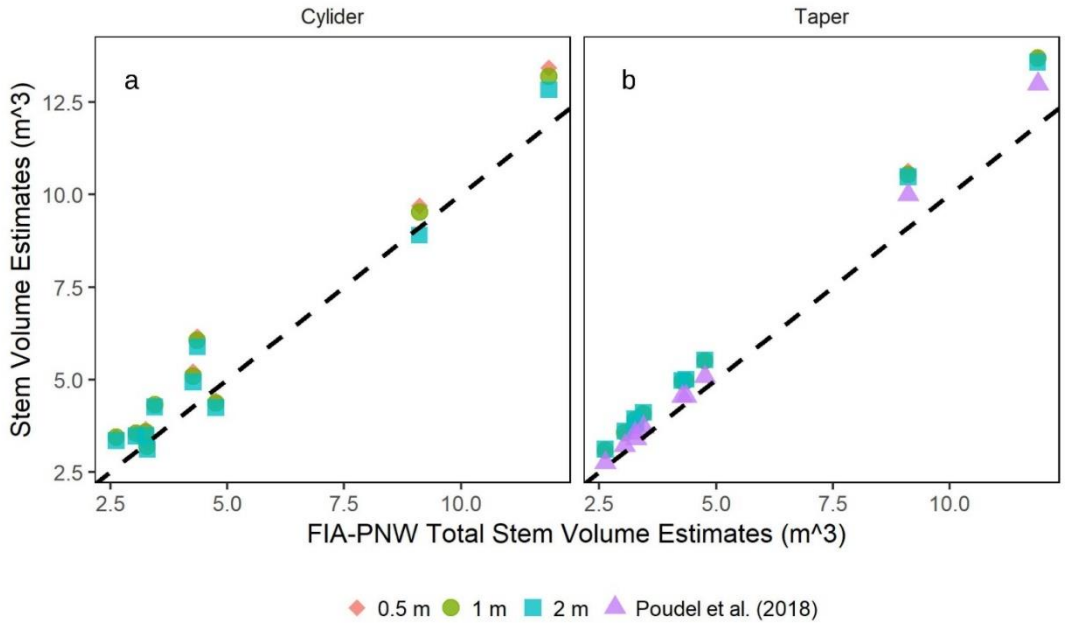

Figure 3.7 Comparison between stem volume estimates of the FIA-PNW equation and other methods. a. Volume estimates of cylinder models. b. Volume estimates of taper-based equations.

3.3.3. Simulated trees

GLM suggested that the mean volume estimates differ in the computation methods, the DBH class of tree and their interaction (p-value < 0.000001) (Table 3.5). As it shows in Figure 3.8 a, increasing divergence exhibited between volume estimates of various computation methods as the DBH class increased. The taper equations (Poudel et al. (2018) and point-cloud-based) produced larger volume estimates, as well as larger standard deviation of estimates, than the FIA-PNW equation (Figure 3.8 a, c). As DBH classes increase from 40 – 60 cm to 100 – 120 cm, Poudel et al.'s mean volume is increasingly greater than the FIA-PNW estimate from 2% to 11% (Table 3.6). The divergence implies the FIA-PNW equation cannot sufficiently yield volume estimates for larger trees. For point-cloud-based taper equations, the mean volume estimates are 14% – 17% (Table 3.6) higher than FIA-PNW estimates across all DBH classes (Figure 3.8 b). All point-cloud-based taper equations yield very similar mean volume estimates for the simulated trees, whereas the standard deviation of volume estimates for a given DBH class increases from model M2 to M05 (Table 3.6), indicating the taper equations developed with smaller segment length could capture more variation of stem volume for a given combination of DBH and tree height. For cylinder-based estimates, the segment length of the sub-cylinders that compose the stem is inversely related to the mean volume estimates, as well as the standard deviation of volume estimates. For a given DBH class, the greatest mean volume estimate and standard deviation of the estimates were observed for model C05 followed by model C1 and C2 (Figure 3.8 a and Table 3.6). For the DBH class of 40 – 60 cm, the mean volume estimates from cylinder models are 1% - 7% smaller mean volume estimates from the FIA-PNW

equation (Figure 3.8 a and Table 3.6). As the DBH class increases, cylinder model estimates grow closer to the FIA-PNW estimates until they eventually surpass them (Figure 3.8 b). For the DBH class of 100 – 120 cm, the mean volume estimates of cylinder models are 2% - 7% greater than the FIA-PNW estimate (Table 3.6). The standard deviation of the relative difference between the cylinder model and FIA-PNW estimates maintain constant but much higher than taper-based estimates for all DBH (Figure 3.8 d), because cylinder models fit directly to the stem shape and yield much variable volume estimates for a given DBH and height combination.

Table 3.5 GLM of volumes estimates as response variable of computation methods and dbh class.

Term	Degree of freedom	Sum square	Mean sum square	F value	P value
Computation methods	8	22047178	2755897	603684.8	<0.000001
Dbh Class	3	7312183	2437394	533916.1	<0.000001
Computation methods × dbhClass	21	19092	909	199.1	<0.000001
Residuals	319968	1460694	5		

Figure 3.8 Simulation results of the 10,000 generated trees by dbh classes: 1 (40 – 60 cm); 2 (60 – 80 cm); 3 (80 – 100 cm); 4 (100 – 120 cm). a. Estimated mean stem volume; b. Mean relative difference between estimates of other methods and the FIA-PNW equation; c. Standard deviation of volume estimates; d. Standard deviation of relative difference.

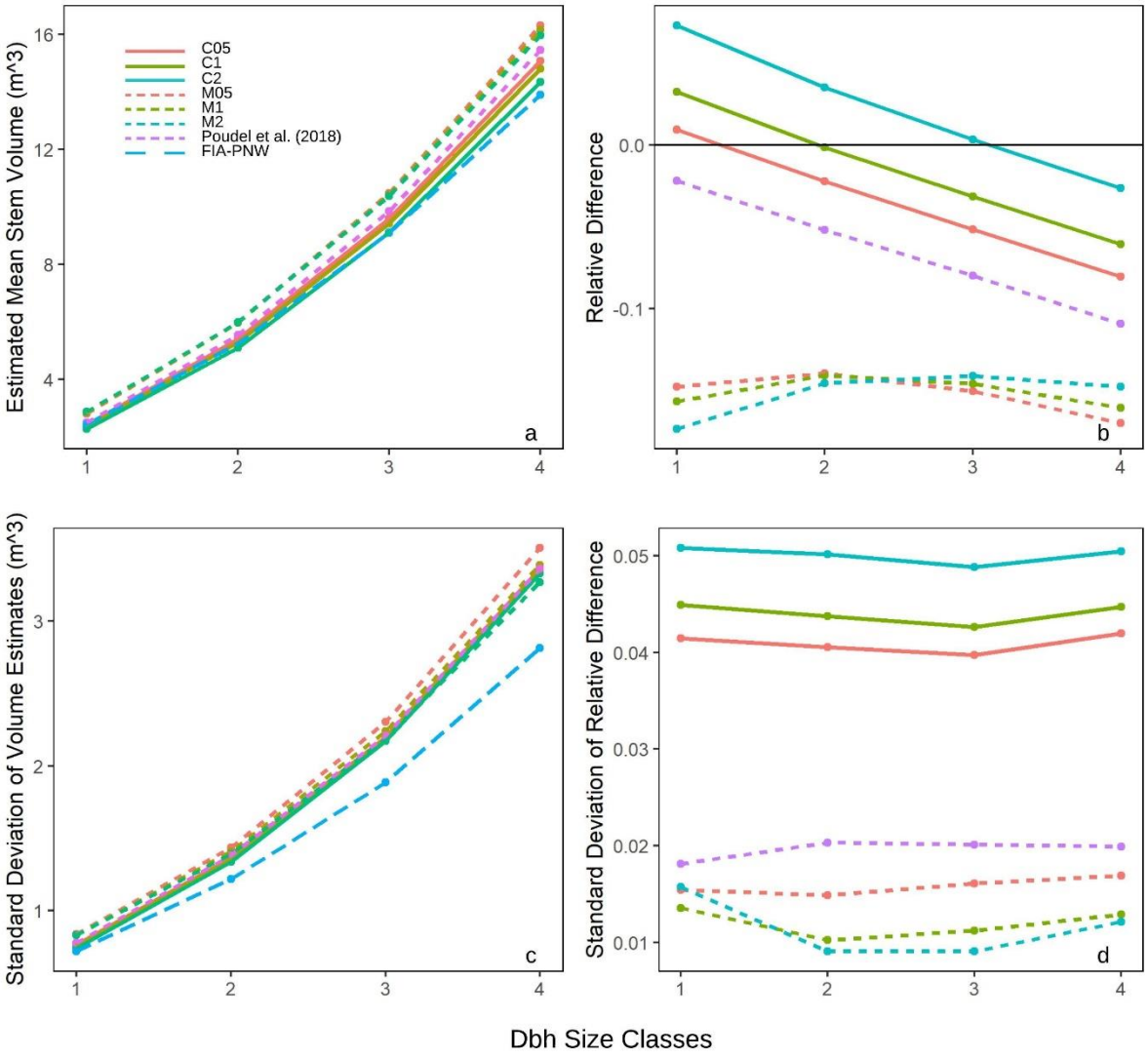

Table 3.6 Simulation results of volume estimates.

DBH Classes (cm)	Model	Mean Volume Estimates(m^3)	Standard Deviation (m^3)	Mean Relative Difference	Standard Deviation of Relative Difference
40 – 60	M05	2.8082	0.8382	-0.1478	0.0154
	M1	2.8271	0.8320	-0.1569	0.0136
	M2	2.8651	0.8319	-0.1738	0.0157
	Poudel et al. (2018)	2.4917	0.7765	-0.0221	0.0181
	C05	2.4172	0.7667	0.0094	0.0415
	C1	2.3630	0.7564	0.0323	0.0449
	C2	2.2670	0.7381	0.0729	0.0508
	FIA-PNW	2.4278	0.7203	NA	NA
60 – 80	M05	5.9627	1.4345	-0.1399	0.0149
	M1	5.9634	1.4086	-0.1410	0.0102
	M2	5.9835	1.3896	-0.1458	0.0091
	Poudel et al. (2018)	5.5445	1.3799	-0.0520	0.0203
	C05	5.3918	1.3685	-0.0224	0.0405
	C1	5.2842	1.3558	-0.0014	0.0437
	C2	5.0969	1.3373	0.0351	0.0502
	FIA-PNW	5.2517	1.2177	NA	NA
80 – 100	M05	10.4850	2.3036	-0.1507	0.0161
	M1	10.4321	2.2410	-0.1460	0.0112
	M2	10.3791	2.1851	-0.1412	0.0091
	Poudel et al. (2018)	9.8503	2.2099	-0.0800	0.0201
	C05	9.5973	2.2000	-0.0517	0.0397
	C1	9.4161	2.1879	-0.0315	0.0426
	C2	9.1065	2.1703	0.0033	0.0488
	FIA-PNW	9.0914	1.8857	NA	NA
100 – 120	M05	16.3040	3.5054	-0.1703	0.0169
	M1	16.1546	3.3857	-0.1608	0.0129
	M2	15.9599	3.2679	-0.1480	0.0121
	Poudel et al. (2018)	15.4604	3.3579	-0.1094	0.0199
	C05	15.0725	3.3638	-0.0807	0.0420
	C1	14.8014	3.3471	-0.0607	0.0447
	C2	14.3383	3.3295	-0.0264	0.0505
	FIA-PNW	13.9021	2.8139	NA	NA

3.4. Discussion

We compared total stem volume estimates for mature Douglas-fir yielded from eight methods, six of which are based on the applications of terrestrial lidar point clouds and two of which are based on empirical equations. Empirical equations are usually developed based on well-known tree allometry studied from destructive samples acquired from field measurements and can be repeatedly used for various inventory purposes. The advantages of using lidar data to develop empirical taper equations are the nondestructive estimates of stem diameter at any specific height and permanent data storage. As being developed with large samples, empirical equations are usually representative of population means of the variables of interest. In contract, direct cylinder model estimates account for individual tree structural variation and produce more accurate volume estimates for individual trees.

A wealth of studies showed that the accuracy of current point-cloud-based stem diameter measurements ranges from 1 – 3 cm (Côté et al., 2011; Hopkinson et al., 2004; Strahler et al., 2008; Tansey et al., 2009; Watt and Donoghue, 2005; Wezyk et al., 2007), and largely depends on the scanner type, number of scans, point density, position of scans, and forest types (Dassot et al., 2011). Previous studies that used the same type of terrestrial laser scanner to model canopy characteristics reported accuracies of DBH estimates within 2 cm (Calders et al., 2015; Huang et al., 2011; Ishak et al., 2015; Tao et al., 2015). Currently, circular or convex hull approximations are commonly used to calculate stem perimeter (Calders et al., 2015; Huang et al., 2011; Liang et al., 2012; Olofsson et al., 2014). In this study, we modeled stems with circular models, as it allows continuous volume estimates along the stem with relative low computation cost.

3.4.1. **Sensitivity of point-cloud-based volume estimates to segment length of cylinder models**

Within the test range of 0.5 m – 2 m, the segment length of sub-cylinders composing the stems did not exhibit a strong influence on the performance of the point-cloud-based taper equations since similar RMSE and R2 were observed for all point-cloud-based taper equations (Table 3.3). For a given DBH class, the difference of mean volume estimates from three point-cloud-based taper equations is less than 3%. The volume estimate difference in the three point-cloud-based taper equation is mainly caused by the variation in the stem tapering rate. For trees with small DBH, the large sub-cylinder length might not adequately capture the tapering rate at the upper stem resulting in overestimates of stem diameters. For trees with large DBH, large sub-cylinder length overgeneralizes the tree stump, where contains most of the tree volume, resulting in underestimates of the stem volumes.

Cylinder volume estimates exhibit a similar pattern with the taper-based estimates that models with smaller sub-cylinder lengths yielded greater volume estimates and standard deviation of the estimates. However, for a specific tree, the difference in volume estimates from cylinder models with different segment lengths ranges from 1% - 14%, which is more variable than the difference observed for estimates from taper-based equations, since individual tree stem variation is fitted locally in the cylinder models but taper equations were developed by minimizing estimation errors of all observations.

For future applications, the cylinder segment length may need to be adjusted proportionally to the total length, the shape, and the diameter of the stem. The fixed segment length could cause errors to the model construction for where sharp angles happen (Binney and Sukhatme, 2009), especially for highly crooked stems, which require fine cylinders to better approximate the stem shapes. Fixed segment lengths less than 0.5 m was used by Thies et al. (2004) to construct sequent cylinder models for highly crooked beech and cherry stems whose lengths were less than 12 m. In our study, the selected segment lengths did not cause problematic model construction for total conifer stem. Variable segment lengths can improve the cylinder models' accuracy of locally approximating the stem (Binney and Sukhatme, 2009), but they are subjected to the decision of segment length of a given stem section and may introduce extra variations to the volume estimates yielded from the model. Defining the segment length as a fixed ratio to the fitted cylinder radius is a way to better approximate the stem tapering shape (Calders et al., 2015; Raumonen et al., 2013b). The protocol of defining the length to radius ratio requires prior information of a taper equation (Raumonen et al., 2013b). As the segment length is dynamically determined from the ongoing construction of successive cylinders, the locally modeled cylinder radius is crucial for successful cylinder construction for the follow-on segment, which works ideally for stems with dense point coverage.

3.4.2. **Difference of total stem volume estimates from various methods**

The mean and standard deviation of the simulated volume estimates reveal the existence of significant difference in the estimated volume from various methods.

Large relative difference between point-cloud-based and the FIA-PNW volume estimates may indicate great divergences between local and regional stem volume estimates. However, a lower standard deviation of the relative difference implies a higher possibility of a systematic calibration to reach consistent estimates when different methods are used in an inventory system.

For the sample trees, the FIA-PNW equation yielded volume estimates that are 6% - 17% lower than other estimates. Especially for trees with DBH greater than 100 cm, the FIA-PNW equation yielded mean volume estimates that are 17% and 10% lower than estimates from model M05 and Poudel et al. (2018) respectively. Slight underestimation of the FIA-PNW equations for stem volume of trees having DBH greater than 90 cm were also observed by Poudel and Temesgen (2016). However, the following study of Poudel et al. (2018) found that the bias of the FIA-PNW volume estimates of Douglas-fir was smaller than the bias of the estimates yielded by the refitted Kozak 04 equation. Therefore, uncertainties arise when regional equations are applied to volume estimation for individual trees at the local scale (Smith et al., 2006) and when plot-level aggregation of individual tree volume estimates were upscaled to estimation at regional scales (Berger et al., 2014; McRoberts and Westfall, 2013). Nevertheless, extraordinarily high correlations were observed between estimates of all point-cloud-based methods and estimates yielded by empirical equations (Figure 3.7), suggesting a high possibility of calibration bringing consistency to volume estimates yielded by different methods.

As the cylinder models in the simulation were directly derived from Poudel et al. (2018)' s equation, they only help investigate the impact from the sub-cylinder segment lengths on stem volume estimation, but their estimates were not directly comparable with estimates yielded by the point-cloud-based taper equations (i.e. M05, M1, and M2), which were developed from the real scanned trees. Considering the high accuracy level that lidar estimates have achieved (Brede et al., 2019b; Lau et al., 2018; Tanago et al., 2018), we assume in reality cylinder models constructed with human-eye interference would yield volume estimates that are closer to the true volumes of a specific tree than volume estimates yielded from an empirical equation, which only produces true mean volume estimates for a large sample that are similar to the samples used to develop the equation. In comparison with volume estimates of the point-cloud-based taper equations, cylinder volume estimates exhibited higher standard deviations of the relative difference to FIA-PNW estimates (Table 3.4), indicating the difference is more associated with individual tree random effects and stem form variation rather than systematic effects from the parameter and model form specification of the equations.

3.5. Conclusion

This study provided a system of using point-cloud-based cylinder models to develop taper equations and generate volume estimates. Despite the small sample size, total stem volumes estimated from both the point-cloud-based taper equations and cylinder models were comparable to the existing values obtained with significant expenses and field effort. For developing taper equations, the sample interval along the stem did not impact the taper equation performance. However, segment length of cylinder models

significantly influenced the stem volume estimates, which are more evident for trees with large dbh. Cylinder models produced more similar volume estimates to the FIA-PNW equation, with a lower relative difference than estimates of the point-cloud-based taper equations. However, the standard deviation of relative difference is much lower for the point-cloud-based taper equations. As they directly fit the stem shape, cylinder models are supposed to produce more accurate estimates of individual stem volume. However, application of cylinder models at regional level could be biased, as depends on the segment length and shape of individual stems. In contrast, the point-cloud-based taper equations are less accurate at predicting individual stem volume, but they are easier to be calibrated to ensure consistency with existing volume equations. I expect that the expensive and time-consuming field measurements that require tree felling would be replaced with point cloud estimates, as are significantly faster, executed on standing trees, and provide a timeless snapshot of the tree or stand. Therefore, considering availability of terrestrial laser scanners and the constant improvement of the algorithms focused on estimation of tree attributes form point clouds, such as DendroCloud or TreeQSM, I think that lidar and photogrammetric point clouds would be the main source of acquiring forest inventory data in the next decade.

References

Avery, T.E., and Burkhart, H.E. 2015. Forest measurements. Waveland Press.

Berger, A., Gschwantner, T., McRoberts, R.E., and Schadauer, K. 2014. Effects of measurement errors on individual tree stem volume estimates for the Austrian National Forest Inventory. Forest Science **60**(1): 14–24.

Biging, G.S. 1984. Taper equations for second-growth mixed conifers of Northern California. Forest Science **30**(4): 1103–1117.

Binney, J., and Sukhatme, G.S. 2009. 3D tree reconstruction from laser range data. *In* 2009 IEEE International Conference on Robotics and Automation. IEEE. pp. 1321–1326.

Brackett, M. 1977. Notes on tarif tree volume computation.

Brede, B., Calders, K., Lau, A., Raumonen, P., Bartholomeus, H.M., Herold, M., and Kooistra, L. 2019. Non-destructive tree volume estimation through quantitative structure modelling: Comparing UAV laser scanning with terrestrial LIDAR. Remote Sensing of Environment **233**: 111355. doi:10.1016/j.rse.2019.111355.

Burkhart, H.E., and Tomé, M. 2012. Modeling forest trees and stands. Springer Science & Business Media.

Burt, A., Disney, M., Raumonen, P., Armston, J., Calders, K., and Lewis, P. 2013. Rapid characterisation of forest structure from TLS and 3D modelling. IEEE. pp. 3387–3390.

Calders, K., Newnham, G., Burt, A., Murphy, S., Raumonen, P., Herold, M., Culvenor, D., Avitabile, V., Disney, M., Armston, J., and Kaasalainen, M. 2015. Nondestructive estimates of above-ground biomass using terrestrial laser scanning. Methods in Ecology and Evolution **6**(2): 198–208. doi:10.1111/2041-210X.12301.

Côté, J.-F., Fournier, R.A., and Egli, R. 2011. An architectural model of trees to estimate forest structural attributes using terrestrial LiDAR. Environmental Modelling & Software **26**(6): 761–777. doi:10.1016/j.envsoft.2010.12.008.

Dassot, M., Constant, T., and Fournier, M. 2011. The use of terrestrial LiDAR technology in forest science: application fields, benefits and challenges. Annals of Forest Science **68**(5): 959–974. doi:10.1007/s13595-011-0102-2.

Fang, R., and Strimbu, B.M. 2017. Stem Measurements and Taper Modeling Using Photogrammetric Point Clouds. Remote Sensing **9**(7): 716.

Fang, Z., Borders, B.E., and Bailey, R.L. 2000. Compatible Volume-Taper Models for Loblolly and Slash Pine Based on a System with Segmented-Stem Form Factors. Forest Science **46**(1): 1–12. doi:10.1093/forestscience/46.1.1.

Garber, S.M., and Maguire, D.A. 2003. Modeling stem taper of three central Oregon species using nonlinear mixed effects models and autoregressive error structures. Forest Ecology and Management **179**(1–3): 507–522.

Gentleman, R., and Ihaka, R. 2014. R. University of Auckland, New Zealand, Auckland, New Zealand.

Hackenberg, J., Spiecker, H., Calders, K., Disney, M., and Raumonen, P. 2015. SimpleTree—an efficient open source tool to build tree models from TLS clouds. Forests **6**(11): 4245–4294.

Henning, J.G., and Radtke, P.J. 2006. Detailed stem measurements of standing trees from ground-based scanning lidar. Forest Science **52**(1): 67–80.

Hopkinson, C., Chasmer, L., Young-Pow, C., and Treitz, P. 2004. Assessing forest metrics with a ground-based scanning lidar. Canadian Journal of Forest Research **34**(3): 573–583.

Huang, H., Li, Z., Gong, P., Cheng, X., Clinton, N., Cao, C., Ni, W., and Wang, L. 2011, March. Automated Methods for Measuring DBH and Tree Heights with a Commercial Scanning Lidar. Text. doi:info:doi/10.14358/PERS.77.3.219.

Ishak, N.I., Bakar, M.A.A., Rahman, M.Z.A., Rasib, A.W., Kanniah, K.D., Shin, A.L.M., and Razak, K.A. 2015. ESTIMATING SINGLE TREE STEM AND BRANCH BIOMASS USING TERRESTRIAL LASER SCANNING. Jurnal Teknologi **77**(26). doi:10.11113/jt.v77.6860.

Kangas, A., and Maltamo, M. 2006. Forest Inventory: Methodology and Applications. Springer Science & Business Media.

Kershaw, J.A., Ducey, M.J., Beers, T.W., and Husch, B. 2017. Forest Mensuration. *In* 5th edition. Wiley Blackwell, Hoboken NJ.

Kozak, A. 2004. My last words on taper equations. The Forestry Chronicle **80**(4): 507–515.

Lau, A., Bentley, L.P., Martius, C., Shenkin, A., Bartholomeus, H., Raumonen, P., Malhi, Y., Jackson, T., and Herold, M. 2018. Quantifying branch architecture of tropical trees using terrestrial LiDAR and 3D modelling. Trees **32**(5): 1219–1231. doi:10.1007/s00468-018-1704-1.

Leica Geosystems. 2019. Leica Cyclone. Leica Geosystems.

Liang, X., Litkey, P., Hyyppa, J., Kaartinen, H., Vastaranta, M., and Holopainen, M. 2012. Automatic Stem Mapping Using Single-Scan Terrestrial Laser Scanning. IEEE Transactions on Geoscience and Remote Sensing **50**(2): 661–670. doi:10.1109/TGRS.2011.2161613.

Maguire, D.A., and Hann, D.W. 1990. Bark Thickness and Bark Volume in Southwestern Oregon Douglas-Fir. west j appl for **5**(1): 5–8. doi:10.1093/wjaf/5.1.5.

McRoberts, R.E., and Westfall, J.A. 2013. Effects of uncertainty in model predictions of individual tree volume on large area volume estimates. Forest Science **60**(1): 34–42.

Mikita, T., Janata, P., and Surový, P. 2016. Forest stand inventory based on combined aerial and terrestrial close-range photogrammetry. Forests **7**(8): 165.

Olofsson, K., Holmgren, J., and Olsson, H. 2014. Tree Stem and Height Measurements using Terrestrial Laser Scanning and the RANSAC Algorithm. Remote Sensing **6**(5): 4323–4344. doi:10.3390/rs6054323.

Pinheiro, J., and Bates, D. 2019. nlme: Linear and Nonlinear Mixed Effects Models. R package version 3.1-138. Available from https://svn.r-project.org/R-packages/trunk/nlme.

Pitkänen, T.P., Raumonen, P., and Kangas, A. 2019. Measuring stem diameters with TLS in boreal forests by complementary fitting procedure. ISPRS Journal of Photogrammetry and Remote Sensing **147**: 294–306. doi:10.1016/j.isprsjprs.2018.11.027.

Poudel, K.P., and Hailemariam, T. 2016. Calibration of volume and component biomass equations for Douglas-fir and lodgepole pine in Western Oregon forests. The Forestry Chronicle **92**(2): 172–182.

Poudel, K.P., Temesgen, H., and Gray, A.N. 2018. Estimating upper stem diameters and volume of Douglas-fir and Western hemlock trees in the Pacific northwest. For. Ecosyst. **5**(1): 16. doi:10.1186/s40663-018-0134-2.

Raumonen, P., Kaasalainen, M., Åkerblom, M., Kaasalainen, S., Kaartinen, H., Vastaranta, M., Holopainen, M., Disney, M., and Lewis, P. 2013. Fast Automatic Precision Tree Models from Terrestrial Laser Scanner Data. Remote Sensing **5**(2): 491–520. doi:10.3390/rs5020491.

Rustagi, K.P., and Loveless Jr, R.S. 1991. Compatible variable-form volume and stem-profile equations for Douglas-fir. Canadian journal of forest research **21**(2): 143–151.

Smith, J.E., Heath, L.S., Skog, K.E., and Birdsey, R.A. 2006. Methods for calculating forest ecosystem and harvested carbon with standard estimates for forest types of the United States.

Smith, W.B. 2002. Forest inventory and analysis: a national inventory and monitoring program. Environmental Pollution **116**: S233–S242. doi:10.1016/S0269-7491(01)00255-X.

Strahler, A.H., Jupp, D.L.B., Woodcock, C.E., Schaaf, C.B., Yao, T., Zhao, F., Yang, X., Lovell, J., Culvenor, D., Newnham, G., Ni-Miester, W., and Boykin-Morris, W. 2008. Retrieval of forest structural parameters using a ground-based lidar instrument (Echidna®). Canadian Journal of Remote Sensing **34**(sup2): S426–S440. doi:10.5589/m08-046.

Tanago, J.G. de, Lau, A., Bartholomeus, H., Herold, M., Avitabile, V., Raumonen, P., Martius, C., Goodman, R.C., Disney, M., Manuri, S., Burt, A., and Calders, K. 2018. Estimation of above-ground biomass of large tropical trees with terrestrial LiDAR. Methods in Ecology and Evolution **9**(2): 223–234. doi:10.1111/2041-210X.12904.

Tansey, K., Selmes, N., Anstee, A., Tate, N.J., and Denniss, A. 2009. Estimating tree and stand variables in a Corsican Pine woodland from terrestrial laser scanner data. International Journal of Remote Sensing **30**(19): 5195–5209. doi:10.1080/01431160902882587.

Tao, S., Wu, F., Guo, Q., Wang, Y., Li, W., Xue, B., Hu, X., Li, P., Tian, D., Li, C., Yao, H., Li, Y., Xu, G., and Fang, J. 2015. Segmenting tree crowns from terrestrial and mobile LiDAR data by exploring ecological theories. ISPRS Journal of Photogrammetry and Remote Sensing **110**: 66–76. doi:10.1016/j.isprsjprs.2015.10.007.

Temesgen, H., Hann, D.W., and Monleon, V.J. 2007. Regional Height–Diameter Equations for Major Tree Species of Southwest Oregon. west j appl for **22**(3): 213–219. doi:10.1093/wjaf/22.3.213.

Thies*, M., Pfeifer, N., Winterhalder, D., and Gorte, B.G. 2004. Three-dimensional reconstruction of stems for assessment of taper, sweep and lean based on laser scanning of standing trees. Scandinavian Journal of Forest Research **19**(6): 571–581. Taylor & Francis.

Walters, D.K., and Hann, D.W. 1986. Taper equations for six conifer species in southwest Oregon.

Watt, P., and Donoghue, D. 2005. Measuring forest structure with terrestrial laser scanning. International Journal of Remote Sensing **26**(7): 1437–1446.

West, P.W., and West, P.W. 2009. Tree and forest measurement. Springer.

Wezyk, P., Koziol, K., Glista, M., and Pierzchalski, M. 2007. Terrestrial laser scanning versus traditional forest inventory: First results from the Polish forests. *In* ISPRS workshop on laser scanning. pp. 12–14.

White, J.C., Coops, N.C., Wulder, M.A., Vastaranta, M., Hilker, T., and Tompalski, P. 2016. Remote sensing technologies for enhancing forest inventories: A review. Canadian Journal of Remote Sensing **42**(5): 619–641. Taylor & Francis.

Chapter 4 Comparison of mature Douglas-firs' crown structures developed with two quantitative structural models using TLS point clouds for neighboring trees in a natural regime stand

Abstract

The Douglas fir crown structure serves important ecological functions in regulating the ecosystem of the Pacific Northwest (PNW). Mapping and modeling of the Douglas-fir crown has traditionally focused on young plantations or old-growth forests. The crown description in natural regime forests is limited by data availability. Terrestrial laser scanning (TLS) enables the acquisition of crown structural attributes, even in dense forests, at a fine-scale. The vertical and horizontal distributions of the fine-scale branch attributes, such as branch diameter, branch length, and branch insertion angle, will reflect the crown behaviors towards light resource availability, as a result of neighborhood competition. The main objective of the study is to compare crown structural models of a group of neighboring trees developed with two TLS-based procedures, namely: semi-automatic (Cyclone software) and automatic (TreeQSM) procedures. The estimated crown attributes are the branch diameter, branch length, branch insertion angle, height of branch insertion point, and branch azimuth. The results show that branch azimuth distribution does not differ between TreeQSM and Cyclone for most of the sample trees. However, the TreeQSM and Cyclone identified branches exhibit different distributions of insertion height. A paired t-test indicates no difference between the mean branch diameter of Cyclone and TreeQSM at an individual tree level. However, Cyclone estimated that the branch length and branch insertion angle are 0.49 m and 9.9° greater than the TreeQSM estimates, respectively.

Repeat measurements of the analysis of variance (ANOVA) suggest that the height along the stem is an influential factor of the difference between the Cyclone and TreeQSM branch diameter estimates. To test whether TLS-based estimates are within the ranges of the previous observations, I computed the tree crown attributes of second- and old-growth trees using Monte Carlo simulations for diameter at breast height (DBH) class 50–55 cm, 60–65 cm, and 85–105 cm. I found that the crown attributes estimated from both of the TLS-based methods are between the simulated second- and old-growth trees, except for DBH 85–105 cm. The TLS-based crown structural models show increasingly diverse distributions of branch insertion angles and increasing branch exclusion as DBH increases. Cyclone-based crown structural models are consistent with previous studies. However, TreeQSM-based crown structural models omitted a significant number of branches and generated crown structures with reduced plausibility.

Keywords: LiDAR; point clouds; TreeQSM; Cyclone software; crown structure; Douglas-fir; branches attributes; neighborhood; light resource availability

4.1. Introduction

Crown structure of Douglas-fir forests plays an important role in shaping abiotic arrangements and eventually determines the biodiversity of the temperate forest ecosystem in Pacific Northwest (Franklin et al., 2002; Ishii et al., 2004; Spies et al., 2006). Characterizing canopy architecture will significantly enhance the understanding of forest microclimate variability (Aussenac, 2000; Chen and Franklin, 1997), foliage distribution (Brunner and Nigh, 2000; Parker, 1997), epiphyte abundance (Clement and Shaw, 1999; Lyons et al., 2000; Sillett and Neitlich, n.d.; Sillett and Bailey, 2003), growth productivity (Barbour et al., 1997; Briggs et al., 2007; Maguire et al., 1998) and distribution of wildlife habitats (Michel and Winter, 2009). Furthermore, knowledge of forest structural dynamics, particularly of the crown, guides silvicultural practices aimed at achieving economic, social and ecological benefits (Barbour et al., 1997; Bauhus et al., 2009; Davis et al., 2007; Swanson and Franklin, 1992).

The crowns of young- to mid-age Douglas-fir plantation trees have been successfully modeled with allometric equations focused on branch diameter (Maguire et al., 1994, 1999, 1991), branch length (Roeh and Maguire, 1997), branch insertion angle (Roeh and Maguire, 1997) and foliage mass (Kershaw Jr. and Maguire, 1996; Maguire and Bennett, 1996; Mori and Hagihara, 1991). In comparison, applications of allometric equations in describing old-growth Douglas-fir crown were less fruitful, as more uncertainties are induced by the complex structural variability caused by canopy closure and stratification (Franklin et al., 2002). In such cases, the crown architectures were conceptually (Ishii and Ford, 2002; Pelt and Sillett, 2008; Van Pelt et al., 2006;

Van Pelt and North, 1996) and numerically (Ishii et al., 2000; Ishii and Wilson, 2001) documented almost exclusively for individual "big trees." Descriptions of mature crowns of trees from natural regime stands are constrained by the difficulties in the acquisition of the branch attributes. Therefore, crown development of trees located inside unmanaged stands is limited.

The point clouds produced by terrestrial laser scanning (TLS) provide a reliable source of data for 3D forest measurements (Coops et al., 2007; Danson et al., 2007; Hilker et al., 2010b). At the stand level, TLS can successfully estimate stand basal area, stem mean diameter, canopy height, and gap fraction (García et al., 2011; Moskal and Zheng, 2012). At the tree level, TLS has also been proven to successfully measure tree crown width, diameter at breast height (DBH), total height and leaf area distribution (Moorthy et al., 2011; Moskal and Zheng, 2012; Srinivasan et al., 2015). Point clouds convey spatial coordinates and laser intensity of reflecting surfaces, with reduced information on the type of surface. Therefore, fine-scale crown geometric measurements, such as branch diameter, branch length, and branch insertion angle, are difficult to be automatically retrieved without external human input or with the use of advanced algorithms. Such algorithms are the quantitative structural models (QSM), which extract tree woody structure based on the topographic relationship between points and approximate tree skeleton with cylinder models (Delagrange et al., 2014; Hackenberg et al., 2015a; Raumonen et al., 2013b; Zeide and Pfeifer, 1991). QSM has effectively reconstructed stems and branches for broadleaf trees and accurately measured tree height (Ghimire et al., 2017), DBH (Ghimire et al., 2017), branch diameter (Lau et al., 2018), branch length (Lau et al., 2018), stem and branch volumes (Burt et al., 2013;

Lau et al., 2018). The accurate stem and branch volume estimations from QSM also enable rapid biomass estimation at tree level (Raumonen et al., 2015; Tanago et al., 2018). From an ecological perspective, QSM also reveals tree structural development in response to ecosystem conditions (Jackson et al., 2019; Malhi et al., 2018).

Despite the successful applications of QSM in estimating big branches of broadleaf trees, QSM tends to overestimate the diameters of smaller branches (Hackenberg et al., 2015a; Lau et al., 2018), because QSM is sensitive to noise, leaf-on points, and disconnected point clouds, which cause poor reconstruction of branch models. Therefore, the application of QSM to coniferous species is challenged by the small leaf on branches. For coniferous trees, TLS-based crown structure studies focus on depicting general crown profile (Ferrarese et al., 2015; van Leeuwen et al., 2013), rather than describing the inside canopy details, particularly branch arrangements and dimensions. To date, few studies have characterized Douglas-fir branch architecture of average trees from stands that experienced limited management (Clement and Shaw, 1999; Maguire et al., 1999; Pelt and Sillett, 2008). The overarching objective of the present study is to numerically describe the crown architecture of average Douglas-fir trees from point clouds. Because the size and location of branches can be estimated using automatic procedures such as QSM, or semi-automatic ones such as Cyclone based, a primary objective of our study is to test the utility of QSM for Douglas-fir crown measurements.

Under similar environmental conditions, Douglas-firs' crown structure reflect the results of the light availability (Pelt and Sillett, 2008). For mature crowns, as the crowns

expand, competition among neighboring crowns triggers the branch exclusion and diversification of branch insertion angles and branch size (Franklin et al., 2002) to ensure sufficient light resource. Previous crown structural modeling has been focused on unrelated individual trees (Ishii et al., 2000; Ishii and McDowell, 2002; Ishii and Wilson, 2001; Pelt and Sillett, 2008; Van Pelt et al., 2006). However, neighborhood density in the canopy is a significant factor on crown dynamic (Getzin et al., 2008; Getzin and Wiegand, 2007; Kramer et al., 2019). In this study, I attempt to develop crown structures of a group of neighboring trees with a variety of sizes using TLS point clouds. A set of plausible crown structural models will reflect the neighborhood impact on crown development as tree size increases. Therefore, the secondary objective of our study is to examine whether TLS-based crown structure will reflect the light-induced neighboring competition's impact on crown structure of varying sized trees.

To achieve the two major objectives, I was interested in addressing four subobjectives:

1. To describe the crown of the average (understood as not-special) dominant and co-dominant Douglas-fir, from different DBH classes using point clouds.
2. To examine whether the TLS-based estimates of the crown fit within the range of existing observations for second-growth plantations and old-growth stands.
3. To compare the branch dimensions estimated using Cyclone, the semi-automatic approach, with the values supplied by TreeQSM, the automatic approach.

4. To examine the neighborhood impact on Douglas-fir crown structure development based on conceptual crown models developed with TLS point clouds.

4.2. Data and methods

4.2.1. Study sites and data collection

The study was conducted in a Douglas-fir stand located in the west side of the Cascades, Oregon, in the HJ Andrews Experimental Forest. Inside the stand, an 80 m × 100 m plot (Figure 4.1 b) with trees on average 38 m tall (standard deviation of 11.5 m), were scanned from 22 locations with a RIEGL VZ400i scanner. The first scan was located at the center of the plot and was programmed for an execution of a complete rotation (i.e., 360º) in 10-min, whereas all subsequent scans took only 5 min. A set of 76 tie-points were placed inside the plot and their coordinates were surveyed with a Trimble RTS633 total station. The registration of individual scans was performed in Leica Cyclone (Leica Geosystems, 2019). Scans were aligned using cloud-to-cloud comparison, constrained by the 76 tie-points. Mean absolute error of constraint and cloud-to-cloud alignments are 0.009 m and 0.016 m respectively. The sample trees selected in this study meet three conditions: 1) trees are composed of abundance of point clouds at least for lower-middle crown, 2) belong to the dominant and codominant crown class (Nyland, 1996), 3) the trees are neighbors, 4) the trees are composed of several DBH classes at least 10 trees fulfill the first two conditions. Therefore, I randomly selected the point clouds of 10 dominant and codominant trees with adjacent crowns (Figure 4.1 a and c). The points associated with each tree were visually delineated in Cyclone (Figure 4.1 a and c). Visual extraction of sample trees is difficult

at the middle section of crowns where a significant number of interlocking branches are found within adjacent crowns. To ensure a clear view of point clouds rendering in Cyclone, individual crowns are roughly divided into sublayers, crown delineation is performed in sublayer level, then, point clouds of sublayers were eventually integrated as an individual tree. Visual delineation of individual crowns largely depends on the connective relationship between stem and branch points. Points rendering based on intensity segregates stem, branch and leaf points and supports visual identification of the stem and its connected branches. The major errors of visual extraction of crowns are the omission of entire or partial branches and inclusion of branches from neighboring crowns. To reduce the sample tree segregation errors, visual delineations were performed from different angles.

Table 4.1 Summary of involved crown attributes.

Attribute	Abbreviation	Formula
Diameter at breast height	DBH	
Total Tree height	THT	
Branch diameter	BD	
Branch length	BL	
Branch insertion angle	α	
Branch azimuth	θ	
Height of branch i's insertion point	h_i	
Height of crown base	h_{BC}	
Crown Length	CL	$CL = THT - h_{BC}$
Branch depth into the crown	DINC	$DINC = THT - h_i$

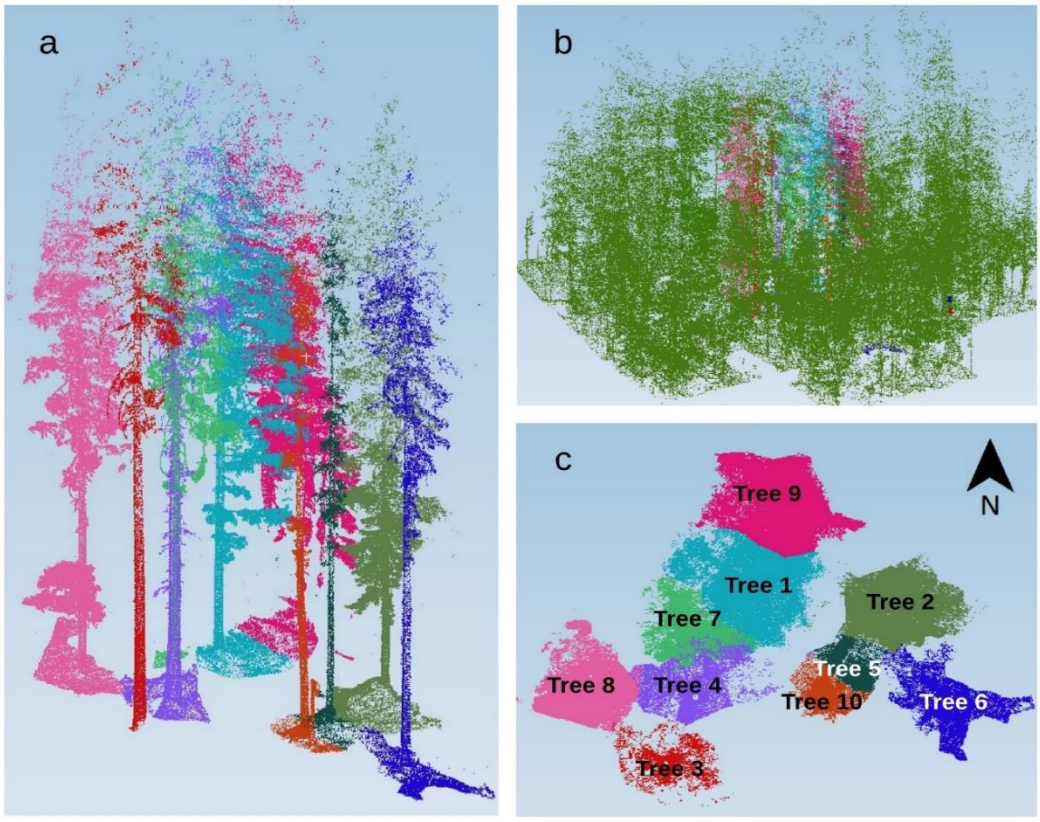

Figure 4.1 Lidar point clouds. a. Rendering of the segmented sample tree point clouds; b. Point clouds of the entire plot and the locations of the 10 sample trees within the plot; c. Nadir view of the sample tree crowns

4.2.2. Cyclone-based estimation of stems and branch dimensions

For each tree, I directly measured tree DBH, height, branch diameter, branch length, branch insertion angle, branch azimuth, and height of branch insertion point (Table 4.1) using crown structural models constructed in Leica Cyclone (Figure 4.2). I also computed five attributes, some of which are commonly used in forest modeling, namely crown length (CL), crown ratio (CR), branch relative height inside the crown (BRH), branch depth inside the crown (DINC), and branch relative depth into the crown (RDINC).

All the branch and stem estimates are based on the region growth algorithm (Pal and Pal, 1993), which requires sufficient points to fit cylinders (Figure 4.2 a). At the top of the crown, not enough points are available for fitting cylinder models (Figure 4.2 b). Therefore, the top stem diameter is determined by assuming the top segment is cone-shaped, with the cone's base diameter equal to the stem diameter of highest available cylinder model. The axis of the top stem segment was aligned with the highest available stem cylinder. Branches at the top of the crown were manually traced with line segments. Thus, branches at the top of the crown were still measured for their height, length, insertion angle, azimuth, and crown radius, but no diameters were estimated.

For the best accuracy, I only measured the first-order live branches that are directly attached to the stems, which were only fitted with cylinders at the insertion point for measuring the basal diameter (Figure 4.2 c). For each cylinder, the extreme coordinates were recorded (i.e., start and end), as well as the axis, diameter, and length. I fitted tree stems with cylinders 1 – 1.5 m long (Figure 4.2 e), for which the taper is negligible in respect with the measurement errors. Dead branches were visually identified in the point cloud, considering that few leaves, and consequently points, are attached to the woody tissue in this case (Figure 4.2 f).

I computed the tree height as the difference between the z values of the highest identified point and the start point of the stem base. I traced the branch skeletons with segments, whose length was summed from the insertion point to the end of the branch and estimated its linear extent (Figure 4.2 d). I computed the branch azimuth with respect to the axis of the base cylinder, while the branch insertion angle was the angle

between the axis of the branch base cylinder and the axis of the stem cylinder (Figure 4.2 c). I determined the crown radius of a branch as the horizontal distance between the end point of the branch and the stem (Figure 4.2 d).

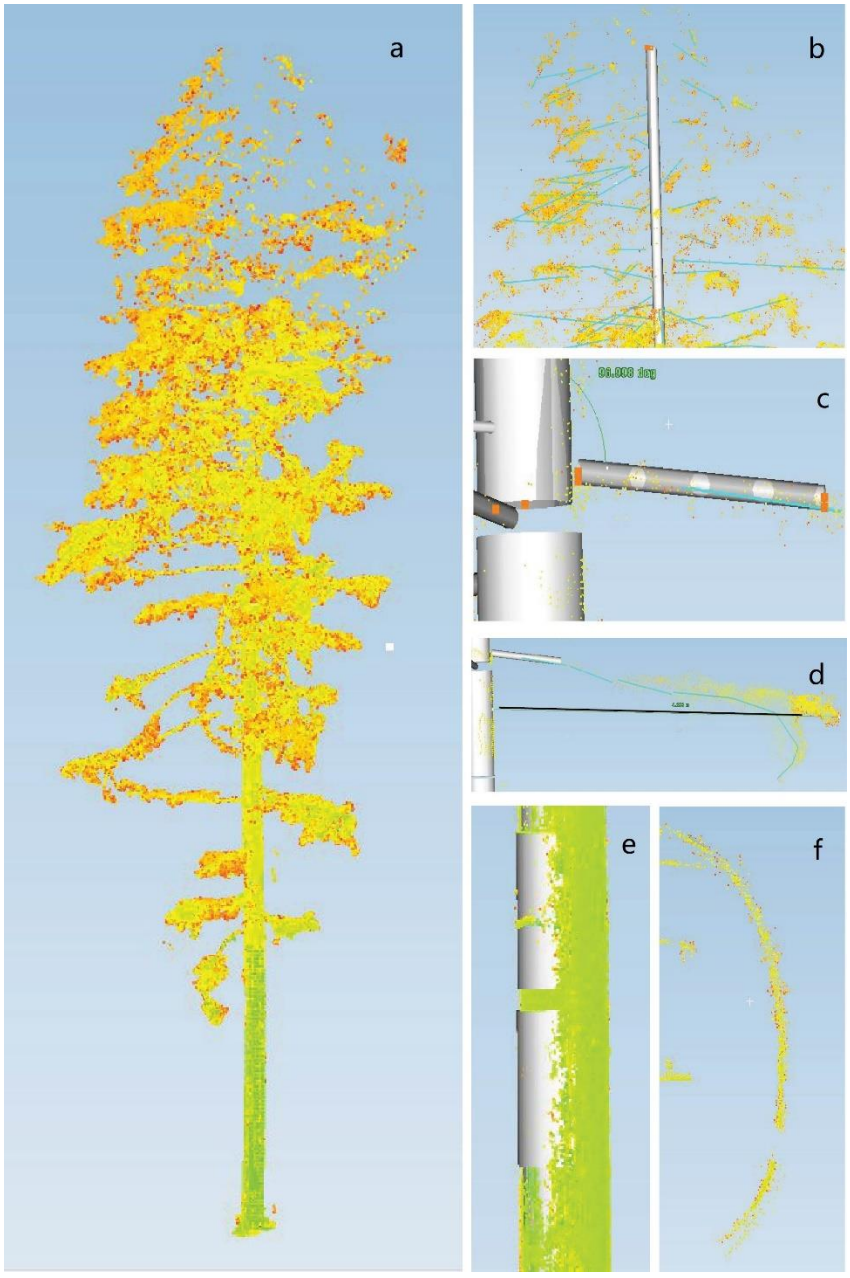

Figure 4.2 Crown measurements in Cyclone. a. The point clouds of a sample tree. b. Incomplete point clouds of the top section of crown. c. Cylinder models of a branch. Branch insertion angle is measured as the angle between the stem axis and branch cylinder axis. d. Branch length measurements: sum

of the length of line segments. The maximum horizontal distance from the stem is the branch projected distance. e. Cylinder model of the stem. f. Dead branch without leaves attaches on it.

4.2.3. Automatic estimates of stem and branches dimensions using TreeQSM

QSM provides an automation process of constructing 3D models from point clouds (Figure 4.3). It segments tree branches by using cover sets, which are connected patches of the tree surface (Raumonen et al., 2013b). Among the QSM models available to 3D model the trees, such as SimpleTree (Hackenberg et al., 2015a), pypetree (Delagrange et al., 2014), or TreeQSM (Raumonen et al., 2013a, 2013b) I chose the TreeQSM. Our software selection is based on the operability and the validity of the results, as only TreeQSM was able to render realistic trees in a feasible amount of time. The other software either were not operational, the case of pypetree, or required a large amount of time to provide valid results, the case of SimpleTree. I used the following parameters to generate the cover sets in TreeQSM:

1. Patch diameter for the first cover: 0.1 – 0.15 m.
2. Minimum patch diameter for the second cover: 0.02 - 0.03 m.
3. Maximum patch diameter for the second cover: 0.06 - 0.08 m.

For each tree, I have estimated the same attributes with TreeQSM as I did with Cyclone, listed in Table 4.1.

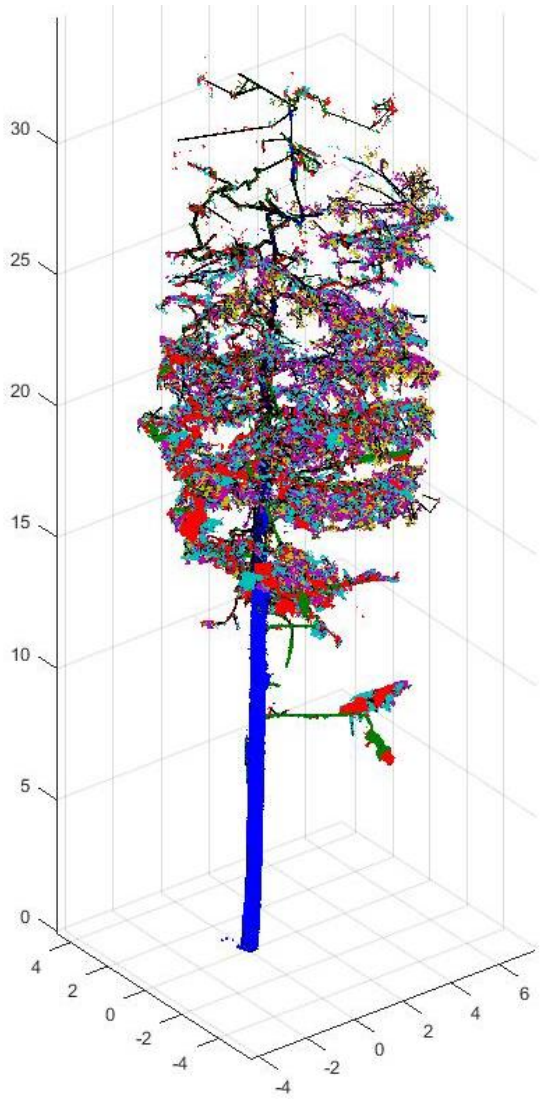

Figure 4.3 An example of QSM created tree model. Different colors represent segments.

4.2.4. Cleaning TreeQSM estimates

I noticed that the tree models constructed with TreeQSM produce significantly more branches than Cyclone. Since the accuracy of TreeQSM is sensitive to the density of the points, and consequently, to the proportion of noise points (Raumonen et al., 2013b), higher order branches located at the upper portion of crowns commonly contain large errors. Therefore, branches that were apparently wrongly created were removed. To eliminate the wrongly constructed branches, I used a series of ad-hoc criteria, which were developed by trial and errors:

1. branches with base diameter above 15 cm;
2. branches with total length less than 1 m;
3. branch height below the lowest identified branch in Cyclone;
4. insertion angle less than 30 degrees;
5. insertion angle less than 50 degrees and length greater than 3 m.

Because TreeQSM wrongly classified some first-order branches as second order, I reexamined all the second-order branches, which were re-classified as first-order branches if the distance between the insertion point and the stem axis is less than stem radius, d (Eq. 4-1):

$$\begin{cases} \sqrt[2]{(x_{branch} - x_{stem})^2 + (y_{branch} - y_{stem})^2} \leq \frac{d}{2} \\ z_{branch} = z_{stem} \end{cases} \quad 4\text{-}1$$

where x_{branch}, y_{branch} and are z_{branch} starting coordinates of a second-order branch, x_{stem}, y_{stem} and z_{stem} are the coordinates of the stem center.

4.2.5. Comparison of the Cyclone and TreeQSM estimates

4.2.5.1. Estimate aggregations by height section

Since one of the interests of this study is the similarities of the trees depicted by the two TLS-based producers (i.e., Cyclone and TreeQSM) I aimed at pair-wise comparison of the branches. However, only 8% of the branches identified with Cyclone and TreeQSM could be paired using visualization and coordinates proximity. Therefore, I compared the aggregated attribute values by height sections of each individual tree rather than comparing paired individual branches. The comparison of aggregated values would reveal whether two procedures generate similar tree structural estimates at individual tree level. The ordinal variable height section is determined based on two criteria: 1) the length of each section < 5 m, except for the bottom and top of the crown; and 2) the number of branches located within each section is relatively equal. The division of the height section is summarized in Table 4.2. For each height section, the branch variables were aggregated by computing the mean (Eq. 4-2):

$$\bar{y}_{\mathrm{method}_{H_{ij}}} = \frac{\sum_{k=1}^{n_{\mathrm{method}_{H_{ij}}}} y_{H_{ijk}}}{n_{\mathrm{method}_{H_{ij}}}} \qquad 4\text{-}2$$

where $\bar{y}_{\mathrm{method}_{H_{ij}}}$ is the average variable (e.g., BD, BL, and α) of height section j of tree i, $y_{H_{ijk}}$ is individually measured branch variable within height section j of tree i, $n_{\mathrm{method}_{H_{ij}}}$ is the number of branches measured by Cyclone or TreeQSM in height section j of tree i, the estimation method is either Cyclone or TreeQSM.

For comparing the branch locational variables insertion height and azimuth, I used nonparametric Kolmogorov–Smirnov test to compare the Cyclone and the TreeQSM estimates, using the R package "stats".

Table 4.2 Summary of number of branches by height section

Height of the Section (m)	Number of Branches	
	Cyclone	TreeQSM
< 15	23	22
15 - 18	28	30
18 - 23	84	51
23 - 26	58	46
26 - 29	88	50
29 - 32	106	33
32 - 35	119	27
35 - 38	116	24
38 - 43	101	5
> 43	34	0

4.2.5.2. Measures for comparing the Cyclone and TreeQSM estimates

I assessed the differences between the two TLS-based branch estimates with four measures:

$$MD_{Hij} = mean\ difference\ by\ height\ section = \bar{y}_{Cyclone_{H_{ij}}} - \bar{y}_{TreeQSM_{H_{ij}}} \quad 4\text{-}3$$

$$\mathrm{MPD_{Hij}} = \text{Mean percent difference by height section} = \frac{\mathrm{MD_{Hij}}}{\bar{\mathrm{y}}_{\mathrm{Cyclone_{H_{ij}}}}} 100\ [\%] \quad 4\text{-}4$$

$$\mathrm{MAD_{Hij}} = \text{Mean absolute by height section} = \left|\bar{\mathrm{y}}_{\mathrm{Cyclone_{H_{ij}}}} - \bar{\mathrm{y}}_{\mathrm{TreeQSM_{H_{ij}}}}\right| \quad 4\text{-}5$$

$$\mathrm{MAPD_{Hij}} = \text{Mean percent absolute difference} = \quad 4\text{-}6$$

$$\frac{\left|\bar{\mathrm{y}}_{\mathrm{Cyclone_{H_{ij}}}} - \bar{\mathrm{y}}_{\mathrm{TreeQSM_{H_{ij}}}}\right|}{\bar{\mathrm{y}}_{\mathrm{Cyclone_{H_{ij}}}}} 100\ [\%]$$

I used paired t-test to access the overall difference between attribute estimates from Cyclone and TreeQSM. The null hypothesis of paired t-test is that mean difference (MD) equals zero. Paired t-test will reveal whether MD follows a normal distribution: $N(0, \sigma_A^2)$, where σ_A^2 is the variance of MD of attribute estimate A (A could be branch diameter, branch length, or branch insertion angle).

Point cloud density decreases with increasing height, suggesting that height section is a possible factor affecting the difference in estimates. Furthermore, the branches belonging to the same stem can be viewed as repeated measurements; therefore, I also used a repeated measures ANOVA (Crowder and Hand, 1990) to evaluate the differences between Cyclone and TreeQSM estimates. To identify the structure of the covariance matrix (required by the repeated measures framework), I considered three structures: autoregressive of order 1 (AR(1)), unstructured variance, and compound symmetry, as recommended by Diggle et al. (Diggle et al., 2002) and Fitzmaurice et al. (Fitzmaurice et al., 2004). The ANOVA equation used to test the difference by height section is

$$\mathrm{MD}_{\mathrm{H_{ij}}} = \text{Height Section Order}_{\mathrm{j}} + \varepsilon_{\mathrm{ij}} \qquad 4\text{-}7$$

The covariance structure for the AR(1) is $\mathrm{cov}(\varepsilon_{\mathrm{ij}}, \varepsilon_{\mathrm{ij-s}}) = \rho^{s}\sigma^{2}$, for the unstructured variance is $\mathrm{cov}(\varepsilon_{\mathrm{ij}}, \varepsilon_{\mathrm{ij-s}}) = \sigma^{2}_{\mathrm{ji-s}}$, and for the compound symmetry is $\mathrm{cov}(\varepsilon_{\mathrm{ij}}, \varepsilon_{\mathrm{ij-s}}) = \sigma_1^2$ (Fitzmaurice et al., 2004), where cov stands for the covariance matrix, $\varepsilon_{\mathrm{ij}}$ and $\varepsilon_{\mathrm{ij-s}}$ are the model residual of tree i at height section of j and j-s, $j \geq s$, ρ is the correlation between two measurements of 1 unit apart, σ^2 is the overall variance of all the measurements.

4.2.6. Simulation of crown architecture

In addition to directly comparing the estimations of branch dimensions and location with two procedures, I conducted a simulation analysis to find whether or not the TLS-based crown estimates can fit in the ranges of the documented Douglas-fir profiles (Ishii et al., 2000; Ishii and McDowell, 2002; Pelt and Sillett, 2008). Most Douglas-fir crown modeling studies have been conducted for plantations or old-growth forests (Ishii et al., 2000; Ishii and Wilson, 2001; Maguire et al., 1999; Roeh and Maguire, 1997). Models for trees with similar crown development stages and sizes as our sample trees are not readily available. Thus, I used both second- (Maguire et al., 1999; Roeh and Maguire, 1997) and old-growth (Ishii and Wilson, 2001) crown models to develop simulated crowns and compare the simulated crown attributes with TLS-based estimates. Our sample trees are located within a natural regime stand with closed canopy and mixed DBH classes. I expect the crown attributes of our sample trees to be at the transitional stage between second- and old-growth trees. Since field measurements are not available, the comparisons between TLS-based estimates and exiting observations also serve as a justification of TLS-based estimation.

4.2.6.1. Second-growth branch size models

Maguire et al. (1999) developed maximum BD models for managed stands. Among all the equations of Maguire et al. (1999), I selected the constrained variable-exponent model to simulate BD:

$$BD_{ij} = \left(\lambda_1 CW^{\lambda_2} + \delta_i\right) W^C + \varepsilon_{ij} \quad (4\text{-}8)$$

$$CW = MCW * CR^{0.01431509*CL+0.07224024\frac{DBH}{Ht}} \quad (4\text{-}9)$$

$$MCW = 1.4081 + 0.22111 * DBH - 0.00053438 * DBH^2 \quad (4\text{-}10)$$

$$W = 1 - BRH^{0.5} \quad (4\text{-}11)$$

$$C = \lambda_3 BRH^{\lambda_4} \quad (4\text{-}12)$$

$$BRH = \frac{h_i - h_{BC}}{CL} \quad (4\text{-}13)$$

$\lambda_1, \lambda_2, \lambda_3$ and λ_4 are coefficients of Eq 6c fitted in Maguire et al. (1999). CW is the stand-grown maximum crown width, MCW is the open-grown maximum crown width, CR is crown ratio, BRH is the branch relative height inside the crown, h_i is the height of branch insertion point, and h_{BC} is the height of crown base. δ_i and ε_{ij} are random errors of tree level and individual branch level, following distribution $\delta_i \sim N(0, \delta^2)$ and $\varepsilon_{ij} \sim N(0, \sigma^2)$.

Roeh and Maguire (Roeh and Maguire, 1997) developed a set of crown profile models for coastal Douglas-firs, in which the estimated attributes were simultaneously corrected across the equations. An examination of the symmetrically modeled BD and BL in Roeh and Maguire revealed that BD and BL are smaller than the estimates from the point clouds of this study. Therefore, I only selected individually developed BL model for the simulation (Roeh and Maguire, 1997):

$$BL_{ij} = e^{d_1} DINC^{d2} e^{d_3 DINC} BD^{d_4} THT^{d_5} \quad (4\text{-}14)$$

where the variables are defined in Table 4.1, BD is estimated branch diameter from Eq. 4-8.

$$Z_{ij} = aRDINC_{ij}^{b}(1 - RDINC_{ij})^{c} \quad (4\text{-}15)$$

$$RDINC_{ij} = \frac{THT_i - h_{ij}}{THT_i - h_{BC_i}} = \frac{DINC_{ij}}{CL_i} \quad (4\text{-}16)$$

4.2.6.2. Old-growth branch size models

Unlike young plantation trees, the branches of old-growth trees are less constrained by tree size and more determined by the depth of the crown. Ishii and Wilson (Ishii and Wilson, 2001) developed crown models for old-growth Douglas-firs, which could adapt to the variation of branch forms. The branch size equation used in this study is:

where Zij is the size of branch j from tree i (BD or BL), RDINCij is relative depth into the crown, a is a coefficient and b and c are scaling exponents, THT_i is the total height of tree i, h_{ij} is branch j insertion height, and h_{BC_i} is height of crown base.

The final crown equation is fitted as a piecewise function since at the lower end of the crown the equation cannot capture the variability of the branch size.

$$\begin{cases} Z_{ij} = aRDINC_{ij}^{b}(1 - RDINC_{ij})^{c}, & DINC_{ij} < h \\ Z_{ij} = ah^{b}(1 - h)^{c}, & RDINC_{ij} \geq h \end{cases} \quad \text{4-17}$$

Previous studies have shown the existence of a relatively simple allometric relationship between BD and BL (Bertram, 1989; Ishii et al., 2000; McMahon and Kronauer, 1976): $BL = aBD^{b}$, where a and b are coefficients. To determine a and b, I used a pre-simulation to decide the range of a and b based on BD and BL models of Ishii and Wilson. The final estimates of branch length model are described as:

$$BL_{ij} = 1.6971 \times BD_{ij}^{0.6237} \quad \text{4-18}$$

4.2.6.3. Simulation algorithm

The simulation was performed for three DBH classes, each following a uniform distribution:

$DBH_{1j} \sim U(50, 55)$, $DBH_{2j} \sim U(60, 65)$, and $DBH_{3j} \sim U(85, 105)$. The selected boundaries cover the DBH range of sample trees and represent crown development at different stages. The number of sample trees within DBH classes 50 – 55, 60 – 65 and 85 – 105 cm are five, three and two respectively. Although trees of DBH classes 50 – 55 and 60 – 65 cm behave similarly in crown structural development, the sample trees are not evenly distributed within the entire DBH range of 50 – 65 cm and the separation of DBH classes would better approximate the transition of crown development. For each size class, I generated 10,000 simulated trees and their crown attributes were estimated with both second- and old-growth models as described above (Hann, 1999; Ishii and Wilson, 2001; Maguire et al., 1999; Roeh and Maguire, 1997).

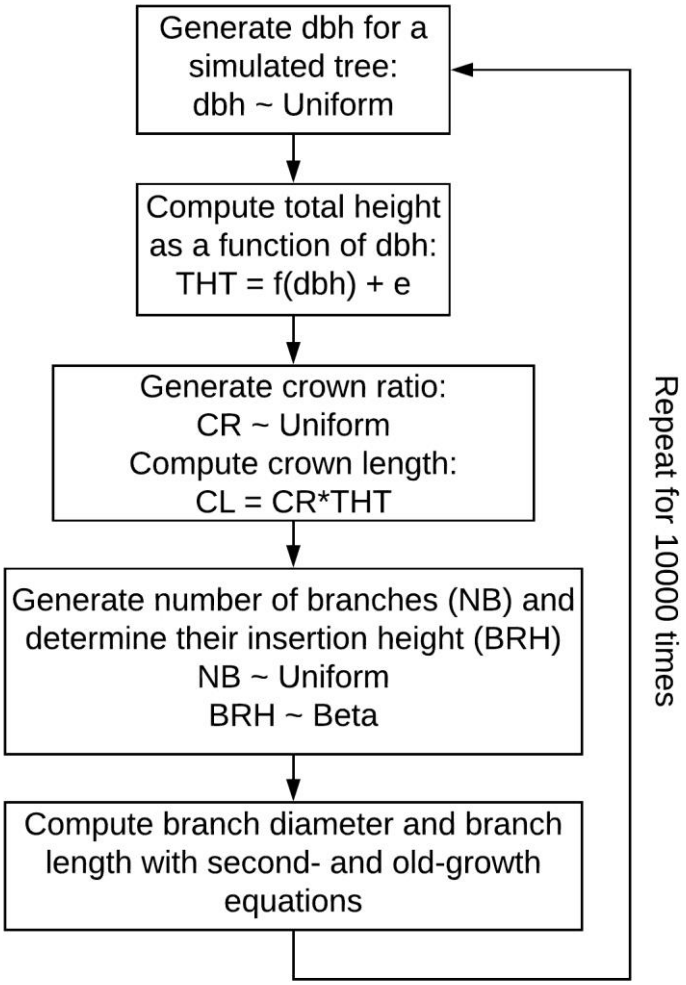

Figure 4.1 The algorithm used to simulate individual trees crown using existing models

The steps of synthetically generating crown attributes are:

Step 1. Select DBH

A random number is drawn from the uniform distribution of DBH for each class.

Step 2. Compute tree height from DBH

An empirical height-DBH equation is used to determine tree total height (Temesgen et al., 2007):

$$\mathrm{THT} = 1.3 + e^{(a+b\times \mathrm{DBH}^c)} + \varepsilon \qquad 4\text{-}19$$

where a = 5.7567, b = -6.7792, c = - 0.2795 and ε is a random error, $\varepsilon \sim \mathrm{N}(0, \sigma_\varepsilon^2)$.

Step 3. Compute crown length

Crown ratio (CR) is generated from a uniform distribution: $\mathrm{CR} \sim \mathrm{U}(0.3, 0.7)$. The selection of crown ratio distribution is based on the observation of our sample trees. Then, crown length is determined from its definition as:

$$\mathrm{CL} = \mathrm{CR} \times \mathrm{THT} \qquad 4\text{-}20$$

Step 4. Select the number of branches and branch insertion height

The number of first ordered branches is established assuming that it follows a uniform distribution, $\mathrm{NB_i} \sim \mathrm{U}(60, 140)$, where $\mathrm{NB_i}$ is the number of branches of simulated tree i. The boundaries of uniform distribution of NB is determined by the observation of sample trees.

Branch insertion height is determined by the BRH, which follows a beta distribution. A pre-simulation was executed to decide the parameters α and β of an assumed beta distribution, which yielded the following ranges for α and β:

$$\begin{cases} \boldsymbol{\alpha} \sim \boldsymbol{U}(\mathbf{1},\mathbf{3}) \\ \boldsymbol{\beta} \sim \boldsymbol{U}(\mathbf{1},\mathbf{3}) \\ \boldsymbol{\beta} \leq \mathbf{1.5} \times \boldsymbol{\alpha} \end{cases} \quad \text{4-21}$$

I simulated BRH following the distribution: $BRH_{ij} \sim \mathrm{Beta}(\alpha, \beta)$, where BRH_{ij} is the ith branch relative height above crown for jth simulated tree.

Step 5. Compute the branch diameter and branch length

For a second-growth tree, the branch diameter and branch length are determined by Eq 4-8 and 4-14 respectively. For an old-growth tree, the branch diameter and branch length are determined by Eq 4-17 and 4-18.

4.3. Results

4.3.1. Tree level estimates

I found no bias in the TreeQSM estimates of DBH (Table 4.3). However, TreeQSM estimated total height consistently smaller than Cyclone, by approximately 10%. For tree #3, a large discrepancy is present between Cyclone and TreeQSM estimated DBH and height, in which TreeQSM overestimated DBH by 17 cm (20%) and underestimated tree height by 10 m (18.5%) (Table 4.3). The difference between Cyclone and TreeQSM crown length estimates ranges from 0.2 – 3.92 m (Table 4.3). A major difference between the two procedures is that TreeQSM identifies fewer first order branches than Cyclone, sometime as low as 31%.

Table 4.3 Semi-automatic (Cyclone) and automatic (TreeQSM) tree attribute estimates.

Tree	DBH (cm)		Tree Height (m)		Crown Length (m)		No. of Branches (First Order)	
	Cyclone	TreeQSM	Cyclone	TreeQSM	Cyclone	TreeQSM	Cyclone	TreeQSM
1	64	65	40.50	36.60	30.58	26.66	96	49
2	60	58	44.00	44.65	35.15	38.30	122	67
3	84	101	53.99	43.83	30.34	29.91	87	32
4	110	113	45.00	45.81	20.71	21.68	47	36
5	56	53	38.06	37.12	24.62	21.35	37	12
6	63	60	44.93	44.39	22.95	24.30	87	27
7	50	52	45.83	46.78	27.37	27.57	77	50
8	52	51	44.76	41.20	28.70	28.82	98	59
9	49	47	39.00	35.29	30.27	26.71	74	34
10	51	54	40.78	40.12	26.33	26.61	39	15
Average	63.9	65.4	43.69	41.58	27.7	27.19	76.4	38.1

4.3.2. Estimation of branch attributes

4.3.2.1. Branches azimuth and insertion height

The majority of the branches identified by TreeQSM are located in the lower portion of the crown, whereas Cyclone generated widely spread branch distribution along the height of the tree (Figure 4.5). The distributions of azimuths for both procedures are similar. The majority of identified branches are facing south, with azimuth ranging from 90° to 270°, except for tree #3 and #4, whose DBHs (> 80 cm) are greater than other trees (Figure 4.5). The distribution of branch azimuth by DBH class is primarily determined by the light condition of the canopy. For small trees, most branches are south facing where light abounds, while for large trees, some branches are facing north where branch exclusion allows some light.

The distribution of branch insertion height exhibits an obvious shift between Cyclone estimates and TreeQSM estimates, suggesting that automatic procedures supplied

values lower than Cyclone procedure (Figure 4.6). The Kolmogorov–Smirnov test confirms the difference between branch insertion height estimated by two procedures, as no tree was found with a similar distribution (p-value < 0.05 Figure 4.6). The largest disagreement in the distribution of branch insertion height occurs between 17 – 36 m. In contrast to branch insertion height, the distributions of the estimated azimuths are much more similar for Cyclone and TreeQSM (Figure 4.6). The Kolmogorov–Smirnov test confirmed similarities of branch azimuth distributions estimated by the two procedures, as only one tree (i.e., 4) has different distributions (p-value < 0.05).

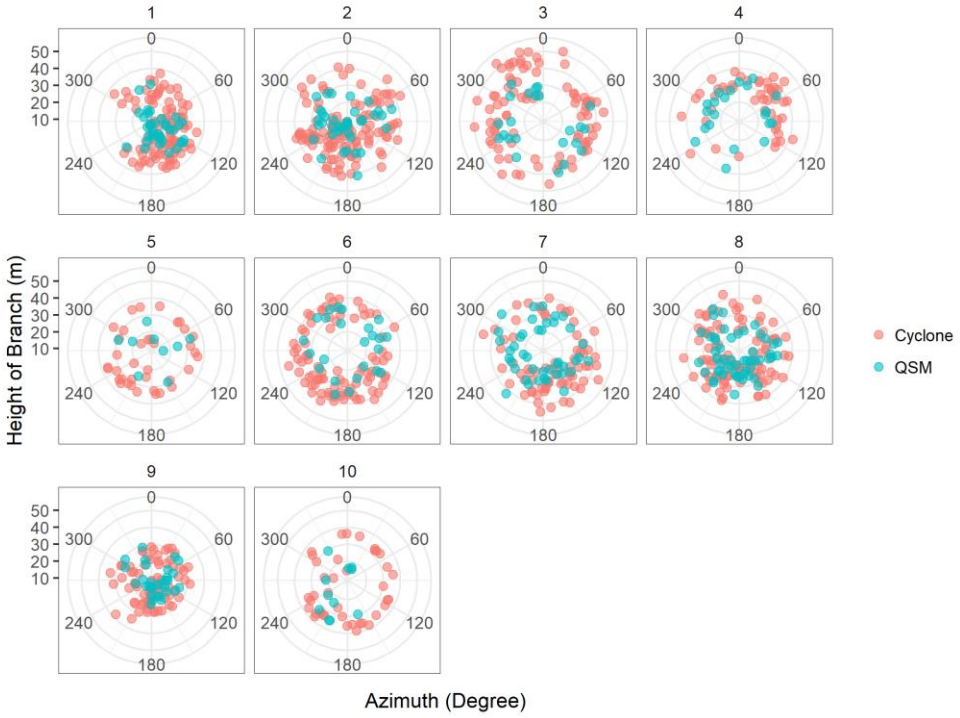

Figure 4.5 TLS identified individual branches by insertion height and azimuth.

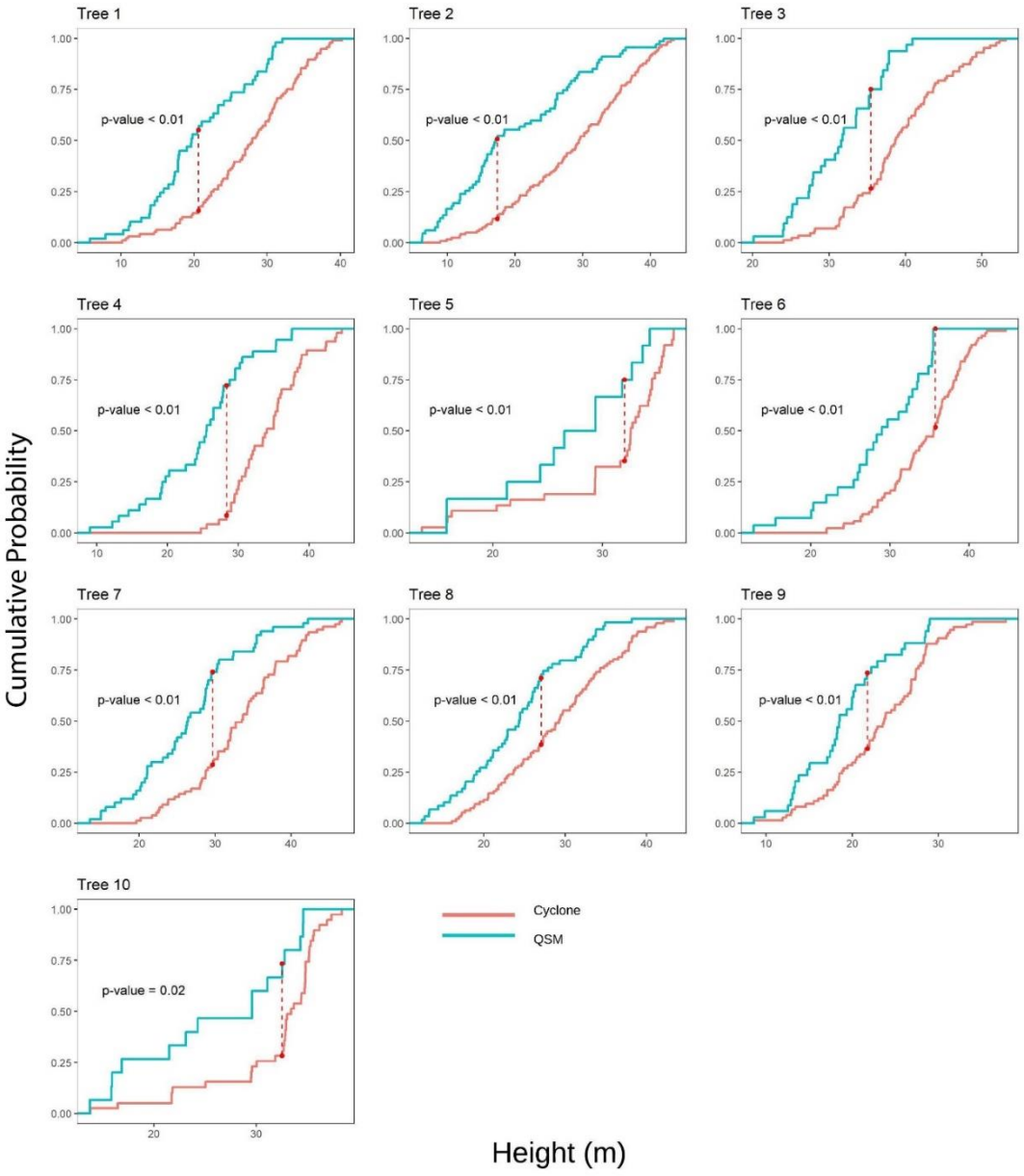

Figure 4.6 Cumulative probability of branch insertion height. The p-values are for the Kolmogorov–Smirnov test used to compare the branch insertion height distribution of TreeQSM and Cyclone. The null hypothesis of the test is that two sets of values have the same distribution. Red dots mark the height at which the largest difference in the cumulative probability of Cyclone and TreeQSM measured height is found.

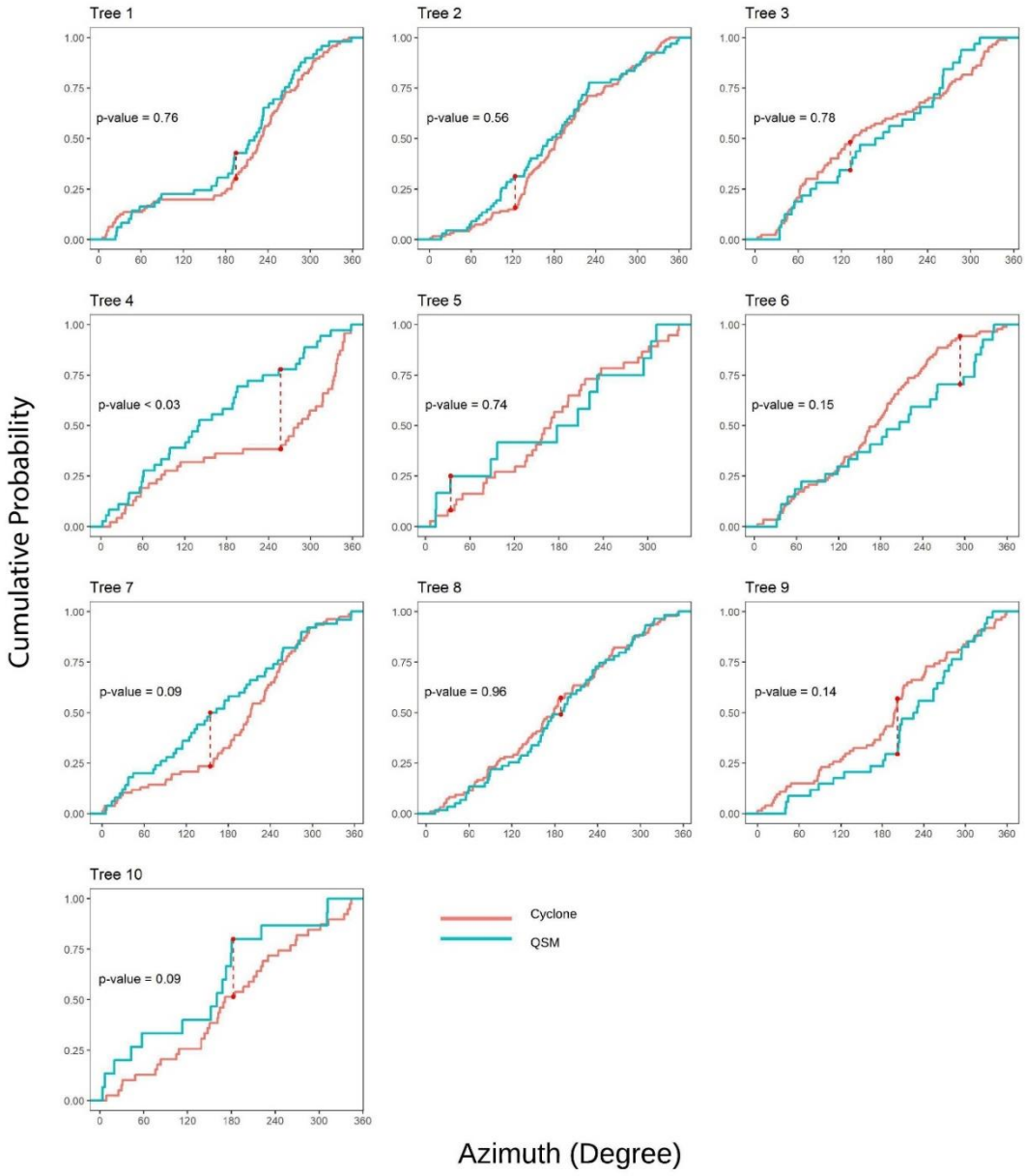

Figure 4.7 Cumulative probability of branch azimuth. The p-values are for the Kolmogorov–Smirnov test used to compare the branch azimuth distributions estimated by TreeQSM and Cyclone. The null hypothesis of the test is that two sets of values have the same distribution. Red dots mark the azimuth at which the largest difference in cumulative probability of Cyclone and TreeQSM estimates are found.

4.3.2.2. Branches diameter

TreeQSM estimated mean BD is greater than Cyclone estimates below insertion height of 29 m (Table 4.4 and Figure 4.8 a). Above 29 m, the TreeQSM estimates are smaller than the Cyclone estimates (Table 4.4 and Figure 4.8 a). The normality of paired t-test is met for BD estimates. The paired t-test indicates no difference between the overall mean of Cyclone and TreeQSM BD estimates (p-value = 0.96) by individual trees over the entire tree profile.

The section-wise comparison reveals that the repeated measurement framework with AR(1) structure yielded smallest AIC value (Table 4.5), suggesting that branch diameter estimates along the stem are not independent but correlated with the insertion height. Cyclone BD estimates are relatively constant across height sections. In contrast, TreeQSM BD estimates decrease with the increase in height section. The largest discrepancy between the BD estimates of the two procedures is at the height section 35 – 37 m (Table 4.4), where TreeQSM underestimated mean BD by 2.34 cm (40.08%). The underestimation was probably the result of the unsuccessful construction of branch structure due to sparse point clouds. Although the abundance of points is supposed to yield similar estimates for branch diameter, the second largest difference is found at the height section below 15 m, where average BD computed with TreeQSM is 1.53 cm (28.75%) greater than Cyclone value (Table 4.4). The overestimation of small size branches by TreeQSM was also found by previous studies (Hackenberg et al., 2015b; Lau et al., 2018), where plenty of points were available.

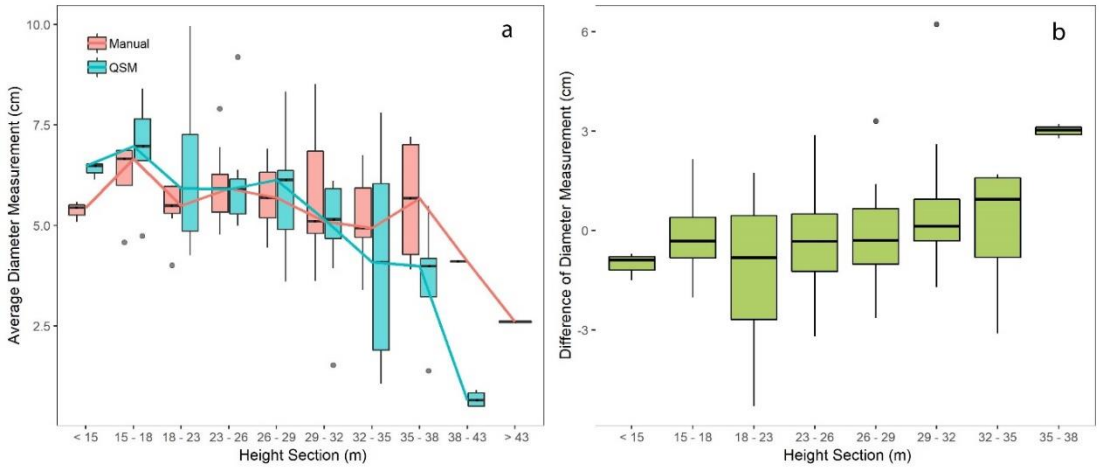

Figure 4.8 Branch diameter estimates at insertion point by height section. a. Comparison of branch diameter estimates of Cyclone and TreeQSM by height section; reference lines connect the mean of the aggregated estimates. b. The difference of the branch diameter estimates between Cyclone and TreeQSM by height section.

Table 4.4 Summary of mean branch diameter estimates by height section.

Height	**Procedure**		**Difference**		**Absolute Difference**	
(m)	Cyclone (cm)	TreeQSM (cm)	(cm)	(%)	(cm)	(%)
<15	5.36	6.89	-1.53	-28.75	1.53	28.75
15-17	6.20	6.40	-0.20	-5.10	0.65	11.82
18-22	5.38	6.54	-1.16	-24.82	1.75	35.32
23-25	5.92	6.04	-0.12	-4.12	1.36	22.71
26-28	5.64	5.95	-0.31	-10.36	1.78	31.53
29-31	5.75	5.09	0.67	4.56	1.48	24.18
32-34	5.38	4.62	0.76	13.65	2.17	44.04
35-37	6.22	3.88	2.34	40.80	2.34	40.80
38-42	4.10	2.89	1.21	29.51	1.21	29.51

Table 4.5 Difference in branch diameter estimates between Cyclone and TreeQSM as a function of height section, within a repeated measurements framework.

Model Type	AIC	BIC
Unstructured	161.8796	175.6169
Repeated measures - AR(1)	153.6215	168.8851
Repeated measures - Compound Symmetry	156.865	172.1286

4.3.2.3. Branch length estimates

Both Cyclone and TreeQSM yielded the longest mean BL estimates at the base of the crown (Figure 4.9). Paired t-test indicates that Cyclone mean BL estimate is significantly larger than TreeQSM estimate (i.e., 0.49 m) by aggregation of height sections (p-value < 0.001). The largest discrepancy in length estimates occurs at the height section 26 – 29 m (Figure 4.9), where mean difference and mean absolute difference are 1.34 m (33.4%) and 1.52 m (37.7%) respectively (Table 4.6). ANOVA does not indicate difference in length estimates in response to height section (i.e., p-value is 0.25). The normality assumption, required for ANOVA, is met, but the homoscedasticity is not, as the variance of the difference between the estimated BL for height section 15 – 18, 23 – 26, and 29 – 32 m is relatively higher than for the other height sections (Figure 4.9).

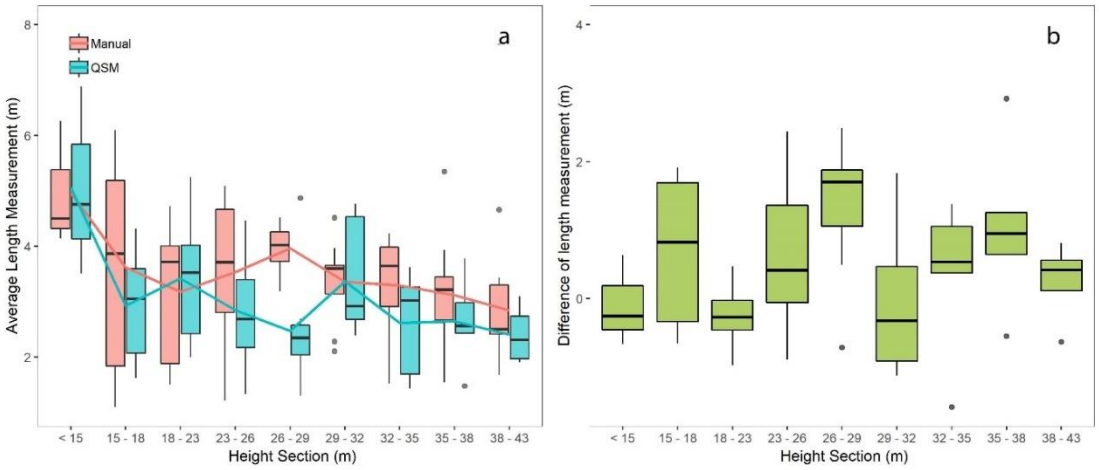

Figure 4.9 Branch length estimates by height section. a. Estimates for Cyclone and TreeQSM; reference lines connect the mean of the aggregated estimates. b. Difference between the branch length estimates of Cyclone and TreeQSM. The dots represents outliers identified with the quantile approach.

Table 4.6 Summary of branch length estimates by height section.

Height	Procedure		Difference		Absolute Difference	
(m)	Cyclone (m)	TreeQSM (m)	(m)	(%)	(m)	(%)
< 15	4.96	5.06	-0.10	0.37	0.52	10.52%
15 - 18	3.62	2.93	0.69	0.58	1.08	34.24%
18 - 23	3.18	3.42	-0.24	-13.87	0.41	18.36%
23 - 26	3.53	2.84	0.69	12.41	0.96	24.90%
26 - 29	3.96	2.62	1.34	33.38	1.52	37.72%
29 - 32	3.38	3.37	0.02	-2.44	0.89	24.57%
32 - 35	3.10	2.62	0.49	8.58	0.88	34.61%
35 - 38	3.68	2.64	1.04	25.53	1.26	32.37%
38 - 43	2.65	2.40	0.25	8.19	0.57	21.09%

4.3.2.4. Branch insertion angle estimates

Both angle estimates do not show strong correlation with height section (Figure 4.10). Paired t-test indicates that the mean Cyclone estimated angle is 9.916° (i.e., 10.52%) greater than the TreeQSM estimates by aggregation of height sections (i.e., p-value < 0.001). The largest mean difference between two estimates occurs at 18 – 23 m (Table 4.7) and is 20.90° (i.e., 22.63%). ANOVA suggests that the difference between angle estimates also does not vary across height sections (i.e., p-value is 0.087). As height is below 18 m, Cyclone mean estimated insertion angles are smaller than TreeQSM estimates. For height above 18 m, Cyclone estimated mean insertion angles are greater than TreeQSM estimates, except for height section of 29 – 32 m (Figure 4.10 b).

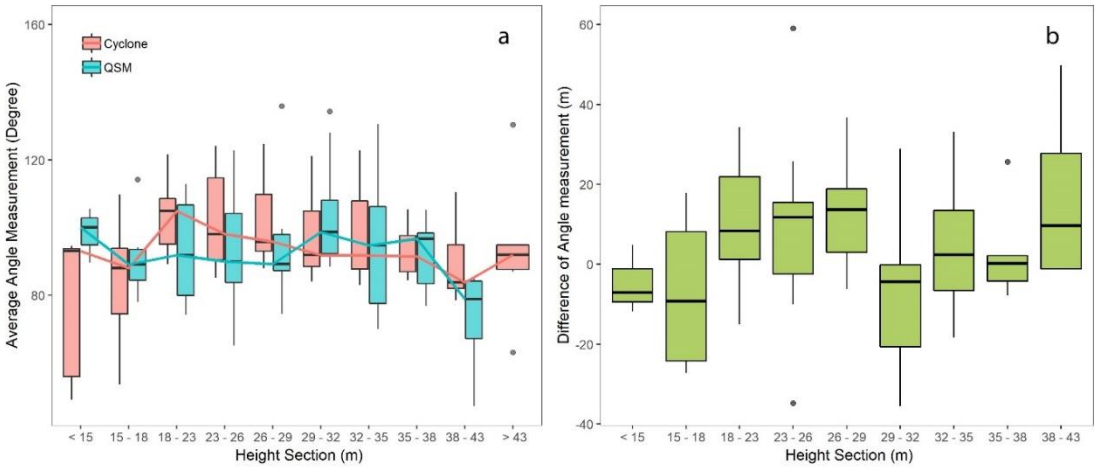

Figure 4.10 Branch angle estimates by height section. a. Estimates for Cyclone and TreeQSM; reference lines connect the mean of the aggregated estimates. b. Difference between branch insertion angle estimates of Cyclone and TreeQSM by height section.

Table 4.7 Summary of branch angle estimates by height section.

Height Section	TreeQSM	Cyclone	Difference		Absolute Difference	
(m)	Angle (º)	Angle (º)	(º)	(%)	(º)	(%)
< 15	88.45	77.27	-11.18	-21.45	12.16	22.49
15 - 18	89.30	84.17	-5.12	-9.85	10.38	15.37
18 - 23	82.92	103.82	20.90	18.91	20.90	18.91
23 - 26	89.81	103.46	13.65	11.86	16.75	15.27
26 - 32	87.60	96.52	8.91	8.32	10.06	9.62
32 - 35	83.60	97.98	14.37	15.06	18.96	20.08
35 - 38	85.35	95.25	9.90	10.08	19.43	20.53
38 - 43	78.94	85.85	6.91	6.63	22.68	26.37

4.3.3. Simulated crowns

TLS-based estimates for BD and BL are compared with the same attributes from the simulated trees without differentiating whorl from epicormic branches. Therefore, I used the maximums to reflect key attributes of crown profile, usually defined by the whorl branches (Hann, 1999; Maguire et al., 1999), and the means to consider all the branches. Furthermore, crown profiles derived from Cyclone and TreeQSM are compared to test whether TreeQSM can develop average tree structures that are comparable with Cyclone.

4.3.3.1. Branch Diameter

Simulated old-growth trees have wider ranges of mean and maximum BD compared to second-growth trees (Figure 4.11), because of greater variability of the old-growth crowns. As the fitted polynomial curves show, both Cyclone and TreeQSM estimated mean BD profiles are slightly greater than simulated second-growth trees (Figure 4.11 a and b), except for DBH 85 – 105 cm. The mean BD profiles of Cyclone and TreeQSM estimates are consistent with simulated second-growth trees, in which largest mean BDs are located in the middle-lower crown and smallest mean BDs are located at the top of the crown (Figure 4.11 a – c). In comparison with Cyclone mean BD estimates, the variance of TreeQSM mean BD estimates are greater. For DBH class of 50 – 55 cm, TreeQSM yielded greater mean BD estimates than Cyclone at the lower crown (Figure 4.11 a). For DBH class of 60 – 65 and 85 – 105 cm, Cyclone, and TreeQSM BD estimates show better agreement.

For both Cyclone and TreeQSM, the maximum BD estimates are similar to simulated old-growth trees for DBH classes 50 – 55 and 60 – 65 cm Figure 4.11 a and e), with mean difference less than 1 cm. However, for DBH class 85 – 105 cm, the overall simulated old-growth trees' maximum BD are 8.51 and 9.60 cm averagely greater than Cyclone and TreeQSM estimates respectively. Instead, mean differences between simulated second-growth trees' maximum BD and TLS-based estimates are within 1.5 cm for DBH class of 85 – 105 cm (Figure 4.11 f). Similar to mean BD estimates, TreeQSM maximum BD estimates are more variable than Cyclone estimates. TreeQSM generated greater maximum BD estimates than Cyclone for DBH class 50 – 55 cm.

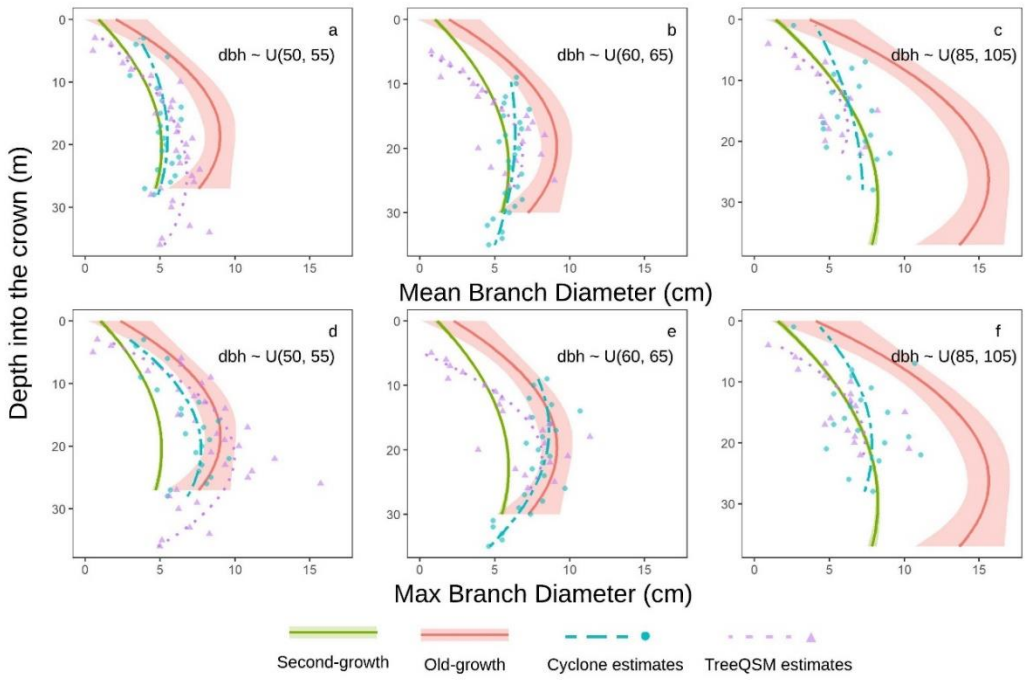

Figure 4.11 Mean (a - c) and maximum (d - f) branch diameter of the 10 trees by DBH class as a function of depth into the crown. The reference lines are second-order polynomial regression lines fit to the simulations and observations. Green and red lines are the simulated trees with second- and old-growth models, namely Ishii and Wilson

(2001) and Maguire (1999) models. The shades represent the 95% confidence intervals of the simulated results of 10000 trees.

4.3.3.2. Branch length

Overall, both simulated second- and old-growth trees have longer mean BL estimates than the TLS-based estimates (Figure 4.2 a - c). The fitted curves on the Cyclone mean BL estimates suggested the presence of three crown shapes: ellipsoid crown for DBH class 50 – 55 cm, where the longest branches are at the middle-lower crown (Figure 4.2 a); conic crown for DBH class 60 – 65 cm, where the longest branches are at the bottom (Figure 4.2 b); and cylindrical crown for DBH class 85 – 105 cm, where the branch lengths are relatively constant along canopy (Figure 4.2 c). In comparison with Cyclone, mean BL estimates supplied by TreeQSM underestimated mean BL for DBH class 50 – 55 and 85 – 105 cm for 0.3 and 1.12 m, respectively (Figure 4.2 a - c).

For maximum BL, both Cyclone and TreeQSM estimates are close to simulated old-growth trees for DBH classes 50 – 55 and 60 – 65 cm, with mean difference less than 1 m (Figure 4.2 d and e). However, great difference is present between TLS-based maximum BL estimates and simulated old- and second-growth trees for trees with DBH ≥ 85 cm (Figure 4.2 f). Unlike ellipsoidal shapes of maximum BL estimates for DBH 50 – 55 and 60 – 65 cm, round crown shapes were present for DBH 85 – 105 cm irrespective the procedure, in which the longest BLs are present in the middle-upper crown. Both simulated second- and old-growth trees have longer maximum BL estimates than Cyclone and TreeQSM estimates for DBH class 85 – 105 cm and the difference is greater than 2 m.

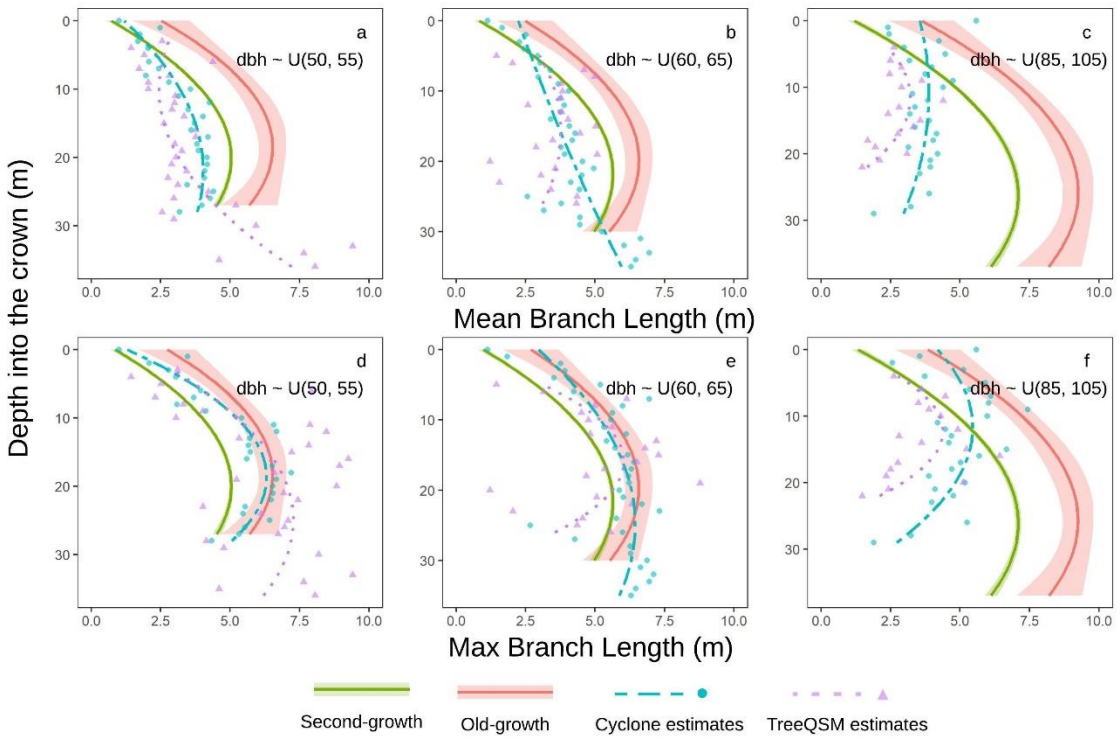

Figure 4.12 Mean (a - c) and maximum (d - f) branch length of the 10 trees by DBH class as a function of depth into the crown. The reference lines are second order polynomial regression lines fit to the individual simulations and observations. Green and red lines are the simulated trees with second- and old-growth models, namely Ishii and Wilson (2001) and Maguire (1999) models. The shades represent the 95% confidence intervals of the simulated results of 10000 trees.

4.4. Discussion

4.4.1. Comparison of TreeQSM and Cyclone crown attribute estimates

The TreeQSM reduces the time and effort of the Cyclone procedure, but the results are still significantly different. In total, the semi-automatic procedure using Cyclone identified 761 branches for the 10 trees, whereas, TreeQSM identified only 38% branches of comparable dimensions and similar locations, mainly for the lower crown. However, for the upper crown where the point cloud is sparse, considerable branches were missed by TreeQSM. For all the sample trees, TreeQSM failed to construct

accurate stem models above 15 m (Figure 4.13 b), where disconnection of point clouds happened due to obstruction of scan view and reduction of point cloud density. Stem model construction is terminated before the process reaches the top of the crown since insufficient point clouds are available for the modeling process. TreeQSM might yield underestimated tree height for tall trees like Tree #3 because of incomplete stem models. However, region grow function in Cyclone still can accurately approximate the remaining point patches for stem model construction at the higher portion of the crown (Figure 4.13 a). TreeQSM miscategorized some first-order branches as second-order (Figure 4.13 c). I examined miscategorized branches, included miscategorized second-order branches and cleaned branches that are wrongly categorized as first-order. TreeQSM failed to construct structural models of stems with irregular form and strong inclination such as Tree #3 (Figure 4.13 f) resulting in incorrect DBH estimation. In Cyclone, stem model construction is controlled with human assistance. The stem cylindrical models are manually adjusted to approximate the point clouds (Figure 4.13 e). TreeQSM also misidentified some stem points as branch points and incorrectly constructed nonexistent branches (Figure 4.13 h).

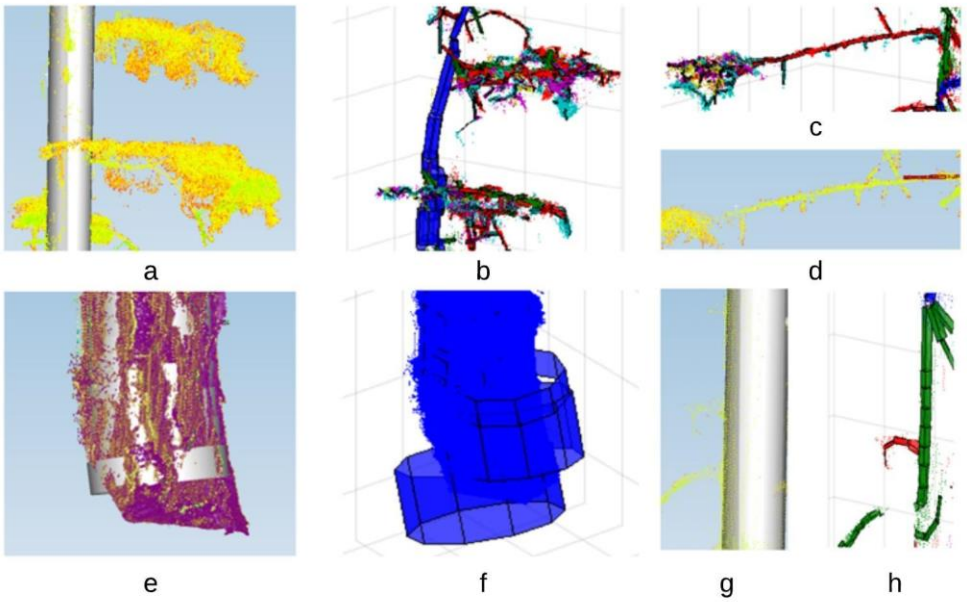

Figure 4.13 Comparisons of quantitative structural models constructed with TreeQSM and Cyclone. Identification of some typical errors of structural models developed with TreeQSM. a. Accurate stem model (silver cylinder) developed in Cyclone. b. Inaccurate stem models developed with TreeQSM (blue cylinders). c. A first-order branch was categorized as second-order in TreeQSM (red cylinder). d. Cyclone rendering of the point clouds of the same branch shown in c. e. Stem models at breast height of Tree #3 in Cyclone. f. Incorrect stem models at breast height of Tree #3 in TreeQSM. Cylindrical models (blue cylinder) deviate from the stem point clouds resulting overestimation of DBH. g. Accurate stem model (silver cylinder) constructed in Cyclone. h. TreeQSM misidentified stem points as branch points and constructed models for a nonexistent branch (green cylinders shown in the right).

For both Cyclone and TreeQSM estimated BD, the accuracy is constrained by the application of pipe models, since real branches have irregular shapes rather than perfect cylinders. With the human-aid computation, Cyclone is believed to generate more accurate BD estimates, especially for complex understory canopy, because noise and leaf points are manually excluded from pipe model construction. TreeQSM can accurately construct pipe models for broadleaf tree stems and branches (Calders et al., 2018; Lau et al., 2019, 2018; Raumonen et al., 2013b), particularly for branches and stem diameters greater than 10 cm (Lau et al., 2019). For branches smaller than 10 cm in diameter, TreeQSM is prone to overestimation (Hackenberg et al., 2015b; Lau et al., 2018). However, the BD estimation with TreeQSM is challenging, since average branch diameter is smaller than 7 cm in this study. Whereas TreeQSM estimates of BD are questionable, the DBH is not, considering that the trees used in this study are mature, with large DBH. Therefore, TreeQSM supplied reliable DBH, as no significant difference was found from the Cyclone values.

Our results suggest that branch height plays a significant role in the accuracy of TreeQSM estimation of BD because branch height is directly related to point cloud density and the abundance of information carried in the point clouds (Calders et al., 2018). Inside the lower crown, where sufficient points are available, TreeQSM yielded greater mean BD estimates than Cyclone, which is probably error introduced by leaves and noise points. Inside the upper crown, TreeQSM provided smaller diameters than Cyclone, because insufficient point density was available to construct and connect the cylinder models. Consequently, the overall means of BD estimates along the entire crown profile are not different between TreeQSM and Cyclone at individual tree level.

Cyclone estimated BL depends only on the identification of the few points defining the overall skeleton of the branches. In contrast, BL estimation with TreeQSM requires enough points for cylinder model construction through the entire branch extent. Thus, BL estimation with TreeQSM is very sensitive to the density of points. False bifurcations caused by noise points and patches of points terminate the branch model construction, resulting in BL estimation errors. The average BL is almost 0.5 m greater in Cyclone than from TreeQSM. Our results are consistent with Lau et al. (Lau et al., 2018), which found that TreeQSM is more reliable in estimating branch diameter than branch length.

Cyclone estimated branch insertion angle would be more accurate in the lower crown since both branch and stem were fitted with sufficient points. For the upper crown sections, the accuracy of branch angle estimation depends not only on the determination of the branch skeleton but also on the accuracy of the projected stem cylinder from the lower section. The average TreeQSM estimated branch insertion angle is 9° smaller than Cyclone values. Since the accuracy of angle estimates is associated with the availability of points, I was surprised to find minute differences in angle estimates between TreeQSM and Cyclone across canopy height. I hypothesize that unlike branch length, which relies on the successful construction of the pipe model for the entire branch, angle estimation is only determined by the main skeleton at the branch base.

4.4.2. Crown architecture and development stage derived with TLS-based estimates

The simulations confirmed our expectation that TLS-based crown estimates would be within the range between second- and old-growth trees. For trees of DBH classes 50 – 55 and 60 – 65 cm, TLS-based mean BD and BL estimates are similar to second-growth trees, whereas, maximum BD and BL estimates fit in the range of old-growth trees, indicating a transitional crown development stage (Franklin et al., 2002). However, crown expansion is not present in trees of DBH class 85 – 105 cm, as crown size is significantly smaller than simulated second- and old-growth trees, which is probably associated with branch exclusion caused by canopy closure (Franklin et al., 2002).

Conceptual crown architectures are drawn based on TreeQSM and Cyclone crown estimates by DBH classes (Figure 4.14 and Figure 4.15). TreeQSM depicted similar crown form with Cyclone for trees with DBH between 50 – 55 cm. However, TreeQSM omitted large numbers of branches for trees with DBH ≥ 60 cm. As the tree grows, branch exclusion occurs on the lower crown given the limited light, resulting in upward migration of crown mass. Therefore, TreeQSM could less accurately retrieve crown attributes for trees with DBH ≥ 60, in which the majority of branches are located at the higher portion of crowns than trees with DBH ≤ 55 cm. Consistent with greater variances of TreeQSM estimated BL and insertion angle, TreeQSM also derived more irregular crown profiles than Cyclone (Figure 4.14), supporting the uncertainties in the estimation of crown attributes using TreeQSM.

Conceptual crown architectures (Figure 4.15) developed based on Cyclone are supported by a previous study of age-related crown development (Ishii and McDowell,

2002). Our results suggest transitions of ellipsoid and conic crown shapes to cylindrical crown with the increase in DBH, as well as increasing gaps from branch loss due to light competition (Franklin et al., 2002) (Figure 4.15). For DBH classes of 50 – 55 and 60 – 65 cm, canopy gaps are mainly found in lower crowns facing north, which likely are caused by the absence of enough light (Figure 4.15 a and b). However, extraordinarily long isolated branches are also found in low canopy gaps, probably as a result of increasing light availability from neighboring branch exclusion (Figure 15 a and b). In addition, the variation of insertion angle increases with growing tree size (Figure 15 c). The diversity of insertion angle eventually will increase the light resource for neighboring branches. For trees with DBH ≥ 85 cm, most branches are surprisingly north facing, possibly because of the light competition from neighboring trees that challenges south-facing branch expansion.

Our findings suggest that point clouds can provide fine scale crown architectural estimates comparable with field measurements. The crown attributes generated from human-aid TLS estimation procedure are consistent with existing studies (Ishii and McDowell, 2002; Ishii and Wilson, 2001; Maguire et al., 1999; Pelt and Sillett, 2008). The comparison of crown attributes by DBH classes provides numerical support for crown development driven by light condition defined by neighboring trees.

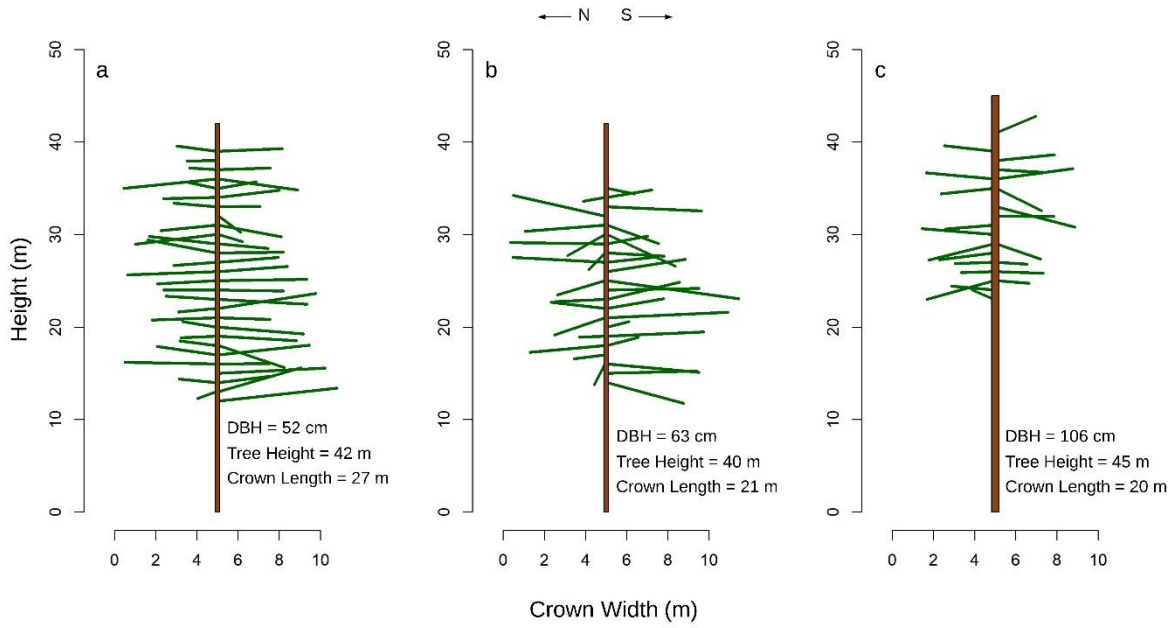

Figure 4.14 Conceptual Douglas-fir tree architectures developed based on TreeQSM crown attribute estimates by DBH classes.

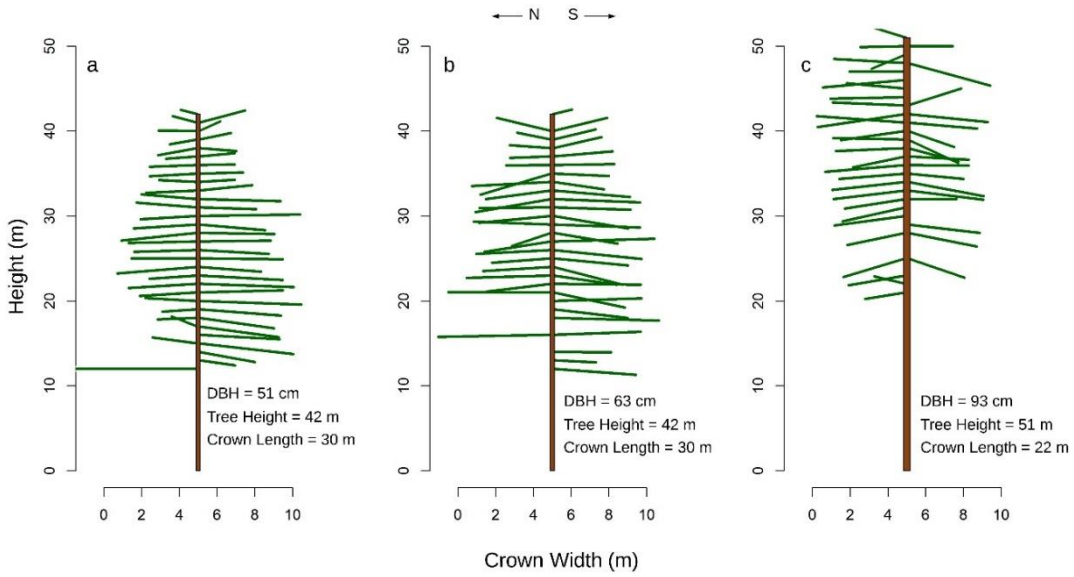

Figure 4.15 Conceptual Douglas-fir tree architectures developed based on Cyclone crown attribute estimates by DBH classes.

4.5. Conclusion

This study evaluated the accuracy of two TLS-based estimation procedures of mature Douglas-fir crown attributes of neighboring dominant and codominant mature trees. Additionally, I assessed the ability of the estimation procedures to describe the crown attributes of mature unmanaged Douglas-firs. The two procedures are a semi-automatic approach — Cyclone, and an automation process, TreeQSM. Although limited human interference is required in TreeQSM process, the uncertainty of TreeQSM estimated crown attributes challenges its application in dense conifer forests. Therefore, significantly more work is needed to implement an operational automatic crown measurement algorithm, similar as TreeQSM, for tall Douglas-firs. I expect that comparable conclusions would be found for other coniferous species, as similar crown architecture is present. Among the estimated attributes, the branch diameters computed by TreeQSM are the closest to the Cyclone values, whereas the branch lengths are significantly shorter than the Cyclone values. The simulated trees based on the TLS estimates suggest an intermediate developmental stage of the trees, as they are between the second- and old-growth stands. The conceptual crown architectures developed based on TLS estimates are similar with other studies, supporting the finding that crown development is driven by light availability.

References

Aussenac, G., 2000. Interactions between forest stands and microclimate: Ecophysiological aspects and consequences for silviculture. Ann. For. Sci. 57, 287–301. https://doi.org/10.1051/forest:2000119

Barbour, R.J., Johnston, S., Hayes, J.P., Tucker, G.F., 1997. Simulated stand characteristics and wood product yields from Douglas-fir plantations managed for ecosystem objectives. For. Ecol. Manag. 91, 205–219. https://doi.org/10.1016/S0378-1127(96)03873-X

Bauhus, J., Puettmann, K., Messier, C., 2009. Silviculture for old-growth attributes. For. Ecol. Manag., Old forests, new management: the conservation and use of old-growth forests in the 21st century 258, 525–537. https://doi.org/10.1016/j.foreco.2009.01.053

Bertram, J.E.A., 1989. Size-dependent differential scaling in branches: the mechanical design of trees revisited. Trees 3, 241–253. https://doi.org/10.1007/BF00225358

Briggs, D., Ingaramo, L., Turnblom, E., 2007. Number and diameter of breast-height region branches in a Douglas-fir spacing trial and linkage to log quality. For. Prod. J. 57, 28-.

Brunner, A., Nigh, G., 2000. Light absorption and bole volume growth of individual Douglas-fir trees. Tree Physiol. 20, 323–332. https://doi.org/10.1093/treephys/20.5-6.323

Burt, A., Disney, M., Raumonen, P., Armston, J., Calders, K., Lewis, P., 2013. Rapid characterisation of forest structure from TLS and 3D modelling. Presented at the 2013 IEEE International Geoscience and Remote Sensing Symposium-IGARSS, IEEE, pp. 3387–3390.

Calders, K., Origo, N., Burt, A., Disney, M., Nightingale, J., Raumonen, P., Åkerblom, M., Malhi, Y., Lewis, P., 2018. Realistic Forest Stand Reconstruction from Terrestrial LiDAR for Radiative Transfer Modelling. Remote Sens. 10, 933. https://doi.org/10.3390/rs10060933

Chen, J., Franklin, J., 1997. Growing-season microclimate variability within an old-growth Douglas-fir forest. Clim. Res. 8, 21–34. https://doi.org/10.3354/cr008021

Clement, J.P., Shaw, D.C., 1999. Crown structure and the distribution of epiphyte functional group biomass in old-growth Pseudotsuga menziesii trees. Ecoscience 6, 243–254.

Coops, N.C., Hilker, T., Wulder, M.A., St-Onge, B., Newnham, G., Siggins, A., Trofymow, J.T., 2007. Estimating canopy structure of Douglas-fir forest stands from discrete-return LiDAR. Trees 21, 295.

Crowder, M.J., Hand, D.J., 1990. Analysis of repeated measures, Monographs on statistics and applied probability. Chapman and Hall, London.

Danson, F.M., Hetherington, D., Morsdorf, F., Koetz, B., Allgower, B., 2007. Forest Canopy Gap Fraction From Terrestrial Laser Scanning. IEEE Geosci. Remote Sens. Lett. 4, 157–160. https://doi.org/10.1109/LGRS.2006.887064

Davis, L.R., Puettmann, K.J., Tucker, G.F., 2007. Overstory Response to Alternative Thinning Treatments in Young Douglas-fir Forests of Western Oregon. Northwest Sci. 81, 1–14. https://doi.org/10.3955/0029-344X-81.1.1

Delagrange, S., Jauvin, C., Rochon, P., 2014. PypeTree: a tool for reconstructing tree perennial tissues from point clouds. Sensors 14, 4271–4289.

Diggle, P., Heagerty, P., Liang, K.Y., Zeger, S.L., 2002. Analysis of longitudinal data. Oxford University Press, New York.

Ferrarese, J., Affleck, D., Seielstad, C., 2015. Conifer crown profile models from terrestrial laser scanning. Silva Fenn 49, 1106.

Fitzmaurice, G.M., Laird, N.M., Ware, J.H., 2004. Applied Longitudinal Analysis. Wiley, Hoboken NJ.

Franklin, J.F., Spies, T.A., Van Pelt, R., Carey, A.B., Thornburgh, D.A., Berg, D.R., Lindenmayer, D.B., Harmon, M.E., Keeton, W.S., Shaw, D.C., 2002. Disturbances and structural development of natural forest ecosystems with silvicultural implications, using Douglas-fir forests as an example. For. Ecol. Manag. 155, 399–423.

García, M., Danson, F.M., Riaño, D., Chuvieco, E., Ramirez, F.A., Bandugula, V., 2011. Terrestrial laser scanning to estimate plot-level forest canopy fuel properties. Int. J. Appl. Earth Obs. Geoinformation 13, 636–645. https://doi.org/10.1016/j.jag.2011.03.006

Getzin, S., Wiegand, K., 2007. Asymmetric tree growth at the stand level: Random crown patterns and the response to slope. For. Ecol. Manag. 242, 165–174. https://doi.org/10.1016/j.foreco.2007.01.009

Getzin, S., Wiegand, K., Schumacher, J., Gougeon, F.A., 2008. Scale-dependent competition at the stand level assessed from crown areas. For. Ecol. Manag. 255, 2478–2485.

Ghimire, S., Xystrakis, F., Koutsias, N., 2017. Using Terrestrial Laser Scanning to Measure Forest Inventory Parameters in a Mediterranean Coniferous Stand of Western Greece. PFG–Journal Photogramm. Remote Sens. Geoinformation Sci. 85, 213–225.

Hackenberg, J., Spiecker, H., Calders, K., Disney, M., Raumonen, P., 2015a. SimpleTree—an efficient open source tool to build tree models from TLS clouds. Forests 6, 4245–4294.

Hackenberg, J., Wassenberg, M., Spiecker, H., Sun, D., 2015b. Non Destructive Method for Biomass Prediction Combining TLS Derived Tree Volume and Wood Density. Forests 6. https://doi.org/10.3390/f6041274

Hann, D.W., 1999. An Adjustable Predictor of Crown Profile for Stand-Grown Douglas-Fir Trees. For. Sci. 45, 217–225. https://doi.org/10.1093/forestscience/45.2.217

Hilker, T., van Leeuwen, M., Coops, N.C., Wulder, M.A., Newnham, G.J., Jupp, D.L., Culvenor, D.S., 2010. Comparing canopy metrics derived from terrestrial and airborne laser scanning in a Douglas-fir dominated forest stand. Trees 24, 819–832.

Ishii, H., Clement, J.P., Shaw, D.C., 2000. Branch growth and crown form in old coastal Douglas-fir. For. Ecol. Manag. 131, 81–91.

Ishii, H., Ford, E.D., 2002. Persistence ofPseudotsuga menziesii (Douglas-fir) in temperate coniferous forests of the Pacific Northwest Coast, USA. Folia Geobot. 37, 63–69. https://doi.org/10.1007/BF02803191

Ishii, H., McDowell, N., 2002. Age-related development of crown structure in coastal Douglas-fir trees. For. Ecol. Manag. 169, 257–270.

Ishii, H., Wilson, M.E., 2001. Crown structure of old-growth Douglas-fir in the western Cascade Range, Washington. Can. J. For. Res. 31, 1250–1261.

Ishii, H.T., Tanabe, S., Hiura, T., 2004. Exploring the Relationships Among Canopy Structure, Stand Productivity, and Biodiversity of Temperate Forest Ecosystems. For. Sci. 50, 342–355. https://doi.org/10.1093/forestscience/50.3.342

Jackson, T., Shenkin, A., Wellpott, A., Calders, K., Origo, N., Disney, M., Burt, A., Raumonen, P., Gardiner, B., Herold, M., Fourcaud, T., Malhi, Y., 2019. Finite element analysis of trees in the wind based on terrestrial laser scanning data. Agric. For. Meteorol. 265, 137–144. https://doi.org/10.1016/j.agrformet.2018.11.014

Kershaw Jr., J.A., Maguire, D.A., 1996. Crown structure in western hemlock, Douglas-fir, and grand fir in western Washington: horizontal distribution of foliage within branches. Can. J. For. Res. 26, 128–142. https://doi.org/10.1139/x26-014

Kramer, R.D., Sillett, S.C., Van Pelt, R., Franklin, J.F., 2019. Neighborhood competition mediates crown development of Picea sitchensis in Olympic rainforests: Implications for restoration management. For. Ecol. Manag. 441, 127–143. https://doi.org/10.1016/j.foreco.2019.03.027

Lau, A., Bentley, L.P., Martius, C., Shenkin, A., Bartholomeus, H., Raumonen, P., Malhi, Y., Jackson, T., Herold, M., 2018. Quantifying branch architecture of tropical trees using terrestrial LiDAR and 3D modelling. Trees 32, 1219–1231. https://doi.org/10.1007/s00468-018-1704-1

Lau, A., Martius, C., Bartholomeus, H., Shenkin, A., Jackson, T., Malhi, Y., Herold, M., Bentley, L.P., 2019. Estimating architecture-based metabolic scaling exponents of tropical trees using terrestrial LiDAR and 3D modelling. For. Ecol. Manag. 439, 132–145. https://doi.org/10.1016/j.foreco.2019.02.019

Leica Geosystems, 2019. Leica Cyclone Register 360. Leica Geosystems.

Lyons, B., Nadkarni, N.M., North, M.P., 2000. Spatial distribution and succession of epiphytes on Tsuga heterophylla (western hemlock) in an old-growth Douglas-fir forest. Can. J. Bot. 78, 957–968.

Maguire, D., Moeur, M., Bennett, W., 1994. Models for describing basal diameter and vertical distribution of primary branches in young Douglas-fir. For. Ecol. Manag. 63, 23–55.

Maguire, D.A., Bennett, W.S., 1996. Patterns in vertical distribution of foliage in young coastal Douglas-fir. Can. J. For. Res. 26, 1991–2005.

Maguire, D.A., Brissette, J.C., Gu, L., 1998. Crown structure and growth efficiency of red spruce in uneven-aged, mixed-species stands in Maine. Can. J. For. Res. 28, 1233–1240.

Maguire, D.A., Johnston, S.R., Cahill, J., 1999. Predicting branch diameters on second-growth Douglas-fir from tree-level descriptors. Can. J. For. Res. 29, 1829–1840.
Maguire, D.A., Kershaw, J.A., Hann, D.W., 1991. Predicting the effects of silvicultural regime on branch size and crown wood core in Douglas-fir. For. Sci. 37, 1409–1428.
Malhi, Y., Jackson, T., Patrick Bentley, L., Lau, A., Shenkin, A., Herold, M., Calders, K., Bartholomeus, H., Disney, M.I., 2018. New perspectives on the ecology of tree structure and tree communities through terrestrial laser scanning. Interface Focus 8, 20170052.
McMahon, T.A., Kronauer, R.E., 1976. Tree structures: deducing the principle of mechanical design. J. Theor. Biol. 59, 443–466.
Michel, A.K., Winter, S., 2009. Tree microhabitat structures as indicators of biodiversity in Douglas-fir forests of different stand ages and management histories in the Pacific Northwest, U.S.A. For. Ecol. Manag. 257, 1453–1464. https://doi.org/10.1016/j.foreco.2008.11.027
Moorthy, I., Miller, J.R., Berni, J.A.J., Zarco-Tejada, P., Hu, B., Chen, J., 2011. Field characterization of olive (Olea europaea L.) tree crown architecture using terrestrial laser scanning data. Agric. For. Meteorol. 151, 204–214.
Mori, S., Hagihara, A., 1991. Crown profile of foliage area characterized with the Weibull distribution in a hinoki (Chamaecyparis obtusa) stand. Trees-Struct. Funct. 5, 149–152.
Moskal, L.M., Zheng, G., 2012. Retrieving Forest Inventory Variables with Terrestrial Laser Scanning (TLS) in Urban Heterogeneous Forest. Remote Sens. 4, 1–20. https://doi.org/10.3390/rs4010001
Nyland, R.D., 1996. Silviculture. Concepts and applications. McGraw-Hill, New York.
Pal, N.R., Pal, S.K., 1993. A review on image segmentation techniques. Pattern Recognit. 26, 1277–1294. https://doi.org/10.1016/0031-3203(93)90135-J
Parker, G.G., 1997. Canopy structure and light environment of an old-growth Douglas-fir/Western hemlock forest.
Pelt, R.V., Sillett, S.C., 2008. Crown development of coastal Pseudotsuga menziesii, including a conceptual model for tall conifers. Ecol. Monogr. 78, 283–311.
Raumonen, P., Casella, E., Calders, K., Murphy, S., Åkerbloma, M., Kaasalainen, M., 2015. MASSIVE-SCALE TREE MODELLING FROM TLS DATA. ISPRS Ann. Photogramm. Remote Sens. Spat. Inf. Sci. II-3/W4, 189–196. https://doi.org/10.5194/isprsannals-II-3-W4-189-2015
Raumonen, P., Casella, E., Disney, M., Åkerblom, M., Kaasalainen, M., 2013a. Fast automatic method for constructing topologically and geometrically precise tree models from TLS Data. Presented at the 7th International Conference on Functional-Structural Plant Models, Saariselkä, Finland, pp. 89–91.
Raumonen, P., Kaasalainen, M., Åkerblom, M., Kaasalainen, S., Kaartinen, H., Vastaranta, M., Holopainen, M., Disney, M., Lewis, P., 2013b. Fast Automatic Precision Tree Models from Terrestrial Laser Scanner Data. Remote Sens. 5, 491–520. https://doi.org/10.3390/rs5020491

Roeh, R.L., Maguire, D.A., 1997. Crown profile models based on branch attributes in coastal Douglas-fir. For. Ecol. Manag. 96, 77–100.
Sillett, S., Neitlich, P.N., n.d. EmergingThemesin EpiphyteResearchin WestsideForestswith SpecialReferenceto Cyanolichens 7.
Sillett, S.C., Bailey, M.G., 2003. Effects of tree crown structure on biomass of the epiphytic fern Polypodium scouleri (Polypodiaceae) in redwood forests. Am. J. Bot. 90, 255–261. https://doi.org/10.3732/ajb.90.2.255
Spies, T.A., Hemstrom, M.A., Youngblood, A., Hummel, S., 2006. Conserving Old-Growth Forest Diversity in Disturbance-Prone Landscapes. Conserv. Biol. 20, 351–362. https://doi.org/10.1111/j.1523-1739.2006.00389.x
Srinivasan, S., Popescu, S.C., Eriksson, M., Sheridan, R.D., Ku, N.-W., 2015. Terrestrial Laser Scanning as an Effective Tool to Retrieve Tree Level Height, Crown Width, and Stem Diameter. Remote Sens. 7, 1877–1896. https://doi.org/10.3390/rs70201877
Swanson, F.J., Franklin, J.F., 1992. New Forestry Principles from Ecosystem Analysis of Pacific Northwest Forests. Ecol. Appl. 2, 262–274. https://doi.org/10.2307/1941860
Tanago, J.G. de, Lau, A., Bartholomeus, H., Herold, M., Avitabile, V., Raumonen, P., Martius, C., Goodman, R.C., Disney, M., Manuri, S., Burt, A., Calders, K., 2018. Estimation of above-ground biomass of large tropical trees with terrestrial LiDAR. Methods Ecol. Evol. 9, 223–234. https://doi.org/10.1111/2041-210X.12904
Temesgen, H., Hann, D.W., Monleon, V.J., 2007. Regional Height–Diameter Equations for Major Tree Species of Southwest Oregon. West. J. Appl. For. 22, 213–219. https://doi.org/10.1093/wjaf/22.3.213
van Leeuwen, M., Coops, N.C., Hilker, T., Wulder, M.A., Newnham, G.J., Culvenor, D.S., 2013. Automated reconstruction of tree and canopy structure for modeling the internal canopy radiation regime. Remote Sens. Environ. 136, 286–300. https://doi.org/10.1016/j.rse.2013.04.019
Van Pelt, R., North, M.P., 1996. Analyzing canopy structure in Pacific Northwest old-growth forests with a stand-scale crown model.
Van Pelt, R., O'Keefe, T.C., Latterell, J.J., Naiman, R.J., 2006. Riparian forest stand development along the Queets river in Olympic National Park, Washington. Ecol. Monogr. 76, 277–298.
Zeide, B., Pfeifer, P., 1991. A method for estimation of fractal dimension of tree crowns. For. Sci. 37, 1253–1265.

Chapter 5 Modeling mature Douglas-fir crown attributes using point clouds-based measurements

Abstract

Crown attributes of a cluster of Douglas-fir were estimated using structural models developed from terrestrial laser scanning (TLS) point clouds. The length, diameter and insertion angles of each branch were described with nonlinear models. Besides dimensional variables, competition indices that measure the proximity of neighboring trees and shading effects were considered in the modeling process. The best models were for the maximum branch length and for the insertion angle of branches identified with maximum diameter at given canopy depth of each individual tree, which explained 79% and 70% of the variation, respectively. The mixed effect model of the maximum branch diameter only explained 60% variation of maximum branch diameter and 20% variation is accounted by random effect. Model of the insertion angle of branches with maximum length only explained 49% variation. Except for model of branches with maximum diameter, height- or crown length- related competition indices largely improved the model explanation power and DBH is not primary predictor variables in any of the models, implying light condition induced by shading and crowding effects determine the branch woody allocation instead of tree size capacity for closed canopy. Two crown profile model systems were developed with nonlinear seemingly unrelated regression (NSUR). One is based on maximum branch length and another is based on maximum branch diameter. The former achieved higher agreement with observations from TLS-based point clouds. Although NSUR did not apparently reduced bias and RMSE of the model, it brought consistency of the estimated coefficients by reducing the standard error of estimation.

Key words: branch attribute estimates, TLS, crown profile, Douglas-fir with mature crown, nonlinear seemingly unrelated regression

5.1. Introduction

Information of Douglas-fir branch allocation and crown profile guide silvicultural and ecosystem conservation practice in Pacific Northwest. Branch attributes, such as diameter, length, crown width and the relative location of the branches inside crowns are important indicators of tree primary production (Ishii et al., 2004; Lewis et al., 2000). Large branches, carrying a great amount of foliage, have superior photosynthesis potential (Oren et al., 1986), but also were argued to have great hydraulic resistance (Bond, 2000; McCulloh and Sperry, 2005) and high relative respiration rate to the stem (Sprugel, 1990), which in turn limits the photosynthetic activities (Hubbard et al., 1999). The crown of large trees, which is an important carbon sink, has been neglected in aboveground biomass estimation, since crowns have relatively lower carbon fixation than stems. However, crown continues to accrue biomass even after stem accumulation rate decrease as stand ages (Ishii et al., 2017).

Traditional crown structure studies applied widely present tree allometric relationships among organisms (Niklas, 1994; West et al., 1999) to predict branch attributes using predictor variables such as depth into the canopy (DINC) and tree-level parameters diameter at breast height (DBH), tree height and crown length. Numerous studies have developed allometric equations for predicting Douglas-fir branch attributes of both plantation trees (Garber and Maguire, 2005a; Maguire et al., 1999; Roeh and Maguire, 1997; Weiskittel et al., 2007) and trees in natural regime stands (Ishii et al., 2000; Ishii and Wilson, 2001; Nemec et al., 2012). The main challenge faced by the development

of crown allometric models is the need of extensive field measurements at multiple sites.

Recently, the focus of individual tree-level crown structural studies, described as the size and distributions of the branches, as well as their relationships with the stem and the neighboring crowns, has been shifted from allometric-model-driven to data-driven, since the advancements in applications of terrestrial laser scans (TLS) enabled fast and accurate acquisition of abundant canopy structural information. Multiple TLS-based crown structural studies applied convex hull algorithms to estimate individual crown volume and surface area (Korhonen et al., 2013; Lin et al., 2017; Trochta et al., 2017) or generalized crown shape with single distribution model such Beta and Weibull distributions (Ferrarese et al., 2015). However, either convex hull or generalized crown profile uses only surface points to describe crown features. A wealth of point clouds inside the crown were omitted, although they convey richness of information about fine-scale branches structural attributes such as branch diameter, branch insertion angle and branch length.

Quantitative structural modeling (QSM) is an automatic approach to model the tree skeleton structure with cylindrical models (Delagrange et al., 2014; Hackenberg et al., 2015a, 2014; Raumonen et al., 2013b). Accurate estimation with QSM requires full coverage of point clouds on the scanned leaf-off branches. QSM could successfully estimate branch diameter that are greater than 10 cm (Hackenberg et al., 2015b; Tanago et al., 2018), but tends to overestimate the smaller branches (Lau et al., 2019, 2018) when the variance of point clouds accuracy approaches to the size of the branch dimension. Therefore, usage of QSM to construct structural models of tall conifer trees

located in dense canopy is limited, especially for the upper crown, where insufficient points are missing from ground-based scans as a result of obstruction (Fang and Strimbu, 2019). Consequently, branch measurements of tall conifer trees using TLS-based point clouds are more reliable with human eye assistance in a computer-aid system than using automatic algorithms, particularly inside the crown (Fang and Strimbu, 2019).

The application of TLS is currently not realistic for extensive forest inventory, as the operation is usually expensive. Besides, processing dense point clouds data requires advanced algorithms and powerful computation capacity. Allometric models still serve as important tools for forest inventory and enhance the understanding of branch woody biomass allocation. Nevertheless, TLS-based branch measurement plays as a supporting role in constructing branch allometric models, reducing the field measurement effort and enabling permanent storage of tree structural information.

Allometric models perform as expected when predicting the branch structure of young plantation trees. As trees age, the complexity of the crown structure increases and branch attributes are less predictable from several tree-level parameters, since crown development is more driven by recent growing conditions (Bartelink, 1996; Ishii et al., 2017) rather than stem size. Variability of light condition is the main factor that triggers the canopy complexity (Ishii and McDowell, 2002; Ishii et al., 2004). For stands with closed canopy, competition for light resource with neighbor trees is a main factor influencing the mass allocation (Bartelink, 1996), which is more prominent in shade-intolerant species. The intensity of competition is mainly determined by the neighbor

trees' size and proximity to the focal trees (Harold E. Burkhart and Tomé, 2012; Rouvinen and Kuuluvainen, 1997). Competition with neighbors alters the symmetric ellipsoid or conic crown geometry to asymmetry for more light availability (Krůček et al., 2019; Rouvinen and Kuuluvainen, 1997) and limits the tree crown volume gain over long period in old-growth forests (Kramer et al., 2019). Considering the immediate effect of light condition on crown development, neighbor competition may be a significant factor influencing the branch woody mass allocation. For natural regime stand, little allometric models are available for branch attribute estimation with consideration of competition impacts.

This study aims to developing branch allometric models of mature Douglas-fir crown located in a natural regime stand using TLS-based branch measurements. The estimated branch attributes include branch diameter, maximum branch diameter, branch length, maximum branch length and branch insertion angle. Size- and distance-dependent competition indices are considered in the model development. First, individual models were developed for each branch attributes. Second, systematic branch models were developed with nonlinear seemly unrelated regression (NSUR). Crown profile was predicted with systematic model sets.

5.2. Data and method

5.2.1. Study site and field data collection

The study site is located at Oregon Cascade HJ Andrews Experimental Forest. An 80 × 100 m plot within a mature natural regime stand was scanned with a RIEGL VZ400i scanner. The plot was scanned from 22 spots, consisting of a 10-min scan with higher

resolution located at the center of the plot and 21 5-min scans evenly spread in the site. A set of 76 reference targets were placed inside the plot and their relative coordinates were surveyed with a Trimble RTS633 total station from 3 survey spots. Individual scans were aligned using reference targets as well as cloud-to-cloud comparison in Cyclone software. The overall mean absolute errors of target and cloud-to-cloud alignment are 0.009 m and 0.016 m respectively.

A cluster of 42 neighboring Douglas firs, with DBH and tree height ranging from 27.6 – 136 cm and 22 – 57 m respectively, are selected from the TLS point clouds and manually delineated in Leica Cyclone software. Tree crown adjacent relationships were identified from the above view of the point clouds. Eventually nine dominant and codominant trees, with total height as important indicator of site productivity, completely located within the center of the cluster were measured in their branch attributes. Other trees inside the cluster were only measured in their DBH and total height.

5.2.2. TSL-based branch estimates in Cyclone

For each tree, I directly measured three tree-level and five branch-level variables with TLS-based point clouds (Table 5.1). I also computed four attributes, which are commonly used in forest modeling, namely branch relative height (RH), branch depth inside the crown (DINC), and branch relative depth into the crown (RDINC), branch relative height inside crown (RHC) (Table 5.1). Maximum branch diameter (BD_{max}) and length (BL_{max}) were also estimated and determined as the maximum values of

branch diameter or length within every one-meter interval along the crown height of a specific tree.

TLS-based tree attribute measurements were performed in Leica Cyclone software. Tree height was estimated as the difference between Z value of the highest and the base points of the target tree (Figure 5.1 a). The branch base where it attaches to the stem was fitted as an approximate cylinder using Region Grow function in Cyclone. The operation of Region Grow requires selection of seed points from the target surface, then the algorithm automatically expand the selection of points by growing from seeds points until all the possible target points are included. Tree DBH was estimated as the diameter of cylinder at height of 1.3 m (Figure 5.1 a). Crown base was identified from the point clouds where lowest branches were identified. Crown length was estimated as the difference between Z values of points of lowest branch base and tree top (Figure 5.1 a). Branch main skeletons were traced with line segments that connect vertexes defining the overall shape of branches (Figure 5.1 d). Branch diameter was estimated as the diameter of cylinder model at branch base (Figure 5.1 c). Branch length was estimated sum of the line segments of a branch skeleton (Figure 5.1 d). Branch insertion angle was estimated as angle between stem axis at branch insertion point and line segment of branch base (Figure 5.1 c). Crown radius is estimated as the projected distance between branch end point and the stem cylinder where the branch attaches to (Figure 5.1 d).

TLS-based point cloud density decreases as canopy height increases. Considerable points that define the branch diameter were missing at the upper crown (Figure 5.1 b).

Since Region Grow in Cyclone requires sufficient points to fit the cylinders, missing points at crown top disabled cylinder fit of branches. However, points that define the branch skeleton and crow radius were still identifiable (Figure 5.1 b). Hence, branches at the top of the crown were still measured for their height, length, insertion angle, and crown radius, but only few branch diameters were estimated at height above 30 m.

Table 5.1 Summary of involved variables branch profile modeling.

Variable	Definition
	Tree Level
DBH_i	Diameter at breast height (1.3 m above the base) (cm)
THT_i	Total tree height (m)
CL_i	Crown Length (m)
	Branch Level
h_{ij}	Height of branch insertion point above the stem bottom (m)
RH_{ij}	Branch relative height: $\frac{h_{ij}}{THT_i}$
$DINC_{ij}$	Depth into the crown (m)
$RDINC_{ij}$	Relative depth into the crown: $RDINC_{ij} = \frac{DINC_{ij}}{CL_i}$
RHC_{ij}	Branch relative height inside crown: $RHC_{ij} = \frac{h_{ij} - HCB_i}{CL_i}$, HCB_i is height of crown base of tree i
CR_i	Crown Radius
BD_{ij}	Branch diameter at the insertion point (cm)
$BD_{max_{ij}}$	Maximum branch diameter of tree i, at DINC j
BL_{ij}	Branch accumulative length of longest path (m)
$BL_{max_{ij}}$	Maximum branch length of tree i, at DINC j
A_{ij}	Branch insertion angle (°)

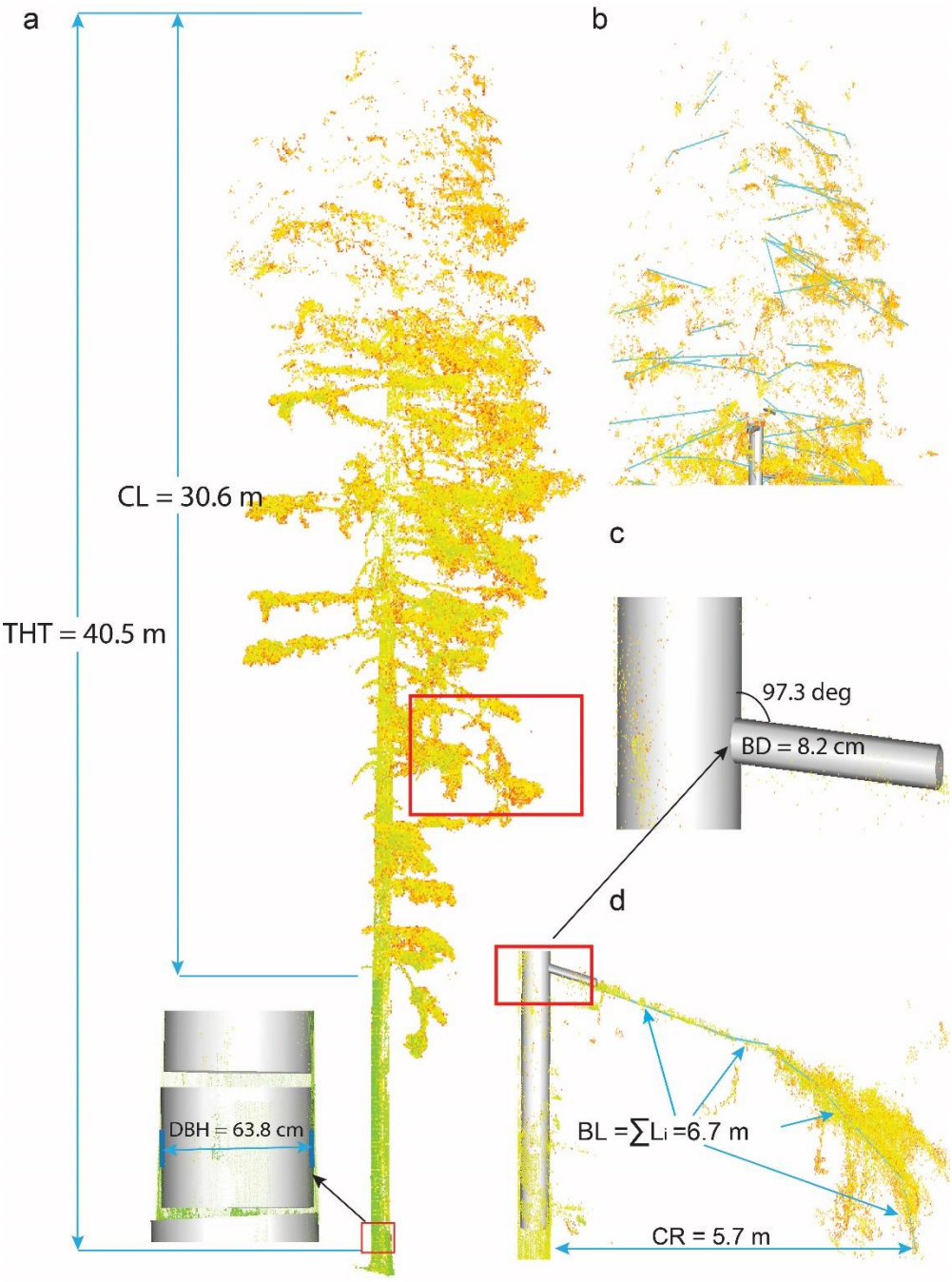

Figure 5.1 An example of tree estimation in Cyclone. a. Tree-level attribute measurements: total height (THT), crown length (CL) and diameter at breast height (DBH). b. a considerable number of points were missing inside the crown, but branch skeletons were still traced with line segments. c. Branch diameter (BD) and insertion angle estimates with the cylinder models. d. Branch length (BL) and crown radius (CR) estimates.

5.2.3. Competition indices

Five size- and distance-dependent competition indices were considered in the modeling procedure to reveal the neighboring trees' impacts on the profile of the focal trees (Table 5.2). Although different studies used various buffering distances to decide the neighboring trees (5 – 11 m) (Contreras et al., 2011; Rouvinen and Kuuluvainen, 1997; Woodall et al., 2003), we considered the neighboring trees as those whose crowns were directly in touch with the focal trees to avoid the arbitrary selection of the buffering distance. The distance between neighboring trees and the focal trees ranges from 2.98 to 14.88 m with an average of 8.68 m. In Table 6.2, indices CI_1 (Hegyi, 1974) and CI_2 (Figure 5.2 a) (Pukkala and Kolström, 1987) quantify the competition intensity as positive and negative effects of the neighboring trees' DBH and their distances to the focal trees respectively. Corresponding to indices CI_1 and CI_2, indices CI_3 (Braathe, 1980) and CI_4 (Figure 5.2 b) (Rouvinen and Kuuluvainen, 1997) use the neighboring trees' height instead of DBH to quantify the competition effects since neighbors' canopy height, rather than DBH, is a more determinant factor of the light condition for the focal tree. A crown-length-based competition index (CI_5 in Table 5.2 and illustrated in Figure 5.2 b) was also developed, because the crown dimensions of neighboring trees directly cause shading effect on the focal trees.

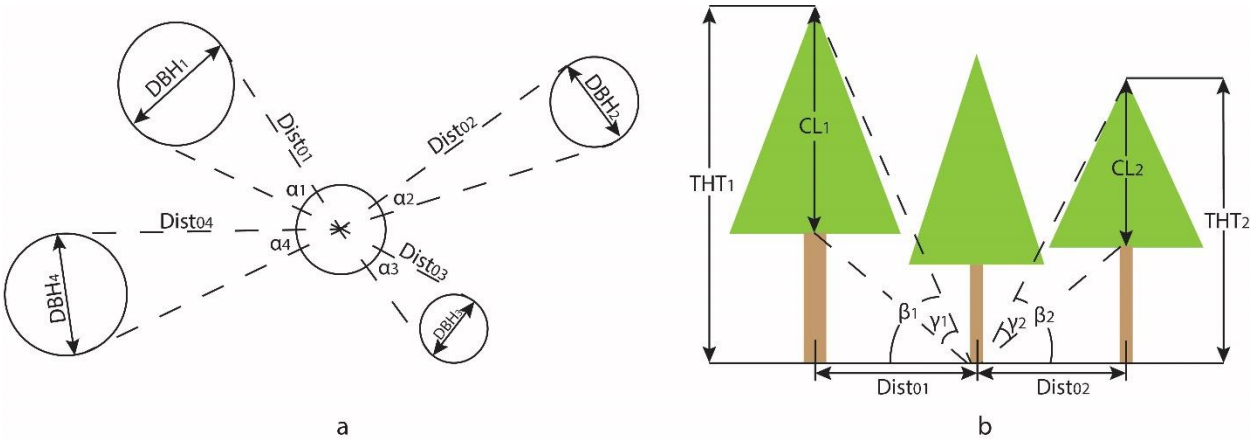

Figure 5.2 Illustration of angular measures in competition indices. a. The horizontal angular measure between the focal and the neighboring trees. The tree in the center is the focal tree; b. vertical angular measures between the focal and the neighboring trees . The tree in the middle is the focal tree. $\alpha_i = arctan\left(\frac{DBH_i}{Dist_{0i}}\right)$. $\beta_i = arctan\left(\frac{THT_i}{Dist_{0i}}\right)$. $\gamma_i = arctan\left(\frac{THT_i}{Dist_{0i}}\right) - arctan\left(\frac{THT_i - CL_i}{Dist_{0i}}\right)$, where DBH_i is the DBH of the ith neighbor of the center tree, $Dist_{0i}$ is the distance between the center tree and the neighbor tree i, THT_i and THT_0 are the total tree height of the neighbor tree i and the center tree respectively, CL_i is the crown length of the neighbor tree i.

Table 5.2 Definitions of competition indices.

Competition Index	Definition	Variables definition
CI1	$\sum_{i=1}^{n} \frac{\frac{DBH_i}{DBH_0}}{Dist_{0i}}$	DBH_i and DBH_0 are the DBH of neighbor tree i and center tree 0 respectively, $Dist_{0i}$ is the distance between tree i and 0.
CI2	$\sum_{i=1}^{n} \alpha_i \frac{DBH_i}{DBH_0}$	$\alpha_i = \arctan\left(\frac{DBH_i}{Dist_{0i}}\right)$, DBH_i is the DBH of tree i and $Dist_{0i}$ is the distance between tree i and 0.
CI3	$\sum_{i=1}^{n} \frac{\frac{THT_i}{THT_0}}{Dist_{0i}}$	THT_i and THT_0 are the total tree height of neighbor tree i and center tree 0 respectively, $Dist_{0i}$ is the distance between the tree i and 0.
CI4	$\sum_{i=1}^{n} \beta_i \frac{THT_i}{THT_0}$	$\beta_i = \arctan\left(\frac{THT_i}{Dist_{0i}}\right)$, THT_i and THT_0 are the total tree height of the neighbor tree i and the center tree 0, $Dist_{0i}$ is the distance between the tree i and 0.
CI5	$\sum_{i=1}^{n} \gamma_i \frac{THT_i}{THT_0}$	$\gamma_i = \arctan\left(\frac{THT_i}{Dist_{0i}}\right) - \arctan\left(\frac{THT_i - CL_i}{Dist_{0i}}\right)$, THT_i and THT_0 are the total tree height of the neighbor tree i and the center tree 0, CL_i is the crown length of the neighbor tree i, $Dist_{0i}$ is the distance between the tree i and 0.

5.2.4. anch attribute modeling

5.2.4.1. Individual modeling

Branch diameter, length and insertion angle were individually regressed against predictor variables of tree-level attributes and height position of the branches (Table 5.1). Whorl and interwhorl branches were not separated in TLS-based estimates. Branch length was modeled for all observations and the maximum values of groups by one-meter interval in the crowns. Complete sets of branch diameter estimates were not acquired from TLS measurements. Branch diameter was only modeled for its maximum observations by one-meter interval in the crowns. The maximum branch diameter and length are supposed to better associate with whorl branch features (Garber and Maguire, 2005a; Maguire et al., 1999; Roeh and Maguire, 1997), which are original branches initiated with the stem annual growth. Candidate models included

weighed/unweighted simple linear and weighed/unweighted nonlinear model forms with various combination of predictor variables. Different error covariance structures, such as first-order autoregressive (AR(1)), compound symmetry and unstructured, were also tested in the selected models. The candidate models were evaluated with goodness-of-fit, root mean square error (RMSE), bias, Akaike information criterion (AIC), and significance of the estimated coefficients, as well as the examination of the residual plots. Final models were selected as those yielded the best evaluation measures (highest coefficient of determination R^2, lowest RMSE, and lowest AIC value) and were explainable from ecological viewpoints. To remove the potential autocorrelation between measured branch attributes from the same individual tree, tree-level random effects were tested in modeling procedures (Garber and Maguire, 2003; Groot and Schneider, 2011; Maguire et al., 1999; Poudel et al., 2018).

All the modeling procedures were performed using R package nlme (Pinheiro and Bates, 2019). The final selected model forms are summarized in Table 5.3. For all and the maximum branch length observations, the selected models were adapted from Kozak (2004) variable-exponent model form. The original variable-exponent model describes the stem taper evolvement along height as proportion of expected maximum stem diameter. In this study, the branch length is predicted as a proportion of the expected maximum estimate, which can be described as:

$$BL = MBL \times Z^{\omega} \qquad 5\text{-}1$$

where BL is branch length, MBL is theoretically expected maximum estimates, $MBL = f(DBH, THT, CL)$, Z is a term of relative position, $Z = \frac{1-RH^{1/3}}{1-(0.01*\frac{CL}{THT})^{1/3}}$, ω is a function of the exponential rate.

The final selected models for all and maximum branch length observations are presented in Table 5.3. For all branch length model, I found that the power function of DBH along explained most variation of MBL. Random effect terms were included to remove potential autocorrelation resulted from the repeated measurements on a single tree (Garber and Maguire, 2005a; Maguire et al., 1999). For maximum branch length model, the power function of crown length explained most variation of MBL. First-order autoregressive (AR(1)) was used in the maximum branch length model to remove autocorrelation of repeated measurements. Both selected models were weighed by the square of RDINC to remove the heteroscedasticity. Error distribution of selected models is described as $N(0, \sigma^2 RDINC^2)$, where σ^2 is the estimated overall variance.

The final selected maximum branch diameter model is polynomial model (Table 5.3). Other candidate models, such as variable exponent model (Maguire et al., 1999) and power model ($BD \propto DBH^{h_1(\mathbf{X}_1)} THT^{h_2(\mathbf{X}_2)} CL^{h_3(\mathbf{X}_3)} DINC^{h_4(\mathbf{X}_4)}$ where $h_i(\mathbf{X}_i)$ is the function of power term, $\mathbf{X}_i$ is the corresponding predictors, i=1…n) could not provide comparable evaluation measures with a relative simple form. Since most available branch diameter estimates were located at the middle-lower crown, to avoid bias estimation, the selected branch diameter model was not constrained to pass the zero point at crown top. All the significant terms were included in the polynomial models.

Correspondingly, branch insertion angle was modeled for observations of branches with maximum length and diameter. Some candidate model forms were provided from previous studies (Osborne and Maguire, 2015; Roeh and Maguire, 1997; Weiskittel et al., 2007). However, none of these models yielded comparable evaluation measures as models selected in this study (Table 5.3 model AML and AMD), which can be described as:

$$A = a_0 CL_i^{a_1} f(DINC, CI_5) \qquad 5\text{-}2$$

where A is the predicte

$a_0 CL_i^{a_1}$ determines the expected value of insertion angle,

$f(DINC, CI_5)$ is an equation of DINC and CI_5 and determines the changing rate of the insertion angle along the crown height.

The change rate of model AML is an exponential function of RDINC and competition index CI5. However, the change rate of model AMD is a power term of DINC, allowing much more gradual change of insertion angle along canopy depth. Unlike studies conducted by Roeh and Maguire (1997) and Weiskittel et al. (2007), maximum branch diameter was not found significantly determining branch insertion angle in this study.

Table 5.3 Selected model forms for developing branch models

Branch Attribute	Model	Form	
Branch length	L	$\mathrm{BL}_{ij} = \mathrm{a}_{11}\mathrm{DBH}_i^{\mathrm{a}_{12}} Z_{ij}^{\left\{\mathrm{a}_{13} DBH_i^{RDINC_{ij}} + \mathrm{a}_{14}\exp\left(\frac{\mathrm{DBH}_i}{\mathrm{THT}_i}\right)^{-1} + \delta_i\right\}} + \mathrm{e}_{ij}$	(5-3)
Maximum Branch Length	LM	$\mathrm{BL}_{max_{ij}} = \mathrm{a}_{21}\mathrm{CL}_i^{\mathrm{a}_{22} CI_{4i}} Z_{ij}^{\left\{\mathrm{a}_{23} + \mathrm{a}_{24} DBH_i^{RDINC_{ij}} + \mathrm{a}_{25}\frac{\mathrm{DBH}_i}{\mathrm{THT}_i} + \mathrm{a}_{26} CI_{5i}\right\}} + \mathrm{e}_{ij}$	(5-4)
Maximum Branch Diameter	DM	$\mathrm{BD}_{max_{ij}} = \mathrm{a}_{31}\mathrm{DINC}_{ij} + \mathrm{a}_{32} DINC_{ij}^2 + \mathrm{a}_{35} RDINC_{ij}^2 \times CI_{4_i} + \delta_{1i} * \mathrm{DBH}_i \times \mathrm{RDINC}_{ij} + \delta_{2i} + \mathrm{e}_{ij}$	(5-5)
Branch Insertion Angle	A_{ML}	$\mathrm{A}_{ij} = \mathrm{a}_{41} CL_i^{\mathrm{a}_{42}} \exp\left(\mathrm{a}_{43} * RINC_{ij} + \mathrm{a}_{44} * CI_{5_i}\right) + \mathrm{e}_{ij}$	(5-6)
Branch Insertion Angle	A_{MD}	$\mathrm{A}_{ij} = \mathrm{a}_{51} CL_i^{\mathrm{a}_{52}} DINC_{ij}^{\{\mathrm{a}_{53} + \mathrm{a}_{54} CI_{5_i}\}} + \mathrm{e}_{ij}$	(5-7)

*Note: $Z_{ij} = \frac{1 - RH_{ij}^{1/3}}{1 - (0.01 * \frac{CL_i}{THT_i})^{1/3}}$

5.2.4.2. Crown profile modeling

Crown profile models, outlining the crown shape, were developed based on the maximum crown radius (CR) through the canopy depth, which is derived from the branch length and branch described as follow:

$$\mathrm{CR} = \mathrm{BL} * \sin(\mathrm{A}) \quad (5\text{-}8)$$

where CR is crown radius, BL is the branch length and A is the branch insertion angle.

In section 5.2.4.1, maximum branch length and branch insertion angle were individually modeled as separate equations in which common tree-level variables serve as predictors. Universal correlations are widely present among tree-level variables. Furthermore, internal constraints of branches' size and their corresponding insertion angle are not accounted by individual models. For example, individual models would yield similar estimates of length and insertion angle for branches located at a given height for different trees with similar size and competition conditions. However, the insertion angle could vary largely among trees as a response variable of the branch length. If strong correlations are present between branch length and insertion angle or other tree-level variables, individual models would not yield consistent and efficient estimates, as ordinary least square (OLS) does not account the relationships between variables across equations (Borders, 1989; Judge et al., 1982; Zellner, 1962).

Instead of minimizing standard error individually for each equation as OLS, systematic modeling using seemingly unrelated regression (SUR) minimizes the standard errors of the estimates simultaneously by considering the correlations among variables across

equations (Zellner, 1962). The estimation of coefficients is subject to minimizing the residual sum of square:

$$R(\boldsymbol{\beta}) = \mathbf{e}^{\mathbf{T}}\boldsymbol{\psi}^{\mathbf{T}}\boldsymbol{\Sigma}^{-\mathbf{1}}\mathbf{e}\boldsymbol{\psi} \quad (5\text{-}9)$$

where $R(\boldsymbol{\beta})$ is the sum of square residuals, $\mathbf{e}$ is the matrix of residuals, $\boldsymbol{\psi}$ is the define diagonal matrix of weighs, and $\boldsymbol{\Sigma}$ is covariance matrix between individual models.

The estimation process of $R(\boldsymbol{\beta})$ is documented by Parresol (2001) in detail. The estimation of $R(\boldsymbol{\beta})$ requires an estimator of $\boldsymbol{\Sigma}$, which is acquired as the error covariance between individual models. The error covariance between individual models is estimated using generalized nonlinear least square (GNLS), which is described as

$$\sigma_{ij} = \frac{1}{(T-K_i)^{0.5}(T-K_j)^{0.5}}\ \hat{e}_i^T\hat{\psi}_j^T\hat{e}_j\hat{\psi}_j, \quad (5\text{-}10)$$

where T is total number of observation, K_i and K_j are the number of the coefficients of model i and model j respectively, $\hat{e}_i$ and $\hat{e}_j$ are the estimated vectors of residuals of model i and j respectively, and $\hat{\psi}_i$ and $\hat{\psi}_j$ are the estimated weighs of model i and j.

An estimator $\hat{\boldsymbol{\Sigma}}$ is the matrix composed of σ_{ij}. $\hat{\boldsymbol{\Sigma}}$, $\hat{e}$ and $\hat{\boldsymbol{\psi}}$ are then used in Eq. 6-9 to derive the estimator of $R(\boldsymbol{\beta})$ using GNLS.

Besides developing systematic crown models of maximum branch length and insertion angle, I also developed crown models based on maximum branch diameter, which serves as an endogenous variable to predict branch length and insertion angle. Branch diameter has been widely used as the predictor variable in models of crown attributes in previous studies (Ishii et al., 2000; Maguire et al., 1994; Roeh and Maguire, 1997),

since branch diameter is more accurately measured in field and strongly correlated with branch biomass. Table 5.4 provides the individual models in two crown model systems.

Although Roeh and Maguire (1997) and Weiskittel et al. (2007) successfully predicted crown radius profile for young plantation trees with Eq. 6-8, the product of branch length and sine of insertion angle is accurate only when the branches maintain straight for the growth period. However, branch bend occurs to acquire sunlight or avoid crowdedness, which is more apparent at the lower canopy. A correction factor of crown competition and relative DINC is applied to Eq. 5-8 to account for the branch curvature effects. The corrected crown radius models can be described as:

$$CR = a_0 CI^{a_1} \times DINC^{a_2} \times BL \times \sin(A) \quad (5\text{-}11)$$

where CR is the crown radius,

CI is selected competition index,

RDINC is relative DINC, BL is branch length,

A is branch insertion angle and a_1 and a_2 are fitted coefficients.

The selected model systems are presented in Table 5.4. Nonlinear seemly unrelated regression was performed in R with package systemfit version 1.1-24 (Henningsen and Hamann, 2007). The systematic models require the modeled branches to contain all the involved attributes. For model system C1, all the modeled branches' length and insertion angles were measured. Similarly, all the modeled branches' diameter, length and insertion angles were measured in model system C2. Branches that have missing attributes from TLS measurements were excluded in the systematic models.

Table 5.4 System modeling model forms

System	Model	Form	
C1	LM_{s1}	$BL_{ij} = a_{11}DBH_i^{a_{12}} Z_{ij}^{\left\{a_{13}+a_{14}DBH_i^{RDINC_{ij}}+a_{15}\exp\left(\frac{DBH_i}{THT_i}\right)^{-1}+\delta_i\right\}} + e_{ij}$	(5-12)
	A_{s1}	$A_{ij} = a_{21}CL_i^{a_{22}}\exp(a_{23} * RINC_{ij} + a_{24} * CI_{5_i}) + e_{ij}$	(5-13)
	CR_{s1}	$CR_{ij} = a_{30}DINC_{ij}^{a_{31}} CI_i^{a_{32}} BL_{ij} \times \sin(A_{ij})$	(5-14)
C2	DM_{s2}	$BD_{max_{ij}} = b_{11}DINC_{ij} + b_{12}DINC_{ij}^2 + b_{13}DBH_i + b_{14}THT_i + b_{15}RDINC_{ij}^2 \times \exp(\frac{DBH_i}{THT_i}) + e_{ij}$	(5-15)
	LM_{s2}	$BL_{max_{ij}} = b_{21}BD_{max_{ij}}^{b_{22}} CL_i^{b_{23}} DINC_{ij}^{b_{24}+b_{25}CI_{3_i}} Z_{ij}^{b_{26}} + e$	(5-16)
	A_{s2}	$A_{ij} = b_{31}CL_i^{b_{32}} DINC_{ij}^{\{b_{33}+b_{34}CI_{5_i}\}} + e_{ij}$	(5-17)
	CR_{s2}	$CR_{ij} = b_{40}DINC_{ij}^{b_{41}} CI_i^{b_{42}} BL_{max_{ij}} \times \sin(A_{ij})$	(5-18)

*Note: $Z = \frac{1-RH^{1/3}}{1-(0.01*\frac{CL}{THT})^{1/3}}$

5.2.5. Model evaluation

Models were evaluated with leave-one-out validation. For each iteration, TLS-based branch estimates from eight trees were used to fit the model, then the fitted model was used to predict branch attributes of the left tree. Model are evaluated with four measures:

$$Fittness\ index = FI = 1 - \frac{\sum_{i=1}^{N}\sum_{j=1}^{n_i}\left(\mathrm{y_{ij}} - \hat{\mathrm{y}}_{\mathrm{ij}}\right)^2}{\sum_{i=1}^{N}\sum_{j=1}^{n_i}\left(\mathrm{y_{ij}} - \bar{y}\right)^2} \quad (5\text{-}19)$$

$$\text{Root mean square error} = \mathrm{RMSE} = \sum_{\mathrm{k}}^{\mathrm{N}} \sqrt{\sum_{\mathrm{i}}^{\mathrm{N}-1} \frac{\sum_{\mathrm{j}=1}^{\mathrm{n_i}}\left(\mathrm{y_{ij}} - \hat{\mathrm{y}}_{\mathrm{ij}}\right)^2}{\mathrm{n_i}}} \Big/ \mathrm{N} \quad (5\text{-}20)$$

$$\mathrm{Bias} = \sum_{\mathrm{k}}^{\mathrm{N}} \left(\frac{\sum_{\mathrm{j}=1}^{\mathrm{n_i}}\left(\mathrm{y_{ij}} - \hat{\mathrm{y}}_{\mathrm{ij}}\right)}{\mathrm{n_i}} \right) \Big/ \mathrm{N} \quad (5\text{-}21)$$

$$\text{Percentation of mean absolute bias} = \%\mathrm{MAB} = \frac{\sum_{\mathrm{k}}^{\mathrm{N}} \left(\frac{\sum_{\mathrm{j}=1}^{\mathrm{n_i}} \left| \mathrm{y_{ij}} - \hat{\mathrm{y}}_{\mathrm{ij}} \right|}{\mathrm{y}_{ij}} \right)}{N} \times 100\% \quad (5\text{-}22)$$

where RMSE, bias and MAB are the mean measures of nine validation iterations, N is the number trees as well as the number of iterations of validation, $\mathrm{n_i}$ is the number of branches in tree i, $\mathrm{y_{ij}}$ is the jth branch estimate of tree i, and $\hat{\mathrm{y}}_{\mathrm{ij}}$ is the model predicted, $\bar{y}$ is the overall mean of all the observations.

5.3. Results

5.3.1. Branch attribute models

5.3.1.1. Branch length

All branch length observations exhibit large variation within and among individual trees (Figure 5.4). The variation of branch length is most pronounced in the middle to lower crown. The fitted coefficients of the modified variable-exponent models are provided in Table 5.5. Model L only explained 40% of the branch length variation

across the canopy depth with the %MAB of 28.22%. Model L could fit the mean of the branch length at a given canopy depth, with the RMSE and bias of 1.19 and 0.06 m respectively. Strong autocorrelation was not detected in model L. Abnormal pattern was not shown in the residual plot (Figure 5.3). Two types of branch length distribution shapes were identified from model L: 1) round or ellipsoid shape with maximum branch length located at the middle crown (tree 1, 3, 4, 5, 7, and 9); and 2) conic shape with maximum branch length located at the crown base (tree 2, 6, and 8). For tree 6, model L largely underestimated the lower branch length and did not capture the conic shape (Figure 5.4). Unlike other tree crown shapes with the maximum length located at the lower middle or bottom of the crown, tree 10 with DBH greater than 100 cm exhibits its maximum length at the upper crown.

Compared with model L, the model of maximum branch length (model ML) reached higher agreement between the observation and the predicts. Model ML explained 78% variation of the maximum branch length observations (Table 5.6). Values of RMSE and %MAB (0.82 m and 15.93%) are much lower for model ML than model L. Model ML included competition indices CI_4 and CI_5, as they could largely improve the model fitness. The negative coefficients of CI_4 and CI_5 indicate the reducing effects from the neighbors' competition on the branch maximum length. The model estimated autocorrelation between adjacent pairs of estimates is 0.31. The variation of the maximum branch length observations is smaller at the crown top but much greater at the middle and lower crown. Model ML apparently underestimated the maximum branch lengths located at the middle- to lower crown for several trees. Especially for

trees 6 and 9, their maximum branch lengths exhibit conic shapes but were predicted as round shape by model ML.

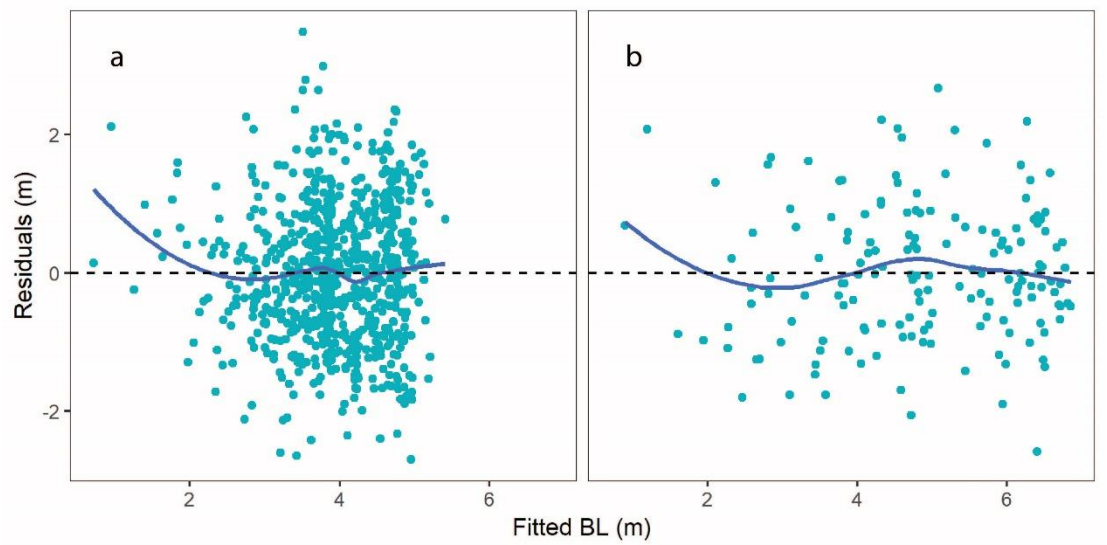

Figure 5.3 a. Residual plot of model L: all branch length observations; b. Residual plot of model ML: the maximum branch length.

Table 5.5 Fitted coefficients of individual branch attributes models.

Branch attributes	Model	Coefficients						
Branch length	L	a_{11}	a_{12}	a_{13}	a_{14}	σ_{δ}^{2}		
		21.2993	-0.2506	1.1547	0.0047	0.0459		
		10.4752	0.1201	0.0924	0.0010	0.0010		
Maximum branch Length	LM	a_{21}	a_{22}	a_{23}	a_{24}	a_{25}	a_{26}	φ
		16.2837	-0.0134	0.7923	0.0068	-0.1882	-0.0914	0.3134
		2.5331	0.0044	0.0515	0.0012	0.0164	0.0167	
Maximum branch diameter	DM	a_{31}	a_{32}	a_{33}	$\sigma_{\delta_1}^{2}$	$\sigma_{\delta_2}^{2}$		
		0.8008	-0.0182	-0.4910	0.0383	1.9589		
		0.0457	0.0017	0.2051	0.0010	0.0126		
Insertion angle of branches with maximum length	A_{ML}	a_{41}	a_{42}	a_{43}	a_{44}			
		264.7904	-0.2909	0.1929	-0.0717			
		51.2068	0.0573	0.0309	0.0132			
Insertion angle of branches with maximum basal diameter	A_{MD}	a_{51}	a_{52}	a_{53}	a_{54}			
		331.3268	-0.4459	0.1817	-0.0367			
		162.4055	0.1509	0.0318	0.0133			

Table 5.6 Evaluation of individual branch models.

Branch Attributes	Model	FI	RMSE	Bias	%MAB
BL (m)	L	0.40	1.16	-0.06	28.22%
Maximum BL (m)	ML	0.78	0.82	-0.04	15.93%
Maximum BD (cm)	MD	0.61	1.52	0.12	21.03%
Insertion angle of branches with maximum length (°)	A_{ML}	0.49	9.75	0.91	8.36%
Insertion angle of branches with maximum basal diameter (°)	A_{MD}	0.70	7.15	0.43	5.47%

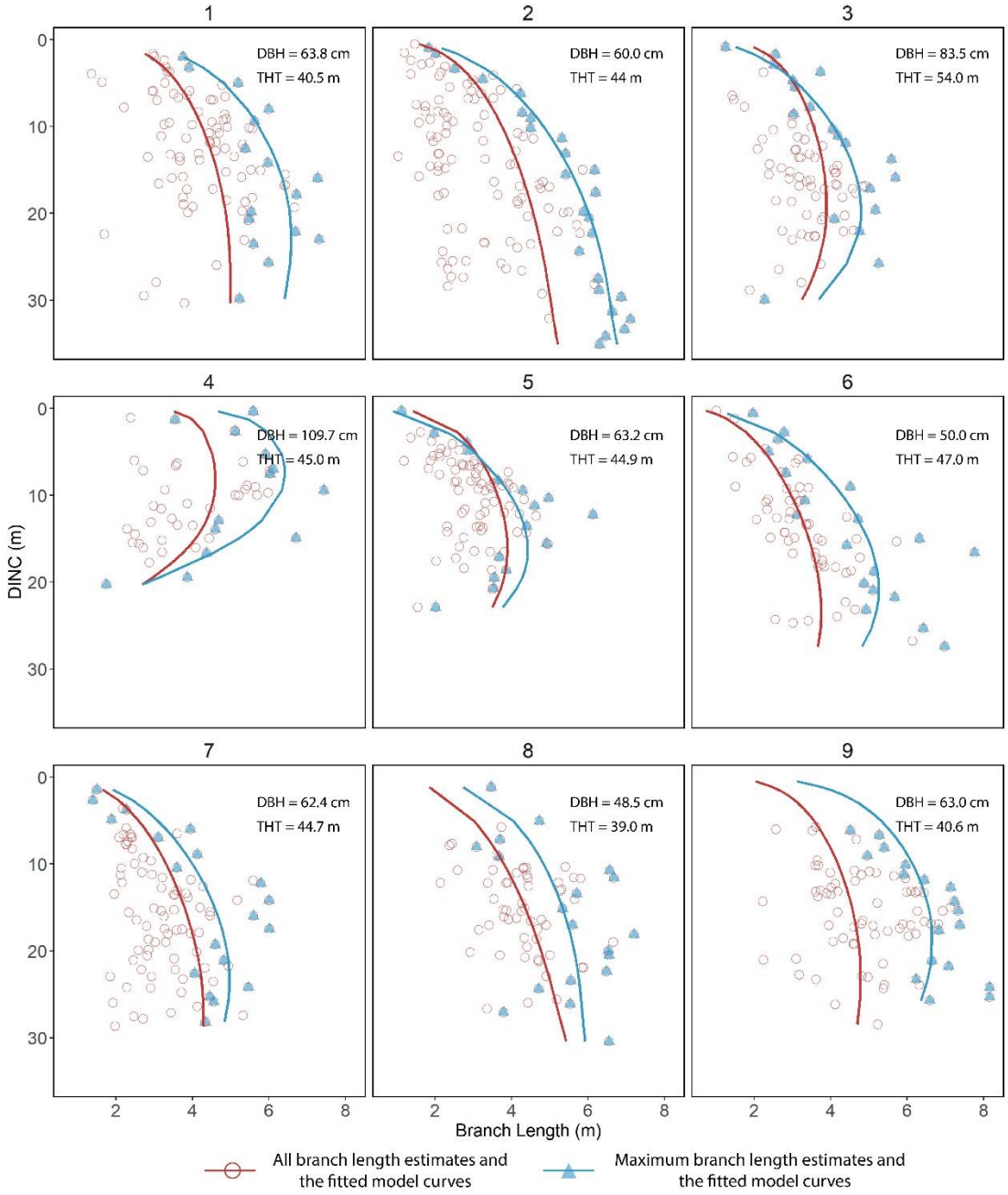

Figure 5.4 TLS-based branch length and maximum branch length estimates and their model fits for nine sample trees.

5.3.1.2. Branch diameter

Most branches that were measured in basal diameters were located at the lower-middle crown, ranging from DINC of 10 m to 30 m. Successful branch diameter measurements were not available at upper crown from TLS due to reducing point cloud density. For all the observations, branch diameter exhibits large variation across the canopy depth and scatters from 2 – 10 cm (Figure 5.6). In comparison to all branch diameter observations, the maximum branch diameter variation is much smaller in the middle-lower crown, ranging from 5 – 10 cm. The selected polynomial model MD conforms with the model form of the segmented polynomial model as documented by Max and Burkhart (1976). Instead of fitting a segmented polynomial equation with first-order derivative continuity, model MD fits the maximum branch diameter as an entire continuous function. Because the random effect of intercept was included, model MD was not constrained to the zero point at the tree top. The upper segment of the original segmented model is constrained to the zero point at the crown top, because the upper segment assumes branch diameter only response to the change of canopy depth not to the tree size effect. But for the lower segment, a non-canopy-depth related term is added to account for the effect of tree size on branch diameter. In this study, since most observations were located at the middle-lower canopy, the random effect of intercept could be viewed as the correction factor accounting for the individual tree effect on branch diameter. Table 5.5 provides the fitted coefficients of model MD. The polynomial model form could account for 61% variation of maximum branch diameter, and yielded RMSE and bias of 1.52 cm and 0.12 cm respectively. Residual plots of model MD did not show strong abnormal pattern

(Figure 5.5). Residual variance is slightly higher for great diameter predictions. Strong autocorrelation was not detected after individual tree random effects were included in model MD. The exponential factor of DBH/THT, negatively related to stand density (Garber and Maguire, 2005a; Weiskittel et al., 2007), is included as an interaction term with $RDINC^2$. The negative value of fitted coefficient a_3 implies DBH to THT ratio limits the growth of the maximum branch diameter. The polynomial model depicts the round shape distribution of branch diameter in which the the smallest and maximum estimates are located at the top and middle of the crown respectively. For most sample trees, the maximum branch diameter estimates peaks in the middle crown at DINC of 15 - 20 m.

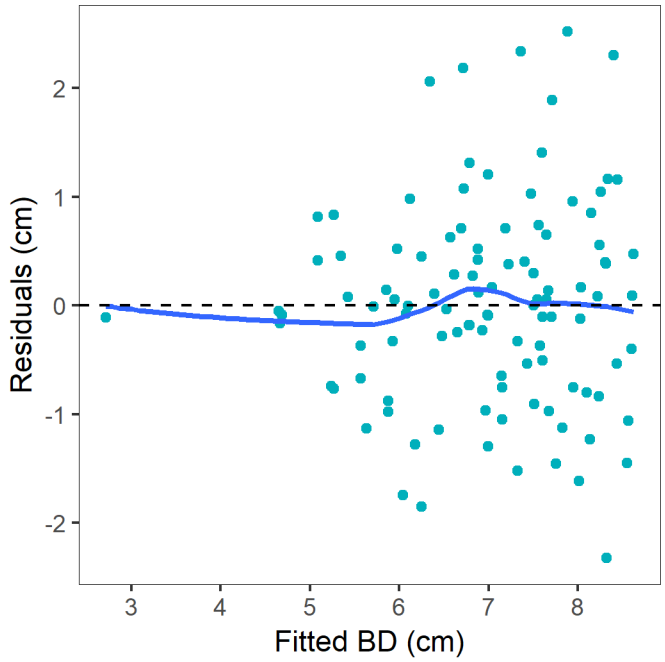

Figure 5.5 Residual plot of model MD: the maximum branch diameter.

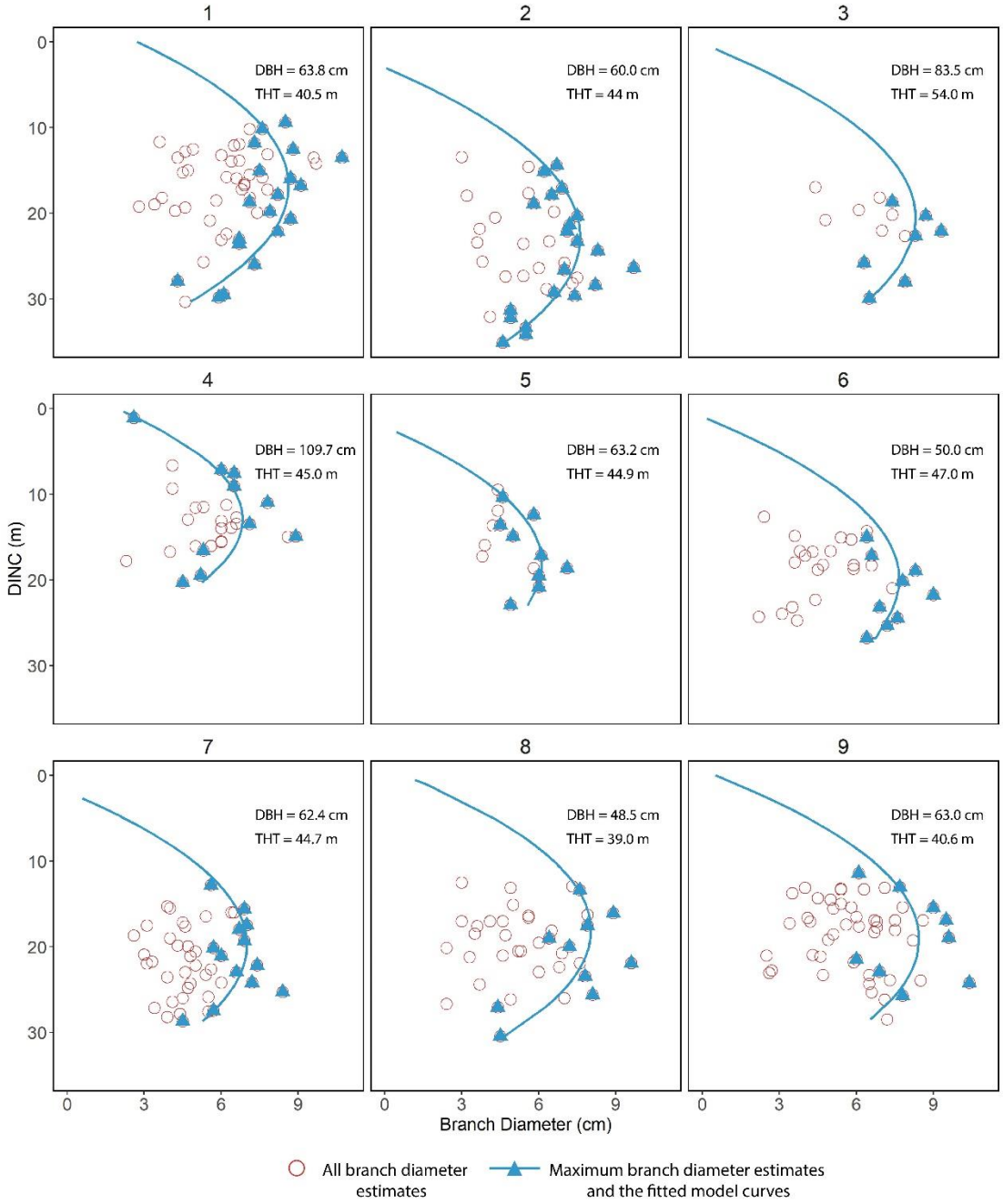

Figure 5.6 TLS-based branch diameter and maximum branch diameter estimates and maximum branch diameter models fit for nine sample trees.

5.3.1.3. Branch insertion angle

TLS-based insertion angle estimates vary remarkably within and cross individual trees (Figure 5.8), especially in the middle crown. Insertion angle of tree 3, 4, 6, and 7 are apparently more variable through the canopy depth than others. Overall, branch insertion angle averages around 90° and increases as canopy depth increases (Figure 5.8). Table 5.5 provides the fitted coefficients of the branch insertion angle models for branches identified with maximum length (AML) and maximum diameter (AMD) respectively. Residual plots of models AML and AMD do not show an abnormal pattern (Figure 5.7). Model AML only accounts for 49% variation of insertion angle and yielded RMSE and bias of 9.75° and 0.91° respectively. Model AMD, though developed with less observations, yielded much higher FI than model AML (Table 5.6), and explained 70% variation of the insertion angle with RMSE and bias of 7.15° and 0.43° respectively. and explained 70% variation of the insertion angle with RMSE and bias of 7.15° and 0.43° respectively. In comparison with model AML, model AMD exhibits more gradual change in branch insertion angle as canopy depth increase (Figure 5.8). For trees 1, 2, 7, 8 and 9, the model AMD and AML yielded similar insertion angle estimates along DINC. Whereas, for tree 3, 4, 5 and 6, model AMD yielded much higher insertion angle estimates than model AML.

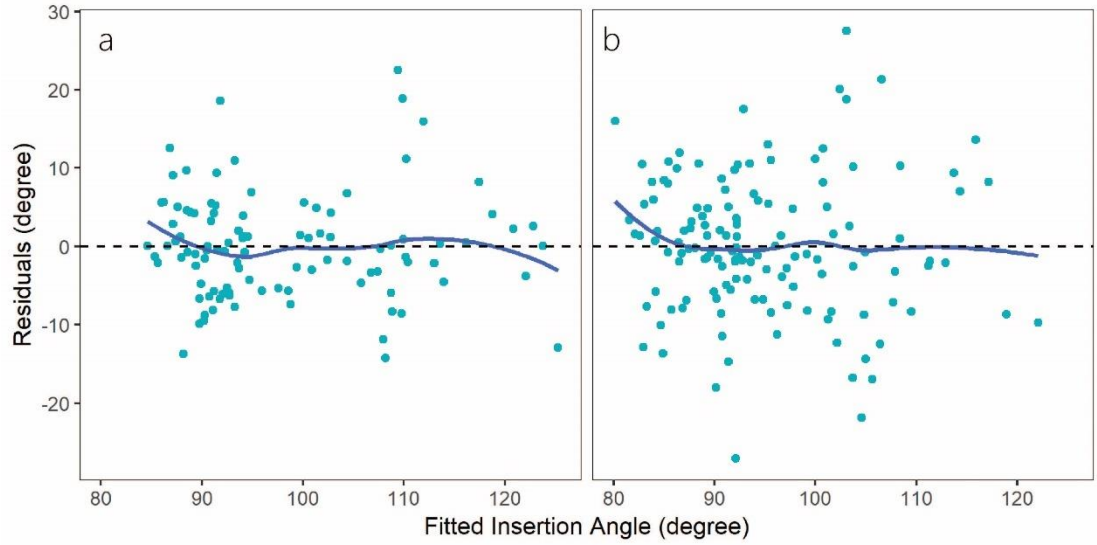

Figure 5.7 a. Residual plot of model AMD: the insertion angle of branches with maximum diameter; b. Residual plot of model AML: the insertion angle of branches with maximum length.

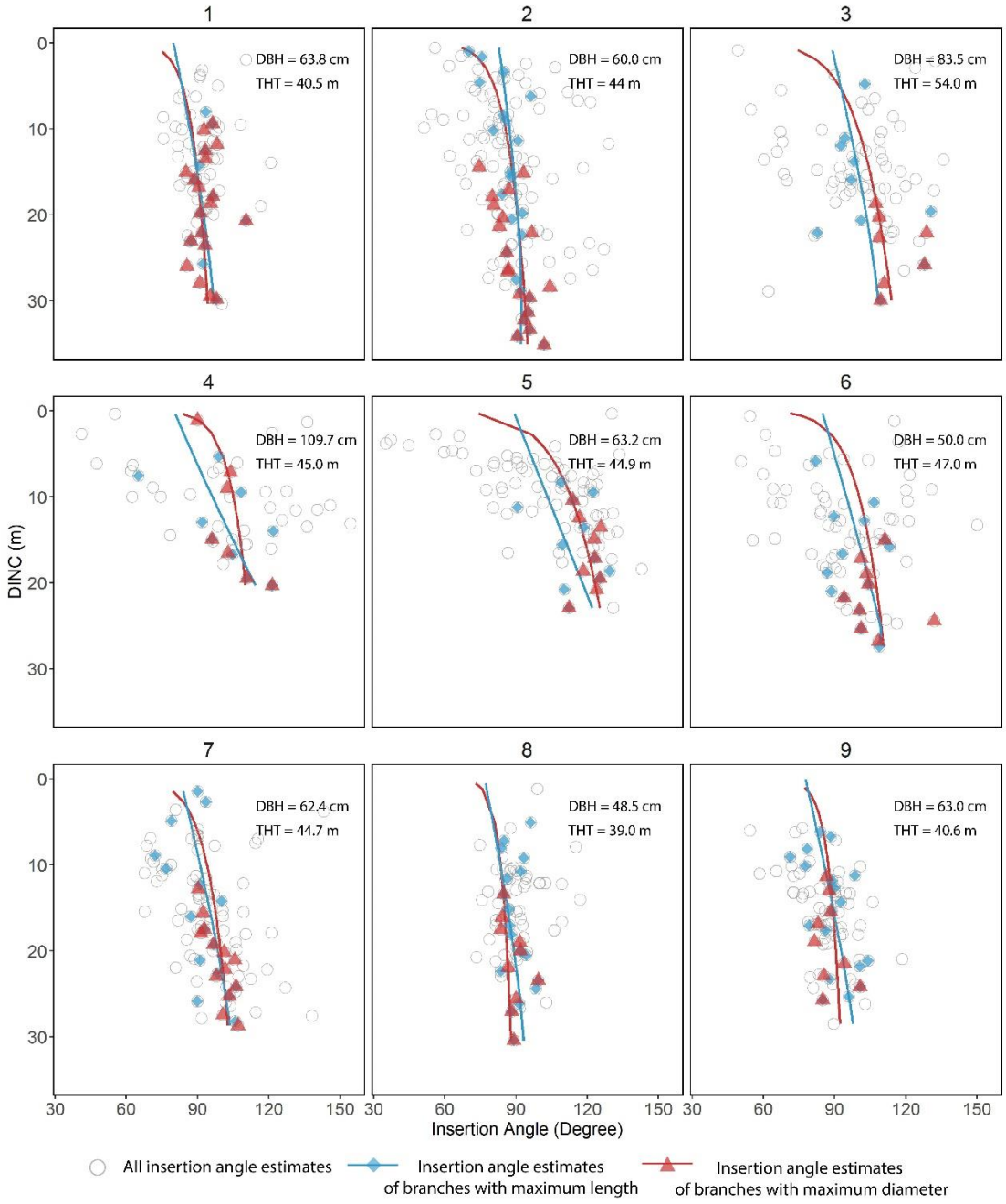

Figure 5.8 TLS-based branch insertion angle estimates and model fits for nine sample trees.

5.3.2. Systematic crown profile modeling

According to the model curves in Figure 5.9, the crown shapes are distinguished as conic and round, in which the largest crown width is observed at the bottom and the middle of the crown respectively. Table 5.7 provides the fitted coefficients of crown profile models. In comparison with individual branch models, systematic branch models with NSUR did not improve the model fit and bias for maximum branch length, branch diameter and branch insertion angle (Table 5.8). In system C1, model ML_{s1} and A_{s1} are the same forms as their corresponding individual models ML and AML. Model ML_{s1}, in comparison with model ML, slightly decreased estimated standard error (Table 5.7). In system C2, MD_{s2} explained 20% less variation of the maximum branch diameter than the individual model MD, because model MD_{s2} did not account for the random effects. In system C2, the maximum branch diameter serves as a predictor variable in branch length model ML_{s2}, which only explained 32% of the branch length variation.

Strong correlation was not present among residuals of equations within the model systems (Table 5.9). None of the competition indices were found significant factor crown models C_{s1} and C_{s2}. Perhaps, competition indices in branch length and insertion angle models could adequately explain the crowding and shading effects on branch structural arrangements. According to model C_{s1}, crown radius of branches with maximum length is increasingly impacted by branch bend as canopy depth increases. However, DINC is not a significant factor in model C_{s2}, implying intensity of branch bend maintains constant for branches with maximum diameter along the canopy. Model C_{s1} and C_{s2} are similar in their FI values but leave-one-out validation shows

model C_{s1} performed much better in terms of RMSE (0.93 m vs. 1.51 m), bias (-0.02 m vs. -0.07 m), and %MAB (19.84% vs. 47.30%). Model C_{s1} yielded overall 1 m larger crown radius estimates than model C_{s2} (Figure 5.9). Overall model C_{s1} yielded slight overestimation of max crown width, especially for the lower crown (Figure 5.10). Model C_{s2}, instead, underestimated crown width at the upper and middle crown (Figure 5.10). Model system C1 could flexibly fit the variable conic (tree 2 and 8) and round (tree 1, 3, 4, 5, 7 and 9) crown shapes than model system C2. Model system C2 could not adequately capture the variation of crown width along the canopy and predicted only cylindrical-like crown shape, in which constant crown width is identified through the canopy depth. Except for tree 6, model system C1 could not well fit the conic shape which was better fitted by model system C2.

Table 5.7 Fitted coefficients of crown shape models. C1 and C2 systematic crown model sets developed with nonlinear seemly unrelated regression (NSUR). C1 is model set developed based on maximum branch length. C2 is model set developed based on maximum branch diameter.

System	Model	Coefficients						
C1	LM_{s1}	a_{11}	a_{12}	a_{13}	a_{14}	a_{15}	a_{16}	a_{17}
		22.2861	-0.0172	0.5770	0.0104	-0.1170	-0.1117	0.3334
		2.7146	0.0038	0.0657	0.0014	0.0283	0.0202	
	A_{s1}	a_{21}	a_{22}	a_{23}	a_{24}			
		230.0181	-0.2400	0.1710	-0.0800			
		46.4795	0.0626	0.0343	0.0135			
	C_{s1}	a_{40}	a_{41}					
		1.0614	-0.0452					
		0.0440	0.0146					
C2	DM_{s2}	b_{11}	b_{12}	b_{13}	b_{14}	b_{15}		
		0.8828	-0.0190	0.0699	-0.1169	-0.7203		
		0.0981	0.0021	0.0151	0.0384	0.1361		
	LM_{s2}	b_{21}	b_{22}	b_{23}	b_{24}	b_{25}	b_{26}	
		8.1031	0.4148	-0.7106	-0.9369	-0.2043	1.1062	
		2.1811	0.1176	0.3764	0.3168	0.0788	0.2801	
	A_{s2}	b_{31}	b_{32}	b_{33}	b_{34}			
		347.6240	-0.4454	0.1574	-0.0358			
		54.0638	0.0520	0.0187	0.0038			
	C_{s2}	b_{40}						
		0.9196						
		0.0081						

Table 5.8 Evaluation of individual models within each systematic model set.

System	Model	FI	RMSE	Bias	%MAB
C1	LM_{s1}	0.70	0.88 m	-0.07 m	15.52%
	A_{s1}	0.46	10.43°	-0.05°	8.97%
	C_{s1}	0.93	0.93 m	-0.02 m	19.84%
C2	DM_{s2}	0.40	1.40 cm	0.13 cm	18.78%
	LM_{s2}	0.32	1.47 m	-0.04 m	33.42%
	A_{s2}	0.72	7.01°	0.04°	5.56%
	C_{s2}	0.93	1.51 m	-0.07 m	47.30%

Table 5.9 Correlation between residuals of individual models in each systematic model set.

		LM_{s1}	A_{s1}	C_{s1}	
C1	LM_{s1}	1	-0.0252	-0.0420	
	A_{s1}		1	0.1516	
	C_{s1}			1	
		DM_{s2}	LM_{s2}	A_{s2}	C_{s2}
C2	DM_{s2}	1	0.0315	0.0965	-0.0075
	LM_{s2}		1	0.0261	0.3087
	A_{s2}			1	0.0697
	C_{s2}				1

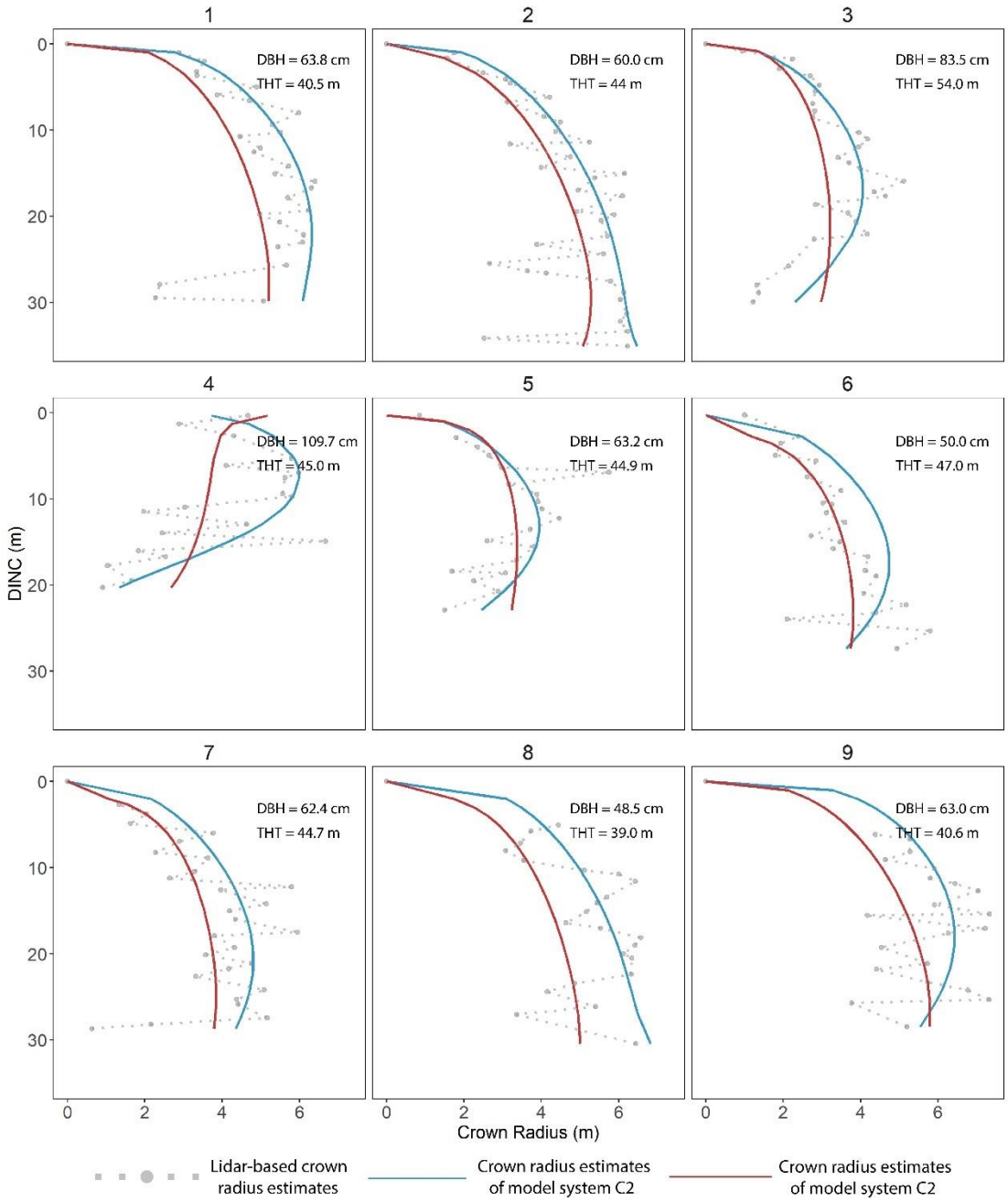

Figure 5.9 Crown radius estimates from four models. C1 and C2 are branch model systems fitted with NSUR.

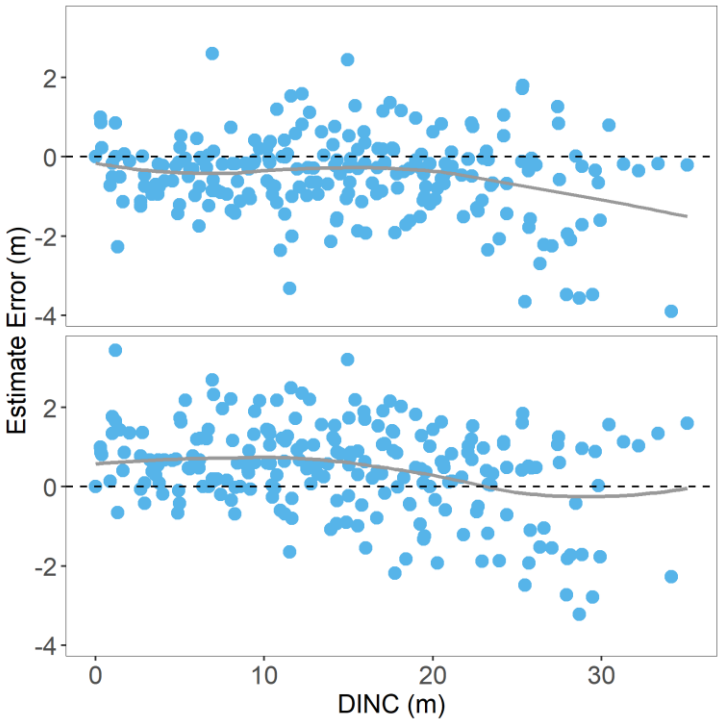

Figure 5.10 Crown width estimation error distributions of systemic models. Upper: model estimation error of model C1; Lower: model estimation error of model C2.

5.4. Discussion

5.4.1. Branch attributes models

In this study, we used TLS-based branch structural estimates to develop allometric models. Meanwhile, we incorporated competition indices derived based on the neighboring trees' size and proximity to the focal trees in the branch models. Attributed to the availability of TLS-based branch estimates, as well as the underlying mechanisms driving branch woody mass allocation, allometric models of branch attributes reached different levels of goodness-of-fit.

5.4.1.1. Branch length

Previously, branch length was seldom directly modeled as a response variable of tree-level attributes. It appeared in most studies as a dependent variable of branch diameter (Monserud and Marshall, 1999; Roeh and Maguire, 1997; Weiskittel et al., 2007), since branch diameter is the most important variable describing branch biomass and is more easily measured in field. From the perspective of lidar point clouds, estimating branch length requires only a few vertex points, which allows successful branch length estimation even for the upper crown where point clouds are sparse. Most branches' lengths were measured with TLS point clouds. But accurately measuring branch diameter was not available at the crown top. Due to the missing diameter estimates of most branches, branch length was directly modeled as a dependent variable of tree-level attributes.

Both all and the maximum branch lengths were modeled with the modified variable exponent model form. For the all branch length model (L), the expected maximum length is modeled as a power function of DBH and the inclusion of competition index

did not improve the model explanation power. Hence, all branch lengths are more likely driven by tree size-related lateral allocation rather than competition intensity induced by canopy closure. For the maximum branch length model ML, the expected maximum branch length value is modeled as a power function of crown length, because crown length explained 3% more variation of the maximum expected than DBH. In comparison with tree DBH, crown length dynamic is more driven by the intensity of competition (Vanninen and Mäkelä, 2000), light resource availability (Ameztegui et al., 2012), and stand spacing of tree initiation (Winter et al., 2002). We observed large reductions of the crown length of trees with DBH greater than 80 cm (trees 3 and 4). Hypothetically, as a shade-intolerant species, large Douglas-fir could take a strategy of enhancing terminal allocation for tree height growth instead of lateral allocation for branch expansion, results in height increment but losses of branches at lower canopy (Chen et al., 1996; Klinka et al., 1992).

A single competition index is hard to comprehensively explain the variation of the maximum branch length (Kaitaniemi and Lintunen, 2010). Competition indices CI5 and CI4, related to stem vertical competition conditions, were included in model ML and explained 7% variation of the maximum branch length. Other horizontal competition indices did not provide a comparable gain in the model prediction ability, suggesting shading and crowding effects induced by the vertical aspects of the neighbors are the determinant factors limiting the branch length expansion. Surprisingly, we observed a negative effect of the DBH-THT ratio on the maximum branch length in model ML. The increasing value of the DBH-THT ratio, indicating an increase in spacing between trees, allows crown expansion (Garber and Maguire, 2005b;

Weiskittel et al., 2007). Since the sample trees were all in dominant crown position and similar in their total height but much more different in their DBH, smaller values of the DBH-THT ratio could be associated with trees in lower social positions, which tend to allocate resources for branch elongation rather than height increment (Gilmore and Seymour, 1997).

The highest FI value yielded by the model of maximum branch length can be two-fold. First, the maximum branch length is the most accurately estimated attribute from TLS point clouds. In comparison, measuring all branch length was increasingly challenging as crown height increases, because distinguishing points from different branches was difficult for small branches intertwined inside the crown and obstruction reduced the available points outlining the skeleton of small branches. Second, branches, that are identified with the maximum branch length, are likely initiated with the annual growth of stem and follow seasonal growth patterns. In contrast, small epicormic branches were initiated as the presence of irregular canopy gaps due to different initiation periods and complex growth conditions (Ishii et al., 2000; Ishii and Wilson, 2001; Pelt and Sillett, 2008). Thereby, a single equation cannot adequately interpret variation of all branch lengths through the canopy but can explain much more variation of the overall crown shape determined by the maximum branch length.

5.4.1.2. Branch diameter

Like branch length estimates, all branch diameter observations vary remarkably in growth conditions such as facing aspect, initiation time, and light conditions. Since TLS-based branch diameter estimates were only available for the lower-middle portion of the crown, models of all branch diameter observations are difficult to interpolate for

the upper crown. We only modeled the maximum branch diameter for the lower portion of the crown. The application of TLS-based branch diameter estimates would be sufficient to test competition effect at the lower crown where competition effect is the most pronounced (Hein et al., 2008).

Accuracy of branch diameter estimates is decreasing dramatically as canopy height increases, where the scanned branches were further away from the terrestrial sensor. Fang and Strimbu (2019) found the accuracy of TLS-based branch diameter estimates is related to the height of branches and first-order autoregressive (AR(1)) structure could quantify the error covariance along the canopy. Garber and Maguire (2005a) also suggested the presence of autocorrelation among residuals of the branch diameter model along whorl lag. In this study, we only observed a marginal gain in model fit from the inclusion of AR(1) in the maximum branch diameter model. The autocorrelation between errors of adjacent measurements on an individual tree was largely reduced by the inclusion of random effects.

The polynomial model MD predicted round shape distribution of maximum branch diameter through the canopy height. Similar patterns were observed for old-growth (Ishii et al., 2000) and plantation (Maguire et al., 1999) trees in which the occurrence of maximum estimates is located at the middle-lower crown. Model MD is a polynomial function of DINC with an additive term of the interaction between $RDINC^2$ and the exp(DBH/THT). Terms of tree DBH and height were not significant in model MD. Therefore, it implies, at least for the lower canopy, the maximum branch diameter did not vary strongly within the DBH and height classes of the sample trees and are

primarily determined by the position of the branches inside the canopy and the spacing effect at a given position of relative DINC. As none of the competition indices could ehance the model explanation power of model MD, the underlying cause of large variation of maximum branch diameter among individual tress is still unclear.

5.4.1.3. Branch insertion angle

Branch insertion angle is important in determining the crown form and knot size of the timbers (Osborne and Maguire, 2015; Weiskittel et al., 2007). In previous studies, models of the branch insertion angle have been developed as a response variable to the increasing canopy depth, light resource availability, plastic stress from the competition with neighbors and other biological causes resistant to gravity (Lintunen and Kaitaniemi, 2010; Osborne and Maguire, 2015; Wilson, 2000). The TLS-based insertion angle estimates exhibit great versatility and are averaged on 90°, with a mean increasing trend responding to the increasing canopy depth. The diverse branch insertion angle of Douglas-fir enables an abundance of light under otherwise scarce light conditions, which is observed during the transformation from young to mature crowns (Pelt and Sillett, 2008).

Canopy depth, crown length and competition index CI5 are the significant factors explained most variation of insertion angles for branches having either maximum diameter or length at given canopy heights. Similarly, Lintunen and Kaitaniemi (2010) found relative height in the crown and interaction between competition indices and species significantly explain the variation of the branch insertion angle. Weiskittel et al. (2007) and Hein et al. (2008) found stand density exerts little effect on the branch insertion angles, but increasing height to DBH ratio and crown length, confounding

with stand density, reduce branch insertion angle, which are supported by our observation of the negative effects from crown-length-related competition index CI5 on the branch insertion angle, indicating surrounding trees' shading effect is a source of formation and orientation of the branches.

The form of model AML suggests a drastic increase in the insertion angle of branches that have the maximum lengths as canopy depth increases. Our observations support the previous findings that branch length growth induces variation in the insertion angle corroborating to light resource and gravity (Castera and Morlier, 1991; Weiskittel et al., 2007). Comparatively, model AMD indicates a more gradual change in the insertion angle of branches that have the maximum diameter through canopy depth. Model AMD had much greater FI value than model ALD, although model AMD was developed with fewer observations, due in part to more accurate insertion angle estimates at the lower crown, and in part to constant light conditions at the lower crown causing less variation of the insertion angle.

5.4.2. Crown form modeling

Two sets of crown profile model systems were based on the maximum branch diameter and length respectively. For both systems, strong correlations between residuals were not present across equations within the system, probably because of small sample size and inconsistent accuracy of TLS-based branch attribute estimates. Besides, the high structural complexity of mature crowns may decrease the strength of internal allometric relationships between crown attributes and tree-level attributes, as the crown structure is increasingly determined by complex light conditions (Ishii and Wilson, 2001). Nevertheless, the application of NSUR would ensure the crown profile models are

consistent with observed branch diameter, length, and insertion angle of a specific branch. The modeling process with NSUR requires complete sets of attribute measurements for all the observations, which challenges field measurements, as some attributes are easier to acquire than others (Roeh and Maguire, 1997). Thus, NSUR could be biased towards the reduced datasets.

Since the inclusion of random effects and autocorrelation increases the difficulty of applying NSUR, the autocorrelation effect was not considered in the modeling process of NSUR. An alternative approach to account for autocorrelation issues in multicollinear models could be a tapering approach that incorporates a tapering factor in the estimation of error covariance matrices of Eq. 9 (Dahlhaus, 1988). In comparison with ordinary NSUR, the tapering approach does not essentially change the mean of the estimated coefficients but only reduces the standard error of estimates (Asikgil, 2014; Aşıkgil and Erar, 2013). Since none of the individual models were detected with the presence of strong autocorrelation between adjacent pairs of branch measurements and the objective of this study is to develop sets of systematic models that depict the mean trend of the crown radius, ordinary NSUR is adequate to address the scopes of this study.

Crown profile models of Douglas-fir have been generalized as a single equation that directly describes the shape of the crown. These models include individual geometric models that are defined as cone, cylinder, ellipsoid, paraboloid (Van Pelt and North, 1996), distribution models such as Weibull and beta equations (Ferrarese et al., 2015), and adjustable segmented model (Hann, 1999). But a generalized model omits large

detailed information inside the crown and would not be adequte to explain large variation of crown radius observed in this study.

5.4.3. Application and limitation

Measuring branch structural attributes with TLS is a computer-aid nondestructive approach. The TLS-based estimation accuracy largely depends on the density of point clouds. Thus, TLS-based branch structural estimates are more accurate for lower crown. Especially for branch diameter, considerable point clouds are required to fit cylinder models. Fusion of terrestrial and airborne lidar data would potentially bring consistency to the accuracy of the structural estimates.

The selected focal trees are a cluster of neighboring trees with varying DBH classes in a natural regime forest. The selections of neighboring trees excluded potential variations caused by environment factors. All the identified whorl and epicormic branches are exhaustively measured for an individual tree. The allometric models developed from this study reveals the mean trend of branch length, branch diameter and branch insertion angle across canopy depth. In inclusion of competition indices in the models reveal neighboring trees' shading and crowding effect on the focal trees' branch allocation. I need to notice that statistical significance of the competition indices in branch models do not necessarily imply a cause and effect relationship between neighboring competition and branch attributes.

In this study, neighbor trees are visually identified and delineated. The definition of competition trees would cause large variations in computation of competition indices (Metz et al., 2013). I aim to minimize the difficulty and variation introduced by

operation of TLS point clouds and develop measures that are consistent with field measurements. For future application, applying different TLS-derived competition indices might improve the model fit, since some TLS-derived competition indices quantified the deep crown interlocking effects.

5.5. Conclusion

A cluster of mature Douglas-fir trees' crown attributes were exhaustively measured using structural models developed with TLS-based point clouds. Branch length was most accurately measured attributes with TLS data. Numeric models were developed for all branch length, length and diameter of branches with maximum length and maximum diameter respectively, and their insertion angles. Model of maximum branch length achieved the highest goodness-of-fit among all the models, following by models of insertion angles for branches with maximum diameter. However, maximum branch diameter is relatively hard to predict with TSL-based estimates. The models imply branch structural attributes were increasingly determined by the canopy depth and correlated light condition shaped by crowding and competition effects. Impact from tree size related attribute DBH is less significant as crown matures and arrival of canopy closure. Two systematic model sets were developed with NSUR for crown radius prediction. As branch length is primary attribute estimates from TLS points, model system based on maximum branch length outperform system based on maximum branch diameter in outlining the maximum edge of the crown profile. Although systematic models did not show strong improvement in terms of model fit, RMSE and bias, they are theoretically superior to individual models in terms of predicting crown profile for its consistency of coefficient estimates.

References

Ameztegui, A., Coll, L., Benavides, R., Valladares, F., Paquette, A., 2012. Understory light predictions in mixed conifer mountain forests: Role of aspect-induced variation in crown geometry and openness. Forest Ecology and Management 276, 52–61. https://doi.org/10.1016/j.foreco.2012.03.021

Asikgil, B., 2014. A Novel Approach for Estimating Seemingly Unrelated Regressions with High-Order Autoregressive Disturbances. Communications in Statistics - Simulation and Computation 43, 2061–2080. https://doi.org/10.1080/03610918.2013.784337

Aşıkgil, B., Erar, A., 2013. Polynomial tapered two-stage least squares method in nonlinear regression. Applied Mathematics and Computation 219, 9743–9754. https://doi.org/10.1016/j.amc.2013.03.088

Bartelink, H.H., 1996. Allometric relationships on biomass and needle area of Douglas-fir. Forest Ecology and Management 86, 193–203. https://doi.org/10.1016/S0378-1127(96)03783-8

Bond, B.J., 2000. Age-related changes in photosynthesis of woody plants. Trends in Plant Science 5, 349–353. https://doi.org/10.1016/S1360-1385(00)01691-5

Borders, B.E., 1989. Systems of equations in forest stand modeling. Forest Science 35, 548–556.

Braathe, P., 1980. Height increment of young single trees in relation to height and distance of neighbouring trees. Mitteilungen der Forstlichen Bundesversuchsanstalt.

Burkhart, H.E., Tomé, M., 2012. Indices of individual-tree competition, in: Modeling Forest Trees and Stands. Springer, pp. 201–232.

Castera, P., Morlier, V., 1991. Growth patterns and bending mechanics of branches. Trees 5, 232–238.

Chen, H.Y.H., Klinka, K., Kayahara, G.J., 1996. Effects of light on growth, crown architecture, and specific leaf area for naturally established *Pinus contorta* var. *latifolia* and *Pseudotsuga menziesii* var. *glauca* saplings. Can. J. For. Res. 26, 1149–1157. https://doi.org/10.1139/x26-128

Contreras, M.A., Affleck, D., Chung, W., 2011. Evaluating tree competition indices as predictors of basal area increment in western Montana forests. Forest Ecology and Management 262, 1939–1949. https://doi.org/10.1016/j.foreco.2011.08.031

Dahlhaus, R., 1988. Empirical spectral processes and their applications to time series analysis. Stochastic Processes and their Applications 30, 69–83. https://doi.org/10.1016/0304-4149(88)90076-2

Delagrange, S., Jauvin, C., Rochon, P., 2014. PypeTree: a tool for reconstructing tree perennial tissues from point clouds. Sensors 14, 4271–4289.

Fang, R., Strimbu, B.M., 2019. Comparison of Mature Douglas-Firs' Crown Structures Developed with Two Quantitative Structural Models Using TLS Point Clouds for Neighboring Trees in a Natural Regime Stand. Remote Sensing 11, 1661. https://doi.org/10.3390/rs11141661

Ferrarese, J., Affleck, D., Seielstad, C., 2015. Conifer crown profile models from terrestrial laser scanning. Silva Fenn 49, 1106.

Garber, S.M., Maguire, D.A., 2005a. Vertical trends in maximum branch diameter in two mixed-species spacing trials in the central Oregon Cascades. Canadian journal of forest research 35, 295–307.
Garber, S.M., Maguire, D.A., 2005b. The response of vertical foliage distribution to spacing and species composition in mixed conifer stands in central Oregon. Forest Ecology and Management 211, 341–355. https://doi.org/10.1016/j.foreco.2005.02.053
Garber, S.M., Maguire, D.A., 2003. Modeling stem taper of three central Oregon species using nonlinear mixed effects models and autoregressive error structures. Forest Ecology and Management 179, 507–522.
Gilmore, D.W., Seymour, R.S., 1997. Crown architecture of Abies balsamea from four canopy positions. Tree Physiology 17, 71–80.
Groot, A., Schneider, R., 2011. Predicting maximum branch diameter from crown dimensions, stand characteristics and tree species. The Forestry Chronicle 87, 542–551. https://doi.org/10.5558/tfc2011-053
Hackenberg, J., Morhart, C., Sheppard, J., Spiecker, H., Disney, M., 2014. Highly Accurate Tree Models Derived from Terrestrial Laser Scan Data: A Method Description. Forests 5, 1069–1105. https://doi.org/10.3390/f5051069
Hackenberg, J., Spiecker, H., Calders, K., Disney, M., Raumonen, P., 2015a. SimpleTree—an efficient open source tool to build tree models from TLS clouds. Forests 6, 4245–4294.
Hackenberg, J., Wassenberg, M., Spiecker, H., Sun, D., 2015b. Non Destructive Method for Biomass Prediction Combining TLS Derived Tree Volume and Wood Density. Forests 6. https://doi.org/10.3390/f6041274
Hann, D.W., 1999. An Adjustable Predictor of Crown Profile for Stand-Grown Douglas-Fir Trees. for sci 45, 217–225. https://doi.org/10.1093/forestscience/45.2.217
Hegyi, F., 1974. A simulation model for managing jackpine stands.–Fries, J, in: Proceedings of IUFRO Meeting S.
Hein, S., Weiskittel, A.R., Kohnle, U., 2008. Effect of wide spacing on tree growth, branch and sapwood properties of young Douglas-fir [Pseudotsuga menziesii (Mirb.) Franco] in south-western Germany. European journal of forest research 127, 481–493.
Henningsen, A., Hamann, J.D., 2007. systemfit: A package for estimating systems of simultaneous equations in R. Journal of statistical software 23, 1–40.
Hubbard, R.M., Bond, B.J., Ryan, M.G., 1999. Evidence that hydraulic conductance limits photosynthesis in old Pinus ponderosa trees. Tree Physiology 19, 165–172. https://doi.org/10.1093/treephys/19.3.165
Ishii, H., Clement, J.P., Shaw, D.C., 2000. Branch growth and crown form in old coastal Douglas-fir. Forest Ecology and Management 131, 81–91.
Ishii, H., McDowell, N., 2002. Age-related development of crown structure in coastal Douglas-fir trees. Forest Ecology and Management 169, 257–270.
Ishii, H., Wilson, M.E., 2001. Crown structure of old-growth Douglas-fir in the western Cascade Range, Washington. Canadian Journal of Forest Research 31, 1250–1261.

Ishii, H.R., Sillett, S.C., Carroll, A.L., 2017. Crown dynamics and wood production of Douglas-fir trees in an old-growth forest. Forest Ecology and Management 384, 157–168.
Ishii, H.T., Tanabe, S., Hiura, T., 2004. Exploring the Relationships Among Canopy Structure, Stand Productivity, and Biodiversity of Temperate Forest Ecosystems. for sci 50, 342–355. https://doi.org/10.1093/forestscience/50.3.342
Judge, G.G., Hill, R.C., Griffiths, W., Lutkepohl, H., Lee, T.C., 1982. Introduction to the Theory and Practice of Econometrics.
Kaitaniemi, P., Lintunen, A., 2010. Neighbor identity and competition influence tree growth in Scots pine, Siberian larch, and silver birch. Annals of forest science 67, 604–604.
Klinka, K., Wang, Q., Kayahara, G.J., Carter, R.E., Blackwell, B.A., 1992. Light-growth response relationships in Pacific silver fir (*Abies amabilis*) and subalpine fir (*Abies lasiocarpd*). Can. J. Bot. 70, 1919–1930. https://doi.org/10.1139/b92-239
Korhonen, L., Vauhkonen, J., Virolainen, A., Hovi, A., Korpela, I., 2013. Estimation of tree crown volume from airborne lidar data using computational geometry. International journal of remote sensing 34, 7236–7248.
Kozak, A., 2004. My last words on taper equations. The Forestry Chronicle 80, 507–515.
Kramer, R.D., Sillett, S.C., Van Pelt, R., Franklin, J.F., 2019. Neighborhood competition mediates crown development of Picea sitchensis in Olympic rainforests: Implications for restoration management. Forest Ecology and Management 441, 127–143. https://doi.org/10.1016/j.foreco.2019.03.027
Krůček, M., Trochta, J., Cibulka, M., Král, K., 2019. Beyond the cones: How crown shape plasticity alters aboveground competition for space and light—Evidence from terrestrial laser scanning. Agricultural and Forest Meteorology 264, 188–199. https://doi.org/10.1016/j.agrformet.2018.09.016
Lau, A., Bentley, L.P., Martius, C., Shenkin, A., Bartholomeus, H., Raumonen, P., Malhi, Y., Jackson, T., Herold, M., 2018. Quantifying branch architecture of tropical trees using terrestrial LiDAR and 3D modelling. Trees 32, 1219–1231. https://doi.org/10.1007/s00468-018-1704-1
Lau, A., Martius, C., Bartholomeus, H., Shenkin, A., Jackson, T., Malhi, Y., Herold, M., Bentley, L.P., 2019. Estimating architecture-based metabolic scaling exponents of tropical trees using terrestrial LiDAR and 3D modelling. Forest Ecology and Management 439, 132–145. https://doi.org/10.1016/j.foreco.2019.02.019
Lewis, J.D., McKane, R.B., Tingey, D.T., Beedlow, P.A., 2000. Vertical gradients in photosynthetic light response within an old-growth Douglas-fir and western hemlock canopy. Tree Physiology 20, 447–456. https://doi.org/10.1093/treephys/20.7.447
Lin, W., Meng, Y., Qiu, Z., Zhang, S., Wu, J., 2017. Measurement and calculation of crown projection area and crown volume of individual trees based on 3D

laser-scanned point-cloud data. International journal of remote sensing 38, 1083–1100.
Lintunen, A., Kaitaniemi, P., 2010. Responses of crown architecture in Betula pendula to competition are dependent on the species of neighbouring trees. Trees 24, 411–424. https://doi.org/10.1007/s00468-010-0409-x
Maguire, D., Moeur, M., Bennett, W., 1994. Models for describing basal diameter and vertical distribution of primary branches in young Douglas-fir. Forest Ecology and Management 63, 23–55.
Maguire, D.A., Johnston, S.R., Cahill, J., 1999. Predicting branch diameters on second-growth Douglas-fir from tree-level descriptors. Canadian Journal of Forest Research 29, 1829–1840.
Max, T.A., Burkhart, H.E., 1976. Segmented polynomial regression applied to taper equations. Forest Science 22, 283–289.
McCulloh, K.A., Sperry, J.S., 2005. Patterns in hydraulic architecture and their implications for transport efficiency. Tree Physiol 25, 257–267. https://doi.org/10.1093/treephys/25.3.257
Monserud, R.A., Marshall, J.D., 1999. Allometric crown relations in three northern Idaho conifer species. Canadian Journal of Forest Research 29, 521–535.
Nemec, A.F.L., Parish, R., Goudie, J.W., 2012. Modelling number, vertical distribution, and size of live branches on coniferous tree species in British Columbia. Can. J. For. Res. 42, 1072–1090. https://doi.org/10.1139/x2012-060
Niklas, K.J., 1994. Plant allometry: the scaling of form and process. University of Chicago Press.
Oren, R., Schulze, E.-D., Matyssek, R., Zimmermann, R., 1986. Estimating photosynthetic rate and annual carbon gain in conifers from specific leaf weight and leaf biomass. Oecologia 70, 187–193. https://doi.org/10.1007/BF00379238
Osborne, N.L., Maguire, D.A., 2015. Modeling knot geometry from branch angles in Douglas-fir (Pseudotsuga menziesii). Canadian Journal of Forest Research 46, 215–224.
Parresol, B.R., 2001. Additivity of nonlinear biomass equations. Can. J. For. Res. 31, 865–878. https://doi.org/10.1139/x00-202
Pelt, R.V., Sillett, S.C., 2008. Crown development of coastal Pseudotsuga menziesii, including a conceptual model for tall conifers. Ecological Monographs 78, 283–311.
Pinheiro, J., Bates, D., 2019. nlme: Linear and Nonlinear Mixed Effects Models. R package version 3.1-138.
Poudel, K.P., Temesgen, H., Gray, A.N., 2018. Estimating upper stem diameters and volume of Douglas-fir and Western hemlock trees in the Pacific northwest. For. Ecosyst. 5, 16. https://doi.org/10.1186/s40663-018-0134-2
Pukkala, T., Kolström, T., 1987. Competition indices and the prediction of radial growth in Scots pine.
Raumonen, P., Kaasalainen, M., Åkerblom, M., Kaasalainen, S., Kaartinen, H., Vastaranta, M., Holopainen, M., Disney, M., Lewis, P., 2013. Fast Automatic

Precision Tree Models from Terrestrial Laser Scanner Data. Remote Sensing 5, 491–520. https://doi.org/10.3390/rs5020491
Roeh, R.L., Maguire, D.A., 1997. Crown profile models based on branch attributes in coastal Douglas-fir. Forest Ecology and Management 96, 77–100.
Rouvinen, S., Kuuluvainen, T., 1997. Structure and asymmetry of tree crowns in relation to local competition in a natural mature Scots pine forest. Canadian Journal of Forest Research 27, 890–902.
Sprugel, D.G., 1990. Components of woody-tissue respiration in young Abies amabilis (Dougl.) Forbes trees. Trees 4, 88–98. https://doi.org/10.1007/BF00226071
Tanago, J.G. de, Lau, A., Bartholomeus, H., Herold, M., Avitabile, V., Raumonen, P., Martius, C., Goodman, R.C., Disney, M., Manuri, S., Burt, A., Calders, K., 2018. Estimation of above-ground biomass of large tropical trees with terrestrial LiDAR. Methods in Ecology and Evolution 9, 223–234. https://doi.org/10.1111/2041-210X.12904
Trochta, J., Krůček, M., Vrška, T., Král, K., 2017. 3D Forest: An application for descriptions of three-dimensional forest structures using terrestrial LiDAR. PloS one 12, e0176871.
Van Pelt, R., North, M.P., 1996. Analyzing canopy structure in Pacific Northwest old-growth forests with a stand-scale crown model.
Vanninen, P., Mäkelä, A., 2000. Needle and stem wood production in Scots pine (Pinus sylvestris) trees of different age, size and competitive status. Tree Physiol 20, 527–533. https://doi.org/10.1093/treephys/20.8.527
Weiskittel, A.R., Maguire, D.A., Monserud, R.A., 2007. Modeling crown structural responses to competing vegetation control, thinning, fertilization, and Swiss needle cast in coastal Douglas-fir of the Pacific Northwest, USA. Forest Ecology and Management 245, 96–109.
West, G.B., Brown, J.H., Enquist, B.J., 1999. A general model for the structure and allometry of plant vascular systems. Nature 400, 664.
Wilson, B.F., 2000. Apical control of branch growth and angle in woody plants. Am. J. Bot. 87, 601–607. https://doi.org/10.2307/2656846
Winter, L.E., Brubaker, L.B., Franklin, J.F., Miller, E.A., DeWitt, D.Q., 2002. Initiation of an old-growth Douglas-fir stand in the Pacific Northwest: a reconstruction from tree-ring records. Can. J. For. Res. 32, 1039–1056. https://doi.org/10.1139/x02-031
Woodall, C.W., Fiedler, C.E., Milner, K.S., 2003. Intertree competition in uneven-aged ponderosa pine stands. Canadian Journal of Forest Research 33, 1719–1726.
Zellner, A., 1962. An efficient method of estimating seemingly unrelated regressions and tests for aggregation bias. Journal of the American statistical Association 57, 348–368.

Chapter 6 General Discussion and Conclusion

Information on the conifer crown structure is vital for ecosystem conservation and silvicultural practices. Previous studies have widely documented structural characteristics and models of conifer trees in various types of forests and species (Baldwin and Peterson, 1997; Ishii et al., 2000; Ishii and McDowell, 2002; Kershaw Jr. and Maguire, 1996; Maguire et al., 1999; Roeh and Maguire, 1997; Weiskittel et al., 2007). Most of these studies were based on traditional fieldwork. However, as technology advances, the emerging application of point clouds provides promising opportunities for displaying, measuring, and analyzing canopy structure. Advantages of point cloud datasets include lively visualization, comparable accuracy as field measurements, reduced efforts for fieldwork, broad coverage of spatial and temporal scales, richness of detailed structural attributes at fine scale, and permanent storage. Through Chapters 2 – 5, this thesis presents the successful utilization of terrestrial point clouds in structural estimation and modeling for conifer species in plantation and natural regime stands.

In the next decade, lidar and photogrammetric point clouds are likely to be the main sources of acquiring forest inventory data. For determining tree stem diameter and volume the two remote sensing techniques have supplied values comparable with ground measurements but a fraction of the cost. The use of point cloud data depends on the targets and the scale of the inventory. Compared with estimates of taper models, direct stem diameter and volume estimates using 3D models constructed with point clouds could be more accurate for individual trees. At the least, stem diameter across several distinct heights of individual tree stem should be sampled to calibrate taper

equation for accurate estimates (Harold E Burkhart and Tomé, 2012; Cao, 2009). For regional inventory, the results of Chapter 3 indicate greater variation of volume estimates from lidar-based individual tree model than the existing FIA equation, which also yielded the smallest volume estimates among all the compared methods. There is an increasing need to update the current inventory equation with estimates from the latest technology. Instant DBH and tree height extraction algorithms are also available for plot level sampling with point cloud data (Liang et al., 2014a; Liu et al., 2018; Mikita et al., 2016; Piermattei et al., 2019; Ye et al., 2020). The combination of point clouds sampling and traditional modeling could merge the consistency of contemporary forest sampling methods with existing forest inventory databases.

In this thesis, 3D stem models were developed for plantation loblolly pine trees (Chapter 2) and natural regime Douglas-fir trees (Chapter 3). In our case, the selection of the data source depended on the stand conditions. PPC was developed for plantation loblolly pine trees, as the clear understory and open canopy ensured the successful RGB photo alignment. By contrast, the relatively low light penetration and increasing complexity of the natural regime stand could lower the success rate of photo alignment in SfM. Laser scanning, which is not restricted by the light condition, was therefore selected as the data source of the natural regime Douglas-fir plot.

The 3D stem models constructed with PPC and lidar point clouds were based on different methods. PPC-based 3D models were developed as polygon mesh, in which point clouds were the vertices of a set of polygon faces that define the surface of objects, whereas the 3D stem models developed from lidar point clouds were cylinders fitted with cross-sectional stem points. While the mesh model reflected the actual shape of

the stem, the cylinder model reflected an approximation of stem shape. The two modeling methods were not restricted by the type of point clouds: mesh models also could be developed from lidar point clouds, and cylinder models could be used to approximate PPC. However, the trade-off is between the model actuality and processing time. The creation of mesh models requires manual clearance of all noise points, as automatic seed point selection is not involved in the model creation approach. Since plantation loblolly pine trees were photographed individually, the reconstructed 3D point clouds for stems were easily segmented from the surrounding. Point clouds of Douglas-fir trees were scanned as the entire plot; thus, manual segmentation of individual tree stem is difficult and time-consuming. Cylinder model fitting could automatically select seed points and reduce the effort of manual removal of noise points. Many sources could introduce bias to 3D models constructed with SfM (Schindler and Bischof, 2003; Zucchelli and Kosecka, 2001; Zucchelli and Košecká, 2008). The usage of PPC requires careful study of the bias in different directions (Smith and Cheeseman, 1986). The bias correction is a trade-off with increasing error variance (Figure 2.6 and Daniilidis and Spetsakis, 1997). The bias could also be alleviated by distance scaling in multiple directions.

Fine-scale branch model constructed with point clouds, although more difficult to construct than stem model, provides detailed crown structural information that would not be acquirable by fieldwork alone. Even though a large sample of field measured branch data was not available, the simulation suggests branch estimates from lidar points using Cyclone and *TreeQSM* fit in the range of existing branch observations (Chapter 4). The poor performance of automatic branch model construction with

TreeQSM for the upper crown is a result of incomplete point cloud coverage plus the interference of leaf points rather than internal shortcomings of the algorithm. The foliage filtering process could reduce the model construction error introduced by leaf points. To filter the leaf points, radiometric features of lidar point clouds are used to distinguish leaf points from wood points (Belgiu and Drăguţ, 2016; Zhu et al., 2018). However, using intensity value could lead to inconsistent estimates for individual trees or different locations, because intensity value varies largely with the distance between the scanned surface and the scanner, the scanning angle, texture of the surface, and moisture conditions. However, extra normalization of intensity could bring consistency to the estimates, but in the present research, the intensity was not normalized because the only geo-coordinate information was used in creating branch structural models. For the semi-automatic method in Cyclone, leaf points were manually excluded from the selection of seed points, and the constructed models were visually examined to reduce the error. For the *TreeQSM*, automatic removal of leaf points is not available, but leaf-on points were used for 3D model construction with *TreeQSM* by previous studies (Calders et al., 2015; Krishna Moorthy et al., 2020; Lau et al., 2019, 2018; Tanago et al., 2018). According to Lau (2019), leaf-on points introduce more errors to higher order branches, which were not the targets of this study, as only first-order branches were modeled.

Only semi-automatic branch estimates with the highest accuracy were used in developing branch profile models (Chapter 5). The branch length was the most accurately measured attribute with the semi-automatic method, as the longest of first-order branches was visually assessed. For *TreeQSM*, the definition of branch length

could be interpreted as either the cumulative length from the stem insertion point to the end of the longest sub-branch or as the length from the stem insertion point to the branch's furthest extension out from the stem. The ambiguity of branch length definition resulted in uncertainty in branch length estimates with *TreeQSM* (Lau et al., 2018). Compared with branch length, which only requires a few vertices to estimate accurately, branch diameter requires a higher coverage of point clouds to achieve similarly accurate estimates; this led to diameter missed in the upper canopy. The model of maximum branch diameter did not reach a high agreement with the predictor variables, due to incomplete coverage of estimates for upper canopy. By contrast, the model of maximum branch length yielded the highest goodness-of-fit, which reflects the combination of effects from the crown length, neighboring competition, crowding condition, and relative position inside the crown. The branch length model, despite being developed from estimates with complete coverage of canopy depth, reached a low agreement with predictor variables, because the mixture of epicormic and original branches are driven by increasing variability of light conditions and internal tree physiology (Ishii et al., 2000; Ishii and Ford, 2001; Pelt and Sillett, 2008).

According to the individual branch and systematic crown models in Chapter 5, the cluster of neighboring trees exhibit two types of crown types: conic and ellipsoid. However, simply categorizing the crown shape into these two types did not adequately encapsulate the large variation of the branch length and crown shapes of individual trees. The observation indicated a weak relationship between crown shape and tree size, as both conic and ellipsoid crown shapes were observed for different DBH classes. The upward migration of the crown gravity center and increasing gaps between branches

were observed for large trees (Chapter 4 and 5). The observations are inconsistent with previous studies (Ishii and McDowell, 2002), indicating light condition is the primary driver of crown development of trees at closed canopy. Other factors including tree interlocking effects, tree genetics, and stand growth conditions may also contribute to the formation of crown shape and its dynamic. Detailed individual tree structural models could support solving unknown factors that drive tree crown development.

6.1. Summary of contributions

Chapters 2 focused on the application of photogrammetry-based point clouds. Chapter 2 demonstrated the applicability and reliability of PPC in stem diameter measurements and modeling for loblolly pines in a plantation. The results of this chapter support PPC as an economically friendly alternative to lidar scanning, as it provides high-quality 3D models for lower stem and improved RGB visualization. Chapter 2 provided the workflow for using affordable photogrammetry for fast and accurate forest inventory. The workflow is easily replicable and could be followed by forestry practitioners with a limited computer programming background.

Chapters 3 to 5 extended the research from the lower stem to upper stem, from the prominent stem features to finer-scale features inside the crown, and from plantation trees to a group of typical trees growing under natural regime.

Chapter 3 continued the study of Chapter 2 and measured Douglas-fir stem diameter with quantitative models derived from lidar point clouds and developed taper equations with the measurements. Chapter 3 compared stem volume estimates from lidar-related models (physical and taper) with an existing taper equation and FIA regional equation. According to the results of the simulation for large samples covering different tree size

class, I found the stem volume estimates varied strongly among various estimation methods and the DBH classes. I demonstrated the possibility of creating lidar-based estimation systems that bridge the inconsistency of estimates at various scales.

Chapter 4 documented crown attributes (branch diameter, branch length, branch insertion angle, and branch azimuth) developed from lidar point clouds using two methods semi-automatic and automatic *TreeQSM* measurements. The semi-automatic branch estimates fit well in the simulated ranges of existing models of plantation (Maguire et al., 1999) and old-growth (Ishii and Wilson, 2001) trees with similar DBH. The conceptual crown profiles developed with semi-automatic methods are also in agreement with previous studies of mature Douglas-fir crown (Ishii and McDowell, 2002). However, automatic measurements could only yield accurate estimates for the lower crown. This chapter contributes to the body of literature from three aspects:

- It documents the sparse research focused on mature Douglas-fir profiles;
- It uses point clouds to estimate tall conifer branch attributes at the upper canopy, which has been rarely executed from terrestrial point clouds;
- It demonstrates that the widely used automatic method QSM is currently unreliable for detailed structural estimates for upper canopy.

Chapter 5 used branch attributes derived from lidar point clouds to develop allometric models of mature Douglas-fir crown profiles. Five individual models of branch attributes and two sets of systematic crown profile models were developed with consideration of neighboring competition effects. The allometric models were added

to the pool of models for forest inventory. The models also enhanced the understanding of neighborhood effects on crown development.

6.2. Limitation and future work

In this study, all point clouds were acquired from terrestrial sensors. Therefore, complete coverage of point clouds through the depth of canopy was not available, and the resulting estimate accuracy is biased towards the lower and understory canopy. Future improvements of point-clouds-based applications rely on two aspects: 1) increasing the point clouds coverage by fusing datasets acquired from multiple platforms, and 2) advancing algorithms for automatic metric extraction.

The structural complexity of dense canopy challenges successful alignment of images via SfM, since the key features connecting sequential images are not easily distinguishable from the surrounding. The advancement of image pattern recognitions would bring opportunities to accurate feature extraction of objects having complex edges. Meanwhile, powerful cloud computing and utilization of graphics processing unit (GPU) will largely reduce image processing time and enable the operation of SfM at a greater spatial scale.

For lidar-based applications, the fusion of terrestrial and airborne lidar point clouds can capture complete coverage of canopy data. Although this thesis demonstrated the inaccurate structural estimates from *TreeQSM* of fine branches at the upper canopy, the automatic estimation algorithm is desirable for delivering fast tree structural estimates for larger branches. Increasing point clouds coverage throughout the entire canopy depth would reduce the modeling error at the upper canopy. Single or sets of traditional numeric models could not adequately generalize the crown structural development. For

future studies, digitization of individual trees point clouds will eventually contribute to large amassed ecological databases. A wealth of crown information would shift crown studies from model-driven to data-driven, and comprehensive knowledge of crown development will be gained from these big databases. The insights provided through this thesis will serve as a foundation for the next wave of computer-supported crown structure analysis.

Reference

Baldwin, J., V. Clark, Peterson, K.D., 1997. Predicting the crown shape of loblolly pine trees. Can. J. For. Res. 27, 102–107.

Belgiu, M., Drăguţ, L., 2016. Random forest in remote sensing: A review of applications and future directions. ISPRS J. Photogramm. Remote Sens. 114, 24–31. https://doi.org/10.1016/j.isprsjprs.2016.01.011

Burkhart, H.E., Tomé, M., 2012. Modeling forest trees and stands. Springer Science & Business Media.

Calders, K., Newnham, G., Burt, A., Murphy, S., Raumonen, P., Herold, M., Culvenor, D., Avitabile, V., Disney, M., Armston, J., Kaasalainen, M., 2015. Nondestructive estimates of above-ground biomass using terrestrial laser scanning. Methods Ecol. Evol. 6, 198–208. https://doi.org/10.1111/2041-210X.12301

Cao, Q.V., 2009. Calibrating a segmented taper equation with two diameter measurements. South. J. Appl. For. 33, 58–61.

Daniilidis, K., Spetsakis, M.E., 1997. Understanding noise sensitivity in structure from motion.

Ishii, H., Clement, J.P., Shaw, D.C., 2000. Branch growth and crown form in old coastal Douglas-fir. For. Ecol. Manag. 131, 81–91.

Ishii, H., Ford, E.D., 2001. The role of epicormic shoot production in maintaining foliage in old Pseudotsuga menziesii (Douglas-fir) trees. Can. J. Bot. 79, 251–264. https://doi.org/10.1139/b00-158

Ishii, H., McDowell, N., 2002. Age-related development of crown structure in coastal Douglas-fir trees. For. Ecol. Manag. 169, 257–270.

Ishii, H., Wilson, M.E., 2001. Crown structure of old-growth Douglas-fir in the western Cascade Range, Washington. Can. J. For. Res. 31, 1250–1261.

Kershaw Jr., J.A., Maguire, D.A., 1996. Crown structure in western hemlock, Douglas-fir, and grand fir in western Washington: horizontal distribution of foliage within branches. Can. J. For. Res. 26, 128–142. https://doi.org/10.1139/x26-014

Krishna Moorthy, S.M., Raumonen, P., Van den Bulcke, J., Calders, K., Verbeeck, H., 2020. Terrestrial laser scanning for non-destructive estimates of liana stem biomass. For. Ecol. Manag. 456, 117751. https://doi.org/10.1016/j.foreco.2019.117751

Lau, A., Bentley, L.P., Martius, C., Shenkin, A., Bartholomeus, H., Raumonen, P., Malhi, Y., Jackson, T., Herold, M., 2018. Quantifying branch architecture of tropical trees using terrestrial LiDAR and 3D modelling. Trees 32, 1219–1231. https://doi.org/10.1007/s00468-018-1704-1

Lau, A., Martius, C., Bartholomeus, H., Shenkin, A., Jackson, T., Malhi, Y., Herold, M., Bentley, L.P., 2019. Estimating architecture-based metabolic scaling exponents of tropical trees using terrestrial LiDAR and 3D modelling. For. Ecol. Manag. 439, 132–145. https://doi.org/10.1016/j.foreco.2019.02.019

Liang, X., Jaakkola, A., Wang, Y., Hyyppä, J., Honkavaara, E., Liu, J., Kaartinen, H., 2014. The use of a hand-held camera for individual tree 3D mapping in forest sample plots. Remote Sens. 6, 6587–6603.

Liu, J., Feng, Z., Yang, L., Mannan, A., Khan, T.U., Zhao, Z., Cheng, Z., 2018. Extraction of Sample Plot Parameters from 3D Point Cloud Reconstruction Based on Combined RTK and CCD Continuous Photography. Remote Sens. 10, 1299. https://doi.org/10.3390/rs10081299

Maguire, D.A., Johnston, S.R., Cahill, J., 1999. Predicting branch diameters on second-growth Douglas-fir from tree-level descriptors. Can. J. For. Res. 29, 1829–1840.

Mikita, T., Janata, P., Surový, P., 2016. Forest stand inventory based on combined aerial and terrestrial close-range photogrammetry. Forests 7, 165.

Pelt, R.V., Sillett, S.C., 2008. Crown development of coastal Pseudotsuga menziesii, including a conceptual model for tall conifers. Ecol. Monogr. 78, 283–311.

Piermattei, L., Karel, W., Wang, D., Wieser, M., Mokroš, M., Surový, P., Koreň, M., Tomaštík, J., Pfeifer, N., Hollaus, M., 2019. Terrestrial Structure from Motion Photogrammetry for Deriving Forest Inventory Data. Remote Sens. 11, 950. https://doi.org/10.3390/rs11080950

Roeh, R.L., Maguire, D.A., 1997. Crown profile models based on branch attributes in coastal Douglas-fir. For. Ecol. Manag. 96, 77–100.

Schindler, K., Bischof, H., 2003. On robust regression in photogrammetric point clouds, in: Joint Pattern Recognition Symposium. Springer, pp. 172–178.

Smith, R.C., Cheeseman, P., 1986. On the representation and estimation of spatial uncertainty. Int. J. Robot. Res. 5, 56–68.

Tanago, J.G. de, Lau, A., Bartholomeus, H., Herold, M., Avitabile, V., Raumonen, P., Martius, C., Goodman, R.C., Disney, M., Manuri, S., Burt, A., Calders, K., 2018. Estimation of above-ground biomass of large tropical trees with terrestrial LiDAR. Methods Ecol. Evol. 9, 223–234. https://doi.org/10.1111/2041-210X.12904

Weiskittel, A.R., Maguire, D.A., Monserud, R.A., 2007. Modeling crown structural responses to competing vegetation control, thinning, fertilization, and Swiss needle cast in coastal Douglas-fir of the Pacific Northwest, USA. For. Ecol. Manag. 245, 96–109.

Ye, W., Qian, C., Tang, J., Liu, H., Fan, X., Liang, X., Zhang, H., 2020. Improved 3D Stem Mapping Method and Elliptic Hypothesis-Based DBH Estimation from Terrestrial Laser Scanning Data. Remote Sens. 12, 352. https://doi.org/10.3390/rs12030352

Zhu, X., Skidmore, A.K., Darvishzadeh, R., Niemann, K.O., Liu, J., Shi, Y., Wang, T., 2018. Foliar and woody materials discriminated using terrestrial LiDAR in a mixed natural forest. Int. J. Appl. Earth Obs. Geoinformation 64, 43–50. https://doi.org/10.1016/j.jag.2017.09.004

Zucchelli, M., Košecká, J., 2008. Motion bias and structure distortion induced by intrinsic calibration errors. Image Vis. Comput. 26, 639–646. https://doi.org/10.1016/j.imavis.2007.08.002
Zucchelli, M., Kosecka, J., 2001. Motion bias and structure distortion induced by calibration errors., in: BMVC. pp. 1–10.

Appendix A. Photogrammetric trees

This appendix describes the point clouds representing the stem of three loblolly pine trees used in Chapter 2. After the images needed for the 3D rendering were captured, the sample trees were felled and their diameters at breast height and at every meter along the stem starting at 1 m above the ground were measured. The diameters measured in the field were stored as ASCII files. The reconstructed models reached over 50% of the relative height – the proportion of the stem on which the majority of the merchantable volume is located. For each tree, two files were produced, a point cloud and a mesh data, to represent the 3D stem and some branches. The point cloud was stored in the LAS format and the mesh in the DXF format. Diameter at breast height was marked on all trees by red rings. The files describing the three trees provide a calibrated dataset that can be used for development of taper models, testing and calibration of segmentation algorithms, and identification of products that can be obtained from a stem.

The photogrammetric point clouds (PPC) were developed for loblolly pines (Pinus taeda Lindl.) positioned in the dominant and codominant crown classes. Field data collection was conducted in February, March, and April 2014. Before any measurement or photo was recorded the trees were prepared for subsequent data processing, particularly scaling of point clouds. To scale the point clouds two metal bars of 304.8 mm (i.e., 1 foot) were freely hanged on the stem, close to breast height, on opposing sides. The diameter at breast height (DBH) was marked with red paint, which provided additional information for calibration. To identify each tree, on the stem on two opposing sides were written the number of the tree (i.e., id of the tree within the study)

and the side of the tree (i.e. 1 or 2). Once preparation was completed, for standing trees, DBH was measured and a sequence of photographs were captured for each standing tree. After the photographs were recorded the trees were cut. On the fallen trees, the diameters every meter and at breast height were measured. Diameter measurement were accurate at 1 mm while stem length was measured with 10 mm accuracy. The precision of the measurements was 1 mm for both diameter and length.

To estimate the total height of the trees, the study site was scanned with airborne laser scanners four months earlier than the actual field sampling. The average point density for the LIDAR point cloud is 30 points / m^2. The total heights for the three trees were determined as the largest normalized elevation, which supplied 25.36 m for tree#1, 26.81 m for tree#2, and 18.91 m for tree #2. The comparison between the LIDAR based values and the the fallen trees measurements suggested the difference was within 3 cm. Larger height estimated from LIDAR is likely the results of breaking the top part of the tree during the falling process, which justifies the heights based on LIDAR. The corresponding DBH measured in the field are 398.5 mm, 326.0 mm, and 268 mm. Table A.1 provided the stem diameters measured for every 1 m increasing along the stem.

The red-green-blue (RGB) images of trees were captured with a Nikon D3200 camera equipped with a Nikkor AF-S DX VR 18–55 mm zoom lens (aperture3.5–5.6). The minimum focal length was used to acquire the images with the largest exposure of the stem of the trees. Multiple images were captured from an approximate circular trajectory surrounding each tree (Figure A.1). Two images were taken at each spot; one was captured for the perpendicular view of the lower part of the stem (i.e., the lens was

approximately horizontal), and one was captured with the lens facing the upper part of the stem (i.e., the lens was tilted upwards). Each pair of such images had at least 50% overlap to ensure the successful feature extraction for 3D construction.

Table A.1 Diameter along the stem measured in the field for the three trees

Length on the stem [m]	Diameter [mm]		
	Tree 1	Tree 2	Tree 3
1.0	397.19	332.42	280
1.3	398.5	326	268
2	408.62	319.72	272
3	375.6	303.21	262
4	381.95	301.94	256
5	378.14	287.97	253
6	369.25	286.7	237
7	362.9	276.54	228
8	350.2	268.92	225

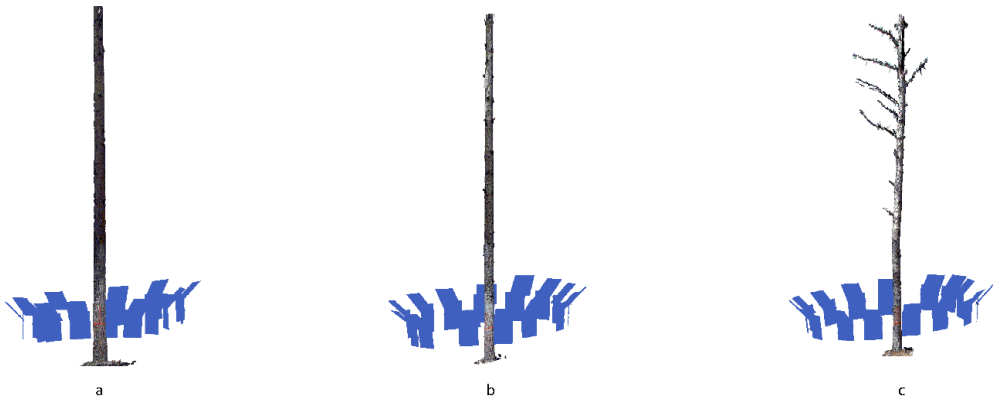

Figure A.1 Position of the cameras to reconstruct the three trees: a. Tree#1, b. Tree#2, c. Tree#3

The reconstruction of the trees with SfM was executed in Agisoft PhotoScan version 1.2 (Agisoft LLC 2014). The SfM workflow in Agisoft PhotoScan contains three serial steps: (1) align photos, (2) build dense point cloud, and (3) build mesh. Photo alignment generates the sparse point cloud, which are the features outlining the tree structure. Then, the dense point clouds were generated based on the sparse points to depict the detailed texture of the stem surface. Finally, the mesh model was derived as polygonal network from the dense point clouds.

The accuracy of the 3D models is determined by the quality of the original images and the settings of the parameter defining each step. However, higher accuracy is achieved at the cost of longer computation time. Thus, the selections of the model accuracy rely on the objectives of the study. There are five accuracy options for photo alignment in Agisoft, varying from lowest to highest. The highest accuracy setting allows the program to use the maximum resolution (i.e., in our case: 3872 2592 pixels) to determine the locations of the cameras. For every decreasing level of accuracy, the program downscales each side of images with half. The images were recorded under the canopy, where GPS signal was weak (i.e., inaccurate positions), which forced their alignment only on the images themselves. To compensate the lack of GPS, I set the accuracy to high. The key point and tie point limits were set to 600,000 and 100,000 respectively. After the images were successfully aligned, Agisoft built the dense point cloud based on the tie points selected during photo alignment. To ensure that the measurements based on PPC are comparable with the field measurements, I set the quality of building dense points to high, with depth filtering disabled. The number of points describing each tree are 2,283,160 for tree #1, 5,148,910 for tree #2, and

1,321,536 for tree #3. After the dense point clouds were created, the mesh was constructed using an arbitrary surface type and the interpolation disabled. Arbitrary surface type is applicable to many types of surfaces, included tree bark. To ensure accurate representation of the stem by the mesh, no interpolations were allowed (Figure A.2- Figure A.4).

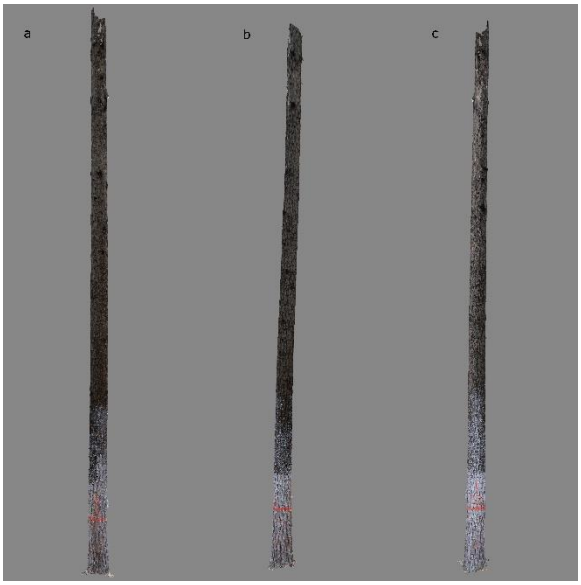

Figure A.1 3D reconstruction of the tree#1, seen from three perspectives (a. south view, b. east view, and c. north view). The top number on the tree represent the tree id, while the bottom the north (i.e., 1) and south (i.e., 2) side.

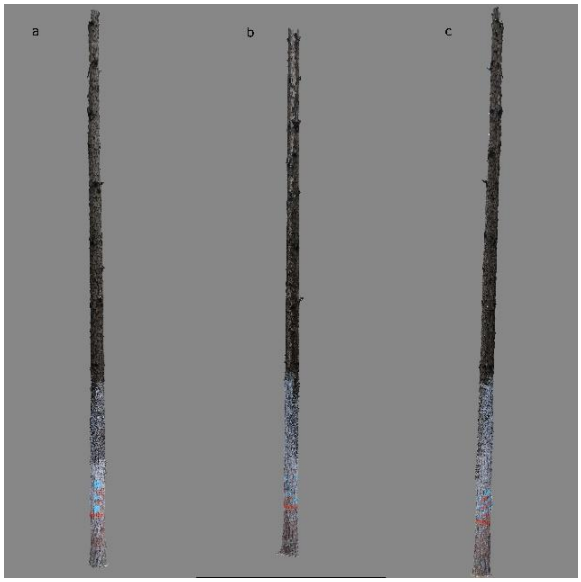

Figure A.2 3D reconstruction of tree#2, seen from three perspectives (a. south view, b. east view, and c. north view). The top number on the tree represent the tree id, while the bottom the north (i.e., 1) and south (i.e., 2) sides.

Figure A.3 3D reconstruction of the tree#3, seen from three perspectives (a. south view, b. east view, and c. north view). The top number on the tree represent the tree id, while the bottom the north (i.e., 1) and south (i.e., 2) sides

The data is hosted by the ScholarArchive@OSU, a digital service supported by Oregon State University. The data can be accessed at the persistent URL http://hdl.handle.net/1957/61881. The metadata are located at the same address and are stored in the file README_PPC_3Dtrees.txt. The data can be used without restrictions, but acknowledgement of their origin is necessary.

For each of the three trees the following files are available:

- an ASCII file with two fields:
    - field #1, titled "Length_m" contains the height in meters along the stem, and
    - field #2, titled "Diameter_mm", contains the diameter in millimeters at the respective height;
- a LAS file with the colored point clouds, and
- an Autodesk drawing interchange format file (DXF) that stores the mesh model.

The files are identified using the following convention: Tree#_field.txt, for the field measurements, Tree#_PPC.las for the photogrammetric point cloud, and Tree#_mesh.dxf for the mesh model of the tree. The "#" represents the tree number: 1, 2, or 3.

Appendix B. Proof of the linear bias reduction for PPC-based tree stem diameter estimates

Estimation of residual bias after application of Eq. 2-7

The selected function to eliminate bias (Eq. 2-7) was not tailored to the data or to the error structure. Therefore, it is likely that bias was reduced not eliminated. After bias reduction, the error, ε_{ht}, become:

$$\varepsilon_h = error_h - BC_h = d_{h,field} - d_{h,ppc} - d_{1.3,field} - d_{1.3,ppc} - RH \times error_{Agisoft} \quad \text{B-1}$$

where the h subscript represents the height at which the respective statistic is computed.

According to Agisoft documentation, the scaling error is a result of the difference between the distance estimated from the point cloud and the distance assigned by the operator after the identification of two points inside ppc:

$$error_{Agisoft} = d_{ppc} - d_{operator} \quad \text{B-2}$$

Figure 2.5 suggests that a linear function could describe the relationship between bias and relative height (RH). A simple linear regression between error and relative height supplied a significant equation (p=0.02), with both coefficients significant:

$$error_h = -1.36 - 1.42 \times RH \quad \text{B-3}$$

The two coefficients were close to the $d_{1.3,}$ error, 1.20 mm, (i.e., intercept in Eq. 2-7) and to the reported error by Agisoft, 1.22, (i.e., slope in Eq. 2-7). In fact, there was no significant difference between the coefficients of regression Eq. 2-7 and the two statistics. The choice of which one will be the intercept and which one will be the

slope was driven by the magnitude of the bias reduction as well as the variation. The model with d1.3 error as slope has a residual bias of 0.15 mm while the alternative was 0.18 mm. However, even that bias was smaller when d1.3 error was slope, the variance was larger (i.e., 2.97 vs. 2.88), which suggested selection of the Eq. 2-7 to reduce the bias.

To assess bias, I computed the expectation of the residual errors εh:

$$\begin{aligned} E[\varepsilon_h] = E[e_h - BC_h] \\ = E[e_h - error_{d1.3} \\ - error_{Agisoft} \times RH_h] = \\ = E[e_h] - E[error_{d1.3}] - RH_h E[error_{Agisoft}] = \\ = E[d_{h,field} - d_{h,ppc}] - E[d_{1.3,field} - d_{1.3,ppc}] \\ - RH_h E[d_{h,ppc} - d_{h,operator}] \end{aligned} \quad \text{B-4}$$

Diameter estimated by the operator from Agisoft suffers from the same lack of accuracy as the one measured in the field; therefore, it can be assumed that

$$E[d_{h,ppc} - d_{h,operator}] = E[d_{h,ppc} - d_{h,field}] \quad \text{B-5}$$

Table 2.3 reveals that errord1.3 is the smallest among all heights (except for height 9 m, which likely is a random occurrence), a direct result of closeness to the operator, and consequently to the camera, of that section of the tree.

Figure 2.6 supports the existence of a linear relationship between the expectation of the error anywhere on the stem and $d_{1.3,}$error:

$$E[d_{h,field} - d_{h,ppc}] = \frac{b}{(1+RH_h)} E[d_{1.3,field} - d_{1.3,ppc}] \quad \text{B-6}$$

where b is a coefficient

Based on Eq. B-4 and Eq. B-5, Eq. B-6 can be rearranged as

$$E[\varepsilon_h] \overset{Eq.16}{\approx} (1 + RH_h) \times E[d_{h,field} - d_{h,ppc}] - E[d_{1.3,field} - d_{1.3,ppc}] \overset{Eq.17}{\approx} \approx bE[d_{1.3,field} - d_{1.3ppc}] - E[d_{1.3,field} - d_{1.3,ppc}] = (b - 1)E[d_{1.3,field} - d_{1.3,ppc}] \quad \text{B-7}$$

Eq. B-7 depends on coefficient b, whose value can be approximated from the observation that

$$E[d_{1.3,field} - d_{1.3,ppc}] = \frac{b}{(1+RH_h)} E[d_{1.3,field} - d_{1.3,ppc}] \rightarrow b = 1 + 1.3/(totalheight) \quad \text{B-8}$$

Therefore, the remaining bias after the application of Eq. 2-7 is 1.3×E[$error_{d1.3}$]/(total height). Considering that field measurements are executed for stands that require immediate attention, such as thinning or regeneration harvests, it can be assumed that the total height of the trees is larger than 13 m, which means that the expected residual bias is less than 10% of E[$error_{d1.3}$]. According to Table 2.3, E[$error_{d1.3}$] is the smallest among errors at all heights (except for 12 m), therefore the residual bias is expected to be approximately1 mm.

Appendix C. Doulgas-fir double bark thickness equation

Double bark thickness is predicted from segmented polynomial equation developed by Maguire and Hann (1990):

$$dbt_{ij} = DBT * (1 + Z_1 + a_2 Z_2 + a_2 Z_3)$$

DBT = predicted double bark thickness at dbh

$$DBT = DOB - DIB$$

$$DIB = 0.3592699 DOB^{0.989388}$$

$$Z_1 = I\left\{\left[\frac{X-1}{k-1}\right]\left[1 + \frac{k-X}{k-1}\right] - 1\right\}$$

$$Z_2 = X + I\left\{\left[\frac{X-1}{k-1}\right]\left[X + \frac{k(k-X)}{k-1}\right] - X\right\}$$

$$Z_3 = X^2$$